UNIVERSITÀ
DEGLI STUDI
DI BRESCIA

DOTTORATO DI RICERCA IN
TECHNOLOGY FOR HEALTH

Area 05 - Scienze biologiche (BIO/14 – Farmacologia)

CICLO XXXIII

Multidimensional approach to Frailty Syndrome of the elderly: preclinical study in a mouse model and set up of a novel optical diagnostic technique in humans

Dott.ssa Agnese
SEGALA

f.to digitalmente ex art.24 D.Lgs. 82/05

RELATORE: Prof.ssa Alessandra VALERIO

f.to digitalmente ex art.24 D.Lgs. 82/05

CO-RELATORE: Prof.ssa Paola TARONI

f.to digitalmente ex art.24 D.Lgs. 82/05

COORDINATORE DEL DOTTORATO: Prof. Alessandra FLAMMINI

f.to digitalmente ex art.24 D.Lgs. 82/05

Abstract

La sindrome di fragilità dell'anziano, risultante del declino cumulativo di molteplici sistemi fisiologici, costituisce una priorità per la salute pubblica a causa dell'aumentata vulnerabilità alle malattie, disabilità, rischio di istituzionalizzazione e mortalità. Caratteristica frequente nell'anziano fragile è la condizione di sarcopenia, una riduzione di massa e forza muscolare, con importanti limitazioni funzionali, che è riconosciuta essere il substrato biologico centrale della sindrome di fragilità fisica. La composizione strutturale e la capacità metabolica del muscolo sono fattori determinanti per la sua funzione. In particolare, ben nota è l'influenza della compromissione della bioenergetica mitocondriale sulla salute muscolare. Numerose evidenze suggeriscono che la co-presenza di obesità, con depositi adiposi ectopici anche nel muscolo, agisce da aggravante della condizione di fragilità fisica. Differenze di genere complicano il quadro della situazione. Sebbene principi di consenso siano stati raggiunti, le eterogenee manifestazioni cliniche e la mancanza di definizioni operative chiare ed univoche per sarcopenia e fragilità fisica ostacolano la progettazione di strategie preventive e terapeutiche efficaci. Studi del mio gruppo di ricerca hanno dimostrato l'efficacia di interventi nutraceutici con peculiari formulazioni di aminoacidi in varie condizioni caratterizzate da deterioramento bioenergetico.

Il presente lavoro di tesi si inserisce nell'ambito dello uno studio multicentrico "Multicomponent Analysis of phYsical frailty BiomarkErs: focus on mitochondrial health - MAYBE" finalizzato a i) identificare biomarcatori in grado di definire e monitorare squilibri mitocondriali alla base di fragilità fisica e sarcopenia; ii) fornire strumenti diagnostici innovativi per queste complesse sindromi "gemelle"; iii) studiare le potenzialità di dieta, esercizio fisico e una nuova formulazione aminoacidica - e delle combinazioni di questi interventi - nel modificare i biomarcatori legati alla fragilità e il decorso della malattia nei topi e nell'uomo. Nel mio lavoro di tesi ho apportato un contributo a queste attività, che comprendevano uno studio preclinico, uno studio tecnologico e una sperimentazione clinica.

Nello studio preclinico, il ceppo murino a senescenza precoce SAMP8 è stato utilizzato per indagare i meccanismi fisiopatologici di declino fisico correlato all'età, con particolare attenzione agli squilibri mitocondriali nel muscolo scheletrico, e per esplorare l'efficacia di interventi terapeutici. Una caratterizzazione fenotipica dei topi a 5, 9, 12 e 15 mesi di età ha

consentito di identificare la corretta tempistica di intervento. In particolare, i primi segni di deterioramento delle condizioni di salute, della forza e resistenza muscolare, e delle funzioni bioenergetiche sono stati riscontrati a 9 mesi di età, con peggioramenti significativi dai 12 mesi di età in poi. La supplementazione dietetica con una innovativa miscela arricchita in aminoacidi a catena ramificata e cofattori del ciclo di Krebs (PD-0E7) nella finestra temporale dai 9 ai 12 mesi di età è stata in grado di contrastare i segni di declino neuromuscolare e di preservare la resistenza all'esercizio nei topi SAMP8. L'effetto benefico di PD-0E7 si associava a un recupero dei fenomeni di mitocondriogenesi, compromessi dall'invecchiamento. Nell'insieme, lo studio preclinico dimostra che PD-0E7 è in grado di ringiovanire i mitocondri e contrastare efficacemente gli effetti deleteri esercitati dall'invecchiamento precoce nei muscoli scheletrici, rappresentando così potenzialmente un nuovo intervento efficace e sicuro per prevenire disabilità e fragilità fisica.

Un punto critico è la varietà dei fenotipi clinici della sindrome da fragilità, da cui derivano sfide diagnostiche rilevanti. La definizione di strumenti diagnostici affidabili è essenziale per supportare la diagnosi, monitorare la progressione della malattia e l'efficacia degli interventi. Sebbene siano stati descritti alcuni parametri misurabili di sarcopenia e/o fragilità fisica, allo stato attuale nessun singolo test clinico è sufficiente per diagnosticare questa complessa condizione. La ricerca di un nuovo approccio diagnostico è dunque necessaria sia a fini clinici che di ricerca.

In questo contesto, tecniche ottiche come la spettroscopia ottica diffusa (DOS) applicata nella regione spettrale del vicino infrarosso possono fornire informazioni in modo non invasivo sulla composizione e struttura dei tessuti e potrebbero essere di grande interesse nello scenario clinico per la diagnosi precoce di sarcopenia e il monitoraggio del suo decorso clinico nel tempo e della risposta al trattamento. Le tecniche di ottica diffusa a risoluzione temporale si basano sull'iniezione di un breve impulso luminoso (~ decine di ps) nel campione e sulla rilevazione temporale della luce riemessa e hanno la capacità unica di stimare simultaneamente le proprietà ottiche di assorbimento e diffusione del tessuto in una singola misurazione. L'unicità del sistema sviluppato dal Politecnico di Milano sta nella disponibilità di una sorgente pulsata nell'ordine dei picosecondi, in continuo e con elevata responsività su un ampio intervallo spettrale (600-1350 nm) entro il quale presentano importanti picchi di assorbimento i principali cromofori tissutali: lipidi, acqua, ossi- e desossi-emoglobina e collagene.

La parte tecnologica del mio lavoro di dottorato si è concentrata sull'applicazione della tecnica TD-DOS (lo strumento utilizzato è stato progettato dal team di collaboratori del Politecnico di Milano) all'indagine del muscolo scheletrico e del tessuto adiposo sottocutaneo nell'uomo. Sono state organizzate due campagne di misurazioni in vivo su volontari sani per comprendere il potenziale della tecnica e disegnare un opportuno protocollo in previsione di un successivo studio clinico. Spettri di assorbimento e diffusione sono stati acquisiti a tre distanze sorgente-rivelatore (ρ) di 1, 2 e 3 cm, e quindi analizzati utilizzando un modello omogeneo di propagazione della luce come passaggio iniziale per comprendere gli effetti degli strati tissutali sulle proprietà ottiche derivate dalle misurazioni.

Un primo studio per indagare le proprietà ottiche del tessuto adiposo è stato condotto sulla regione addominale su 10 volontari sani maschi. I risultati mostrano una chiara influenza della natura stratificata del tessuto sulle proprietà ottiche derivate. Da questo primo studio pilota sono stati osservati tre principali effetti, ovvero: i) la presenza di un'elevata variabilità tra soggetti, relativa a differenze costituzionali; i) l'aumento dell'assorbimento tissutale complessivo a $\rho = 3$ cm, quando il tessuto adiposo è sottile, suggerendo che il muscolo è raggiunto dalla misurazione; ii) l'aumento del picco di assorbimento dell'acqua a $\rho = 1$ cm supponendo un contributo dell'idratazione della cute; e iii) l'aumento della pendenza dello spettro di scattering ancora per la $\rho = 1$ ipotizzando un contributo del collagene. Tutti questi risultati sono coerenti con un modello a 3 strati dell'addome che comprende la pelle, il tessuto adiposo e il muscolo sottostante e che dovrebbe quindi essere considerato per ottenere un'analisi quantitativa.

In secondo luogo, abbiamo valutato la capacità di tale tecnologia nel contesto di un altro studio pilota su 26 volontari sani a livello delle regioni di addome e coscia (vasto laterale) al fine di caratterizzare struttura e componenti del tessuto adiposo sottocutaneo e del muscolo. Dal secondo studio pilota sono stati osservati cinque effetti, ovvero: i) una differenza di genere negli spettri di assorbimento e diffusione sia a livello di addome che di vasto laterale; ii) il contenuto di HbO2 ha una tendenza all'aumento con ρ sia nei maschi che nelle femmine nella regione dell'addome e questo potrebbe essere correlato al raggiungimento del muscolo alle profondità maggiori; iii) una conferma dell'effetto di "contaminazione della cute" ottenuto dal primo studio; iv) nelle femmine a livello del vasto laterale è stata osservata un maggiore prevalenza di lipidi a supporto dell'ipotesi che probabilmente il muscolo sottostante non sia stato effettivamente raggiunto dalle misurazioni; v) il contenuto di lipidi, acqua e collagene a tutte e 3 le distanze sorgente-rivelatore nella regione del vasto laterale

differiscono tra maschio e femmina supportando l'ipotesi che il muscolo sia raggiunto solo nei soggetti maschi.

Nell'era della medicina personalizzata e di precisione, aumentare le nostre conoscenze sui tessuti adiposo e muscolare potrebbe consentirci di superare i limiti dei tradizionali indici antropometrici nella valutazione di obesità e sarcopenia. La disponibilità di una tecnica non invasiva per monitorare lo stato del tessuto adiposo in risposta alla dieta, all'esercizio fisico o al trattamento terapeutico è di particolare interesse scientifico. Le intuizioni ottenute da questo studio verranno utilizzate per ottimizzare sia il protocollo di misurazione che la metodologia di analisi dei dati per successivi studi clinici. Nell'ambito del programma MAYBE è infatti in corso uno studio nel quale lo strumento TD-DOS è applicato, nell'ambito di una valutazione geriatrica multidimensionale, per esaminare l'efficacia di cambiamenti dello stile di vita associati a integrazione nutrizionale con PD-E07 (AminoTher) nella prevenzione della fragilità in pazienti anziani con obesità sarcopenica.

Preface

The work presented in this thesis is part of the multicenter project **"Multicomponent Analysis of phYsical frailty BiomarkErs: focus on mitochondrial health"** (MAYBE) financed by the Cariplo Foundation. Experiments have been carried out mainly at the **Department of Molecular and Translational Medicine, University of Brescia** (Prof. Alessandra Valerio), and the **Department of Physics, Politecnico di Milano** (Prof. Paola Taroni). Other project partners were the **Department of Medical Biotechnology and Translational Medicine of the University of Milan** (Prof. Enzo Nisoli); **the Department of Medicine, Division of Geriatrics, University of Verona** (Prof. Mauro Zamboni), and the **National Institute of Health and Science on Aging (INRCA) in Ancona** (Prof. Mauro Provinciali).

One of the most notable changes that accompany ageing is a condition termed sarcopenia, i.e., the progressive loss of skeletal muscle mass. Sarcopenia and its clinical correlates result in reduced muscle strength, functional limitations, and ultimately physical disability. A body of recent evidence indicates sarcopenia as the central biological substrate of the physical frailty syndrome. No effective pharmacological therapies exist for this common geriatric condition that has dramatic consequences on the quality of life of the elderly. Notably, older adults are weaker than the loss of muscle mass alone would predict. Muscle's structural composition, fat infiltration, and metabolic capacity are important factors impacting their physical function. Indeed, a key feature affecting muscle health in sarcopenic individuals is the impairment in mitochondrial bioenergetics. While inadequate intake of essential nutrients might contribute to sarcopenia, older age and unhealthy lifestyles predispose to obesity and its complications, also associated with disability and frailty. Mounting data suggest that the co-presence of obesity acts as a modifier of physical frailty and aggravates its consequences. Age-related sex differences complicate the picture. An overview of ageing pathophysiology, focusing on sarcopenia and physical frailty in terms of definitions, mitochondrial involvement, diagnostic tools and possible treatments, is presented in **Chapter 1**.

Though consensus principles have been reached, the heterogeneous clinical manifestations and lack of unique operational definition(s) for sarcopenia and physical frailty hamper the

design of effective preventive and therapeutic strategies. The MAYBE project has been designed to i) explore multidimensional, non-invasive biomarkers able to track mitochondrial derangements and contribute innovative diagnostic tools for these complex "twin" syndromes; ii) study the ability of diet, exercise, nutrient supplements, and their combinations, to modify frailty-related biomarkers and the course of the disease in mice and humans. My PhD thesis fits in the context of this comprehensive project, comprising a preclinical study and a clinical trial. A general description of the MAYBE program and my PhD work is presented in **Chapter 2**.

My research group seminal studies demonstrated the efficacy of designer formulations amino acids, enriched in branched-chain amino acids, as nutraceuticals in various conditions characterised by bioenergetic impairment. During my PhD program, I took part in the preclinical study to investigate the potentiality of a novel dietary supplement in ameliorating mitochondrial dysfunction as a strategy of intervention in mouse models of age-related sarcopenia. The results are presented in **Chapter 3**.

A critical point in frailty syndrome is the variety of clinical phenotypes, which poses relevant diagnostic challenges. Establishing reliable diagnostic tools is essential to support the diagnosis, track disease progression over time, and monitor the efficacy of interventions. Fulfilling the gap of the diagnostic approach is of particular importance in terms of prevention. Sarcopenic individuals at risk of physical frailty should be identified before their decline in physical function reaches a critical threshold, beyond which recovery is not possible and extreme risk of adverse health outcomes occur. Though several measurable changes have been described, the current state of the art suggests that no single clinical test will be sufficient to diagnose this complex condition. Research toward a novel diagnostic approach has been advocated to be utilized in clinical and research settings. Thus, the MAYBE program has the purpose of identifying a multidimensional diagnostic approach to frailty syndrome. In this context, my PhD project focused on an upgraded version of an existing broadband time-resolved instrument (time-domain diffuse optical spectroscopy, TD-DOS) designed for non-invasive clinical applications. **Chapter 4** describes this system and the results obtained during two *in-vivo* measurement campaigns to understand the technique's potential use in the abdominal region and thigh muscle of human volunteers. The insights presented in this chapter will aid in designing optimized measurement protocols and data analysis methodology for its application in clinical research settings.

The MAYBE program comprises a clinical trial to examine the combination of lifestyle changes and amino acid-based nutrient supplements to modify frailty-related symptoms in elderly sarcopenic obese patients. **Chapter 5** describes the clinical trial protocol, comprising the sub-study for the possible employment of the TD-DOS instrument to identify frailty-related phenotypes and monitor the response to the experimental therapy.

Finally, a brief conclusion on the whole work of the thesis is reported in **Chapter 6.**

Index

1 Introduction

1.1 On ageing: from physiological decay to frailty syndrome

Defining ageing is one of the most demanding challenges in the current research scenario. It is not easy to attribute ageing to the mere flow of time. Since the causes of ageing are largely unknown, and ageing could be studied from different perspectives, it is usual to find many different definitions, sometimes contrasting[1]. We can consider ageing a natural multifactorial process that implies a gradual decrease in physiological functions, resulting in reduced resistance to stress, high vulnerability to diseases, and increased probability of death. In particular, ageing is characterised by a plethora of changes such as a gradual reduction in bone and muscle mass (resulting in decreased physical performance), longer reaction time and cognitive decline, compromised metabolic activity, changes in the endocrine system, reduced sexual activity, as well as a general decline of auditory, olfactory, renal, pulmonary and immune functions[1]. Although immune functions low down with age (immunosenescence phenomena), a crucial ageing determinant is the presence of a basal chronic inflammatory state corresponding to the rise of the pro-inflammatory cytokines, that is at the basis of various age-related diseases such as neurodegenerative diseases, atherosclerosis, arthrosis[1]. These complex ageing mechanisms are influenced by underlying genetic factors combined with environmental variables and epigenetic mechanisms, which regulate the differential gene expression in cells. Ageing is considered the result of the lifelong accumulation of molecular and cellular damage caused by multiple mechanisms under the regulation of a complex maintenance and repair system. There is uncertainty regarding the precise threshold of cellular damage required to cause impaired organ physiology. Notably, many organ systems exhibit considerable redundancy, which provides the physiological reserve required to compensate for age and disease-related changes[2].

In 2015, 617 million (8.5%) people in the world were aged 65 and over and these numbers are estimated to rise to 1.6 billion by 2050[3]. Longevity steadily increased over the past several decades, owing to changes in economy, society and medical care. In western countries, the proportion of people over age 60 is increasing faster than any other group[4]. However, the longer life and the postponement of death are inevitably linked to increased occurrence of disease and functional deterioration. Thus the promotion of "healthy ageing"

– as opposed to "sick ageing"– is an obvious emerging target in the pursuit of well-being and successful ageing[5]. Life expectancy for women in the EU was, on average, 5.5 years longer than that for men in 2019. Despite the increase in life expectancy, there is no corresponding increase in healthy life expectancy: the number of healthy life years at birth was estimated at 65.1 years for women and 64.2 years for men in the EU, this represented approximately 77.5 % and 81.8 % of the total life expectancy for women and men. Indeed, at just 0.9 years difference in favor of women, the gender gap was considerably smaller in terms of healthy life years than for overall life expectancy. Men, therefore, tend to spend a greater proportion of their somewhat shorter lives free from activity limitations[6].

Among the multiple age-related chronic disorders leading to disability, the frailty syndrome is a significant public health priority. It is defined as a state of vulnerability characterised by decreased reserve and diminished resistance to stressors, with greater functional impairment in women[2][7].The prevalence of frailty increased steadily with age, being 4% between 65-69 years; 7% between 70-74 years; 9% between 75-79 years; 16% between 80-84 years and 26% over 85 years. Most frailty models were developed in Caucasian populations. The prevalence of frailty may be higher in inhabitants, of Southern Europe and older Hispanic and African Americans so different cut-offs for frailty diagnosis may be required in different populations[2].

Frailty is a long-established clinical expression that implies concern over an older person's vulnerability and prognosis, in which an apparently small insult (e.g. a new drug; "minor" infection; or "minor" surgery) results in a dramatic and disproportionate change in health state: from independent to dependent; mobile to immobile; postural stability to falling; lucid to delirious (*Fig. 1*). While a gradual decline in physiological reserve occurs in normal ageing, this decline is accelerated in frailty due to the failure of homeostatic mechanisms. Therefore, a key question is whether there is a critical threshold of age-related, cumulative decline in multiple physiological systems beyond which frailty becomes evident[2].

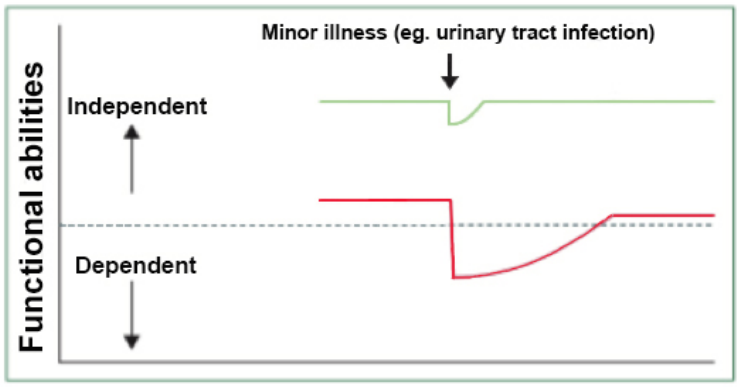

Figure 1. Vulnerability of frail older people to a sudden change in health status after a minor illness

The green line represents a fit elderly individual able to returns to homoeostasis, after a minor stressor event. The red line represents a frail elderly individual unable to return to baseline homoeostasis, after a similar stressor event, manifesting a functional dependency. The horizontal dashed line represents the cut-off between dependency and independency[2].

1.1.1 *Sarcopenia and muscular ageing as a substrate of physical frailty syndrome*

The 'frailty cycle' may be triggered by the separate or joint effects of multiple stressors on the background of ageing, including lack of physical exercise, inadequate nutrition, unhealthy environment, injuries, disease, hormonal alterations, chronic systemic inflammation and polypharmacy. Among these interconnected factors, chronic undernutrition causing loss of bone and skeletal muscle mass, plays a major role in the development of sarcopenia[5].

The physical phenotype of frailty, as described by Fried and co-workers (see below)[8], shows significant overlap with sarcopenia; low grip strength and slow gait speed are characteristic of both conditions. Weight loss, another diagnostic criterion for frailty, is also a major etiologic factor for sarcopenia[9]. Though frailty syndrome is more multifaceted than sarcopenia alone, sarcopenia is currently recognised as a core component of frailty (*Fig. 2*). These definitional ambiguities are also reflected by the absence of reliable biomarkers that could be utilised in clinical and research settings to identify the two conditions, track their progression over time, and monitor their response to interventions[10].

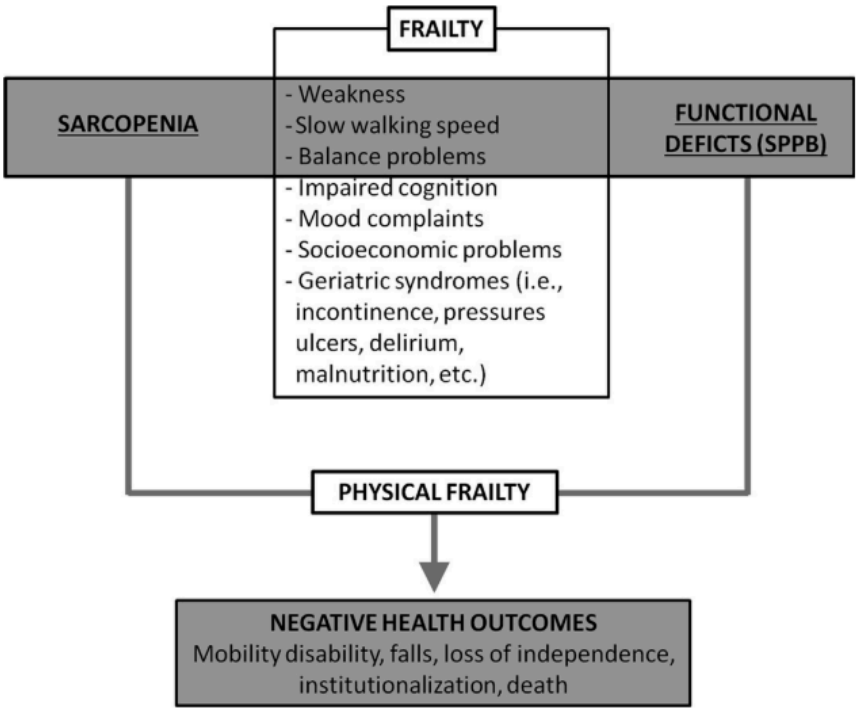

Figure 2. Frailty, physical frailty and sarcopenia interlinks. The grey areas highlight the operationalisation of the 3 components defining physical frailty and the adverse outcomes associated with this condition[11]

The term sarcopenia comes from the Greek words 'Sarx' meaning flesh and 'penia' meaning loss and has been used to describe the age-related decline in muscle mass[12], originally by Rosenberg in 1989. Many authors since[13][14], have used sarcopenia as an all-encompassing term, to describe the accompanying loss of strength and functional capability with age[15]. In 2010, the European Working Group on Sarcopenia in Older People (EWGSOP) published a sarcopenia definition that was widely used worldwide as the presence of both low muscle mass and low muscle function (strength or performance) for the diagnosis of sarcopenia[14][9]. Muscle strength does not depend solely on muscle mass, and the relationship between strength and mass is not linear[14]. Sarcopenia is now formally recognised as a muscle disease with an ICD-10-MC Diagnosis Code that can be used to bill for care in some countries[9]. Its prevalence increases with age and it has been estimated 5-13% in the 60 to 70-year-old population, rising up to 50% in subjects aged 80 or older[5].

In 2019, a second report EWGSOP2 recommended using SARC-F questionnaire to elicit self-reports from patients on signs that are characteristic of sarcopenia. SARC-F can be readily used in community healthcare and other clinical settings[9]. The SARC-F is a 5-item questionnaire, inexpensive and convenient, used method for sarcopenia risk screening[9][16].

Responses are based on the patient's perception of their limitations in strength, walking ability, rising from a chair, stair climbing and experiences with falls. SARC-F has a low-to-moderate sensitivity and a very high specificity to predict low muscle strength. Further, EWGSOP2 newly identifies subcategories of sarcopenia as acute and chronic. Sarcopenia that has lasted less than 6 months is considered an acute condition, while sarcopenia lasting ≥6 months is considered a chronic condition. Acute sarcopenia is usually related to an acute illness or injury, while chronic sarcopenia is likely to be associated with chronic and progressive conditions and increases the risk of mortality[9].

It has been found that total muscle mass and muscle size peak at about the age of 24 years. Similar to strength, muscle mass is well maintained throughout the fifth decade as only a modest (10%) decrease in muscle size occurs between 24 and 50 years of age. Between 50 and 80 years of age an additional reduction of 30% occurs, with an annual 1% decrease in muscle cross-sectional area beyond the fifth decade of life[5]. The ageing-related muscle atrophy is the most common type of muscle atrophy in humans. It is associated with significant impairment of function, such as slowing of movement and muscle weakness. The importance of ageing-related muscle function changes is also associated to socioeconomic factors related to the demographic development with a growing proportion of old individuals due to improved living conditions and health care[17]. Under normal circumstances, muscle homoeostasis is maintained in a delicate balance between new muscle cell formation, hypertrophy and protein loss. This delicate balance is coordinated by the brain, endocrine system and immune system and is influenced by nutritional factors and level of physical activity. The combined declines in the neurological, endocrine and immune functions can destabilise this delicate homeostatic balance and accelerate the transition toward muscle atrophy and physical frailty.[2] Indeed, many ageing-related phenomena are closely related and impact skeletal muscle and sarcopenia, adding complexity when interpreting results[17].

The impaired muscle function observed in elderly individuals is related to both quantitative and qualitative changes in muscle structure and function. *Figure 3* show the principal causes of skeletal muscle disfunction which determine sarcopenia. Skeletal muscle fibres are multinucleated cells, and the size of muscle fibres is related to the number of nuclei present within a fibre. During disuse or injury, muscle fibres lose nuclei. Satellite cells, normally quiescent between the basal lamina and the fibre plasma membrane, following injury or exercise, become activated, migrate to the site of injury, proliferate, and fuse to regenerate the fibre by providing an additional source of nuclei. The density and regenerative capacity

of satellite cells declines in an age-dependent manner[18]. This decline can prolong the time to muscle recovery after eccentric injury (i.e., the gradual accumulation of incompletely repaired contraction-induced microdamage). Overtime this likely contributes to the slow, progressive loss in muscle mass that occurs with sarcopenia[18].

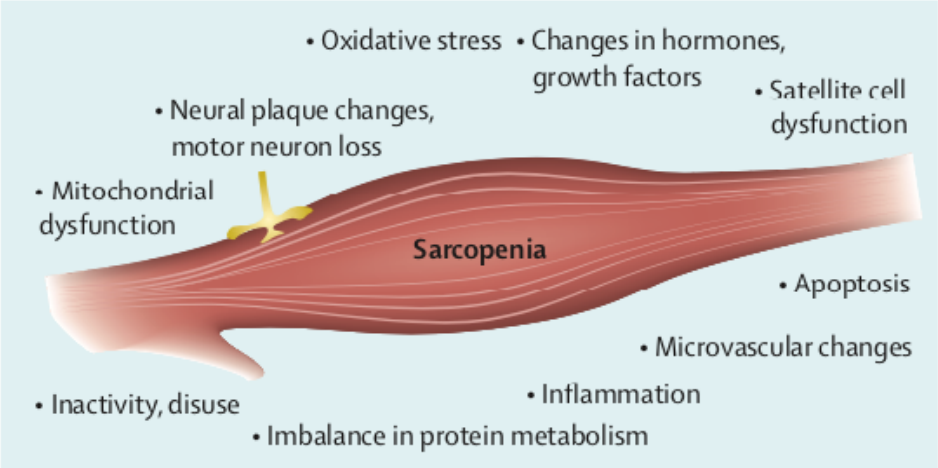

Figure 3. Causes of sarcopenia[19]

Reduced muscle fibre number and size can be partly the consequence of the progressive loss of motor neurons occurring with ageing[17]. Inadequate compensation by muscle fibres reinnervation by the remaining motor neurons, contributes to the progressive decline of muscle function.[17] Further, a fast-to-slow myosin isoform (fibre type) switching with age has been reported in both humans and experimental animal models. This transition may contribute to the slowing of movement as well as decline in maximum force because of the high force generation capacity of fast muscle fibres compared to slow fibres. However, the relative changes in fibre type proportions or myosin isoform expression in ageing human muscle are relatively small. It may be questioned whether these changes will have a major impact on overall motor performance[17].

An adequate blood supply is critically relevant to maintain muscle size and function, as suggested by the ensuing atrophy during prolonged ischemia and a by the onset of muscle fatigue during a series of intermittent isometric contractions in ischemic conditions[17]. Since capillary rarefaction or hypoperfusion may play a causal role in muscle atrophy, their possible contribution to ageing-related sarcopenia deserve to be investigated. In fact, an adequate microvascular network is not only required for oxygen supply and removal of heat and metabolites, but also for the delivery of nutrients and (anabolic) hormones[17].

Computed tomography studies demonstrate that loss of muscle mass is accompanied by replacement of contractile material with fat and connective tissue in elderly humans. As a result, non-contractile mass can account for 15% of total muscle cross-sectional area, about 2.5 fold greater than in young subjects[20][15]. These changes are associated with an increase in inter and intramuscular adipocyte content[21] that is thought to directly impair cross-bridge kinetics[22].

1.1.2 *Ageing and obesity: the relationship with sarcopenia*

Profound changes in body composition with increased body fat mass and decreased muscle mass have been reported in association with advancing age[17]. Global mean body mass index (BMI, calculated as the weight in kilograms divided by the square of the height in meters) had increased at an annualised rate of 0.4 kg/m2/ decade for men and 0.5 kg/m2/decade for women[23]. However, the recent coining of obesity as "adiposity-based chronic disease" (ABCD) recognises this complexity and the limits of BMI as the parameter to define obesity and its grading[24], especially in older people.[25]

From a physiological point of view, fat mass and its distribution mainly depend on age, gender, and ethnic differences. Total fat content, corresponding to the whole-body weight, declines after birth until young age, then gradually increases along adulthood. In particular, abdominal fat progressively increases with age, more in men and in post-menopausal women, often accompanied by chronic low-grade inflammatory processes. Fat accumulation can also occur without overt weight changes in the elderly, due to the concomitant reduction of lean mass. From a pathological perspective, obesity – often simplistically defined as an excess of fat mass – is a complex chronic disease characterised by changes in total adipose amount, distribution and function, as well as by adipocyte death and low-grade chronic inflammation.[25] In particular, visceral white adipose tissue (WAT) undergoes inflammation (metaflammation) in obese individuals and is closely involved in the onset of some of the more severe medical complications of obesity[26]. Subclinical inflammation induced by obesity may contribute to the development of sarcopenia[27]. Both ageing and inflammation may influence adipose tissue differentiation[28][29]. Inflammation decreases the lipid storage capacity of adipose tissue by inhibiting preadipocyte differentiation and increasing lipolysis. This supports the importance of adipose tissue's fat storage capacity, influenced by inflammation, to prevent ectopic fat deposition[30][31][32]. Moreover, it is known that the ability of preadipocytes to replicate and differentiate declines with ageing[33].

Obesity exacerbates the age-related decline in physical function and contributes to frailty[5]. Indeed, obesity is increasingly being interpreted as a state of premature ageing[34]. It has been stated that "the most common frailty phenotype in the future may be an obese, disabled, older adult", affected by the so-called sarcopenic or dynapenic obesity[35]. In this scenario, the hypothesis is emerging that lean mass loss, together with muscle fat accumulation and metabolic derangement, with or without obesity, are at the core of the functional defects of the elderly frail population[5].

Sarcopenic-obese subjects are more likely to have insulin resistance and the metabolic syndrome, both increasing cardiovascular disease risk. For instance, in men, the prevalence of metabolic syndrome is 60.9% in sarcopenic-obese, but only 29.2% in sarcopenic-non-obese subjects; 48.6% in obese non-sarcopenic, but just 11.6% in non-sarcopenic non-obese phenotype, with similar trends seen in women. This suggests that in the induction of the metabolic syndrome, there is an additive effect of sarcopenia and obesity[36].

Ageing is also associated with a progressive loss of subcutaneous fat, accumulation of visceral fat, and ectopic fat deposition[33] (*Fig. 4*). Ectopic fat infiltration is associated with lipid deposition outside the adipose tissue into muscle, liver, heart and bone, in which its presence contributes to organ dysfunction. There is evidence that ectopic fat in muscle, in the form of intramuscular adipose tissue (IMAT) may not be an inert fat depot: in young (~20 years) healthy individuals subjected to 30 days of leg disuse by suspension, IMAT increased (15%–20%) and exceeded the loss of lean calf and thigh muscles[37]. This suggests that IMAT does not just "fill" the space left by lean mass loss but may negatively affect muscle function. In elderly obese or type 2 diabetic people, elevated levels of IMAT are associated with both insulin resistance[38] and reduced muscle strength[39][38]. The cause of this improper ectopic lipid deposition in skeletal muscle (and the liver) is an imbalance between energy intake and energy expenditure, resulting in spill-over of energy storage from adipose tissue to the liver and skeletal muscle[29]. Such cascade is indirectly supported by the presence in obese individuals of enlarged, lipid overloaded adipocytes, which are presumably unable to accumulate additional fat. However, this "spill-over" hypothesis cannot explain why some non-obese patients suffering from metabolic disorders could also be accompanied by ectopic lipid accumulation[5].

Figure 4. Age-related changes in fat distribution in human body.
This figure shows the changes in muscle and fat mass over time and the changes in fat storage. Yellow cells represent subcutaneous fat, red cells represent visceral fat, and yellow cells within muscle represent ectopic fat depots. Muscle mass decreases through the years, whereas fat mass (visceral and subcutaneous) increases until midlife. Elderly age is associated with decreased subcutaneous fat (parallel to the loss of lean body mass) and the emergence of ectopic fat, mainly in skeletal muscles[5].

Muscle mass loss and fat accumulation in the muscle in the elderly, with or without the presence of obesity, may explain some of the functional and metabolic defects shown in the frail, sarcopenic population. Fat mass and muscle mass are interconnected via many pathways. Loss of muscle mass induces a 2%–3% decline in basal metabolic rate per decade after the age of 20 years, and a 4% decline per decade after the age of 50 years. This may lead to an increased risk of weight gain, with lower physical activity performed in the background[5].

1.1.3 *Role of mitochondrial homoeostasis in ageing*

Mitochondria are important cell organelles involved in a plethora of different functions, from energy production and fatty acid oxidation to regulating cell cycle and cell death[40]. They have a central role in metabolism as key actors in energy (ATP) production via oxidative phosphorylation (OXPHOS). In the matrix, tricarboxylic acid cycle (TCA) enzymes generate electron carriers (NADH and FADH2), which donate electrons to the inner membrane-localised electron transport chain (ETC). The ETC consists of four protein machines (I–IV), which undergo conformational changes to pump protons from the matrix into the intermembrane space through sequential redox reactions. The first and largest respiratory complex, complex I, is a sophisticated microscale pump consisting of 45 core subunits. The proton gradient generated by complexes I, III, and IV is released through the rotary turbine-like ATP synthase machine or complex V, which drives phosphorylation of ADP to ATP.

An increased need for ATP is met by increasing mitochondrial mass and inducing OXPHOS. For example, an increase of mitochondrial mass and activity is observed after endurance exercise[41]. The regulation of mitochondrial biogenesis is tightly coordinated with pathways that induce vascularisation, enhance oxygen delivery to tissues, and enable oxygen supply to facilitate efficient mitochondrial oxidisation of glucose and fat[42].[43]

The main regulator of this complex chain of events is the transcriptional activator proliferator-activated receptor γ coactivator 1α (PGC-1α). The activity of the transcription factor PGC-1α is induced by SIRT1-mediated deacetylation and by AMPK-mediated phosphorylation in response to changes in nutritional elements or energy depletion. AMPK also acts as a link between PGC-1α and mTORC1 (mechanistic target of rapamycin complex 1), a key element in the regulation of protein synthesis and cell growth in response to nutrients. Through the inhibition of TORC1, AMPK can promote the clearance of defective mitochondria by stimulating autophagy. Further, as reported by Nisoli et al., the complex processes of mitochondrial biogenesis are induced by nitric oxide (NO), a gaseous mediator produced by the enzyme endothelial nitric oxide synthetase (eNOS)[44]. Further work highlighted the role of the eNOS-NO-SIRT1-PGC-1α signalling pathway in the regulation of mitochondrial homoeostasis during caloric restriction[45] or specific nutritional interventions [46][47]. This pathway, involving the activation of signals consisting of NO, AMPK, SIRT1 and mTORC1, is complex and not yet fully understood[48].

Complexes I and III also generate reactive oxygen species (ROS), including oxygen radicals and hydrogen peroxide, capable of damageing key cell components, including lipids, nucleic acids, and proteins[49][50]. ROS has been suggested to contribute to diseases associated with mitochondrial dysfunction, including neurodegeneration. Multiple evidence also indicates that low levels of mitochondrial ROS influences homeostatic signalling pathways contribute to adaptive stress signalling pathways, such as hypoxia[34].

One of the most successful theories to explain the ageing process has been the so-called "oxidative stress theory" initially proposed by Harman[51]. Since the production of the great majority ROS species occurs as a side-effect of the mitochondrial respiratory metabolism, this theory has been subsequently modified as the "mitochondrial theory of ageing", indicating mitochondria as a leading cause of organism ageing. Indeed, substantial deterioration of mitochondria occurs with age from ultrastructural, bioenergetic, biochemical and genetic points of view (*Fig. 5*). It has been shown that mitochondria of cells from old

animals decrease in number, accumulate vacuoles, cristae abnormalities and paracrystalline inclusions[52]. Mitochondrial respiratory chain enzyme activities and ATP production decrease[53]. In addition, the amount of oxidative damage to proteins and mitochondrial DNA (mtDNA) increases, with an associated accumulation of mtDNA mutations[54]. Nevertheless, in recent years the hypothesis that ROS are the leading cause of ageing has been put under discussion by studies in animal models and in humans. Strikingly, a number of clinical trials with antioxidants (including β-carotene, vitamin A and vitamin E) reported an increase in mortality rather than a decrease[54]. Hence, the importance of ROS as physiological effectors in redox-sensitive signalling pathways, rather than pathological agents, has progressively increased[54].

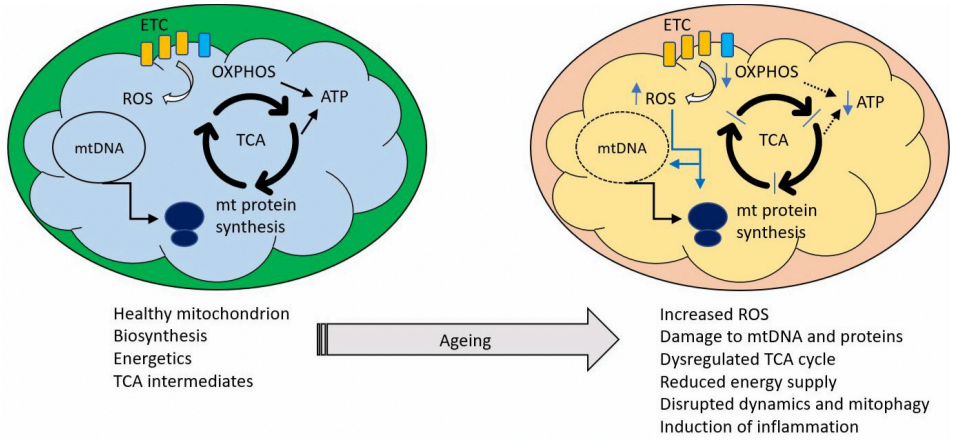

Figure 5. Age-related mitochondrial derangements.
Healthy mitochondria perform a variety of functions, including ATP production and synthesis of metabolites required for cell maintenance. Black arrows indicate major processes; blue arrows indicate changes occurring during ageing[55].

Mitochondria are organised in dynamic networks, undergoing cycles of fission and fusion mediated by a dedicated set of dynamin-related GTPases. Mitochondrial fusion is an essential cellular process that helps to merge fragments of mitochondria, mediating the exchange of mtDNA, proteins, and metabolites[56]. It involves the fusion of the outer and the inner mitochondrial membranes. Fusion of the inner mitochondrial membrane is mediated by the GTPase protein called OPA1. OPA1 is proteolytically cleaved into different fragments. Long forms determine fusion; long or short forms alone build cristae, whereas long and short forms together tune mitochondrial morphology[57]. Mitochondria can also break their network down into smaller fragments in the fission process, which is required for removing

damaged parts of mitochondria, which get eventually cleared by mitophagy. Mitochondrial fission also has a critical role in replicating mitochondria during the cell cycle[40].

Of central importance in the pathophysiology of muscular ageing is the loss of mitochondrial function. The correct functioning of the mitochondrial system is entrusted to "quality control" systems that provide for a balanced synergy between the processes of mitochondrial biogenesis (formation of new functionally active organelles) and mitophagy (demolition of damaged organelles). The mitochondrial biogenesis process includes mtDNA replication mechanisms and mitochondrial protein synthesis, as well as mitochondrial dynamics with phenomena of fusion and fission of the organelles themselves. These mechanisms contribute to the function of the mitochondria in different conditions. PGC-1α levels are reduced at both the mRNA and protein level muscles of elderly subjects, and the decreased mitochondrial biogenesis and mitochondrial protein expression probably contribute to the reductions in mitochondrial volume[58]. As previously mentioned, the mitochondrial dysfunction characterising the ageing processes, in addition to the energy imbalance with reduced ATP production and increased AMP/ATP ratio, causes a huge increase in ROS production, with free radical-associated damage. Of note, persisting oxidative stress renders eNOS uncoupled (i.e., O2 reduction is uncoupled from NO synthesis), such that the enzyme no longer produces the protective gaseous messenger NO, but superoxide[34]. In addition, the inhibition of mTORC1 itself, resulting from the reduced expression of PGC-1α, negatively affects mitochondrial biogenesis and the functionality of the mitochondria, as suggested above. The reduced activation of mTORC1 determines a reduction in protein synthesis, as well as in lipids and nucleotides. In conditions of cellular senescence and, more generally, of ageing (particularly in the myocytes of elderly sarcopenic and fragile patients) the processes of autophagy, normally responsible - as seen - for the elimination of dysfunctional and ROS-generating organelles, are deficient (*Fig. 6*)[59]. The accumulation of damaged mitochondria in this context of compromised mitophagy promotes the extracytoplasmatic release of multiple substances (N-formyl peptides, cardiolipins) and mtDNA fragments, as well as residues of damaged organelles, which stimulate inflammation. Circulating levels of mtDNA progressively increase with age and correlate with the amount of pro-inflammatory cytokines, such as IL-6 and TNF-α, usually present both in plasma and in various metabolically active tissues, such as muscle, of elderly subjects[59].

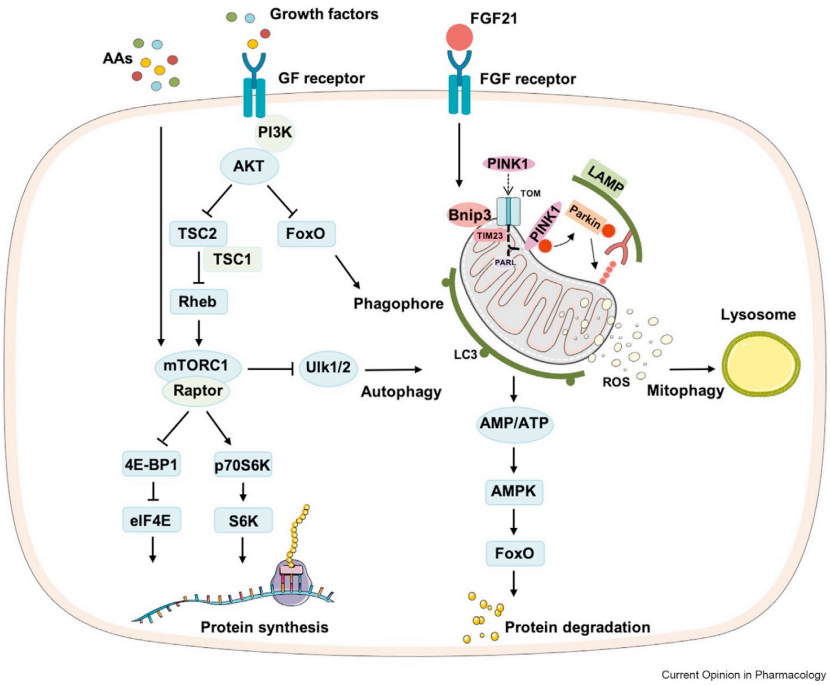

Figure 6. Mammalian target of rapamycin (mTOR) and the autophagy-lysosomal system in muscle protein synthesis and degradation. Growth factors indirectly activate mTOR complex 1 (mTORC1), which is also directly triggered by amino acid availability. mTORC1 activation promotes muscle protein synthesis and inhibits autophagy. Fibroblast growth factor 21 (FGF21) stimulates the expression of Bnip3, which favor the mitophagic degradation of depolarised mitochondria and their delivery to lysosomes for disposal.[59]

Gene expression studies have shown that the mitochondrial deficit in ageing processes is tissue-specific and particularly relevant in tissues strongly dependent on oxidative metabolism, such as brain, heart and skeletal muscle. Having a post-mitotic nature, myocytes and neurons, the homoeostasis of these cells depends solely on the "quality control" systems of the mitochondria. For this reason, the impairment of the mitochondrial renewal system in the skeletal muscle, with a bioenergetic deficit, oxidative stress and damage to mtDNA, leads to the loss of muscle fibres and the development of sarcopenia and fragility[48].

1.2 Frailty Syndrome: the gap to fill from the definition to the diagnosis

There is to date no clear consensus regarding the definition and diagnostic criteria of frailty. The two main models of frailty are the so called “phenotype model” and the “cumulative deficit model”. The **phenotype model** is based on the landmark study by Fried and colleagues[8] who focused on evaluating five domains (nutritional status, energy, physical activity, mobility, and strength). The authors undertook a secondary analysis of data obtained

from the Cardiovascular Health Study (CHS), a prospective cohort study involving 5,210 men and women aged 65 years and older. A frailty phenotype was operationalised using a cluster of variables: unintentional weight loss, self-reported exhaustion, low energy expenditure, slow gait speed, weak grip strength. The lowest quintile values were used to define absence/presence of these variables. People with three of the five factors were considered frail, one or two factors as pre-frail, and no factors as fit older people. This work is important as it suggests a frailty phenotype can be defined and might be a basis to detect frailty in routine care. However, it is not clear how the variables might reliably be translated into clinical practice[60].

The **cumulative deficit model**, based on the Frailty Index (FI) proposed by Rockwood and colleagues, was developed as part of the Canadian Study of Health and Ageing (CSHA)[61]; a five years prospective cohort study on 10,263 participants designed to investigate the epidemiology and burdens of dementia in older people in Canada (mean age: 82 years). Ninety-two baseline parameters of symptoms (e.g. low mood), signs (e.g. tremor) and abnormal laboratory values, disease states and disabilities, collectively referred to as deficits, were used to define frailty. The FI was a simple calculation of the presence or absence of each variable as a proportion of the total (e.g. 20 deficits present out of a possible 92 gives a FI of 20/92 = 0.22). In this way, frailty is defined as the cumulative effect of individual deficits. This is attractive clinically because it allows making frailty quantifiable rather than present/absent. Importantly, a value of 0.67 appears to identify a level of frailty beyond which further deficit accumulation is not sustainable, and death is likely to supervene.[2] Subsequent work by the same group has demonstrated that the initial list of 92 variables can be reduced to a more manageable 30 or so without loss of predictive validity[62]. Several studies demonstrated that the FI is strongly related to the risk of death and institutionalisation. The phenotype and cumulative deficit models demonstrate overlap in the identification of frailty and considerable statistical convergence[2].

Among the tools for frailty identification are questionnaires such as the *Frail Elderly Functional Questionnaire* (19 items). It is identified as a potential outcome measure for frailty intervention studies, as it is suitable for use by telephone or proxy, valid and reliable[63]. Further, it is worth mentioning The *Groningen Frailty Indicator*[64] and the *Tilburg Frailty Indicator*[65] that are simple and similar[66] questionnaire-based approaches to detecting people with frailty. Aspects of validity have been investigated, but importantly, studies of diagnostic accuracy against well-defined community populations of older people are not yet available[2]. The

Edmonton Frail Scale is a multidimensional assessment method. It is quick to administer (less than 5 minutes) and is valid, reliable and feasible for routine use, but the diagnostic accuracy has not been investigated[2].

Comprehensive geriatric assessment (CGA) has become an internationally established tool to assess older people in clinical practice. It is a multidisciplinary diagnostic process to determine the medical, psychological and functional capability of an older person, to develop a plan for his treatment and follow up[2].

1.2.1 Measuring sarcopenia

It is possible to measure sarcopenia in its determinant parameters such as muscle strength, quantity, quality and function. Parameters and measuring methods are extensively described in the original EWGSOP2 article[9].

Muscle strength measure (i.e., *grip strength*) is simple and inexpensive. Low grip strength is a powerful predictor of poor patient outcomes such as longer hospital stays, increased functional limitations, poor health-related quality of life and death. Accurate measurement of grip strength requires the use of a calibrated *handheld dynamometer* under well-defined test conditions with interpretive data from appropriate reference populations. Grip strength correlates moderately with strength in the whole body, so it serves as a reliable surrogate for more complicated arm and leg strength measures. The *chair stand test* (also called chair rise test) can be used to assess the strength of leg muscles (quadriceps muscle group). The chair stand test measures the amount of time needed for a patient to rise five times from a seated position without using arms. Alternatively, the timed chair stand test is a variation that counts how many times a patient can rise and sit in the chair over a 30-second interval[9].

Muscle quantity or mass can be estimated by a variety of techniques, and there are multiple methods of adjusting the result for height or for BMI. *Anthropometry* reflects nutritional status in older adults, but it is not a good measure of muscle mass, especially in this category of subjects. *Calf circumference* has been shown to predict performance and survival in older people and may be used as a diagnostic parameter for older adults in settings where no other muscle mass diagnostic tools are available[9]. Muscle quantity can be reported as total body skeletal muscle mass, as appendicular skeletal muscle mass (the sum of the muscle mass of the 4 limbs), or as muscle CSA of specific muscle groups or body locations. *Magnetic resonance imageing (MRI)* and *computed tomography (CT)* are considered gold standards for non-invasive

assessment of muscle quantity/mass. However, MRI and CT are expensive and technically difficult to manage. Moreover, cut-off points for low muscle mass are not yet well defined for these methods. *Dual energy X-ray absorptiometry (DXA)* is a more widely available instrument to determine muscle quantity. The technique provides an objective and sufficiently reliable measure of muscle or fat-free mass, of which muscles comprise the majority. Unfortunately, such imaging tools lack portability and are not immediately available in primary care (e.g. the general practitioner's office), which represents the first diagnostic step for most sarcopenic elderly. These techniques also provide different estimates of the body composition profile in terms of explored anatomical regions, applied methods and units, and accuracy in defining thresholds of risk, making difficult (if not impossible) direct comparisons across their results[10]. *Bioelectrical impedance analysis (BIA)* has been explored for estimation of total or appendicular muscle mass. BIA equipment does not measure muscle mass directly, but instead derives an estimation based on whole-body electrical conductivity. BIA equipment is affordable, widely available and portable. However, the estimation of muscle mass differs when different instrument brands are used. In addition, BIA measurements can also be influenced by the hydration status of the patient. For their affordability and portability, BIA-based determinations of muscle mass are widely used; however, it is necessary to validate prediction equations[9].

Muscle quality is a relatively new term, referring both to micro- and macroscopic changes in muscle architecture and composition and to muscle function delivered per unit of muscle mass. MRI and CT have been used to assess muscle quality in research settings, e.g. by determining infiltration of fat into muscle. Alternatively, the term muscle quality has been applied to ratios of muscle strength to appendicular muscle mass or muscle volume. As yet, there is no universal consensus on assessment methods for routine clinical practice in estimating muscle quality[9]. *Ultrasound* is a widely used research technique for the evaluation of muscle condition[9]. It is reliable and valid, even in older subjects, and is starting to be used at the bedside by trained clinicians. Ultrasound was shown to have good validity to estimate muscle mass as compared to DXA, MRI and CT. The use of ultrasound has recently been expanded in clinical practice to support the diagnosis of sarcopenia in older adults. Echogenicity reflects muscle quality, since non-contractile tissue associated with myosteatosis shows hyper-echogenicity[67]. Thus, ultrasound has the advantage of being able to assess both muscle quantity and quality[9].

Muscle function or **Physical performance** has been defined as an objectively measured whole-body function related to locomotion. This is a multidimensional concept that not only involves muscles but also central and peripheral nervous function, including balance.[9] Physical performance can be variously measured by *Gait speed*, a quick, safe and highly reliable test widely used in clinical practice. It can predict adverse outcomes related to sarcopenia (disability, cognitive impairment, need for institutionalisation, falls and mortality). A commonly used gait speed test is called the *4-m usual walking speed test* (a cut-off speed ≤0.8 m/s indicates severe sarcopenia). The *Short Physical Performance Battery* (SPPB) is a composite test that includes assessment of gait speed, a balance test, and a chair stand test. The *Timed-Up and Go (TUG) test* evaluates physical function. Individuals are asked to rise from a standard chair, walk to a marker 3 m away, turn around, walk back and sit down again. Each of these physical performance tests can be performed in most clinical settings. Since it takes at least 10 min to administer, SPPB it is more often used in research[9].

Quality of life in sarcopenic patients can be evaluated by the *SarQoL questionnaire*[68]. SarQoL assists the healthcare provider in assessing a patient's perception of his or her physical, psychological and social aspects of health. The SarQoL tool has been validated, and it can be used in both clinical care and research studies[68][9].

The EWGSOP2 updated algorithm can be applied in clinical setting for sarcopenia case-finding, diagnosis and severity determination. A pathway of Find-Assess-Confirm-Severity (F-A-C-S) is recommended for use across clinical practices and in research studies (*Fig.7*).

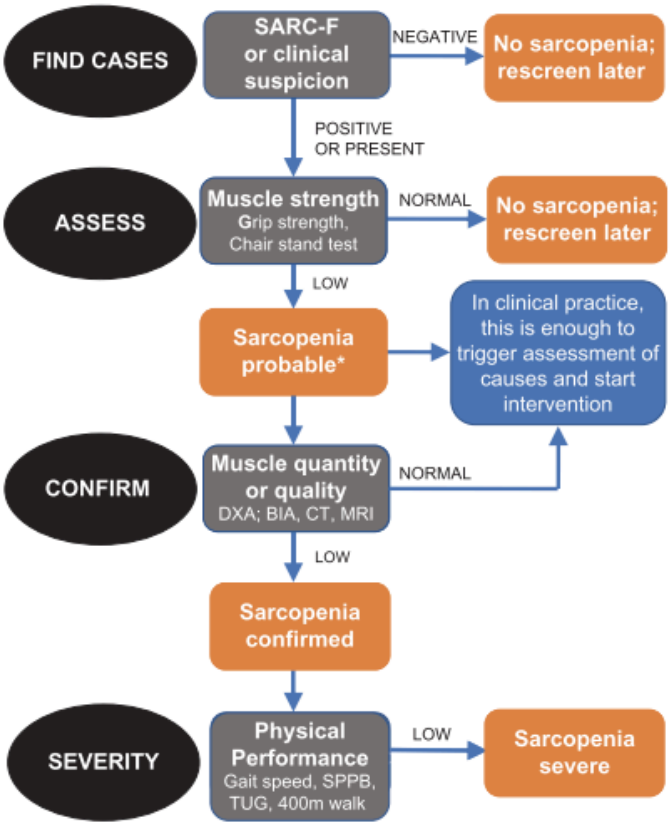

Figure 7. EWGSOP2 algorithm for case-finding, making a diagnosis and quantifying the severity of sarcopenia in practice. The steps of the pathway are represented as Find-Assess-Confirm- Severity or F-A-C-S.[9]

1.2.2 Physical frailty and sarcopenia biomarkers

While the combined assessment of muscle mass and function is an essential requirement for the identification of sarcopenia, a major challenge resides in defining the threshold of pathological muscle ageing resulting in physical frailty. The development and validation of a single biological marker might be an easy and cost-effective way to guide the diagnosis and facilitate the monitoring of sarcopenia, marking a substantial step forward in this field.[10] However, because of the complex pathophysiology of physical frailty, it is unlikely that a single biomarker will be able to identify the condition in a heterogeneous population.[9]·[10]

A panel of complementary and multidimensional biomarkers (likely within multiple classes: imageing, circulating biomolecules, and functional tests) should be proposed. This approach may promote (i) the early detection of otherwise subclinical conditions; (ii) the diagnostic assessment of clinically manifest physical frailty; (iii) the risk stratification of subjects with a suspected or confirmed diagnosis; (iv) the tracking of the conditions over time; (v) the

selection of an appropriate therapeutic intervention; and (vi) the monitoring of the response to treatment.[10] A multivariate strategy has been proposed for the development of a panel of biomarkers. This approach could aid in the early identification of sarcopenia and physical frailty to activate primary prevention strategies.[10]

1.2.3 What role does diffuse optical imaging (DOS) play in this context?

To date, reliable clinical tools for the diagnosis and the follow-up of the frailty syndrome are to be established yet[10]. Research toward a novel approach would possibly play a pivotal role in the early detection of frailty, leading to prompt intervention and avoiding or delaying the decline of physical function, and in monitoring the effects of therapeutic interventions. The ability to monitor *in-vivo* the human muscle and adipose tissue is of great practical use and hence of growing interest in the fields of clinical diagnostics and preventive medicine.

Biological tissues are considerable diffusive media in the near-infrared (NIR) spectral region, with absorbing agents or chromophores and scattering centers. Consequentially, when light interacts with tissue, its constituents and microscopic structure are responsible for two main phenomena, namely *absorption* and *scattering*.

NIR is used in a diagnostic contest because the attenuation in this range of wavelengths is sufficiently low to permits the penetration of light in tissue. When light interacts with diffusive media can be considered as photons, which are quantized particles, colliding elastically with the scattering centers and being absorbed by the chromophores. Quantification of these phenomena is then obtained from the probability of the occurrence of an absorption or scattering event. These quantities are defined as the absorption μa and scattering coefficients μs, respectively. In a medium with sufficiently high number of scattering centers, the photons undergo to scattering events as well as absorption. A medium is considered diffusive when is characterised by a considerably higher number of scattering events than absorption events. The scattering centers in diffusive media tend to divert the photons in random directions. At a microscopic level, the major contribution to scattering phenomena is given by cellular membranes, organelles and nuclei. These microscopic tissue features results in the diffusion of light at macroscopic level[69].

Biological tissue is strongly scattering in the visible and near infra-red (NIR) wavelength regions. Therefore, to study biological tissues, it is resorted the radiation in the wavelength range between 600-1100nm, which permits a better penetration into the tissue[70]. This low

attenuation, corresponding to high penetration of light in tissue, is consistent to the fact that the absorption in this spectral region is very low. Tissue chromophores concentrations can be retrieved from broadband or multi-wavelength measurements.

The key chromophores contributing to the absorption in biological tissue in the already mentioned wavelength region are: water, lipid, collagen, oxy and de-oxy hemoglobin (*Fig. 8*)[69]. Concerning the absorption spectrum, the key features are the absorption tail of haemoglobin – mainly Hb – in the region below 700 nm, the peak of Hb overlapped to a small water shoulder around 760 and 740 nm respectively, the clear peak of lipid at 930 nm with a second minor one at 1020 nm, the water contribution around 980 nm followed by the collagen peak around 1030 nm (*Fig. 8*). The concentration of these chromophores has been evaluable in different biomedical settings. For instance, concentrations of oxy and de-oxy haemoglobin can be studied to monitor the activation of brain regions[71]. Furthermore, the amount of collagen, lipid and water present in the breast was found to be related to the risk of breast cancer[72][73][74]. Similarly, diffusive optics was applied in thyroid cancer detection[75].

Information on the morphology and structure of the biological tissue can be obtained from the scattering coefficient and the scattering spectra can be described by this empirical law:

$$\mu_s = a\left(\frac{\lambda}{\lambda_0}\right)^b$$

With the Mie theory, the coefficients a and b can be linked to the density and effective radius of the scattering centers modeled (approximated) as independent spheres[76]. When this assumption is too far from the experimental situation, numerical simulations are necessary[69].

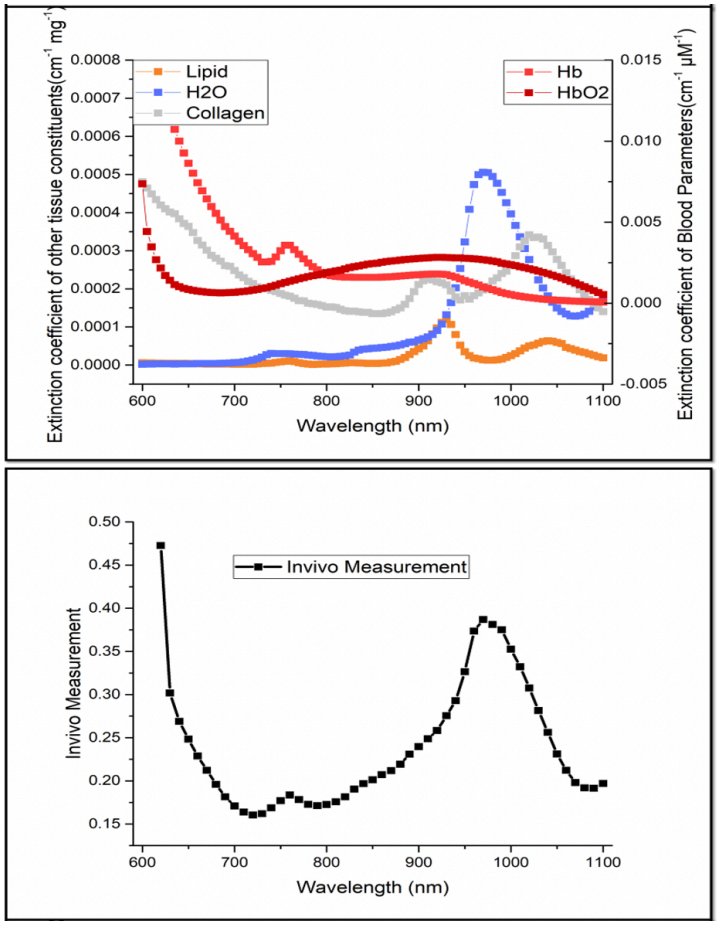

Figure 8. (above) Extinction Coefficients of some of the key biological tissues chromophores in the wavelength range between 600-1100 nm. (below) Example of absorption coefficient spectra of the biological tissue (in this case human forehead)[69].

Optical techniques such as diffuse optical spectroscopy (DOS) described above can non-invasively provide information on tissue composition, structure and physiology (blood parameters) and could be of great interest in the clinical scenario for the early diagnosis of sarcopenia/physical frailty syndrome, the tracking of its clinical course over time, and the monitoring of the response to treatment.

Different experimental approaches to diffuse optics are employed for the retrieval of the optical properties of diffusive media. The classification is based on the spatial distribution and temporal characteristics of the source and the detection strategies used. Time-domain (TD) or time-resolved modality injects picosecond pulses into the tissue or diffusive medium. An attenuation and broadening from picosecond to nanosecond pulse occurs in the tissue as a result of the scattering and absorption phenomena. The scattering properties concern with the photons have travelled a relatively short path length and thus have a lower

probability of being absorbed by the tissue. Differently absorption events occur within the tissue and concern with longer path length of the photons[69]. Thus, a single TD measurement with a proper analysis allows for an estimation of both optical properties[77]. Performing measurements at more wavelengths then allows the estimate of tissue composition.

Instruments based on TD approach are characterised by sources providing pulsed light and detector with high temporal resolution (sub nanosecond). These detectors should also have high sensitivity and should be able to detect single photon events[69]. In conclusion, is important to highlight that tools of this type in the past years were difficult to obtain or, in any case, very complex and expensive. Nowadays, it is possible to produce instruments suitable for clinical use and relatively easy to manage and low cost.

1.3 Interventions strategy to counteract physical frailty and sarcopenia: a call to action

A variety of strategies that alleviate age-related deficits in mitochondrial biogenesis and activity, including calorie restriction (CR) and moderate physical exercise, promote survival in mammals. These interventions increase the expression of PGC-1a and SIRT1, thus reducing oxidative damage in metabolically active tissues of mice and humans[78][45] [79].[46] As mentioned before, mitochondrial biogenesis, dynamics, and clearance of damaged mitochondria by mitophagy cooperate to assure efficient energy production. Nitric oxide (NO), a short-living signal molecule produced by endothelial NO synthase (eNOS), induce the expression of the master regulator of PGC-1a, promoting mitochondrial respiration in various tissues[44]. As superbly reviewed by Farah et al.[80], physiological levels of NO favor angiogenesis, blood flow, as well as brown adipocyte differentiation and "browning" of white adipose tissue (WAT). Interestingly, within a finely tuned cellular range, eNOS-mediated NO production activates mithormesis, an adaptive stress resistance program contrasting age-related chronic diseases and prolonging healthspan[34]. Significantly, the eNOS-PGC-1a-mediated mitochondrial renewal mechanisms are at the basis of the beneficial effects of CR[45], exercise[81], and BCAA supplementation[46][82] (*Fig. 9*).

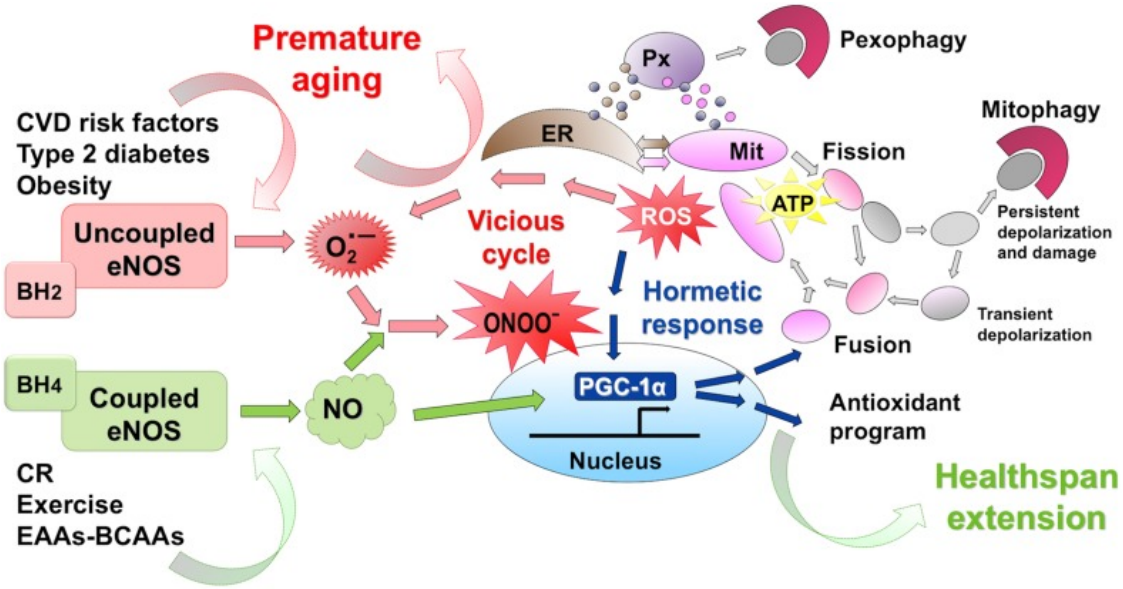

Figure 9. eNOS activation promotes mithormesis and healthspan extension. Unhealthy lifestyles and cardiovascular risk factors uncouple eNOS and increase ROS production of powerful oxidants that initiates a vitious cell-damageing cycle favoring chronic age-related diseases. Calorie restriction (CR), exercise and dietary supplementation with balanced EAA-BCAA formula enhance eNOS expression and production of low-levels NO and ROS. The eNOS-NO-PGC1α pathway boosts mitochondrial renewal, with efficient energy production, and activates the endogenous antioxidant response, favoring healthspan extension.[48]

1.3.1. Physical exercise: the gold standard "therapy" to counteract sarcopenia

The lower levels of physical activity and increased sedentary behaviour in old age is considered a major cause of the ageing-related loss of muscle mass and strength. The negative effect of inactivity on protein synthesis may add to the ageing-related decline in skeletal muscle contractile capacity, making the elderly more vulnerable to a period of immobilisation. Given these observations, it is not surprising that significant attention has been paid to the potential of exercise to improve the quality of life and independence. Muscle hypertrophy, per se, is only valuable if it also leads to improvement in the ability to perform daily life activities, in terms of improving gait velocity, stair-climbing power, and spontaneous activity levels in elderly subjects.[17]

Accordingly to the observation that mitochondrial dysfunction precedes sarcopenia[83], the beneficial effects of physical activity impinge on the mitochondrial quality control system and mitochondrial energetics in older adults[84]. Metabolic remodelling of skeletal muscle to exercise training is the consequence of a coordinated genetic response that boosts PGC-1α-dependent mitochondrial biogenesis, increases the size and number of mitochondria, and

induces the GLUT4 (insulin-sensitive) isoform of the glucose transporters[85]. Current evidence suggests that exercise remains the most potent behavioural therapeutic approach for improving mitochondrial health both in muscles and in other tissues[58]. Even though somewhat attenuated compared with young adults, regular exercise has significant benefits for muscle strength and endurance in old age. Of note, different exercise modalities do not impinge on the same molecular patterns, and therefore, they slightly diverge in terms of functional effects in older people. Interestingly, only aerobic exercise induces the biggest changes of gene expression regardless of age, whereas both aerobic and resistance training enhance proteins involved in the translational machinery irrespective of age[17]. Various reports suggest that exercise in frail individuals may be useful to increase functional performance, walking speed, chair stand, stair climbing, and balance[86]. Consequently, investigating exercise modalities that are both capable of inducing robust mitochondrial adaptations and convenient is useful in fostering more widespread adherence to exercise programs in older individuals[58]. Interestingly, exercise and nutrients partially affect the same signalling pathways. Thus, it would be useful to investigate their interaction to potentiate each other because of their synergistic action[34].

1.3.2. Calorie restriction: benefits and limits

Chronic CR, the reduced caloric intake without malnutrition, acting as a low-energy stress condition, is considered the gold standard intervention to extend lifespan in most species, and its effects seem to be sex-independent. CR is challenging in the long-term, mainly in older people, and various fasting-mimicking diets are under examination to promote health benefits while minimising the burden of chronic restriction.[82]

CR reduces ROS production and induces a shift from glucose to fatty acid metabolism and reduces insulin growth factor I (IGF-I) and insulin. As IGF-I is important for muscle growth, one may expect that a CR-induced reduction in IGF-I has a negative impact on muscle strength, but no such effect was seen in caloric restricted mice.[17] CR–reduced DNA damage in progeroid mice with deficiencies in DNA-repair genes, preserving their motor neurons and full motor function[87].

There are some potential pitfalls in applying CR to humans, such as lowered blood pressure, slower wound healing, risk of osteoporosis, and increased danger of malnutrition, especially

in older people. In older subjects with sarcopenic obesity, CR may lead to undesired loss of muscle mass, suggesting that weight loss by CR in these individuals should be avoided.[17]

Alternative energy restriction strategies involve various protocols of intermitted fasting (e.g., 60% energy restriction on two days per week or every other day), periodic fasting (e.g., a five-day diet providing 750-1100 kcal) or time-restricted feeding (e.g., limiting the daily period of food intake to eight hours or less). These approaches involve adaptive response signalling pathways that enhance mitochondrial health, DNA repair and autophagy[88]. By activating the eNOS-mediated NO production, CR – achieved through alternate-day fasting – promotes mitochondrial biogenesis in skeletal muscles and other mice tissues[45]. Time-restricted feeding is more potent than chronic CR in enhancing insulin oscillation. Further, the periodic fluctuation of mTOR activity better sustains autophagy in aged mice. These findings suggest that exercise or intermittent fasting by acting as acute stress stimuli might be more effective than CR in preserving muscle function and counteracting sarcopenia[17].

Other approaches could include combined interventions of CR, exercise and/or dietary supplementation. A recent study showed that while resistance exercise training improves muscle force of older obese persons both at the single myofibre level and in whole muscle, CR does not enhance such improvements[89]. A body of research has also focused on developing CR-mimetic compounds or nutraceuticals, providing some of the CR benefits without reducing caloric intake. Dietary supplementations are also being investigated as adjuvants in CR or fasting interventions.[82]

1.3.3. EAAs and BCAAs: a strategy targeting mitochondria

Nutrition is one of the most significant determinants of health. Among the three primary macronutrients, proteins - particularly the quantity and quality (i.e., the specific amino acid profile)- play a crucial role in regulating metabolic health and longevity. Significantly, the restriction (e.g., leucine, methionine, or tryptophan) or supplementation (e.g., leucine, glycine, or arginine) of single amino acids can substantially modulate metabolic health. A positive correlation between high consumption of animal-derived proteins and the increase in overall mortality has been described, suggesting that a relatively modest protein regimen may have clinical benefits in healthy individuals.[82] Although basal protein synthesis rates are not different between age groups, protein malnutrition is often observed in older people. Of note, consumption of a high protein diet or increased amino acid intake in older people

has been associated with a reduced overall mortality rate, probably due to the positive effect of amino acids on muscle wasting.[82]

The essential amino acids (EAAs) are considered the most relevant nutritional input for protein synthesis, with a crucial role in controlling glucose and lipid metabolism and the maintenance of energy balance. In particular, the branched-chain amino acids (leucine, isoleucine, valine; BCAAs) constitute ~35% of the amino acids in muscle proteins. Multiple reports demonstrate that balanced combinations of different amino acids are safe and more effective than single amino acid supplementation. BCAA-based supplements are widely administered to maximise muscle protein synthesis during energy deficit or prevent exercise-induced muscle damage.[82] Balanced EAA-BCAA formulations have shown beneficial effects in numerous pathologic conditions in older people. A body of clinical data has proven that these supplements counteract protein disarrangement and preserve energy homoeostasis in acute and chronic hypercatabolic conditions without influencing renal function.[82]

By activating mTORC1, BCAAs take part in vital pathways linking nutrition with health and ageing.[82] Amino acid formulations containing the BCAAs are capable of counteracting muscle wasting in elderly, cachectic or sarcopenic patients[90][91][92]. Chronic supplementation with a specific amino acid mixture enriched in BCAAs, referred to as BCAA-enriched mixture (BCAAem) preserved mitochondrial metabolism and enhanced physical endurance in middle-aged mice and increased average lifespan[46]. Of note, the lifespan-promoting effects of the BCAAem are eNOS-dependent and occur via the mTORC1-SIRT1-PGC-1a pathways, with enhanced mitochondrial biogenesis and function and improved endogenous anti-ROS defence in cardiac and skeletal muscles of aged mice. A virtuous cycle between eNOS and mTORC1 seems to be involved in the BCAAem beneficial effects[46]. The BCAAem was also able to mitigate muscular dystrophy in mdx mice (the experimental model of Duchenne muscular dystrophy)[93] and preserve skeletal muscles from rosuvastatin-induced myopathy[93].

More importantly, this original formula has proven health-promoting effects in a variety of clinical settings.[82] In the recent MATeR study (a 2 month, open-label randomised trial conducted in collaboration with our group) Buondonno and colleagues[92] administered BCAAem or provided diet advice to 155 elderly malnourished patients. The study demonstrated that BCAAem enhances physical performance and ameliorates cognitive performance thanks to an improvement of systemic mitochondrial bioenergetics[92].

Our group recently investigated two novel amino acid formulations containing balanced EAA-BCAA stoichiometric ratios and Krebs' cycle precursors and cofactors (i.e., citric, succinic, and malic acid), designed to optimise their effects on mitochondrial bioenergetics (*Fig. 10*). These mixtures show enhanced amelioration of mitochondrial dysfunction in ageing and diverse preclinical models.[82]

Essential amino acids	BCAAem	α5	PD-E07
L-Leucine	30.01	31.09	22.45
L-Lysine (chlorhydrate)	19.58	16.90	21.13
L-Isoleucine	15.00	10.36	11.23
L-Valine	15.00	10.36	11.23
L-Threonine	8.40	7.25	13.1
L-Cysteine	3.60	3.11	2.81
L-Histidine	3.60	3.11	2.81
L-Phenylalanine	2.40	2.07	1.87
L-Methionine	1.20	1.04	0.94
L-Tyrosine	0.72	0.62	–
L-Tryptophan	0.48	2.07	0.94
Vitamin B1 (thiamine chlorhydrate)	–	0.004	0.02
Vitamin B6 (pyridoxine chlorhydrate)	–	0.004	0.02
Citric acid	–	8.00	7.65
Malic acid	–	2.00	1.92
Succinic acid	–	2.00	1.92
Leucine : isoleucine : valine ratio	2 : 1 : 1	3 : 1 : 1	2 : 1 : 1

Figure 10. Composition of the essential amino acid mixtures All values are reported as a percentage (g/100 g). BCAAem, branched-chain amino acid-enriched mixture.[82]

In particular, the first formula (termed a5) was able to boost mitochondrial function and ROS scavenging mechanisms, promoting neuronal stem cell differentiation[94]. It also exerted mitochondrial biogenic and antioxidant effects and efficiently prevented doxorubicin-mediated cardiac damage[95]. The second mixture (PD-0E7) was investigated for its effects in Senescence-Accelerated Mouse Prone 8 (SAMP8) mice, a progeroid model showing age-related muscular and cognitive alterations[96]. The PD-0E7 experiments on skeletal muscle mitochondrial biogenesis and physical performance in SAMP8 mice are part of the present thesis.

2 Multicomponent Analysis of phYsical frailty BiomarkErs: focus on mitochondrial health (MAYBE)

My PhD project is included as a part of the broader and more complex program MAYBE financed by Cariplo Foundation in 2016 and engaging several partners.

University of Milan
Enzo Nisoli, MD PhD – project leader

University of Brescia
Alessandra Valerio, MD

Politecnico di Milano
Paola Taroni, MSc Nucl Eng

University of Verona
Mauro Zamboni, MD

University of Padua
Gerolamo Lanfranchi, PhD

INRCA Ancona
Mauro Provinciali, MD

2.1 Scientific background

Although life expectancy is undoubtedly increased in high-income countries, elderly subjects spend several years in prolonged disability. Gender differences also emerge, with greater functional impairment in women. Among the multiple chronic disorders possibly leading to disability, the geriatric syndrome of frailty is a significant public health priority. While early detection and prevention of frailty are crucial in this scenario, unfortunately, no healthcare programmes or pharmacological treatments are available for frail older people, largely due to the lack of a precise, operational definition of frailty, linked in turn to the multidimensional nature of the condition. Increasing evidence recognises sarcopenia, a state of age-related quantitative muscle loss[14] as the central biological substrate of frailty[60]. Reduced relative muscle mass is significantly and independently associated with disability in older subjects,

particularly in women[60]. The physical frailty phenotype overlaps substantially with sarcopenia[86][10] whose pathogenic mechanisms may represent the pathways through which the adverse health outcomes of frailty ensue.

A sarcopenia-linked global health challenge in the elderly population is obesity. Mean body mass index (BMI) is increasing in the elderly population in both genders[23]. Notably, obesity exacerbates the age-related decline in physical function and contributes to frailty[5]. In particular, visceral obesity (excess abdominal fat) is accompanied by subcutaneous fat dysfunction, with spillover of energy storage to other organs and insulin resistance[97]. Further, ageing and obesity share the presence of a basal chronic inflammatory state, corresponding to the rise in the pro-inflammatory cytokines. Intramyocellular lipid accumulation and/or intermuscular adipocyte formation occur in muscle, contributing to functional impairment. Notably, intramuscular fat deposition is advocated as a critical factor responsible for the declines in muscle function even in non-obese elderly subjects[98]. In this scenario, the hypothesis emerged that lean mass loss, together with muscle fat accumulation and metabolic derangement (with or without obesity), is at the core of the functional defects of the elderly frail population[5]. As already mentioned in the previous chapter, it was stated that "the most common frailty phenotype in the future may be an obese, disabled, older adult", affected by the so-called sarcopenic or dynapenic obesity[5].

While the complex, interlinked causal mechanisms are far from being established, age-dependent decrements in mitochondrial function play a key role in the frail phenotype[5]. Indeed, mitochondrial dysfunction (e.g., changes in mitochondrial biogenesis and dynamics, reduced mitochondrial hormesis, and impaired crosstalk among mitochondria and other cellular organelles) take part in the energetics decline of the elderly[99][34], and their contribution to frailty pathophysiology deserves to be elucidated. Muscle-specific microRNAs (miRs, small non-coding RNAs regulating gene expression through miR-mRNA interaction) - also termed myomiRs - have recently been identified, playing significant roles in skeletal muscle atrophy or regeneration[100]. Remarkably, selected miRs are known to modulate pathophysiological processes including muscle fibre type switching, neuromuscular junction activity, inter- and intra-muscular lipid infiltration, and satellite cell activation[101]. Further, miRS have a translational regulatory capacity within mitochondria, and recently unique sets of mitochondrial miRs (mitomiRs) were described for human skeletal muscle[102]. Thus, exploring miRs role in sarcopenia and physical frailty could be of extreme interest.

The efforts devoted by geriatric clinicians and gerontology basic researchers to identify interventions against the "twin"' conditions of sarcopenia and frailty are hampered by the lack of a unique, standardised, and universally accepted operational definition for these conditions. The main critical point is that the variety of clinical phenotypes of sarcopenia, sarcopenic obesity, and physical frailty pose a challenge to establishing reliable diagnostic tools that could be utilised in clinical and research settings to support the diagnosis, track disease progression over time, and monitor the response to interventions[10].

Though several measurable changes have been described, the current state of the art suggest that no single clinical test will be sufficient to diagnose these complex conditions. Research toward a novel approach a multidimensional diagnostic approach has been advocated for a reliable diagnosis[10]. Preclinical models of accelerated and physiological ageing could be useful to identify specific patterns of circulating biomarkers (including inflammatory cytokines, myomiRs and mitomiRs). Distinct biomarker profiles could be subsequently analysed with multivariate statistical approaches together with indexes of physical performance, muscle volume, and intermuscular fat infiltration in older people. The ability to monitor in-vivo the human tissues such as muscle and adipose tissue is of great practical use and hence of growing interest in the fields of clinical diagnostics and preventive medicine. In this context, optical techniques such as diffuse optical spectroscopy (DOS) applied in the near-infrared spectral region can non-invasively provide information on tissue composition, structure and physiology and could be of great interest in the clinical scenario to early diagnosis of sarcopenia/physical frailty syndrome, the tracking of its clinical course over time, and the monitoring of the response to treatment.

Lifestyle interventions, including exercise and nutritional care, could play a role in sarcopenic elderly subjects[60][103], while interventions combining diet and exercise have been shown to ameliorate physical frailty scores in sarcopenic-obese subjects[35][104]. Diet and exercise may differently affect mitochondrial biology, energy metabolism, and muscle tissue homeostasis. Accordingly, mitochondrial networks are targets of CR and exercise, and "mitochondrial rejuvenation" prevents age-related decline. We recently designed and studied several novel amino acid mixtures containing BCAA-enriched EAAs with different stoichiometric ratios and Krebs' cycle precursors and co-factors to optimise their effects on mitochondrial bioenergetics[95]. Dietary supplementation with such EAA-BCAA mixtures deserves to be investigated in both preclinical and clinical settings. For the MAYBE project, we selected the PD-0E7 formulation, with a leucine:isoleucine:valine 2:1:1 stoichiometric

ratio and added citric, succinic, and malic acids. The PD-0E7 mixture has been included in the Italian register of dietary supplements as AminoTher (Professional Dietetics S.p.A, Milan, Italy) with the code number 95457.

2.2 An overview of my PhD thesis and the interlinks with MAYBE project

2.2.1 Outline of the MAYBE project

The MAYBE project has been designed to i) investigate the contribution of mitochondrial dysfunction in the development of sarcopenia and physical frailty, to disentangle its complex pathophysiology; ii) identify multidimensional, non-invasive biomarkers able to track mitochondrial derangements and contribute innovative diagnostic tools for sarcopenia and frailty syndrome; iii) study the ability of diet, exercise, nutrient supplements, and their combinations, to modify frailty-related biomarkers and the course of the disease. Preclinical studies (mouse models of physiological or accelerated ageing of both sexes) and clinical trials (in elderly sarcopenic and sarcopenic obese male and female patients) are planned.

To accomplish these tasks, this project involves an outstanding team of experts in mitochondrial biology and ageing research (E. Nisoli, University of Milan and A. Valerio, University of Brescia), miR expression profiling (G. Lanfranchi, University of Padova) and non-invasive in vivo imaging techniques (P. Taroni, Politecnico di Milano). Mouse ageing models have been supplied and monitored within an internationally recognised gerontology research institution (M. Provinciali, INRCA of Ancona). Elderly subjects with sarcopenic obesity are recruited and assessed by M. Zamboni (Geriatric Unit, University of Verona), an expert leader in the European consensus working group on sarcopenia definition and diagnosis[14]. Statistic analyses are entrusted to S. Calza and M. Vezzoli (collaborating with A. Valerio at Brescia University). Prof. Alessandra Valerio and prof. Paola Taroni acted as a tutor and co-tutor, respectively,are in my Ph.D. thesis.

The COVID-19 pandemic has affected the possibility to complete every planned task of the MAYBE project. My laboratory at Brescia University has been closed for several months. Most importantly, the clinical trial in Verona has been interrupted in the enrolment phase (please, see chapter 5 for details). Thus, my scheduled PhD program has been partly revised in agreement with my tutors.

2.2.2. Main objectives of my PhD thesis

My project within the PhD program in Technology for Health comprised three main tasks, spanning from biomedical and translational research to applied technological research:

1) **Preclinical study in the SAMP8 progeroid mouse strain** to investigate the role of skeletal muscle mitochondrial dysfunction in the development of physical frailty and the effects of a nutraceutical intervention with PD-0E7 (chapter 3)
2) **Pilot studies in healthy human volunteers** to set up the non-invasive investigation of skeletal muscle and adipose tissue by time-domain diffuse optical spectroscopy (TD-DOS) (chapter 4)
3) **Clinical trial sub-study** on the use of TD-DOS for the evaluation of the characteristics of fat and muscular tissues in sarcopenic obese patients undergoing combined interventions of diet, exercise and PD-0E7 (AminoTher) supplementation (chapter 5)

The SAMP8 mouse model has been previously shown to develop early sarcopenia and a cognitive decline with Alzheimer-like phenotype at early ages[105]. In particular, SAMP8 mice showed a peak of muscle mass at month 7, and the onset of an ex-vivo contractility decline of the gastrocnemius was observed from month 8. Compared with month 8, most of the functional parameters at month 10 decreased significantly[105]. Therefore, we decided to use SAMP8 male mice as a model of accelerated ageing to characterise a wide panel of physical performance parameters and mitochondrial activity and to test the effects of PD-0E7 supplementation. This part of the work was carried out at Brescia and Milan University in collaboration with the Prof. Provinciali team of the INRCA of Ancona.

Secondly, the capacity of TD-DOS has been investigated for *in vivo* imaging. An instrument for broadband TD-DOS, able to estimate tissue composition, was developed by researchers of the Politecnico di Milano team[106] and the pilots studies were conducted in the same institution. Time-resolved diffuse optical techniques rely on the injection of a short light pulse (~ tens of ps) into the sample and on the temporal detection of the re-emitted light. Such techniques have the unique capability to simultaneously estimate absorption and reduced scattering coefficients from a single measurement. The uniqueness of the system developed by Politecnico di Milano is in the availability of a picosecond pulsed, continuously tunable source and in its high and almost flat responsivity over a broad spectral range (600-1350 nm), which provide the capability to better quantify tissue composition. To this purpose, the instrument has two different detectors, with a complementary spectral

sensitivity (600-940 nm and 940-1350 nm, respectively). The broadband estimation of absorption (μ_a) and reduced scattering (μ_s') coefficients yields information about chromophore concentrations and tissue structure, respectively[107].

A first study to investigate adipose tissue and skeletal muscle optical properties was performed on the abdomen region of 10 healthy male volunteers. After this, a second pilot study on 26 healthy male and female volunteers was carried out to better understand the influence of the tri-layered nature of these tissue types on the time distribution of the diffusively reflected light and investigate how gender affects the optical measurements, in view of a potential general application of the technique.

Subsequent planned clinical trial in sarcopenic-obese elderly subjects of both sexes have the objective of i) include TD-DOS measurements in a panel of multiple measurable aspects of physical frailty, including circulating miRNAs, pro-inflammatory cytokines, optical property measured as well as comprehensive geriatric assessment and physical performance tests; ii) investigate the power of interventions strategies, with particular attention on possible changing in optical property, on counteracting physical frailty decline.

The project's overall aim is to help cope with the multidimensional nature of physical frailty, by contributing diagnostic and risk/benefit-assessment tools, which might enable early, gender-targeted and phenotype-oriented interventions. Particular interest is posed on fulfilling the knowledge gap on sarcopenia and physical frailty by studying the pathophysiological mechanisms involved, improving the diagnosis method and investigating new treatment strategies. This will be the basis for exploring a multidimensional, non-invasive approach to define, track, and counteract these "twin" conditions. This project aims to respond to this challenging task thanks to the multidisciplinary effort of experts of diverse disciplines, including biomedical researchers, engineers and clinicians with vast experience in geriatric research. The project will further explore the capability of the novel metabolic modulator PD-0E7, combined with nutritional interventions and exercise training, to ameliorate the physical frailty score.

3 Preclinical studies: a focus on mitochondria dysfunction in sarcopenia

The results of the preclinical study obtained during my PhD have been published as part of the following article:

Brunetti D, Bottani E, Segala A, Marchet S, Rossi F, Orlando F, Malavolta M, Carruba M O, Lamperti C, Provinciali M, Nisoli E and Valerio A. Targeting Multiple Mitochondrial Processes by a Metabolic Modulator Prevents Sarcopenia and Cognitive Decline in SAMP8 Mice. Frontiers in Pharmacology, Front Pharmacol 11:1171, 2020. doi: 10.3389/fphar.2020.01171.

As mentioned in the previous chapters, an age-dependent decline of skeletal muscle mass and function occurs in elderly subjects. Although physical difficulties can occur independently of cognitive decline, physical deterioration often coexists with cognitive impairment in the aged population, with a consequent erosion of older people's independence[108]. The underlying pathophysiological mechanisms share common features of mitochondrial dysfunction, which plays a central role in the development of overt sarcopenia and/or dementia. Dietary supplementation with formulations of essential and branched-chain amino acids (EAA-BCAA) is a promising preventive strategy because it can preserve mitochondrial biogenesis and function. The senescence-accelerated mouse prone 8 (SAMP8) is considered an accurate model of age-related muscular and cognitive alterations. Hence, our research group aimed to investigate the progression of mitochondrial dysfunctions during muscular and cognitive ageing of SAMP8 mice and study the effects of a novel EAA-BCAA-based metabolic modulator on these changes. During my PhD program, I contributed to this preclinical study with regards to the characterization of the age-related mitochondrial dysfunction in the skeletal muscles. I also contributed to studying the effects of the dietary supplementation with the EAA-BCAA mixture on mice physical decay.

SAMP8 mouse model: characteristics and reasons for the choice

Senescence-Accelerated Mouse (SAM) comprise 18 strains: 11 senescence-prone inbred strains (SAMP) and 7 senescence-resistant inbred strains (SAMR). The SAMP8 strain has been considered a good choice for sarcopenia study[109][110]. According to a previous study on SAMP8 mice at 10 (young), 25 (adult) and 60 (old) weeks of age[111], SAMP8 exhibited typical features of accelerated muscle ageing with a short life span and fast ageing progress due to high oxidative stress status[112][113], a greater decrease in muscle mass and contractility, larger reduction of type II muscle fibres size[114][115][116]. In particular, SAMP8 mice showed the peak of muscle mass at month 7, and the onset of an ex-vivo contractility decline of the *gastrocnemius* was observed from month 8. Compared with month 8, most of the functional parameters at month 10 decreased significantly[105]. Furthermore, mitochondrial dysfunction is the primary cause of high oxidative stress status in SAMP8, hence inducing senescence acceleration[112]. The advantage of SAMP8 mouse is the short lifespan accelerated senescence process. Further, previous studies demonstrated that the age-related pathological phenotypes in SAMP8 are similar to human geriatric disorders[109]. Therefore, SAMP8 is recommended as a high cost-effective animal model for sarcopenia research[116].

A brief summary of the research

We performed a phenotypical evaluation of body condition and motor endurance of SAMP8 mice at 5, 9, 12, and 15 months of age. Parallel changes in mitochondrial respiratory chain subunits' protein levels, regulators of mitochondrial biogenesis and dynamics were measured in the *quadriceps femoris*. The same variables were assessed in 12-month-old SAMP8 mice that had received dietary supplementation with the novel EAA-BCAA formulation, containing tricarboxylic acid cycle intermediates and co-factors (PD-0E7, 1.5 mg/kg/body weight/ day in drinking water) for 3 months. Contrary to untreated mice, which had a significant molecular and phenotypic impairment, PD-0E7-treated mice showed preserved healthy body condition, muscle weight to body weight ratio and motor endurance at 12 months of age. The PD-0E7 mixture increased the protein levels of mitochondrial complex I, II, and IV and the expression of PGC1α and optic atrophy protein 1 (OPA1) in skeletal muscles. In summary, this study found that a dietary supplement tailored to boost mitochondrial respiration preserves skeletal muscle mitochondrial quality control and health. When

administered at the early onset of age-related physical decline, this novel metabolic inducer counteracts the deleterious effects of physical ageing.

3.1 Material and methods

3.1.1 Animal management and ethical aspects

All experiments were performed following the European Community Council Directive 2010/63/EU. According to current Italian law (D. Lgs. n. 26/2014), the protocol was approved by the General Direction of Animal Health and Veterinary Drugs of the Italian Ministry of Health with the authorization n. 131/2018-PR. Male SAMP8 mice (SAMP8/AKR/J, ENVIGO) were housed under specific pathogen-free (SPF) conditions with room temperature set at 22 ± 2°C and a 12-h light-dark cycle, with ad libitum access to food (Rodents standard diet cat. 4RF25, Mucedola, Settimo Milanese, Milan, Italy) and water.

3.1.2 Experimental plan and dietary supplementation

The experimental design included four groups (n=6 mice/group) of untreated mice aged 5, 9, 12, and 15 months. Another group of 9-month-old mice (n = 12) was randomly divided into two experimental groups, unsupplemented and PD-0E7-supplemented (n=6/each), the latter receiving the PD-0E7 for 3 months (1.5 mg/g body weight/day in drinking water). The composition of the PD-0E7 supplement (Professional Dietetics S.p.A, Milan, Italy) is detailed in *Table 1*.

PD-0E7 mixture composition	
L-Leucine	23.46
L-Lysine HCl (chlorhydrate)	17.59
L-Isoleucine	11.73
L-Valine	11.73
L-Threonine	13.68
L-Cysteine	2.93
L-Histidine	2.93
L-Phenylalanine	1.95
L-Methionine	0.98
L-Tyrosine	0.00
L-Tryptophan	0.98
Vitamin B1 (thiamine chlorhydrate)	0.0137
Vitamin B6 (piridoxine chlorhydrate)	0.0166
Citric acid anhydrous	7.99
Malic acid	2.00
Succinic acid	2.00
Leucine:Isoleucine:Valine Ratio	**2:1:1**

Table 1. Composition is expressed as percentage of total amount (%, g/100 g)

The PD-0E7 dose was selected based on our previous experience with the BCAAem formula[46][and of the safety and efficiency of a peculiar EAA- BCAA formula containing Krebs' cycle precursors and co-factors (i.e., citric, succinic, and malic acids with the same percent composition of PD-0E7)[95][117]. A decade of knowledge shows that BCAA-based mixtures are safe in both rodents and humans and, in particular, do not harm the liver nor the kidney[47][118]. The amount of PD-0E7 to be dissolved in water was calculated by recording the average body weight and the average daily water consumption of each experimental group for 2 weeks before starting the treatment and regularly adjusted based on the same parameters. Body weight was measured once a week, and water intake was checked twice a week. Fresh PD-0E7 was replaced three times per week. PD-0E7 dietary supplementation did not affect food consumption and slightly but not significantly increased water consumption in SAMP8 mice (*Tab. 2*). At the end of the study, mice were culled by cervical dislocation. Muscles for Western blot analysis were snap-frozen in liquid nitrogen

and stored at −80°C. All chemicals and reagents were purchased from Sigma Aldrich (Milan, Italy) unless otherwise stated.

	untreated	**PD-0E7**
Food intake (g)	5.49 ± 0.43	5.52 ± 0.62
Water intake (ml)	6.58 ± 0.91	7.37 ± 1.11

Table 2. Data are from measures in 12-month-old mice (6/group).
Values represent mean ± D.S.

3.1.3 Health status and behavioural assessment

Mice were monitored weekly for general health or behavioural changes and the onset of postural abnormalities. Body condition score (BCS) was assessed according to an established method[119]. Kyphosis, a characteristic dorsal curvature of the spine (frequently due to backbone muscle weakness in older people and progeroid mice models)[120], was assessed by visual inspection. The presence of hind limb clasping reflex (a common manifestation of neurological disease in mice)[121] was assessed by suspending the mice by the tail for 20 sec and observing if they clasped their hind limbs together; normal mice splay their limbs apart. Motor skills were evaluated measuring endurance as previously described[122] using a treadmill apparatus (Ugo Basile, Italy) with a gradually accelerating protocol (the speed was initially set at 3.8 m/min and increased by 3 m/min every 2 min). The test was terminated by exhaustion, which was defined by 10 falls/min into the motivational grid.

3.1.4 Western blot analysis

Mouse *quadriceps femoris* were homogenized in ten volumes of radioimmunoprecipitation assay (RIPA) buffer [150 mM NaCl, 5 mM EDTA, 50 mM Tris, 1% NP-40, 0.5% sodium deoxycholate, and 0.1% sodium dodecyl sulfate (SDS)] in the presence of protease and phosphatase inhibitors, with the use of automatic homogenizer (Omni international, Kennesaw, GA). Samples were incubated on ice for 30 min and centrifuged at 14,000 x g for 20 min at 4°C. Protein concentration was determined with the BCA protein assay Kit (Pierce Biotechnology, Rockford, IL). Aliquots (20 mg each) were run through a 4–12% SDS–polyacrylamide gel electrophoresis (PAGE), electroblotted onto a PVDF or nitrocellulose membrane and probed with different primary antibodies: total oxidative phosphorylation (OXPHOS) rodent antibody cocktail (Abcam, ab110413, dilution 1:1,000); OPA1

(Immunological Sciences, 1:1,000); GAPDH (Immunological Sciences, 1:2,000), PGC-1α (Novus Biological, 1:1,000), SIRT1 (Cell Signaling Technology 1:1,000), Nrf2 (BioSource, 1:500), chemiluminescence-based immunostaining (ECL Western Blotting Detection Kit, Amersham) was performed. Images were acquired with the use of ChemiDoc Imaging System apparatus (Bio-Rad Laboratories, Milan, Italy) and analysed with Image LabTM software, version 6.0.1 for Windows (Bio-Rad Laboratories, Milan, Italy).

3.2 Statistical analysis

One-way ANOVA with Tukey's post-test for multiple comparison or Student's t-test were used to compare the means among four age groups or between two groups, respectively. Fisher Exact test was performed to evaluate significance of frequency records among four age groups. The data were analysed using GraphPad Prism version 5.00 for Windows (GraphPad Software, San Diego, CA). A linear model fitted using generalized estimating equation (GEE) accounting for the within-subject correlation was used to analyse longitudinal experiments, either with Gaussian error distribution for quantitative data or with binomial distribution for binary events. Models were fitted using R (version 3.6.3). All tests were two-sided and assumed a 5% significance. See text or figure legends for details.

3.3 Results

3.3.1 Characterization of age-related physical decline in SAMP8 male mice

We first performed a comprehensive characterisation of age-related changes in the general health status and motor abilities in male SAMP8 mice at 5, 9, 12, and 15 months of age. (*Fig. 11*). In particular, at 5 months of age, SAMP8 mice appeared healthy and well-conditioned, without prominence of vertebrae and dorsal pelvis; conversely, in the 9- and 12-month-old groups, mice progressively appeared under-conditioned, with evident segmentation of vertebral column and palpable dorsal pelvic bones. At 15 months of age, SAMP8 mice looked emaciated, with an extremely prominent skeletal structure (*Fig. 11*). The changes were reminiscent of an age-dependent decrease in body condition score (BCS)[119] (*Fig. 11*).

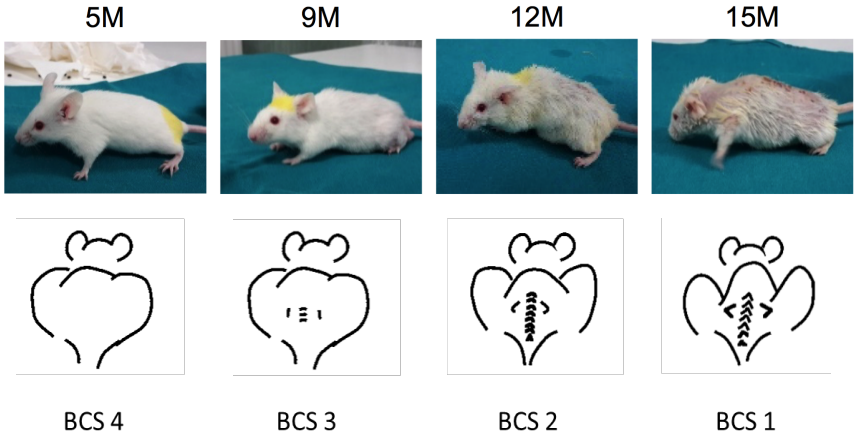

Figure 11. Phenotypical characterization of SAMP8 mice at different ages.
Representative pictures of SAMP8 mice at 5, 9, 12, and 15 months of age show a progressive appearance of signs of aging, corresponding to a reduction of the body condition score (BCS)

Quantification of the BCS demonstrated an age-dependent decrease of this score, which was significant starting at 12 months of age (*Fig. 12A*). We observed a non-significant decrease in the body weight along with mice age (*Fig. 12B*). SAMP8 mice showed an ever-increasing prevalence of kyphosis that became statistically significant in the 12-month-old group (*Fig. 12C*), with further intensification at 15 months, suggesting a progressive impairment of back muscle mass and strength. SAMP8 mice also revealed an age-related increase in the frequency of the hind limb clasping reflex (*Fig. 12D*). Exercise endurance, as assessed by the capacity to run until exhaustion during a treadmill test, gradually and significantly diminished with age (*Fig. 12E*). Taken together, these data indicate that SAMP8 mice developed an age-related impairment of skeletal muscle function.

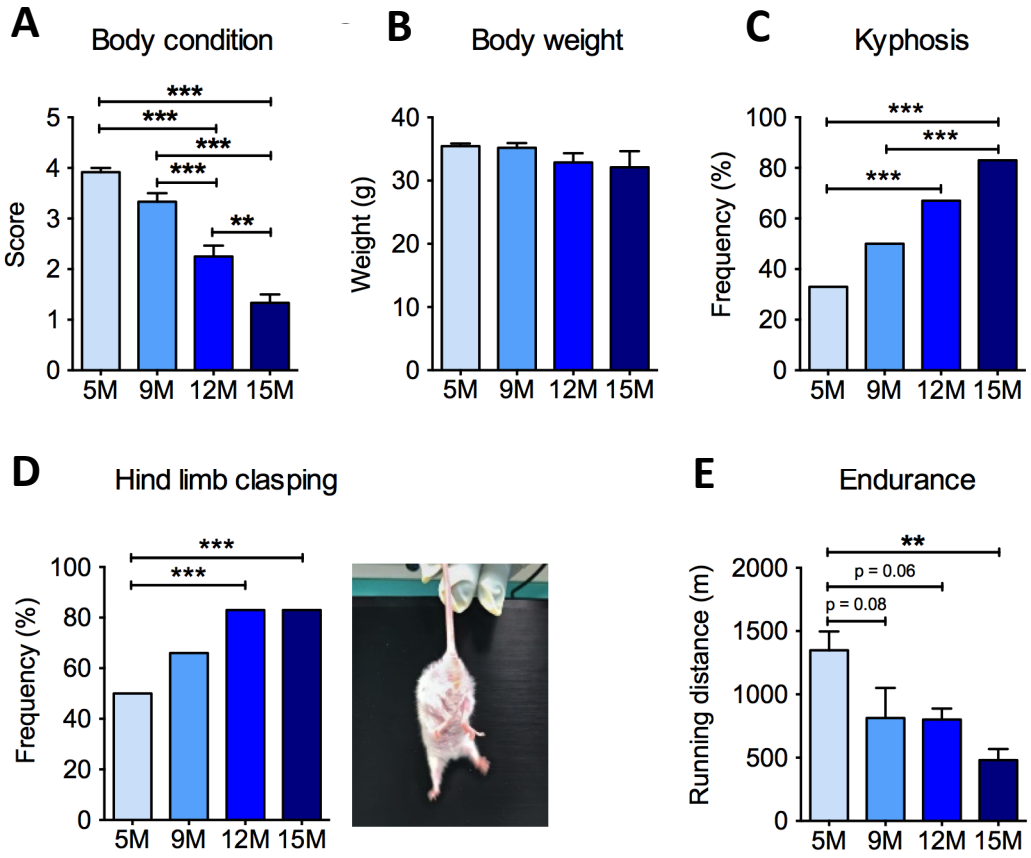

Figure 12. progressive neuromuscular impairment in SAMP8 mice at different ages.
SAMP8 mice at 5, 9, 12, and 15 months of age showed a progressive deterioration, as quantified by means of body condition score (A), frequency of kyphosis (C), increased limb clasping reflex (D), and progressive reduction in exercise endurance measured by treadmill exhaustion test (E). Body weight is also shown (B). Statistical analyses were performed with one-way ANOVA and Tukey's multiple comparison test (A, B, E) or Fisher test (C, D). Error bars represent SEM; n=6 mice/group; **p < 0.01, ***p < 0.001.

3.3.2 Characterization of age-related mitochondrial dysfunction in skeletal muscle in SAMP8 male mice

Because muscular mitochondrial function declines with age[123], we analysed mitochondrial function in the skeletal muscles of the four groups of SAMP8 mice. Significant, age-related reductions of the protein levels of several subunits of the oxidative phosphorylation pathway were detected by Western blot analysis (*Fig. 13*) of *quadriceps femoris*. In particular, the amount of the nuclear-encoded subunits of complex I (NDUFB8, NADH:ubiquinone oxidoreductase subunit B8), complex II (SDHB, succinate dehydrogenase complex iron sulfur subunit B), complex III (UQCRC2, ubiquinol-cytochrome C reductase core protein 2), and complex V (ATP5A, ATP synthase F1 subunit alpha), as well as the mitochondrially-encoded subunit of complex IV (MTCOI, mitochondrial cytochrome c oxidase subunit 1)

were reduced by more than 50% from 9 months of age onwards (*Fig. 13*). As previously observed in aged C57BL/6J mice[124], the master transcriptional regulator of mitochondrial biogenesis PGC-1α was reduced in skeletal muscle of aged SAMP8 mice (*Fig. 13*). The mitochondrial dynamin-like GTPase optic atrophy protein 1 (OPA1), which is required for mitochondrial fusion, cristae remodelling, and mitochondrial respiration[57] also decreased along with age in SAMP8 quadriceps femoris (F*ig. 13*). These data confirm that mitochondrial deterioration is a key hallmark of ageing in the SAMP8 mouse model.

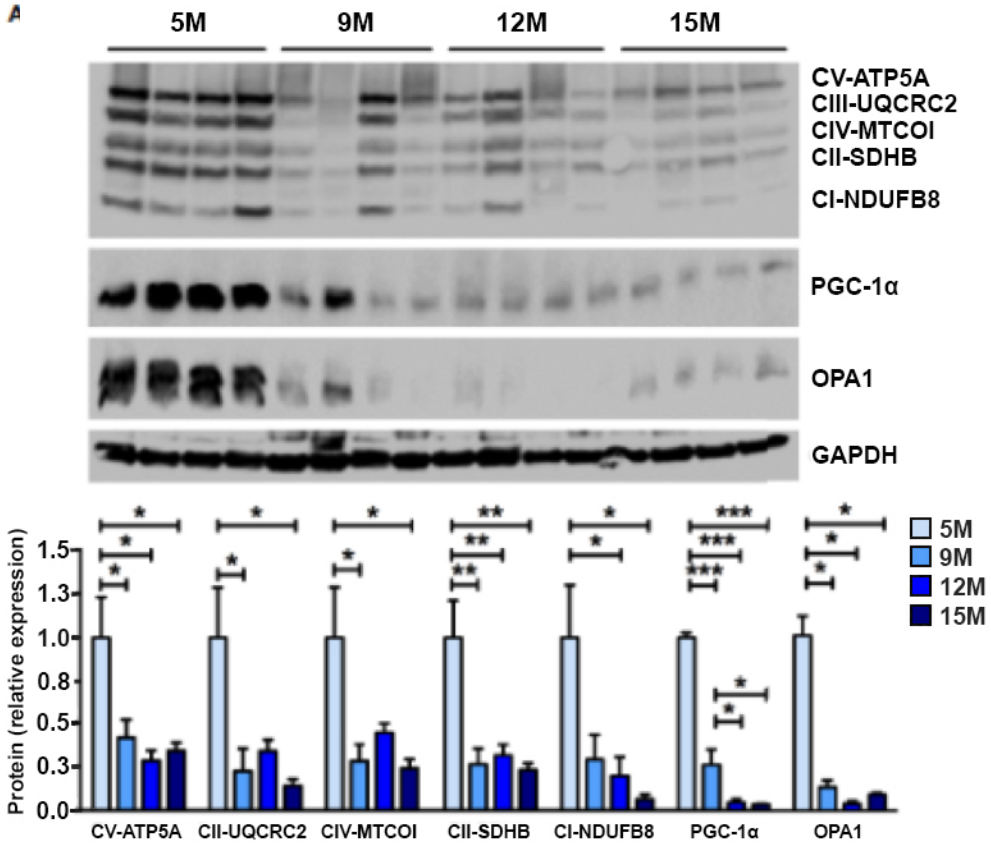

Figure 13. Age-dependent mitochondrial dysfunction in the skeletal muscle of SAMP8 mice. Western blot analysis of the MRC subunits ATP5A (complex V), UQCRC2 (complex III), MTCOI (Complex IV), SDHB (Complex II) and NDUFB8 (Complex I) and of PGC-1α and OPA-1 was performed in *quadriceps femoris* at different ages. The quantification of each signal was normalized to the amount of GAPDH and represented below the images. Statistical analysis was performed with one-way ANOVA and Tukey's multiple comparison test. Error bars represent SEM; n=4 mice/group; *p < 0.05, **p < 0.01, ***p < 0.001.

3.3.3 Effects of 3 months dietary supplementation with PD-0E7 on the physical status of SAMP8 male mice

In this part of the study, we tested whether dietary supplementation with the PD-0E7 formula could counteract the deterioration of general health status and motor abilities in aged mice. Nine-month-old male SAMP8 mice (n = 12) underwent physical and phenotypical assessment at baseline, as described above. Mice were then randomly divided into two experimental groups (n=6/each), either unsupplemented or supplemented with PD-0E7 for 3 months. At the end of the experimental protocol, a second physical and phenotypical assessment was performed. Twelve-month-old, PD-0E7-treated mice appeared healthier and better conditioned than the age-matched untreated mice, which showed prominent kyphosis and apparent hyposthenia of fore and hind limb muscles (*Fig. 14A*); moreover, PD-0E7-treated mice had thick, glossy fur, which was instead lost and replaced by thinning fur in untreated animals (*Fig. 14A*). Contrary to untreated mice, PD-0E7-treated mice retained their BCS (time x treatment interaction, $p < 0.001$; GEE) (*Fig. 14B*) and their body weight (time x treatment interaction, $p = 0.047$, GEE) (*Fig. 14C*) for the duration of the treatment. The frequency of kyphosis (*Fig. 14D*) and hind limb clasping (*Fig. 14E*) showed non-significant trends toward a reduction in PD-0E7-treated mice (time x treatment interaction, $p = 0.2$ and $p = 0.128$, respectively; GEE with binomial distribution). While the endurance performance on the treadmill test was significantly reduced in untreated mice, it remained unchanged after the 3 months PD-0E7 treatment (time x treatment interaction, $p=0.25$; GEE) (*Fig. 14F*). On the whole, these results demonstrate the efficacy of the dietary supplementation with the PD-0E7 mixture in counteracting age-associated skeletal muscular decline.

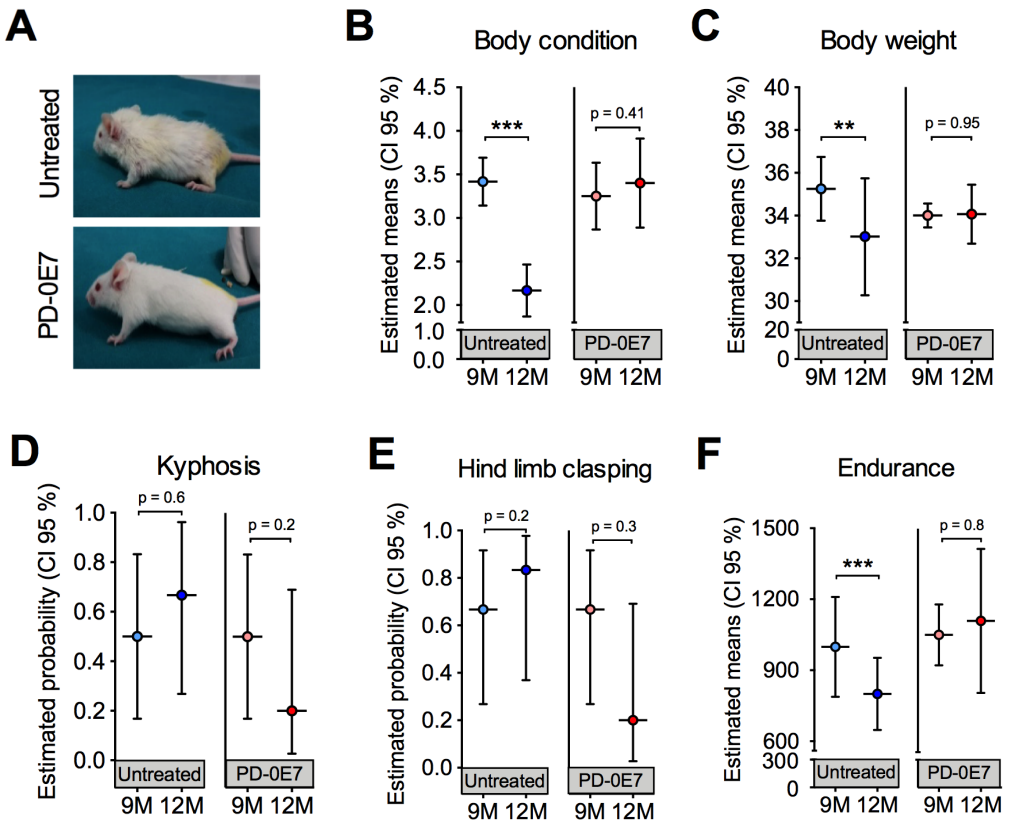

Figure 14. Effect of PD-0E7 supplementation on physical phenotype and on skeletal muscular function in aged SAMP8 mice. (A) Representative pictures of 12-month-old untreated and PD-0E7-treated mice. Treatment effects on body condition score (B), body weight (C), frequency of kyphosis (D) frequency of hind-limb clasping (E) and endurance capacity (E). Treatment effects across time (B, C, F) were analysed with generalized estimating equation (GEE) with Gaussian error distribution. Frequency data (D, E) were analysed with GEE with binomial distribution. Error bars represent 95% confidence interval; n=6 mice/untreated group; 5 mice/PD-0E7-treated group, due to one death after baseline assessment. **p < 0.01; ***p < 0.001.

3.3.4 Effects of 3 months dietary supplementation with PD-0E7 on mitochondrial health in skeletal muscle in SAMP8 male mice

Post-mortem examination of the skeletal muscles showed that PD-0E7-treated SAMP8 mice had significantly higher *gastrocnemius* muscle mass than the untreated group (*Fig. 15A*), supporting its efficacy in reducing sarcopenia. Western blot analysis on total homogenates of *quadriceps femoris* showed that the amount of phosphorylated p70 S6 kinase 1 (S6K1) was significantly augmented in the PD-0E7-treated group compared to unsupplemented controls (*Fig. 15B*), demonstrating the activation of the mTORC1/S6K1 pathway[125], as we reported previously with the in vivo administration of the BCAAem formula[46]. We also previously found evidence that BCAAem-activated mTOR signalling enhances PGC-1α-

mediated mitochondrial biogenesis[46]. Previously evidence found that BCAAem-activated mTOR signalling enhances PGC-1α-mediated mitochondrial biogenesis[46]. Accordingly, from Western blot analysis, the protein amount of PGC-1α was significantly increased in *quadriceps femoris* from PD-0E7- treated animals compared to untreated controls (*Fig.15D*), together with the amount of the sirtuin family deacetylase SIRT1, which is known to promote PGC-1α activation and expression in the skeletal muscle[126] (*Fig. 15D*), both suggesting that the mitochondrial biogenesis pathway was activated upon PD-0E7 supplementation. The amounts of the nuclear factor, erythroid 2 like 2 (NFE2L2 or Nrf2-ARE), which regulates the expression of antioxidant genes and is involved in a mitochondrial biogenic regulatory loop involving PGC-1α[127], was also increased in *quadriceps femoris* from PD-0E7-treated animals (*Fig. 15C*). The protein content of the respiratory chain subunits ATP5A, UQCRC2, MTCOI, and SDHB, were significantly higher than those detected in untreated mice (*Fig. 15D*). Notably, skeletal muscles of the PD-0E7-treated group also showed increased levels of OPA1 (*Fig. 15D*).

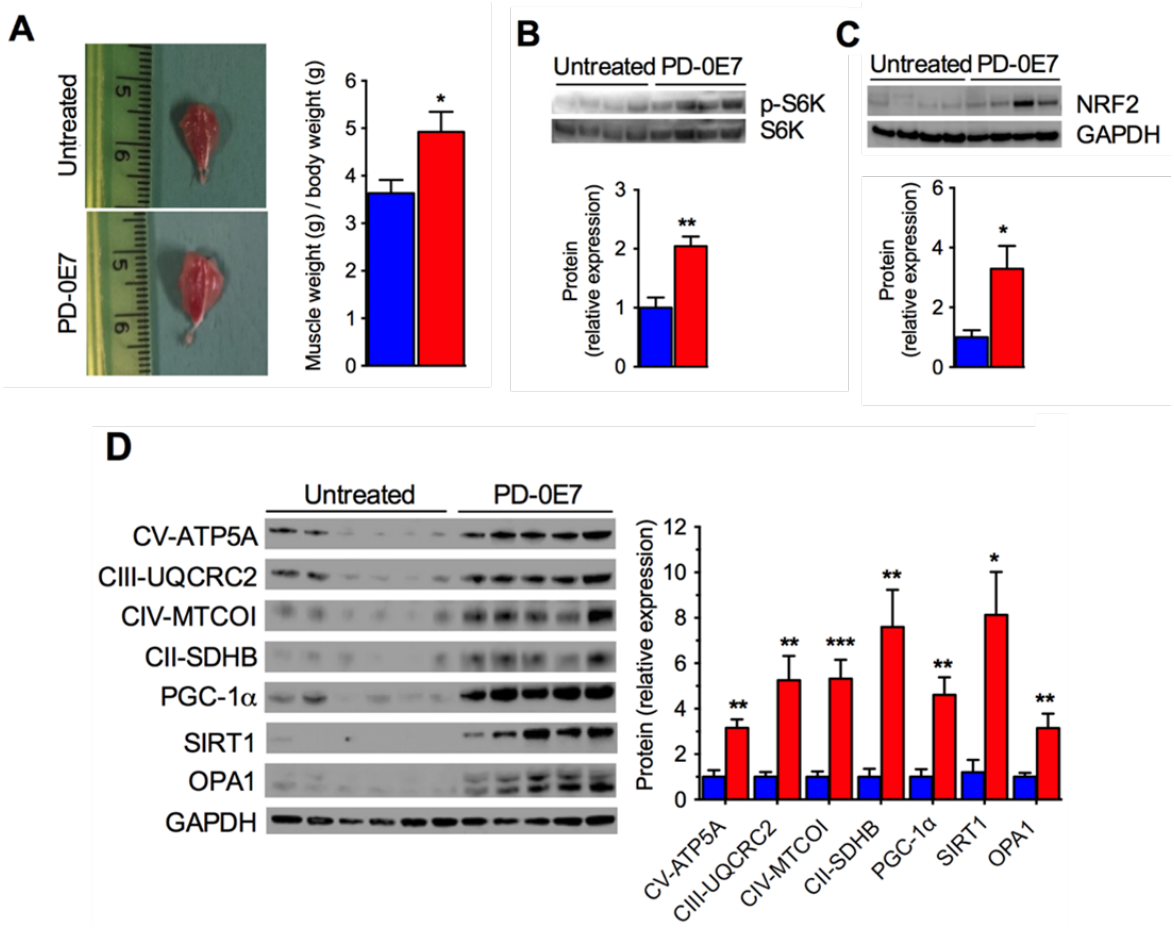

Figure 12. Effects of dietary supplementation with PD-0E7 on skeletal muscles of aged SAMP8 mice. (A) Representative pictures of *gastrocnemius* muscles of untreated and PD-0E7-treated mice; quantification of muscle weight/body weight is shown on the right (blue bars, untreated mice, red bars, PD-0E7-treated mice). (B) Western blot analysis of phosphorylated p70 S6 kinase 1 (p-S6K) and total S6K in quadriceps femoris; quantification of pS6K/S6K ratio is shown below the image. (C) Western blot analysis of NRF2-ARE in *quadriceps femoris*, with quantification relative to GAPDH shown below the image. (D) Western blot analysis of PGC-1α, SIRT1, OPA1 and of the respiratory chain subunits ATP5A, UQCRC2, MTCOI, and SDHB in quadriceps femoris; relative quantification of proteins to GAPDH levels is shown on the right. Statistical analysis was performed with Student's t test. Error bars represent SEM; n=6 mice/group; *$p < 0.05$, **$p < 0.01$, ***$p < 0.001$.

As a whole, these data strongly support the role of PD-0E7 in promoting mitochondrial biogenesis, oxidative phosphorylation, and antioxidant response through the mTORC1/S6K1/ PGC-1α pathway in the skeletal muscle of SAMP8 mice.

3.4 Discussion

In the present study, we provided evidence of the beneficial effect of a novel nutritional intervention, acting as a metabolic inducer, in rescuing age-related motor function in senescent mice. We used the SAMP8 mouse strain—which is prone to accelerated ageing with impairments affecting both muscle and brain—to investigate the pathophysiological mechanism(s) of physical decline, with a particular focus on mitochondrial derangements, and to explore the effectiveness of a novel metabolic modulator in preventing indexes of sarcopenia and physical frailty.

It has been reported that SAMP8 mice spontaneously develop a pre-sarcopenic status at 8 months of age, which results in overt sarcopenia at 10–12 months of age[128][116]. To identify the proper timing of intervention at the early onset of motor impairment, we first performed an in-depth phenotypical characterization of the SAMP8 mice, by recording established scores of their general health status, as well as of their motor skills, at 5, 9, 12, and 15 months of age. In line with previous studies[116][129], we observed an age-dependent physical and neuromuscular decline in this mouse strain. In particular, the early signs of inadequate general health conditions were detectable at 9 months of age, with a trend in the reduction of BCS, as well as in the increased frequency of kyphosis (a sign accompanying age-associated loss of muscle mass in mice)[120] and hind limb clasping (an unspecific sign of neurological dysfunction)[121]. These changes were significant at 12 months of age and further worsened with ageing. Of note, a marked reduction of exercise tolerance was observed as early as at 9 months of age, with a subsequent further decline.

By post-mortem examination, the observed physical deteriorations evolved in parallel with a progressive impairment of the mitochondrial function in skeletal muscles. By analysing *quadriceps femoris,* we found a significant age-dependent reduction of PGC-1α and several MRC subunits. We also identified an age-dependent down-regulation of the mitochondria-shaping protein OPA1 in the *quadriceps femoris* of SAMP8 mice, as reported in muscles of sarcopenic rodents[130] and in muscle biopsies of old subjects, in whom OPA1 reduction and defects of mitochondrial dynamics correlate with muscle mass loss and muscle force drop[131][132].

A body of research efforts is currently devoted to boosting mitochondrial bioenergetics as novel therapeutic approaches to treat sarcopenia[133]. Given that these conditions will continue to rise worldwide alongside the population ageing, a focus on prevention is urgently

needed. Studies in preclinical models are necessary to investigate the effects of compounds that could sustain age-related skeletal muscle and brain dysfunctions. The long-standing experience of my research group with the BCAAem formula has demonstrated its effect on preserving skeletal muscle health by targeting mitochondrial function via the mTORC1/PGC-1α pathway[46][134][93]. The BCAAem has recently proven to be effective in improving muscular and cognitive performance in elderly subjects[92]. Further, our research group recently demonstrated that adding tricarboxylic acid cycle intermediates and co-factors to an EAA-BCAA mixture increases oxidative metabolism much more than the previous formula and potentiates its protective effects against mitochondrial dysfunction[95][117][82]. Here, we tested the novel EAA formulation PD-0E7, with an optimized stoichiometric ratio of BCAAs, and added Krebs' cycle precursors and co-factors, in SAMP8 senescent mice.

We found that supplementation with PD-0E7 in the temporal window between 9- and 12-month of age beneficially affected the whole body and counteracted the age-related signs of neuromuscular and decline of SAMP8 mice. These effects were accompanied by increased activation of the mTORC1 pathway (as demonstrated by increased S6K1 phosphorylation) in the skeletal muscle of PD-0E7 treated mice. Of note, mTORC1 activation plays a role in exercise-mediated health benefits on physical performance[135]. In particular, increased mTORC1 signalling is responsible for changes in skeletal muscle growth that occur in response to exercise in rodents and humans[136][137]. In turn, exercise—which in normal mice extends healthspan (i.e. disease-free life span)—remains the only currently available intervention to mitigate and even reverse the age-related decline in muscle mass and function of sarcopenia. Notably, in older people, mTORC1 becomes less responsive to contraction-induced activation compared with young adults[138]. Additionally, exercise upregulates PGC-1α, hence counteracting its age-related decline[139]. Activation of mTORC1 favours PGC-1α coactivation of its own promoter[140] and positively correlates with cellular oxidative capacity[141]. Accordingly, we found that chronic treatment with PD-0E7 increased PGC-1α protein levels and upregulated several MRC subunits in SAMP8 mouse skeletal muscle. Raised SIRT1 levels in both tissues of PD-0E7-treated mice could further amplify the mitochondrial responses by deacetylating and activating PGC-1α[142]. Finally, skeletal muscle of PD-0E7-treated mice displayed augmented levels of Nrf2, a transcription factor that activates antioxidant genes upon binding to antioxidant-responsive elements (ARE) motifs in their promoters[143]. Increased mitochondrial respiration can augment

ROS production if appropriated mitochondrial quality control lacks. Although optimal levels of ROS act as essential biological signals regulating various physiological processes[144], excessive ROS levels can damage cellular components contributing to age-related pathology. Notably, both PGC-1α and Nrf2 are involved in mitochondrial biogenesis and in the endogenous antioxidant response, and a positive regulatory loop has been described between the two factors, overall contributing to maintain mitochondrial mass and redox homeostasis[145]. Hence, simultaneous activation of the PGC-1α and Nrf2 pathways is being considered one of the most promising strategies in gerontoprotection[127].

PD-0E7-supplemented mice showed higher muscle weight when compared to the age-matched untreated controls. The preserved exercise endurance observed in the 12-month-old PD-0E7- supplemented mice might be explained by the increased levels of MRC complex subunits. Interestingly, the protein levels of OPA1 were significantly increased in the muscle of the PD-0E7-treated group. In addition to its role in mitochondrial fusion, OPA1 regulates mitochondrial cristae remodelling by promoting the juxtaposition of the cristae membranes[146][57]. Cristae tightness, in turn, determines the assembly and stability of respiratory chain complexes into SC structures[147]. These functional quaternary structures increase the electron flow channelling during respiration, minimizing electron leaks[148][149], and stabilizing individual respiratory chain complexes such as complex III[150], thus affecting mitochondrial respiratory efficiency. Indeed, OPA1 overexpression optimizes the ATP production and ameliorates mitochondrial dysfunction in vivo[151]. A similar link between OPA1 levels, SC organization, and muscle mass was recently described in humans[132]. Alterations in SCs have been described in brain and muscle during ageing, and interestingly, besides increasing individual MRC subunits, exercise affects the stoichiometry of SC formation in old age[152]. In particular, exercise training promoted the redistribution of CIII into SCs in *vastus lateralis* muscle of sedentary older subjects[152]. Altogether, these observations suggest that PD-0E7 might act as an exercise mimetic in older people.

In conclusion, dietary supplementation with the metabolic modulator PD-0E7 rejuvenates mitochondria and efficiently counteracts the deleterious effects exerted by premature ageing in skeletal muscles, thus potentially representing aw efficacious and safe intervention to prevent disability and physical frailty in elderly subjects.

4 In vivo time-domain diffuse optical spectroscopy (TD-DOS): two pilot studies

The results of the first pilot study obtained during my PhD have been published in the following article:

Lanka P, Segala A*, Farina A, Konugolu Venkata Sekar S, Nisoli E, Valerio A, Taroni P, Cubeddu R, and Pifferi A. Non-invasive investigation of adipose tissue by time domain diffuse optical spectroscopy. Biomedical Optics Express, Vol. 11, No. 5, 1 May 2020. *Equal contributors*

Time domain (TD) Diffuse Optics can provide information on tissue chromophore concentrations and on the microstructure of the tissue; these properties are hardly exploited in available commercial and clinical instruments. Most instrumentation and studies, both *in vivo* and otherwise, assume only oxy and deoxy haemoglobin as the absorbers due to usage of a limited number of wavelengths. Moreover, carrying out clinical measurements *in vivo* further complicates the issue. Broadband instruments, like the one discussed in this chapter, can effectively quantify other tissue constituents that are of clinical interest. Lipid, collagen and water are some of the key constituents of tissue that exhibit particular changes in the wavelength region around 1 μm. The instrument of choice needs to be portable, robust, easy to use, well automated and safe to handle. All these parameters were taken into account while designing the broadband, multi-distance, time domain, diffuse optical spectrometer.

4.1 Adipose tissue and skeletal muscle: introduction on pathophysiology and diagnostic techniques

Adipose tissue

During the last decades, increasing evidence defined adipose tissue (AT) as an organ, highly vascularised and innervated, with a precise anatomy; endocrine properties and a high degree of plasticity are both characteristics of this tissue[153][154][155]. There are two morphologically and functionally distinct AT types: white adipose tissue (WAT) and brown

adipose tissue (BAT)[156]. WAT accumulates fat during nutrient abundance state and releases fatty acids during fasting. The principal depots of WAT are visceral AT (VAT), centrally located and enclosed by the peritoneum, the subcutaneous AT (SAT) located directly below the skin, and finally ectopic AT, which consists of depots in areas not directly associated with storage[153]. The SAT compartment comprises more than 80% of the total body fat and consists of gluteal, femoral and abdominal AT. SAT adipocytes appear larger than perivisceral adipocytes[153]. Abdominal fat depots are characterised by rapid uptake and storage of energy from the diet and a high lipid turnover (i.e., lipolysis)[157]. AT expands by a combination of an increase in adipocyte size (hypertrophy) and number (hyperplasia)[158]. In obese subjects, the subcutaneous adipose tissue may fail to appropriately expand to store the energy surplus. This may lead to ectopic fat deposition in other tissues such as skeletal muscle and liver and to metabolic dysfunctions. Thus, it is mandatory to provide a tool to better understand the role of adipose tissue function and other potential biological mechanisms in obesity-related complications[157].

While VAT is a source of proinflammatory cytokines and free fatty acids that contribute to glucose production, insulin resistance, and metabolic syndrome[29], SAT is an independent predictor of lower cardiovascular risk (CVR) and diabetes-related mortality and protects against impaired glucose metabolism[159][160].[161] It has been well-documented that adipose tissue of the leg in women, in opposition to intra-abdominal and trunk adipose tissue, is negatively related to CVR[162][163]. The described positive metabolic activity of SAT located in lower body parts in women may be associated with higher lipoprotein lipase activity. Interestingly, this relationship was not observed in the male population[164][165]. In a research that compared the morphological construction of the thigh's SAT between genders using US[165] was observed that sex is the strongest factor affecting thigh's SAT. A strong correlation was shown between the BMI and the thickness of SAT layers in women.[165]

Thus, the preference in storage compartments of lipids is gender-affected: women preferentially store fat in the gluteal–femoral region. A hypothesis "evolutionary-based" asserts that women accumulate energy reserves in the subcutaneous depot for adipose tissue mobilisation required during lactation. The decline in circulating estrogens during menopause leads to a shift in adipose tissue deposition favouring the visceral depot. In men, the evolutionary-based explanation to deposit more fat in the visceral area may be due to the fact that this fat depot is more readily usable.[161]

Moreover, the subcutaneous and dermic architecture is similar between female and male, with non-uniform distribution of collagen fibres within the compartments and surrounding fat lobules. However, in females, the adipose lobules in subcutaneous tissue appeared better organised and homogeneous in dimensions. In males, collagen fibres appeared more randomly organised, and the adipose lobules assumed different forms and dimensions. Furthermore, in male, the collagen bundles are detectable in the dermis, while the female dermis presented only small depots.[166]

Since different types of obesity have various fat distributions, further investigation of SAT morphology in different body locations seems important. Thus, AT examinations could be a new perspective in the diagnosis of numerous diseases obesity-related. Moreover, this work of thesis is focused on physical frailty and sarcopenia, which possibly and mostly occur in concomitance to obesity, then a great interest is posed on the investigation of AT.

Over recent years, there has been an increased interest in methods useful in evaluating both the morphology and function of this tissue[165]. Numerous techniques become available for body fat assessment, with a different validity in obese individuals and specific populations. However, despite the importance of AT in disease, there are no widely-used methods for assessing its physiology in humans[167], the strengths and limitations being due to the accuracy, costs, safety and portability of the device. BMI is the most frequently used index in epidemiological studies, but it does not show a strong correlation with body fat in obese individuals[153] and older subjects with decreased muscle mass[157]. Further, BMI does not locate fat depots. Diversely, waist circumference, hip circumference, waist-to-hip ratio, and waist-to-height ratio are indirect indexes for VAT or SAT valuation. Bioelectric impedance and dual-energy X-ray absorptiometry are widely used, indirect techniques that derive body fat percentage from specific equations and cannot differentiate between different fat depots. Computerised tomography and magnetic resonance imaging are the most accurate techniques available for measuring fat sub-compartments, however, they are highly expensive, not portable and have huge limitations in clinical practice[153]. In addition to these methods, studies to validate ultrasound techniques in the estimate of SAT and VAT in the abdomen and for muscle thickness are ongoing. New devices with specific software are needed to increase accuracy and reduce operator variability to provide a method that is efficient in both clinical practice and epidemiological studies[153].

The knowledge of the optical properties (at several wavelengths) of tissues allows defining tissue properties: composition in terms of its major constituents (water, lipid, and collagen),

haemoglobin content and oxygenation level, and also information on the structure derived from scattering parameters. Diffuse optical spectroscopic imaging, combining continuous wave (CW) broadband (650-1000 nm) acquisition with frequency domain (FD) measurements at 4 discrete wavelengths, was applied to estimate the optical and then the physiological properties of abdominal AT in 10 overweight or obese adults during three-months on calorie-restricted diet[167]. Changes were observed in scattering, possibly indicating reduction in adipose cell volume, as well as water and haemoglobin content, suggesting improved AT perfusion and oxygen extraction. The combined use of two approaches (CW and FD) allowed disentangling scattering from absorption. Optical techniques have obtained interesting initial results suggesting their high potential for the non-invasive investigation of adipose tissue. However, optical techniques will succeed in providing valuable feedback only if they can grant reliable and quantitative information.

Skeletal muscle

As described in chapter 1, ageing-related muscle dysfunction involves quantitative and qualitative changes in skeletal muscle structure and function. This process is typically slow, and the functional impairment varies significantly among individuals, but is observed in all humans. Although the fundamental biological processes underlying ageing remain mostly obscure, it is clinically important to acquire detailed knowledge about muscle tissue-specific mechanisms of ageing.[17]

After the age of 35 years, a healthy subject has a rate of loss of muscle mass at 1% to 2% per year with a 1.5% annual decline in strength, which accelerates to around 3% per year after the age of 60[168]. As a consequence, the muscle cross-sectional area (CSA) of the thigh decreases by about 40% between 20 and 60 years of age. The decline in fat-free mass is twice as great in men than in women, and is amplified in sedentary subjects[168]. Contextually to the losing lean body mass, an average adult could be expected to gain approximately 0.50 kg of fat mass per year between the ages of 30 and 60[169]. This modification in body composition is frequently masked by unchanging body weight and can results in sarcopenic obesity disorder[170].[11]

However, ageing-related changes in muscle power appear to precede detectable changes in various morphological and electrophysiological changes.[17] Moreover, it has been shown that the capillary supply to a fibre depends more on the size. This supports the idea that a

potentially slow but gradual capillary rarefaction and hypoperfusion contribute during ageing contributes, and may even precede, sarcopenia[17].

Further, it is known that disuse resulting in muscle atrophy and also induces capillary rarefaction[171][172][173]. In the *vastus lateralis* muscle of 65- to 74-yr-old men, it was shown that both endurance and resistance training can induce[174][175][176], although not always[177], angiogenesis. In resistance training, angiogenesis is proportional to the increase in fibre size[175]. However, the angiogenic response to the endurance training is attenuated in old (62 yr) men relative to young (20 yr) and may even be associated with muscle fibre atrophy that occurs with ageing[178].[17]

In quadruped and biped mammals, the forelimb (arm) and hindlimb (leg) appear to be affected differently by ageing, with hindlimb (leg) muscles being more severely affected than forelimb (arm) muscles[17]. Further, the anterior compartment of the thigh region undergoes a preferential age-related decline in skeletal muscle (SM) and force.[15] In accordance with this, the predictive value of the muscle weakness is stronger when muscle force is measured at a speed of movement[179]. However, grip strength measurements have frequently been preferred for studying ageing-related impairment in skeletal muscle function due to the simplicity of the procedure and the high prevalence of disabilities and walking problems in elderly. However, it may be argued how well grip strength reflects the ageing-related motor handicap and decreased quality of life in old age related to impaired mobility and risk of falls and fall-related injuries.[17]

Several attempts have been made to normalize *in vivo* muscle force, such as the average muscle cell CSA in muscle biopsy specimens or with *in vivo* measurements of total muscle CSA determined from limb circumference, ultrasound, or computed tomography or MRI scans[17]. However, muscle CSA and muscle weights overestimate the amount of contractile material in old age[180]. Nowadays, there is a lack of a reliable method or tool to properly assess skeletal muscle quantity, quality and function. Moreover, in this context, as said before for the AT, investigating the optical properties (at several wavelengths) of tissues allows to define tissue properties in terms of composition, haemoglobin content and oxygenation level, and also information on the structure and is interesting also in the field of skeletal muscle study. In particular, this match the purpose of my thesis to disentangle the principal mechanism underlying age-related sarcopenia and sarcopenic obesity.

4.2 Materials and methods

4.2.1 The instrument

An upgraded version of an existing broadband time-domain instrument specifically designed for clinical measurements was used for this study[107]. The probe was specifically designed for these studies, and the system was modified (as described in the following) to allow time domain measurements to be performed at multiple source-detector distances minimising the overall time required for the measurements. A schematic of the setup is shown in (*Fig. 16*). A broadband (450-1750 nm) pulsed supercontinuum fibre laser (Fianium WhiteLase SC360, NKT Photonics, Denmark) with repetition rate of 60 MHz and pulse width of a few tens of picoseconds, was chosen as the illumination source. A Pellin Broca prism was used to spatially disperse the white light pulses, and a rotation of this prism allowed for wavelength selection. The spectrally selected light, with an average power of 0.5 to 5 mW, was then focused into a 50-μm core fibre. Due to prism dispersion, the bandwidth at the selected wavelength varied between 3 and 10 nm over the wavelength range of 600–1100 nm. A motorised, circularly variable, neutral-density filter (NDC-50C-2, Thorlabs, Germany) was placed in front of this fibre to adjust the power. A 1 × 4 fibre optic switch (Leoni, Germany) was employed to create 3 separate source points to facilitate multi-distance measurements. Light diffusely reflected by the sample, in this case, a specific location on the subject's abdomen, was then collected by a detector fibre bundle made of two 1-mm diameter step-index fibres bundled together on the sample side and coupled to two different detectors, to provide high responsivity over the entire wavelength range of interest: 1) A silicon photomultiplier SiPM (S10362-11-050C, Hamamatsu, Japan) with home-made front-end electronics[181], and 2) an InGaAs photomultiplier (H10330A-45, Hamamatsu, Japan). The signal from the detectors was processed by two time-correlated single photon counting (TCSPC) boards (SPC-130, Becker & Hickl, Germany) to produce the temporal point spread functions (TPSFs). A reference arm coupled the source light at the selected wavelength directly to the detectors shifted in time not to interfere with the sample response. This allowed for continuous monitoring of the instrument response and for compensating any temporal distortions or thermal drifts affecting the signal.

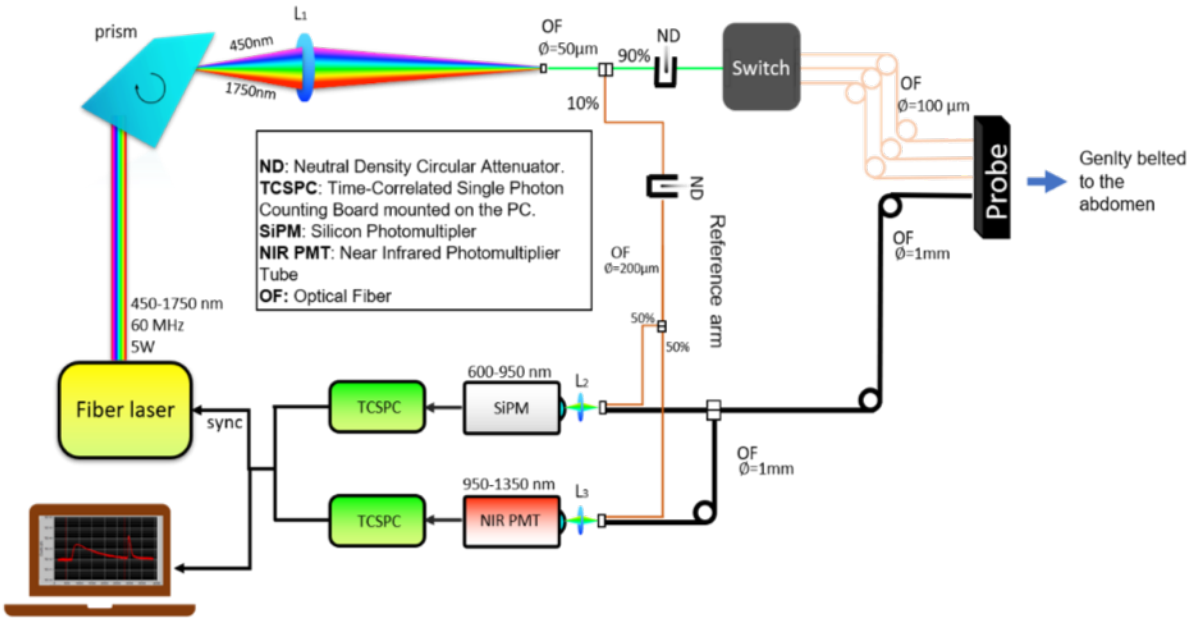

Figure 16: Scheme of the instrument [25]

The system has been extensively characterised following internationally agreed protocols[182][183] and proved to be reliable and accurate in its standard operating conditions[107]. The entire system operation and acquisition at multiple source detector separation was completely automated using proprietary software.

4.2.2 Data analysis: estimate of optical properties

A numerical method based on Monte Carlo (MC) simulations was employed to retrieve the absorption (μ_a) and reduced scattering (μ'_s) coefficients at a given wavelength[184]. First, a library of temporal point spread functions (TPSFs) for time resolved reflectance with different possible scattering coefficients and null absorption were generated using a CUDA (Compute Unified Device Architecture) accelerated MC code[185]. A linear interpolation between the generated data was performed to account for arbitrary reduced scattering coefficient values. To account for the absorption, these TPSFs were then multiplied by the Lambert–Beer exponential term:

$$\exp(-\mu_a v t)$$

where μ_a is the absorption coefficient, t is the photon time-of-flight and v is the speed of light in the medium. A Levenberg–Marquardt optimisation procedure was performed between the experimental data and this simulated curve after convolution with the

instrument response function (IRF) to determine the optical properties satisfying the best-fit conditions. The fitting range for the experimental data was chosen to be all the datapoints having counts greater than 80% of the peak value on the rising edge of the curve and greater than 1% on the trailing edge. Based on previous studies[186], this range offers a good balance between stability and accuracy of the fit. Also, it is the standard range selected in the validation of the instrument on reference solid phantoms[107] and adopted in several time-resolved reflectance studies. Absorption and reduced scattering spectra were then obtained by plotting the optical properties against their corresponding wavelength. The time required to retrieve the optical properties at a single wavelength was under 1 s.

4.2.3 Data analysis: estimate of tissue composition and scattering-related parameters

The absorption and reduced scattering spectra obtained from the fitting procedure described above could be exploited to evaluate key information regarding the tissue, such as tissue composition, blood parameters and information on the size and density of the scattering centres in the tissue. A linear combination of the extinction coefficient spectra of different chromophores and tissue constituents of the tissue, such as oxy (HbO_2) and deoxy (Hb) haemoglobin, water, lipid and collagen were fit to the absorption coefficient spectra, according to:

$$\mu_a(\lambda) = \sum_i c_i \varepsilon_i(\lambda)$$

where $\varepsilon_i(\lambda)$ is the specific absorption of the *i*th constituent at wavelength λ. The c_i retrieved from this equation represents the concentration of the *i*th constituent. The key absorbers mentioned above have been studied thoroughly and their specific absorption has been reported in the literature[187][188][189]. The total blood content was obtained from the concentration of the two blood parameters with the formula THb = Hb + HbO_2 and the oxygen saturation StO_2 = HbO_2 / THb.

Similarly, assuming that all the scattering events are caused by homogeneous spheres, an empirical model derived from Mie theory relates the wavelength dependence of the reduced scattering coefficient spectra to the size and the density of the scattering centres present in the tissue[76]:

$$\mu_s'(\lambda) = A(\lambda/\lambda_o)^{-b}$$

where λ_o is a reference wavelength (600 nm in this case) and A and b are the scatter amplitude and power parameters which correlate to the density and size of the scattering centres, respectively. These parameters are related to the tissue microstructure.

The just-described method is the conventional procedure for secondary fitting to retrieve the constituent concentrations, but a robust and more accurate procedure for time-resolved data has been developed by D'Andrea et al.[190]. This method evaluates the constituent concentrations and structural parameters directly from the raw experimental data (TPSFs) with a global fitting procedure that operates on data at all wavelengths simultaneously. The constituent concentrations and structural information presented in these two pilot studies were obtained by applying this method to our data.

4.3 Investigating adipose tissue optical properties: a first pilot study on the abdomen region

In order to characterize structure and composition of adipose tissue, a first study was performed on the abdomen region of 10 healthy male volunteers. TD-DOS measurements were performed to estimate optical properties and tissue composition, and information on the thickness of tissue layers was obtained from ultrasound measurements to better interpret the data. Further, for a better understanding of the in vivo measurements, and more generally of the physical problem under study, Monte Carlo simulations were performed assuming a simple three-layered model of the abdomen with the three layers being i) skin ii) SAT and iii) underlying muscle.

4.3.1 Subjects and experimental protocol

Ten adult male volunteers were recruited among the staff and students of Politecnico di Milano (Milan, Italy) and informed on the main study objective, the protocol of TD-DOS measurements and the safety of the instrument. A signature of informed consent was obtained. Data on general information like age, height and weight were collected. A commercially available portable ultrasound machine (Model E2exp, SonoScape, China) was used to estimate the thickness of the skin and SAT layers. *Table 3* summarizes the general anthropometric data for the ten subjects involved in the study. Approval was obtained from the Ethical Committee of Politecnico di Milano prior to the in vivo measurements.

Table 3 Demographics of the subjects involved in the study

Subject	Age (y)	Height (m)	Weight (kg)	BMI (kg/m^2)	Thickness (mm)	
					Skin	SAT
#1	53	1.75	67	21.9	1.8	24.6
#2	74	1.73	78	26.1	1.8	18.4
#3	25	1.91	87	23.8	1.6	17.0
#4	24	1.70	64	22.1	1.5	6.6
#5	37	1.80	76	23.5	1.9	14.3
#6	41	1.80	86	26.5	1.9	28.6
#7	48	1.83	100	29.9	2.1	35.0
#8	58	1.73	59	19.7	1.0	6.6
#9	38	1.78	74	23.4	1.7	4.1
#10	47	1.90	115	31.9	2.2	26.4

BMI = Body Mass Index | WC = Waist Circumference | Thickness = Thickness of the two layers measured by ultrasound imaging

Measurements were performed on the abdomen with the subject lying in supine position. The wavelength range of choice was 600-1100 nm with a step size of 10 nm, at the three inter fibre distances of 1, 2 and 3 cm. Five positions were tested: 2 cm left to the navel (2L); 4 cm left to navel (4L); 2 cm left and 2 cm below the navel (2L2D, D stands for down); 4 cm left and 2 cm down to the navel (4L2D); 8 cm left to the navel (8L). All distances were taken with reference to source 2 with the probe positioned in a direction perpendicular to the waistline with the detector downwards (*Fig. 17*). The total measurement time required to acquire the spectra at the three interfibre distances at one location was 5 minutes.

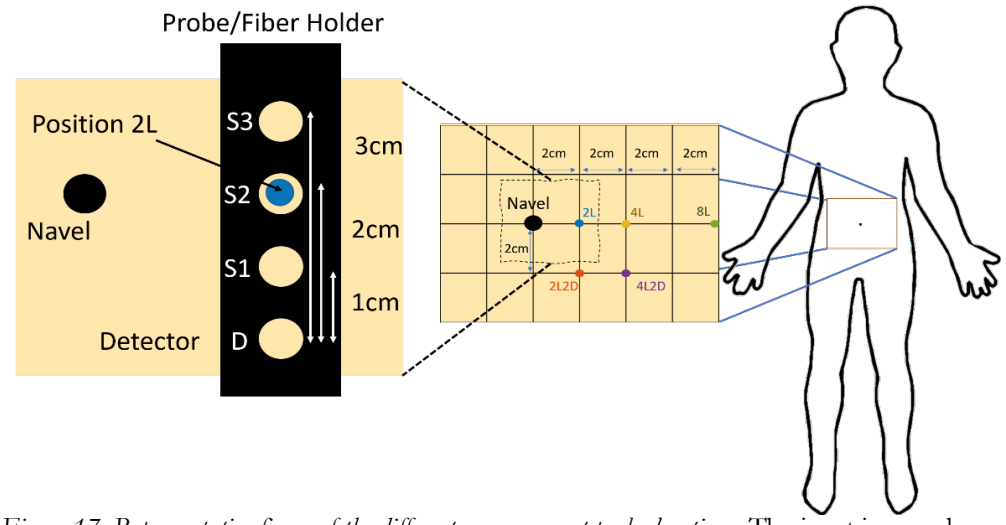

Figure 17. Representative figure of the different measurement probe locations. The inset image shows the positioning of the probe/fibre holder at a given measurement position (in this case 2L) [25]

4.3.2 Data for simulations

While the thickness of each of these layers was varied as described in the following paragraph, the base optical properties and constituent concentrations of the layers were fixed to values obtained from the literature. The average refractive index for the three layers was assumed to be constant over the wavelength range of interest and chosen to be 1.38 for skin[191], 1.44 for the SAT and 1.37 for muscle[192]. Regarding the optical properties spectra, the values for the skin or dermal layer were obtained from the literature [193], while those for the muscle were estimated assuming the constituent concentrations to be 14.5 g/dL of blood[194], 5% lipids, 80% water and 15% collagen[195]. Finally, SAT was assumed to comprise 95% of lipids and 5% water with negligible concentration of blood.

4.3.3 Results and discussion

As a first overview of the overall spectral variability, *Figure 18* shows the absorption (left) and reduced scattering (right) spectra of all the subjects at interfibre distance ρ = 2 cm in the same location (4 cm left of the navel). Clearly, there is wide variability, both in spectral features and in absolute values, mostly related to the heterogeneity of the abdomen and differences among subjects, as discussed in the following. Concerning the absorption spectrum, the key features are the absorption tail of haemoglobin – mainly Hb – in the region below 700 nm, the peak of Hb overlapped with a small water shoulder around 760 nm, the

clear peak of lipid at 930 nm with a second minor one around 1020 nm, and the water contribution around 980 nm. HbO_2 is definitely present, but less evident since its decreasing tail in the red is overcome by Hb, and the broad maximum around 900 nm is overlapped to the other sharper spectra. Upon decreasing the thickness of the upper layer (skin + SAT), the overall absorption increases with the marked contribution of water and blood as a clear sign that the muscle tissue is reached by the measurement.

For what concerns the reduced scattering spectrum, there are no distinct spectral features, as expected from the simple power-law dependence of μ'_s on wavelength for biological tissues in this spectral range[76]. Still, there is a large intersubject variability both in amplitude and in slope of the scattering spectrum.

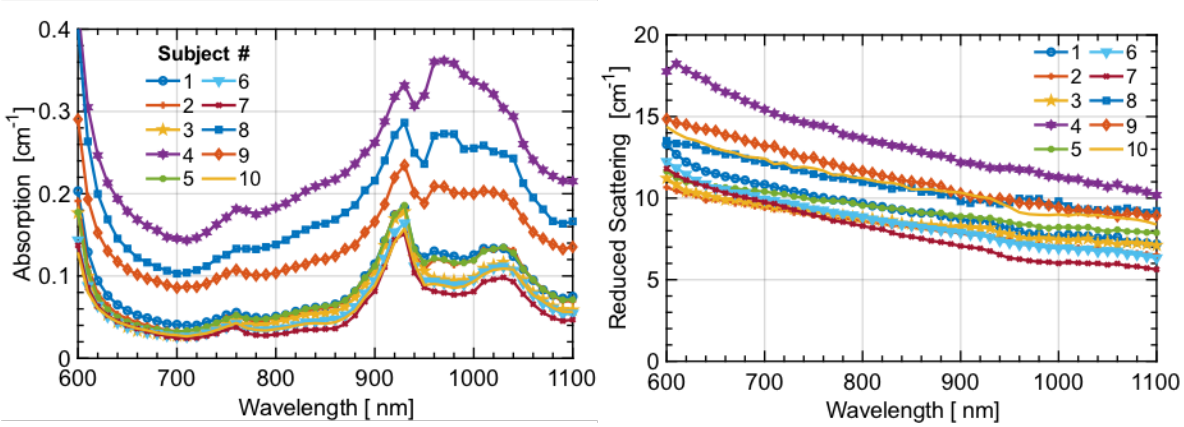

Figure 18. Absorption and reduced scattering spectra measured on the abdominal region of the 10 subjects enrolled in this study. The measurements were performed at a source detector separation ρ = 2 cm at a location 4 cm to the left of the navel. [25]

Figure 19 shows the absorption (top) and reduced scattering (bottom) spectra for the 3 interfibre distances again at 4 cm left of the navel from 3 representative subjects. For the absorption, basically two main effects are observed. The first, most obvious one, is the progressive increase in μ_a upon increasing ρ, (except for the region around 980 nm, where water contribution is dominant, as discussed below). This effect is evident in Subject #4 (centre) with possibly some minor hints also in the other two cases. It can be ascribed to the increased relevance of the muscle layer (with higher blood content) upon increasing ρ, and therefore to the larger probing depth.

What is more unexpected is the mild increase in μ_a around the water peak (980 nm) for the shortest ρ = 1 cm, as observed in Subject #1 (left) and #7 (right). Since a shorter ρ is more sensitive to shallower structures, the leading hypothesis attributes such an increase to the

contribution of the skin that is more hydrated (70%)[196] as compared to the underlying adipose tissue. Still, the relatively small thickness of this layer (*Tab. 3*) calls for some caution in a straightforward attribution. In fact, very thin superficial layers are not expected to affect much the temporal shape of the diffuse photon distribution, and consequently of the estimated μ_a. A deeper discussion of this interpretation was made with the aid of simulations.

The reduced scattering spectra display a clear increase in slope upon reducing ρ, for all subjects, also for the middle one where the SAT thickness is small. Again, increased relevance of the superficial layer (dermis) can be speculated due to the expected steepest scattering spectrum caused by collagen fibrils. In particular, a bi-component scattering spectrum is observed for Subject #1 (left) and #7 (right) for ρ = 1 cm, with the steepest slope in the red (<700 nm). This observation is consistent with the small dimension of collagen fibrils, which are expected to cause a behaviour close to Rayleigh scattering[197].

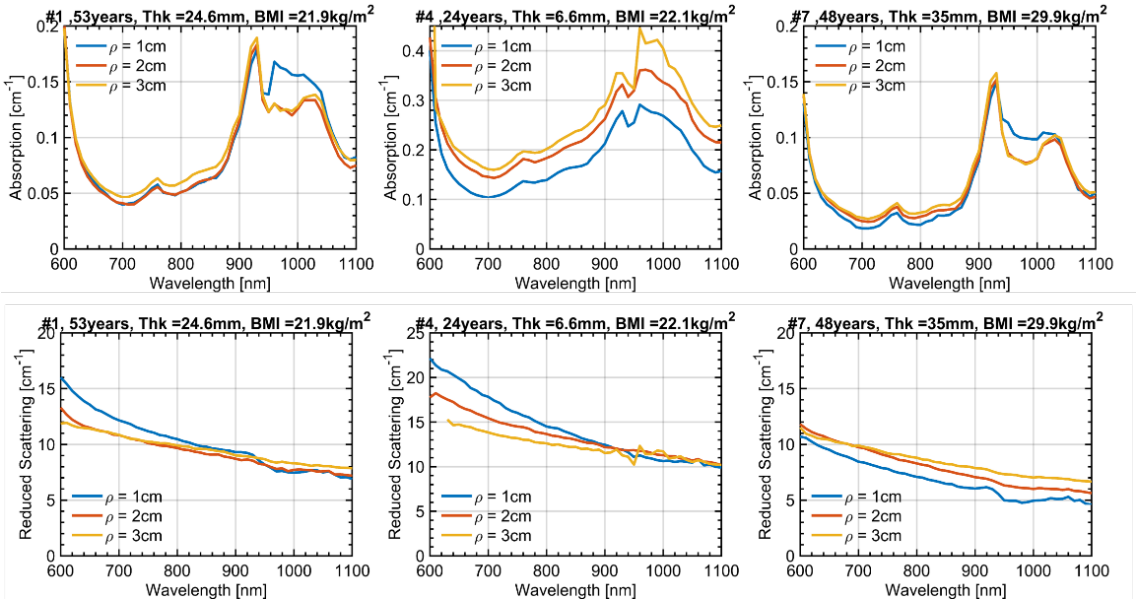

Figure 19. Absorption and reduced scattering spectra at the 3 interfibre distances ρ = 1, 2 and 3 cm. Results are presented for 3 subjects with further information about the subject in the title of each subplot (Age, Thk=Thickness of the SAT layer, and BMI). The measurement was taken 4 cm to the left of the navel. [25]

The variations in absorption (top) and reduced scattering (bottom) spectra for different locations on the abdomen are shown in *Figure 20* for 3 subjects, representative of the whole study, while spectra of all 10 subjects are reported in **Appendix A**. In general, all key spectral features are preserved for different locations on the same subject. Yet, some intra-subject variability is observed, which is more marked in the case of thinner adipose layer. In detail,

the coefficient of variation CV = (stdev/mean) is 5.2%, 4.0%, 11.0% for μ_a at 800 nm (left to right) and 3.9%, 14.1%, 5.4% for μ'_s. Considering the whole set of subjects, the median / max CV is 8.6% / 18.0% for μ_a and 6.6% / 18.1% for μ'_s.

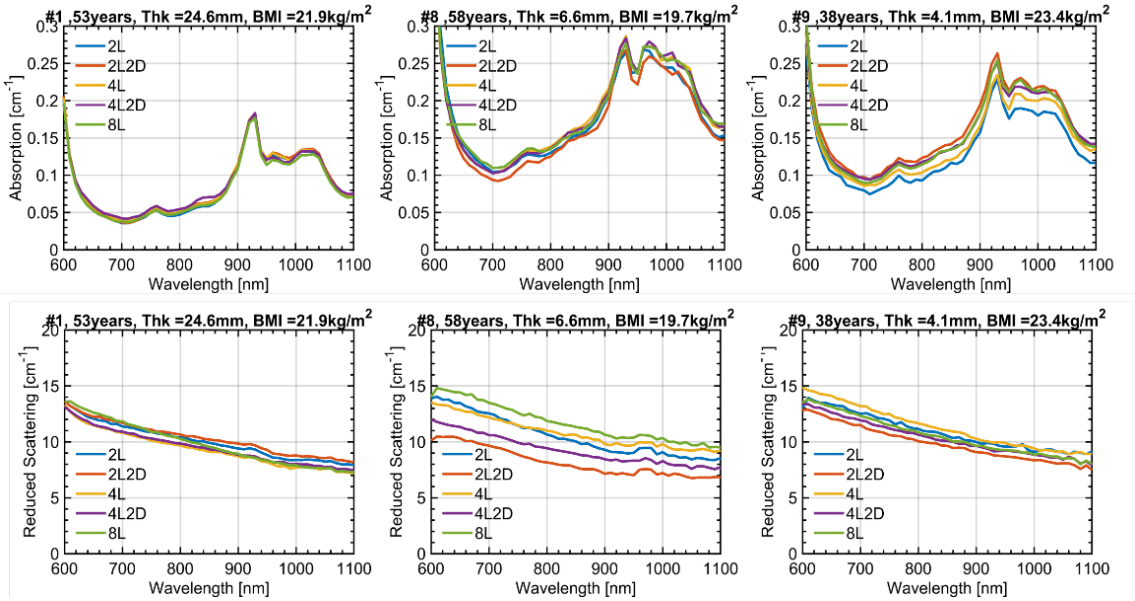

Figure 20. Absorption and reduced scattering spectra at 5 different locations in the abdominal region. The legend identifies the measurement position with reference to the navel. For example: (4L2D – corresponds to a point 4 cm to the left and 2 cm below the navel). Results are presented for 3 subjects with further information (Age, Thk=Thickness of the SAT layer and BMI) about the subject in the title of each subplot. For all the measurements ρ = 2 cm. [25]

From the comparison of the absorption spectra at the different measurement positions, no statistically significant differences were not found (Spectra and tables with statistics are included in **Appendix A**). Instead, some significant differences emerge from the analysis of reduced scattering coefficients at the different abdomen positions at ρ=2 and 3 possibly reflecting a different morphology of the tissue or they could result from increased sensitivity to a different thickness of the top layer at different locations (Spectra and tables with statistics are included in **Appendix A**). However overall the optical property retrieved from all measured points on abdomen didn't show differences of great entity and those denote similar features of the tissue examined in all positions tested.

The absorption and reduced scattering spectra were further analysed to retrieve the concentration of key absorbers (Hb, HbO_2, lipid, water, collagen) as well as the scattering amplitude and power (A, b). Results for all subjects and all ρ distances for the location 4 cm on the left of the navel are reported in *Table 4*. It is important to remind that the optical

properties were derived using a simple homogeneous tissue model. Due to the heterogeneous nature of the abdomen, these numbers are meant as averages over different volumes depending on the source-detector distance. Further, spectral distortion is expected due to different spatial sensitivity maps for different wavelengths. Therefore, these values must be taken with caution, not considering them as absolute reliable estimates but rather as indications of qualitative trends observed in the spectra.

The key observations made in the analysis of the spectra for different ρ are confirmed. In subjects where the SAT thickness is < 7 mm (#4, #8, #9) the total Hb content is high and increases for increasing ρ, as a clear indication that the muscle tissue is probed (THb > 30 μM for ρ = 3 cm). This is an expected effect and, of course, must be carefully considered when studying the adipose tissue to avoid contamination from the underlying muscle. For the very same subjects, also the collagen content is higher on average. Again, this could be attributed to the contribution of muscle, since collagen is the major structural protein in skeletal muscle[198]. Concurrently, we observe an increased background value, which is possibly ascribed to a missed collagen contribution (very flat and subtle spectral features) or to the inadequacy of the homogeneous model under such strong heterogeneous conditions.

The more unexpected contamination from the thin superficial skin layer seems to be confirmed, since in subjects with the greatest thickness (> 10 mm, that is all cases except the three subjects mentioned above) an increase in water content is observed for the shortest ρ, with the only exception of Subject #6 at ρ = 30 mm. For the previous 3 subjects, the muscle contamination is possibly dominant and overwhelms the water increase at a shorter ρ.

The comments on the scattering spectra are confirmed by the corresponding values (A, b) reported in *Table 4*. In fact, ρ = 1 cm always shows the highest value for b, supporting again the contamination of the skin. Indeed, b > 1 is an indication of steep scattering spectrum arising from small scattering centres as for collagen fibrils[197], whereas adipose tissue with large adipocytes (where a lipid droplet can represent up to 90% of the cell volume) exhibits a flatter (b < 1) spectrum.

In general, tissue oxygenation (StO_2) is unrealistically high because of a possible underestimation of Hb, which is actually often close to zero. This behaviour might be due to the line shape alterations of the absorption spectrum arising from spectral differences in the sampled volume or by inadequacy of the homogeneous model to deal with the clear heterogeneous structure.

Table 4. **Tissue composition, blood oxygenation, and scatter parameters for all the subjects at the three source detector separations for location at 4 cm to the left of the navel.**

Subject #	ρ cm	Hb μM	HbO_2 μM	THb μM	StO_2 %	lipid g/cm^3	water g/cm^3	collagen g/cm^3	bkg cm^{-1}	A cm^{-1}	b
1	1	0.83	10.83	11.66	93	0.955	0.216	0.090	0.001	14.5	1.26
	2	0.20	15.89	16.09	99	0.969	0.185	0.088	0.020	18.7	0.38
	3	0.13	14.40	14.53	99	0.884	0.141	0.075	0.019	13.7	0.44
2	1	2.86	5.29	8.15	65	0.664	0.221	0.000	0.010	12.0	1.21
	2	0.09	18.60	18.68	100	1.164	0.154	0.054	0.020	15.5	0.03
	3	0.07	16.14	16.21	100	1.188	0.043	0.071	0.015	12.3	0.52
3	1	2.89	4.90	7.79	63	0.605	0.197	0.000	0.010	13.6	1.08
	2	0.00	17.08	17.08	100	0.930	0.136	0.022	0.021	14.9	0.00
	3	0.23	15.56	15.79	99	0.977	0.085	0.030	0.015	12.2	0.43
4	1	0.33	33.30	33.64	99	0.994	0.281	0.140	0.036	22.2	1.56
	2	0.08	42.52	42.61	100	0.483	0.535	0.143	0.073	23.2	0.00
	3	0.05	50.25	50.30	100	1.247	0.291	0.205	0.084	18.9	0.24
5	1	2.84	5.52	8.36	66	0.690	0.236	0.000	0.010	15.0	0.83
	2	0.05	19.25	19.30	100	0.994	0.108	0.033	0.024	17.3	0.00
	3	0.01	18.11	18.12	100	1.046	0.57	0.043	0.019	13.1	0.29
6	1	2.90	4.72	7.63	62	0.574	0.185	0.000	0.010	12.4	1.42
	2	0.33	12.21	12.54	97	0.950	0.132	0.035	0.018	16.0	0.29
	3	2.66	6.62	9.28	71	0.720	0.286	0.000	0.011	11.8	0.67
7	1	2.90	4.69	7.59	62	0.568	0.182	0.000	0.010	10.3	1.41
	2	0.07	9.96	10.03	99	1.171	0.116	0.086	0.006	16.7	0.70
	3	0.15	7.89	8.03	98	1.085	0.106	0.077	0.003	12.9	0.74
8	1	2.02	32.19	34.21	94	0.811	0.010	0.056	0.031	15.7	1.07
	2	0.01	43.62	43.63	100	0.824	0.368	0.141	0.075	25.7	0.15
	3	0.74	40.71	41.46	98	0.899	0.202	0.133	0.060	15.6	0.18
9	1	0.27	15.89	16.16	98	1.028	0.145	0.132	0.002	18.0	1.48
	2	0.12	25.95	26.07	100	0.888	0.312	0.131	0.062	26.7	0.43
	3	0.00	30.24	30.25	100	0.997	0.203	0.143	0.049	16.0	0.36
10	1	2.90	4.76	7.66	62	0.583	0.186	0.000	0.010	18.6	1.37
	2	0.03	10.81	10.84	100	0.984	0.101	0.057	0.015	19.3	0.33
	3	0.02	8.51	8.53	100	0.985	0.075	0.059	0.008	13.7	0.51

THb = total haemoglobin content | StO_2 = oxygen saturation | bkg = wavelength independent value added as a fitting parameter to account for possible tissue absorbers not included in the fitting procedures and for limitations of the theoretical model.

The key trends observed in the in vivo measurements are I) increase in blood-related absorption for the largest ρ when the SAT is thin (< 7 mm); II) increase in water content for short ρ; III) increase in scattering slope for short ρ. The first effect is consistent with the

probing of muscle tissue, while the other two with a contribution from the skin. Since this latter statement is less obvious, we ran a set of Monte Carlo simulations on possible scenarios in order to corroborate our hypothesis. We tried to match as much as possible the measurement conditions (e.g., convolution with the IRF, number of counts, geometry) and analysis (homogeneous model, fitting range) so as to closely replicate the experiment. As for the tissue structure (layers) and optical properties, we inferred values from the literature or from realistic assumptions, as described in section 4.3.2 (*Fig.* 21). Four possible scenarios are considered, spanning all combinations of thin (15 mm) and thick (40 mm) SAT layer with thin (1 mm) and thick (3 mm) skin.

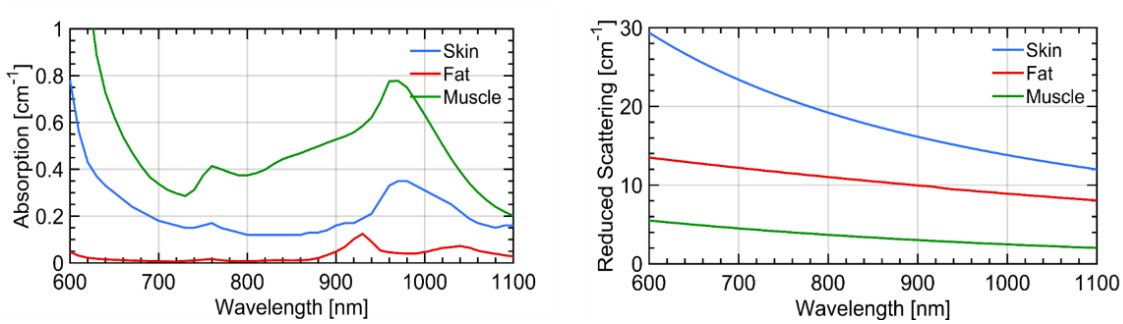

Figure 21. Absorption (left) and reduced scattering (right) spectra of the three primary layers of the abdominal tissue (namely skin, SAT and underlying muscle) used in the simulation studies. [25]

The resulting fitted absorption and reduced scattering spectra are displayed in *Fig. 22* and *Fig. 23*, respectively. The increase in absorption due to the underlying muscle for a thin fat layer is confirmed [*Fig. 22(c) and Fig. 22 (d)*]. The water contribution from the skin arising at ρ = 1 cm is consistent with a skin thickness of 3 mm [*Fig. 22(b)*] and is possibly masked for the same skin thickness when the muscle is visible [*Fig. 22(d)*], similarly to what observed in vivo.

Finally, the increase in scattering slope for ρ= 1 cm, possibly due to skin collagen, is definitely observed for any skin thicknesses when the fat layer is thick enough to isolate from the muscle. Instead, contamination from the muscle is masking this effect for thin fat layers.

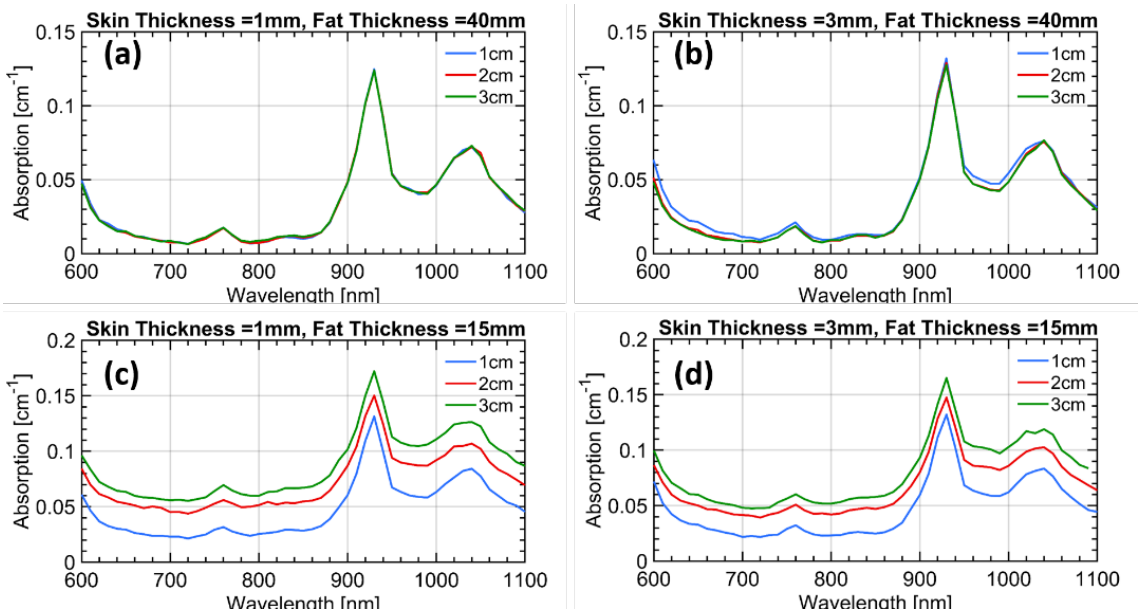

Figure 22. Absorption spectra at the three inter-fibre distances retrieved from the simulations for the four different combinations of layer thicknesses. The assumed thickness of the first two layers in each case is mentioned in the title of the corresponding subplot. The third layer was assumed to be infinitely thick in all cases. [25]

Overall, the simulations confirm the proposed hypothesis that the superficial skin yields a tangible effect in the in vivo measurements at least for a thickness of 3 mm or greater. Surely, these simulations are derived using simplified assumptions on the geometry and using literature data for the estimate of layered absorption. Still, they provide an indication of the plausibility of our interpretation. Indeed, the *in vivo* effects both on the water increase and on the scattering slope seems to be stronger than what predicted based on literature information. This may suggest either that the skin thickness is larger than 3 mm or that the skin scattering is higher than the values depicted in *Fig. 21*.

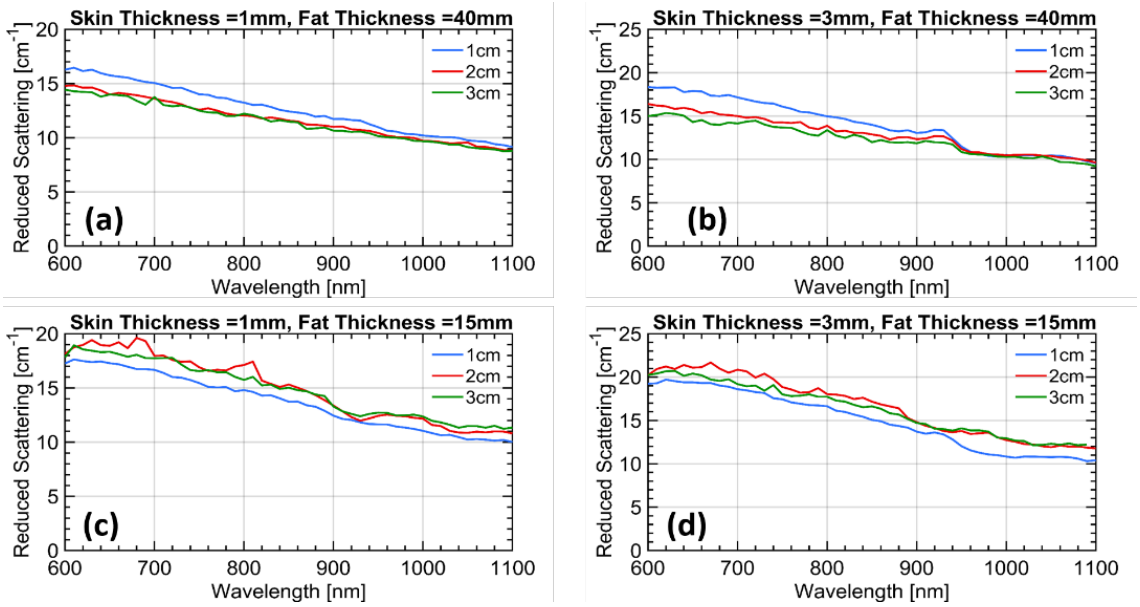

Figure 23. Reduced scattering spectra at the three inter-fibre distances retrieved from the simulations for the four different combinations of layer thicknesses. The assumed thickness of the first two layers in each case is mentioned in the title of the corresponding subplot. The third layer was assumed to be infinitely thick in all cases. [25]

Incidentally, while these findings make data interpretation more complex, they also indicate that time domain diffuse optical spectroscopy is sensitive enough to skin properties and could be studied more specifically for the non-invasive in vivo sensing of skin properties, such as hydration or collagen content.

4.4 The influence of the tri-layered nature of biological tissues and gender on optical property: a second pilot study on healthy male and female

A second study has been conducted on 26 adult volunteers in order to better understand the capacity of TD-DOS technology in characterising structure and components of subcutaneous adipose tissue and muscle and in investigating gender differences and how they may affect the potential of the technique for diagnostic purposes.

4.4.1 Subjects and measurement protocol

26 adult male and female volunteers were recruited among the staff and students of Politecnico di Milano (Milan, Italy) and informed on the main study objective, the protocol of TD-DOS measurements and the safety of the instrument. One male subject (#20) was excluded from the *vastus lateralis* measurement due to a knee problem. A signature of

informed consent was obtained. Approval was obtained from the Ethical Committee of Politecnico di Milano prior to the in vivo measurements.

Data on general information like age, height and weight were collected for each subject at the recruitment.

A commercially available portable ultrasound machine (Model E2exp, SonoScape, China) was used to estimate the thickness of the skin and SAT layers (*Fig.24*).

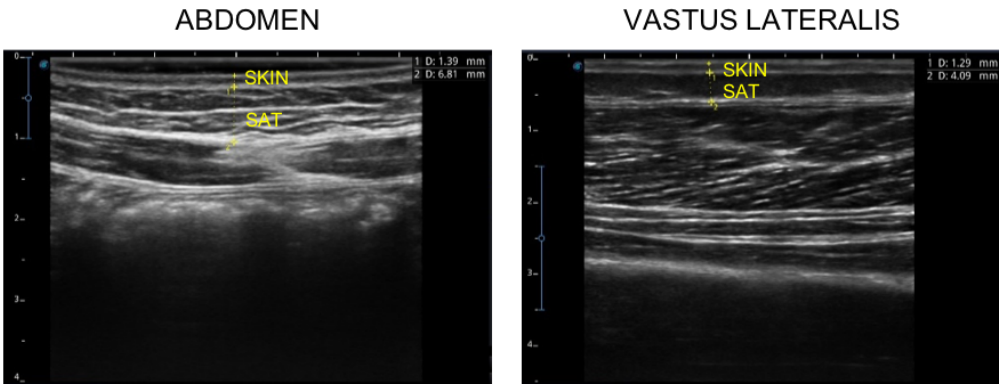

Figure 24. Representative images obtained with ultrasound machine from abdomen and vastus lateralis regions.

In the analysis of the gender differences in the concentration of the tissue constituents, only normal BMI volunteers (18<BMI<25) are considered; then #10 (overweight); #14 (obese; BMI>29); #24 (underweight) are excluded in order to study the mere inter-gender variability and to remove a possible confounder which affects SAT. Considered that, it is good to underline that the recruited population (without the outliers already mentioned) is BMI- and age-matched between male and female groups (*Fig. 25*).

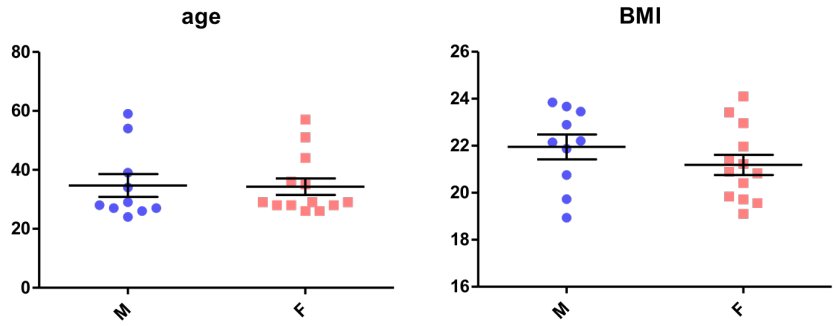

Figure 25. Age and BMI comparison between male and female groups.
Statistical analysis was performed with Student's t test. Error bars represent SEM; n=10 male, n=13 female

Table 5 **summarises general and anthropometric data for the twenty-six subjects involved in the study**

Subject	Gender	Age (y)	BMI (kg/m²)	ABD 4L Thickness (mm)		ABD 4R Thickness (mm)		VL Thickness (mm)	
				Skin	SAT	Skin	SAT	Skin	SAT
#0	M	54	22.2	1.6	20.7	2.6	22.9	1.6	2.7
#1	M	24	22.1	1.8	6.0	1.3	6.7	1.2	9.0
#2	F	26	20.9	1.7	10.5	1.6	9.3	1.3	4.0
#3	M	27	23.5	1.9	6.1	1.7	5.0	1.4	4.0
#4	M	26	23.8	1.8	19.1	1.8	21.3	1.3	11.0
#5	M	29	20.8	2.3	6.5	2.0	6.4	1.0	4.8
#6	M	28	19.7	1.0	7.7	1.9	6.1	1.3	6.8
#7	F	29	23.4	1.7	15.6	1.9	19.9	1.9	5.8
#8	F	29	23.0	1.3	10.6	1.3	11.0	1.1	11.9
#9	M	34	23.7	2.0	12.2	1.9	11.9	1.2	9.4
#10	M	76	25.4	1.7	16.8	1.8	16.2	1.2	5.3
#11	F	36	22.0	1.3	11.5	1.3	10.8	0.9	7.6
#12	M	27	21.9	1.7	22.7	1.9	22.0	1.1	6.4
#13	F	44	19.6	1.2	12.5	1.2	11.8	1.2	11.8
#14	M	48	30.5	2.7	28.7	2.5	30.2	2.5	30.2
#15	F	29	20.8	1.4	7.8	1.4	6.6	1.4	6.6
#16	F	57	19.1	1.4	8.0	1.3	9.0	1.3	9.0
#17	M	59	18.9	1.3	7.0	1.4	7.9	1.4	7.9
#18	F	28	21.2	1.3	11.0	1.3	11.0	1.3	11.0
#19	F	35	20.4	1.2	9.7	1.3	9.8	1.3	9.8
#20	M	39	22.9	1.2	14.7	1.3	18.1	n.a	n.a.
#21	F	51	21.4	1.3	8.0	1.4	6.0	1.4	6.0
#22	F	26	19.8	1.2	5.7	1.1	8.5	1.1	8.5
#23	F	28	19.7	1.7	5.2	1.5	6.6	1.5	6.6
#24	F	50	17.4	1.4	6.5	1.3	5.6	1.3	5.6
#25	F	28	24.1	1.2	16.6	1.3	19.6	1.3	19.6

BMI = Body Mass Index | Thickness = Thickness of the two layers measured by ultrasound imaging | ABD = abdomen | VL = vastus lateralis

Measurements on the abdomen were performed with the subject lying in supine position while measurements on the thigh with the subject seat on a chair (right leg at 90° position). The wavelength range of choice was 600-1100 nm with a step size of 10 nm, at the three interfibre distances of 1, 2 and 3 cm. Two positions were tested on the abdomen region: 4 cm left to the navel (4L); 4 cm right to navel (4R). For the thigh measurement one position was tested: one-third of the femoral length (hip to knee) measured from the knee on the right *vastus lateralis* muscle. All distances were taken with reference to source 2 with the probe positioned in a direction perpendicular to the waistline with the detector downwards (*Fig.26*).

The total measurement time required to acquire the spectra at the three interfibre distances at one location was 5 minutes.

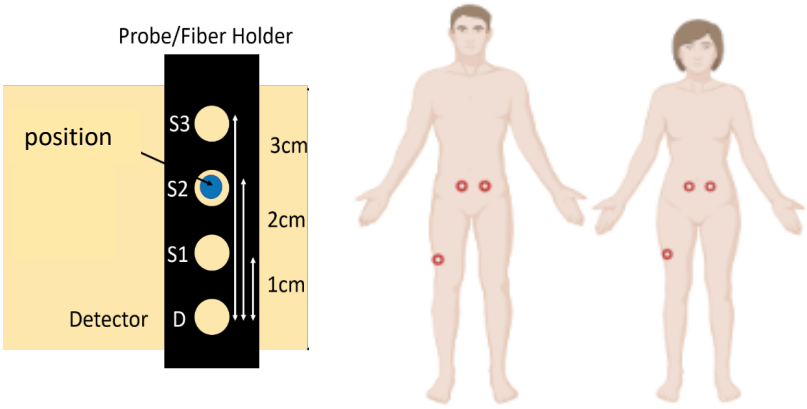

Figure 26. Representative figure of the different measurement probe locations: 4 cm left to the navel (4L); 4 cm right to navel (4R); one-third of the femoral length measured from the knee on the *vastus lateralis* muscle

4.4.2 Results and discussion on the abdomen region

The resultant absorption spectra for the abdominal region for both subject groups (male and female) at all the source-detector separations (ρ) are dominated by the lipid peak at 930 nm (*Fig. 27*). Moreover, an increase in absorption is evident over the entire spectral range with increasing ρ. This phenomenon possibly suggest that the muscle is reached by the measurements confirming the result the first pilot study.

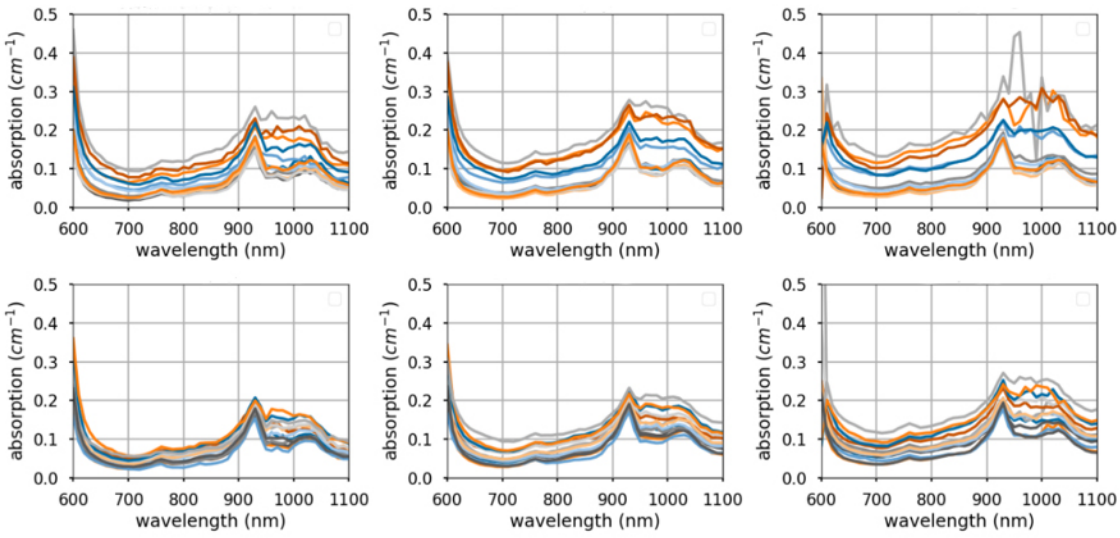

Figure 27. Absorption spectra. Inter-subject variation in the broadband absorption in males (top row) and in females (bottom row) of the position 4L on the abdomen at

three different source-detector distances, ρ = 1 cm, ρ = 2 cm ρ = 3 cm from left to right.

The distinctive shape of the reduced scattering (*Fig. 28*) at ρ = 1 cm (larger slope, higher initial value) is assumed to be a consequence of the influence of the (collagenous) dermal layer on the recovered optical properties at short ρ. Thus, this second pilot study confirms that both in males and females the three layers have a significant influence on the recovered optical property spectra at different ρ in the case of the abdominal region.

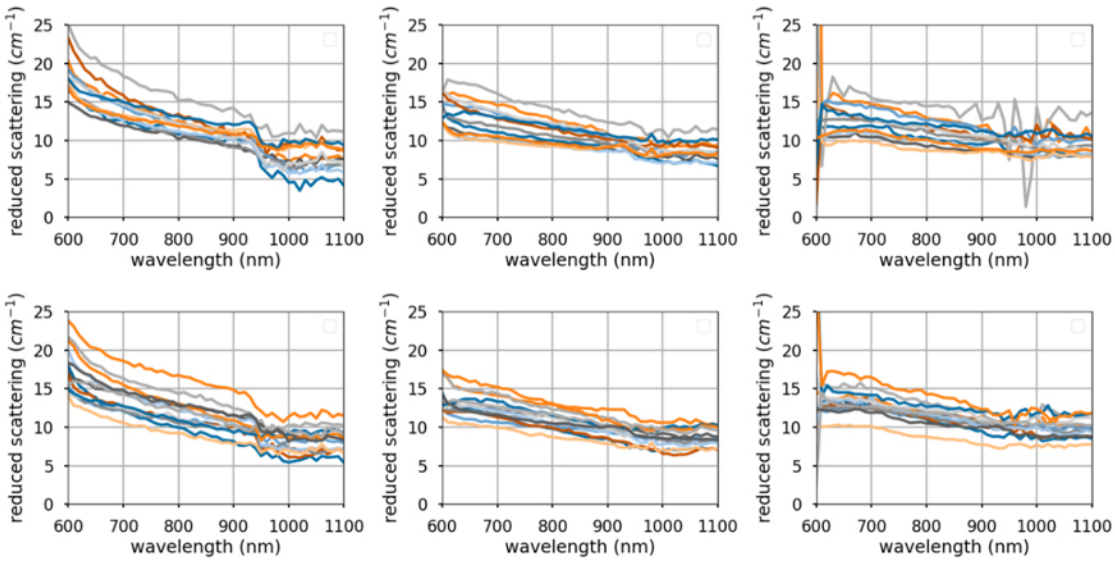

Figure 28. Reduced scattering spectra. Inter-subject variation in the broadband reduced scattering spectra in male (top row) and female (bottom row) of the position 4L on the abdomen at three different source-detector distances ρ = 1 cm, ρ = 2 cm ρ = 3 cm from left to right.

From the analysis of the three interfibre distances dataset from all the subjects at each position, differences were found in absorption between ρ=1 and 3 but not between ρ=1 and 2 and ρ=2 and 3 (Spectra and tables with statistics are included in **Appendix B**). This corroborate the necessity of a second step of analysis with a multilayered model.

The retrieved concentrations of key tissue chromophores (Hb, HbO_2, lipid, water, collagen) as well as the scattering amplitude and power (A, b) are reported in **Appendix** B.

In accordance to the increase in absorption with increasing ρ, emerges from the analysis an augmentation of the HbO_2 content resulted in both males and females with the depth of probing (*Fig. 29*). Furthermore, no statistical differences were observed in lipid and water content between males and females. Supporting these data, from ultrasound measurements,

no statistical differences between male and female were found in SAT thickness in the measurement positions on the abdomen region (*Fig. 30*).

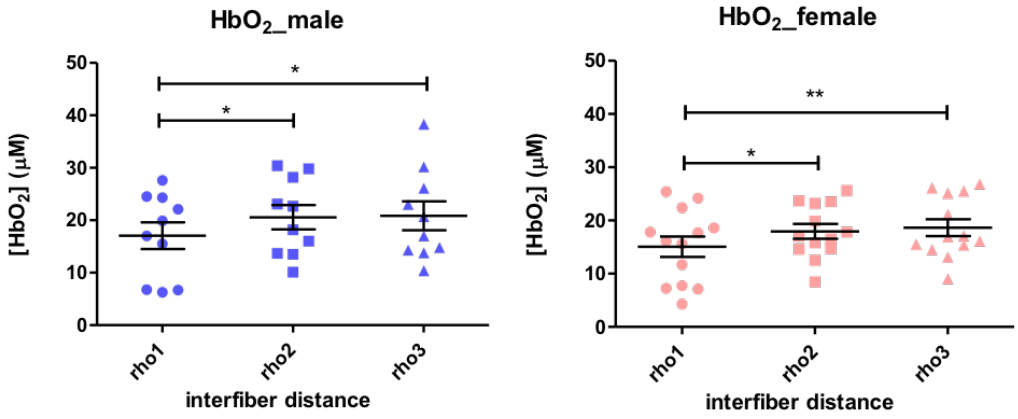

Figure 29. differences in HbO_2 content with ρ in both male and female at 4L position. Statistical analysis was performed with one-way ANOVA and Bonferroni's multiple comparison test. Error bars represent SEM; n=10 male, n=13 female; *p < 0.05, **p < 0.01.

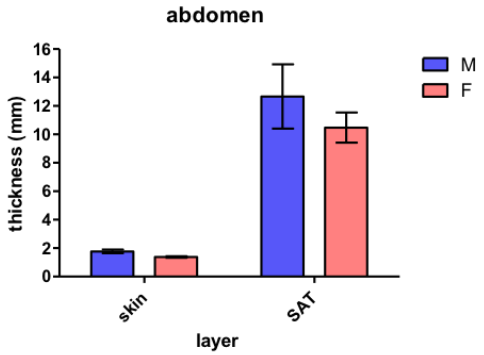

Figure 30. *Skin and SAT thickness from abdomen measurements with US instrument.* Mean values from right and left positions. Statistical analysis was performed with two-way ANOVA and Bonferroni's multiple comparison test. Error bars represent SEM; n=11 male, n=13 female.

Further, the trend of A and b scattering parameters confirmed the result obtained in the previous study and corroborates the skin contamination effect (*Fig.31*). No significative differences in these scattering parameters were found between male and female.

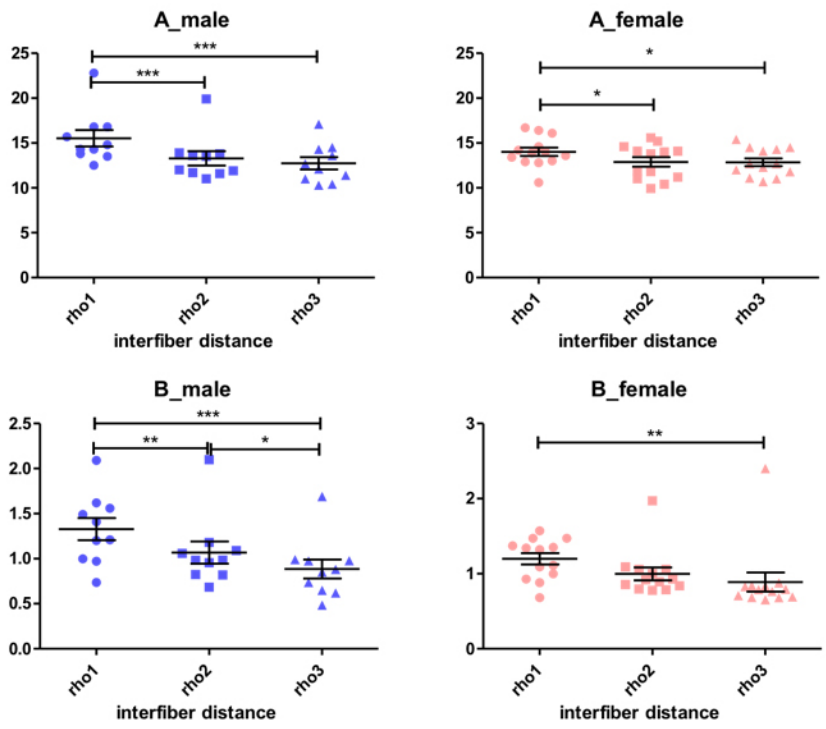

Figure 31. A (row above) and b (row below) scattering parameters difference with ρ in both male and female at 4L position. Statistical analysis was performed with one-way ANOVA and Bonferroni's multiple comparison test. Error bars represent SEM; n=10 male, n=13 female; *p < 0.05, **p < 0.01, ***p<0.001.

4.4.3 Results and discussion on the thigh region

From the comparison of the absorption and reduced scattering spectra at the three different measurement positions from all the subjects, no statistically significant differences were found between left and right positions on the abdomen, while the differences between the two positions on the abdomen and the *vastus lateralis* position are well appreciated at all interfibre distances (Spectra and tables with statistics are included in **Appendix B**). This is obviously related to the different nature of these tissues. In particular, it is evident how the absorption coefficients of the *vastus lateralis* are higher than those of abdomen subtending higher values of haemoglobin and water in this region.

From the analysis of the interfibre differences at each position from all the subjects differences were found in absorption between ρ=1 and 3 and between ρ=1 and 2 (Spectra and tables with statistics are included in **Appendix B**). Similarly to what was previously mentioned for the abdomen, this corroborate the necessity of a second step of analysis with a multilayered model.

The results from the measurements on the *vastus lateralis* muscle of male subjects show significantly higher absorption in the red spectral region, which can be ascribed mostly to haemoglobin, relative to the abdomen (*Fig. 32*). In the male population, for all the three source-detector distances we observe a strong peak at 980 nm, corresponding to the water absorption, which often dominates lipid absorption at 930 nm. Differently, on average, apart from the contribution of haemoglobin at short wavelengths, the data on the female population resemble the spectrum of lipids, with major absorption at 930 nm and a secondary peak around 1020-1030 nm.

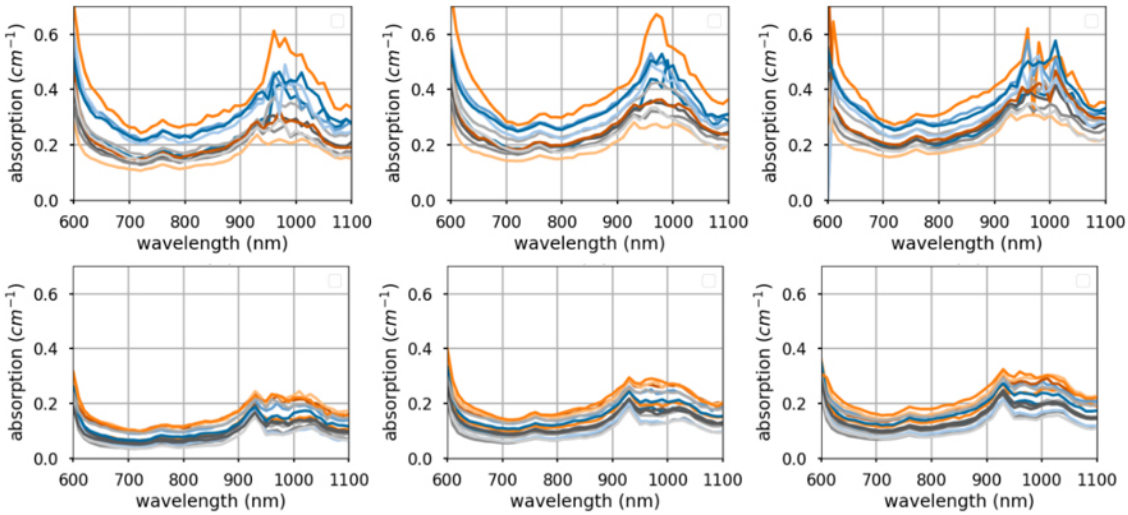

Figure 32. Absorption spectra. Inter-subject variation in the broadband reduced scattering spectra in male (top row) and female (bottom row) of the thigh position at three different source-detector distances $\rho = 1$ cm, $\rho = 2$ cm $\rho = 3$ cm from left to right.

Further, the reduced scattering spectra for women volunteers, in particular at source-detector distances of 2 and 3 cm, are flat relative to the male spectra (*Fig. 33*). An expected flatter spectrum in adipose tissue is ascribed to the bigger dimension of adipocytes relative to myocytes. This phenomenon possibly suggests that in the *vastus lateralis* region the volume being probed is mainly adipose (subcutaneous fat) and the underlying muscle is not effectively reached by the measurements in female subjects.

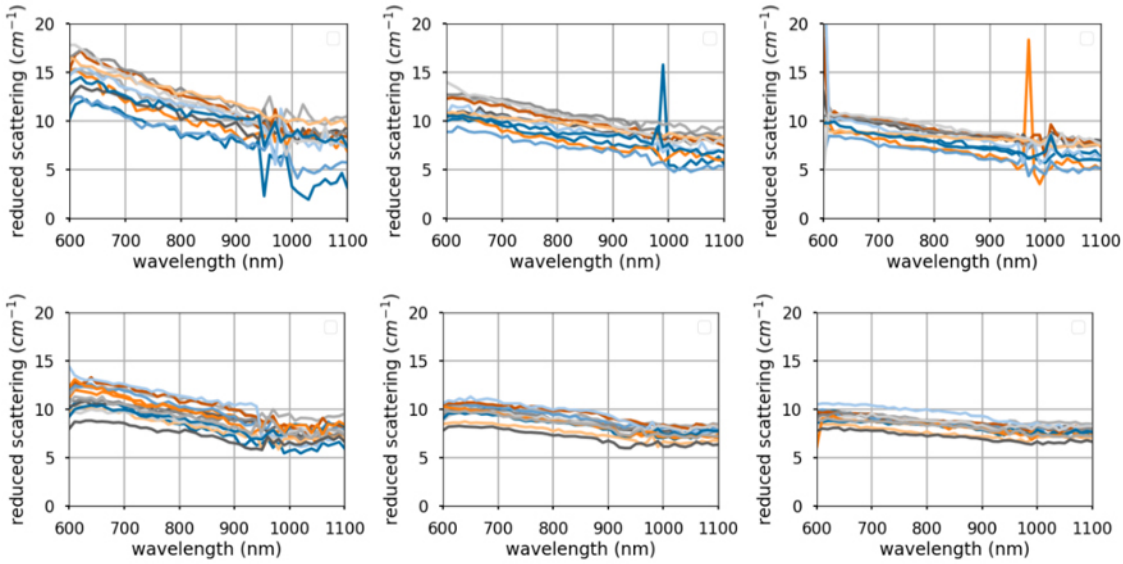

Figure 33. Reduced scattering spectra. Inter-subject variation in the broadband reduced scattering spectra in male (top row) and female (bottom row) at the *vastus lateralis* position at three different source-detector distances ρ = 1 cm, ρ = 2 cm ρ = 3 cm from left to right.

The retrieved concentrations of key tissues chromophores (Hb, HbO_2, lipid, water, collagen) as well as the scattering amplitude and power (A, b) are reported in **Appendix B**.

The results already mentioned are consolidated by the fact that the thickness of the fat layer in this region (measured using an ultrasound imaging system) is on an average lower for the male volunteers compared to the female ones (*Fig.* 34) and also by the fact that from the analysis of the constituents were found significant differences in lipid and water content at all the 3 source-detector distances between male and female (*Fig. 3*5).In particular, a significantly higher water content in males and lipid content in females were found. This is in accord with the literature showing that the lipid storage compartments are gender-affected, with most fat deposition in the gluteal–femoral region in women.[165]

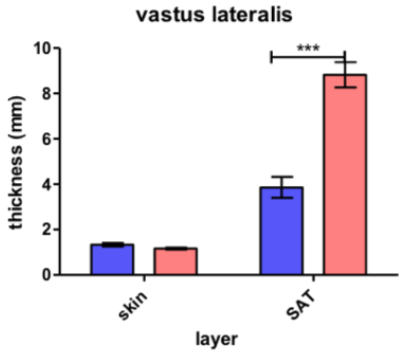

Figure 34. Skin and SAT thickness from vastus lateralis measurements with US instrument. Statistical analysis was performed with two-way ANOVA and Bonferroni's multiple comparison test. Error bars represent SEM; n=10 male, n=13 female; ***p < 0.001

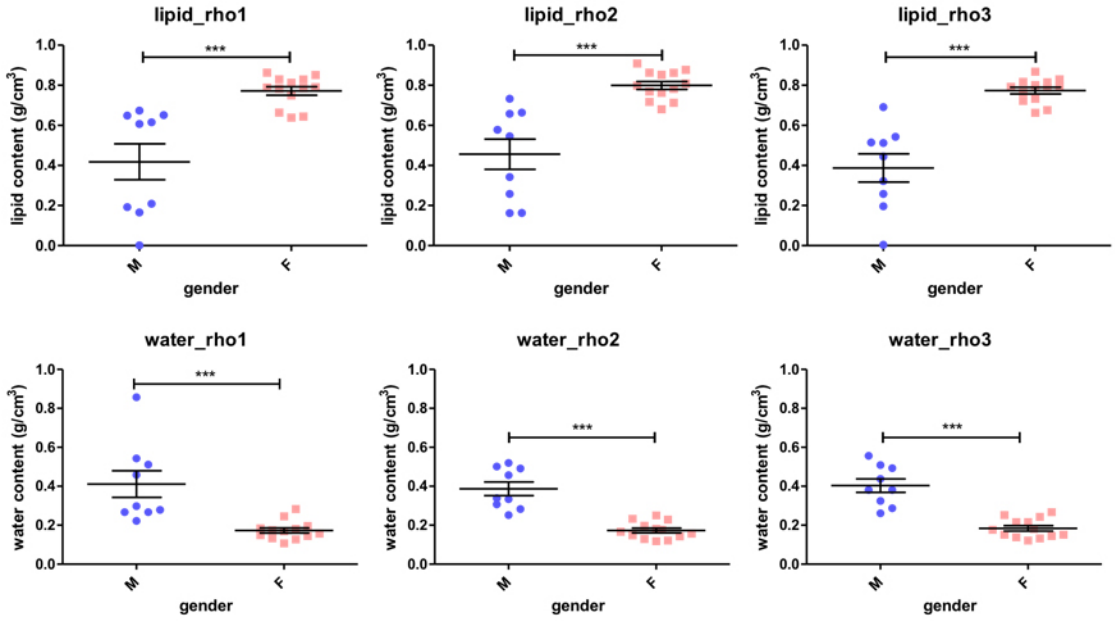

Figure 35. Lipid (row above) and water (row below) content in both male and female on vastus lateralis position at all the 3 ρ. Statistical analysis was performed with one-way ANOVA and Bonferroni's multiple comparison test. Error bars represent SEM; n=10 male, n=13 female; ***p < 0.001.

In addition, sex differences in collagen content (*Fig. 36*) were found at all the 3 ρ, and this might come from the fact that the muscle (more collagenous relative to fat) was better reached by the measurements in male than in female subjects. Another hypothesis is that this gender-related difference in collagen content might be due to the diverse collagen organisation in male and female previously mentioned in literature [166].

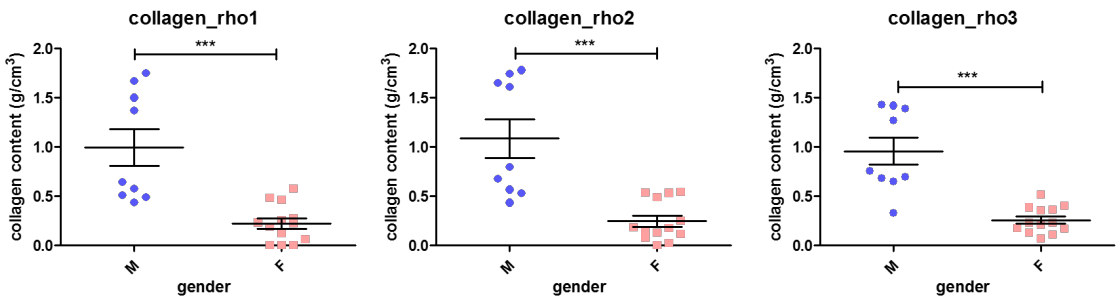

Figure 36. *Collagen content in both male and female at vastus lateralis position.* Statistical analysis was performed with one-way ANOVA and Bonferroni's multiple comparison test. Error bars represent SEM; n=10 male, n=13 female; ***$p < 0.001$.

4.5 Limits

The present results on tissue composition were derived by interpreting the experimental data with a simple homogeneous model; a preliminary step of analysis, which allowed us to observe the effects the different tissue' layers on the retrieved optical properties. This step brought out the need to adopt a multi-layered model. A more advanced analysis including multi-layered geometries could provide more reliable quantitative results on abdomen and thigh regions. Still, the retrieval of 3-layer properties with proper accuracy is not straightforward due to the risk of overfitting the data yielding unreliable results. Therefore, the validation of spectral multi-layered approaches is ongoing for a second-level analysis of the experimental dataset.

Preliminary TD-DOS measurements also permitted to test the designed protocol for the clinical trial in elderly sarcopenic subject evaluations.

4.6 Conclusions

In conclusion, we have investigated the optical spectroscopy of the abdomen and *vastus lateralis* regions in vivo using time domain broadband diffuse optics at 3 source-detector distances (ρ). Wide inter-subject variability was observed related to the specific subject's constitution. From the first pilot study upon changing ρ, three effects were observed, that is: i) the increase in the overall tissue absorption at the largest ρ = 3 cm, when the superficial adipose tissue thickness is < 8 mm, suggesting that the muscle is reached by the measurement; ii) the increase in water absorption for the shortest ρ = 1 cm); and iii) the

increase in the scattering slope again for the shortest ρ. All these findings are consistent with a 3-layer model of the abdomen comprising the skin, the adipose tissue, and the underlining muscle.

Secondly, we evaluated the capacity of time-domain diffused optical spectroscopy (TD-DOS) technology in the context of pilot studies in healthy volunteers on abdomen and thigh (*vastus lateralis*) regions in order to characterise structure and components of subcutaneous adipose tissue and muscle. From the second pilot study five effects were observed, that is: i) a gender difference in the absorption and reduced scattering spectra both on the abdomen and *vastus lateralis* regions, with a flatter absorption and reduced scattering spectra for female subjects at all the three ρ; ii) the HbO_2 content has an increasing trend with ρ both in male and female on abdomen region and this is might correlate with muscle probing at deeper depth; iii) a confirmation of the skin contamination effect on the abdomen obtained from the first study; iv) in the *vastus lateralis* region the volume being probed is mainly adipose and probably the underlying muscle is not effectively reached by the measurements in female; v) lipid, water and collagen content at all the 3 source-detector distances in *vastus lateralis* region differ between male and female supporting the hypothesis that muscle is reached only in male subjects. Previously mentioned evidence [165] [166] report substantial structural sex-differences in SAT layer and could explain the founded differences.

A proper optical investigation of the adipose tissue should cope with this multilayer structure in order to properly disentangle true fat properties from contamination from the skin or the underlying muscle.[25]

It is also important to underline that the tissue chromophores are more than those investigated through the analyses carried out in the studies presented in this thesis; it could therefore be interesting to evaluate others. In particular, since previous studies[199] have shown the possibility of discriminating the spectra of haemoglobin and myoglobin, it could be interesting try to evaluate the myoglobin content. However, the myoglobin content in the patients of our studies (elderly sedentary sarcopenic) could be very low. This additional assessment could therefore be difficult to implement reliably in our analyses.

In the era of personalised and precision medicine, increasing our knowledge on adipose tissue and muscle might enable us to overcome the limitations of the traditional anthropometric indices of obesity and sarcopenia. The availability of a non-invasive technique to monitor adipose tissue status in response of nutrition, lifestyle habits or medical

treatment is fascinating for the possibilities of providing feedback and non-invasive insight. Diffuse optics is a potentially powerful option, also in view of the wealth of information it can provide – related to both tissue composition and microstructure. Yet, a preliminary understanding of the origin of optical measurements is a prerequisite for proposing diffuse optics in clinical studies. The present work sets a first observational ground on fat and muscle spectroscopy, clearly identifying the next step to provide an accurate and quantitative optical characterisation of adipose and muscle tissues. The insights obtained from these pilot studies will be used to optimize both measurement protocol and data analysis methodology for a clinical study aimed at monitoring the physical frailty in older people.

5 The MAYBE Sarco-Ob clinical trial: current status and future perspectives

Geriatric clinicians and basic gerontology researchers' efforts to identify appropriate interventions to prevent the frailty syndrome of the elderly are hampered by the lack of a single standardized and universally accepted operational definition for this condition. A critical point remains the great variety of clinical phenotypes that make it challenging to define diagnostic tools useful to support the diagnosis, monitor the disease's progression over time, and verify the efficacy of therapeutic interventions[10]. Although various clinical-diagnostic definitions have been proposed so far, identifying a panel of multidomain biomarkers could bring a significant advance in this context [10]. In particular, recognizing sarcopenic individuals at risk of physical frailty before the functional decline reaches a critical threshold - beyond which recovery is not possible - is an essential step in a prevention perspective.

No specific drugs have been approved for the treatment of sarcopenia and physical frailty. Recent systematic reviews and meta-analyses focused on pharmacological interventions to improve muscle mass, strength, and physical performance in older people. A few pharmacological interventions emerged, including hormonal therapies such as testosterone, but caution should be taken regarding their safety profile. The majority of studies failed to identify the baseline sarcopenia status, so the findings could only be generalized to older people rather than sarcopenic or frail patients[19].

The MAYBE project (as described in Chapter 2) aims to respond to this ambitious purpose thanks to the multidisciplinary effort involving researchers from different disciplines and geriatric clinicians. In the context of my PhD work, the last two steps should have been: i) the investigation of the TD-DOS techniques as a novel non-invasive diagnostic tool in sarcopenic and sarcopenic obese elderly subjects; and ii) the translation of the results obtained during our preclinical studies into an interventional clinical trial aimed at evaluating the effects of the PD-0E7 mixture, in combination with diet and exercise training, in elderly sarcopenic obese patients. The TD-DOS techniques should have been applied to monitor the therapeutic response.

The COVID-19 pandemic has created cumbersome disruptions to clinical research worldwide, severely affecting the possibility to conduct trials in safe and effective ways[200]. *This situation is especially true when considering trials recruiting vulnerable subjects. The slowdown or cancellation of trials negatively impacts early career researchers*[200].

The Ethical Committee approved the protocol of the TD-DOS sub-study of the MAYBE clinical trial in November 2019. Recruitment of patients had just begun when the trial had to be interrupted at the end of February 2020. Brescia and Verona belong to Italian regions (Lombardy and Veneto) heavily affected by the COVID-19 pandemic. Geriatricians of Verona University were pulled away from the clinical trial to work in COVID-19 medical care. To date, the enrolment of new patients has not been restarted yet. Notably, subjects to be recruited are at particular risk of severe outcome if undergoing SARS-CoV-2 infection, being of advanced age[201] *and obese*[202][203].

Accordingly, the schedule of my PhD program had to be revised and adapted to the circumstances. Below is reported the original plan of the MAYBE clinical study to be reconsidered as a future perspective.

5.1 Experimental plan

The trial is an open-label, randomized study. Participants, on a low-calorie diet and exercise training, are randomized into three dietary supplementation groups with placebo, low dose AminoTher (AA-1) or double-dose of AminoTher (AA-2).

The study is conducted in obese sarcopenic patients (Sarco-Ob) aged > 65 years in moderately low-calorie diet therapy. It aims to compare the effects of different dietary supplementations with amino acids - combined or not with exercise - on physical performance and sarcopenia. A further aim is to investigate the potential of TD-DOS technology as a novel diagnostic tool capable of evaluating fat and muscle status. The supplementation intervention will be conducted in a double-blind manner.

5.2 Participants

Subjects with BMI> 30 kg / m2 and with low lean mass values normalized by BMI will be defined as obese sarcopenic (Sarco-Ob)[36][86]. Obese sarcopenic subjects (Sarco-Ob) in moderately low-calorie diet therapy are recruited at the Nutrition ambulatories of the Clinical

Nutrition of Geriatrics B of the AOUI of Verona if they meet the following requirements of the eligibility criteria:

Inclusion criteria:

- Sarco-Ob diagnosis: will be defined as obese sarcopenic (Sarco-Ob) subjects with BMI> 30 kg/m^2 and with low lean mass values indexed by BMI[36][86]
- Male and female subjects
- Age between 65 and 80 years
- BMI > 30 kg/m2
- Resident in Verona (Italy)
- Stable weight in the last 2 months
- Sedentary (less than one hour of exercise per week for the previous 6 months)
- Signature of the informed consent for participation in the study

Exclusion criteria:

- Unstable Angina or recent myocardial infarction
- Malignant or unstable arrhythmias (ventricular tachycardia, atrioventricular block II or III degree, atrial flutter, junctional rhythm)
- Heart failure NYHA class > II
- Severe respiratory failure
- Severe heart valve disease (severe aortic stenosis)
- Abdominal and/or thoracic aortic aneurysm
- Recent intracerebral or subdural haemorrhage
- Poorly controlled arterial hypertension
- Presence of pacemakers or metal prostheses
- Severe chronic renal failure
- Symptomatic musculoskeletal pathology
- Symptomatic disc herniation
- Symptomatic arthrosis
- Acute joint, tendon and ligamentous injuries and pathologies
- Hip or knee prostheses recently placed (<6 months) or with joint instability
- Symptomatic or large inguinal or abdominal hernia
- Acute retinal detachment or bleeding
- Recent eye surgery (laser, cataract, retinal surgery, glaucoma surgery)
- History of malignant cancer within the previous 5 years
- Diagnosis of dementia
- Eating disorders

5.3 Objectives

In general, the objective of the study is to evaluate the effect of the supplementation with different doses of a peculiar EAA-BCAA mixture (placebo, supplementation with amino acids at 2 different doses) on physical performance and on biomarkers of frailty in obese sarcopenic subjects aged> 65 on a moderately low-calorie diet. The physical performance outcome is evaluated in terms of the Short Physical Performance Battery (SPPB) quantitative index.

The timing has been selected based on published studies evaluating the response to diet and exercise treatment of elderly sarcopenic-obese subjects of both sexes.[35][104]

Primary objectives

- Evaluate the effect of the interactions between A) amino acid intake and exercise, and B) amino acid intake and gender on the primary outcome (SPPB) after 5 (T5) and 9 (T9) months of treatment
- Investigate the potentiality of the TD-DOS instrument as a novel diagnostic tool for sarcopenia

Secondary objectives

Evaluate the effect of the interactions reported above on SPPB after 9 months of treatment and on biomarkers of frailty after 5 and 9 months of treatment. Selected biomarkers are:

- muscle strength (dynamometer)
- muscle mass and muscle quality (bioimpedance and DEXA)
- routine blood parameters
- miRNA dosage in circulating blood
- blood levels of cytokines

ENDPOINTS OF THE STUDY

Primary endpoints

- Short Physical Performance Battery (SPPB score) at T0 (enrolment), T5.

Secondary endpoints

- Short Physical Performance Battery (SPPB score) at T9,

- Muscle strength of the dominant limb (kg) at T0, T5, T9
- Bio-impedentiometry: skeletal muscle mass (kg and%) and fat mass (kg and%) in T0, T5, T9
- DEXA: Total Body Fat-free Mass (Kg and%), Total Body Fat mass (Kg and%) and Appendicular Fat-free Mass (Kg e.%) In T0, T5, T9
- miRNA dosage in circulating blood (%) in T0, T5, T9
- blood levels of inflammatory cytokines (TNF-α, IL-6) in T0, T5, T9

5.4 Procedure and methods

All participants undergo a nutritional intervention with a moderately low-calorie diet and are included in a training program. Further, participants will be randomized into three groups that will receive a dietary supplement with placebo, low dose amino acid (AA-1) or high-dose amino acid (AA-2).

All subjects will be subjected to:

- T0: medical examination and anamnesis collection, functional and psychological questionnaires, anthropometry, body composition (BIA and DEXA), Short Physical Performance Battery (SPPB), measurement of muscle strength in the upper limb (handgrip), blood sampling (for blood chemistry tests, miRNA assay), indirect calorimetry for the assessment of basal energy expenditure.
- T5 and T9: same ratings (except calorimetry)

5.4.1 Nutritional intervention

All obese sarcopenic subjects will undergo moderately low-calorie diet therapy to achieve a weight loss of 5% compared to the initial weight in 6 months and 8-10% compared to the initial weight in one year. The caloric restriction initially proposed will be 500 Kcal below the resting energy expenditure calculated by indirect calorimetry, multiplied by 1.4. Each subject will receive nutritional indications capable of providing 60% carbohydrates, 25% fat, 15% protein and 20 g of fibres, divided into three meals and two snacks; in particular, the protein content will be calculated in order to guarantee 1 g of protein per kg of ideal body weight. Compliance with dietary treatment will be assessed by clinical-nutritional follow-up every 3 months. The calorie restriction prescription will be adjusted in order to achieve the expected weight loss.

5.4.2 Supplementation with amino acid mixture

Patients will be randomized into double-blind groups that will receive different dosages of an oral amino acid mixture (AminoTher, see the PD-0E7 composition in chapter 3) or an isocaloric product containing maltodextrins instead of amino acids[204].
In particular:

- Placebo groups: one dose of placebo in the morning and one in the afternoon, for a total of 0 g amino acids/day;
- Group AA-1: one dose of placebo in the morning and one dose of amino acids (4 g) in the afternoon, for a total of 4 g amino acids/day;
- Group AA-2: one dose of amino acids (4 g) in the morning and one dose of amino acids (4 g) in the afternoon, for a total of 8 g amino acids/day.

The doses are dissolved in half a glass of water and taken between meals, mid-morning and mid-afternoon. On the days in which the exercise is carried out, they will be taken 1 hour before the exercise sessions.

5.4.3 Physical activity

All subjects will participate in a supervised muscle strength training program at the Sports Science facilities of the University of Verona. The main goal is to increase strength and muscle mass. In sarcopenic patients, strength training can benefit body composition, muscle strength and functional capacity[205]. To achieve this goal, strength training will be prescribed following the guidelines of the American College of Sport Medicine (ACSM, 2009).

The proposed exercises mainly stimulate the development of resistant strength and marginally of maximal strength. Some exercises stimulate large muscle groups (quadriceps, glutes, pectorals). Other exercises stimulate smaller muscle groups (triceps, biceps, calf). Together with the exercises with the strength machines, some free body exercises will be carried out.

The proposed training modality has been repeated in numerous intervention studies and demonstrated to be effective and safe. In particular, for the type of patients to whom this study is addressed, it does not present risk because it is a type of activity in which contacts are avoided, the speed of execution of the exercises are limited, patients are monitored throughout the training sessions , and workloads increased progressively (the patient has

time to adapt to different workloads based on the improvements obtained in previous training sessions)[206].

Training is planned 3 times a week and provides squats, leg presses and flat bench presses to reach maximum and resistant strength on large muscle groups. Moreover, other exercises are planned to be carried out in "free body" and using elastic bands to modulate the load (small muscle groups - resistant force).

At the beginning of each session, all subjects perform a warm-up phase (5-10 minutes) consisting of dynamic stretching exercises in preparation for the subsequent strength work. At the end of the session a 5-10 min cool-down phase and static stretching. In total, each training session will last approximately 60 minutes.

5.4.4 Clinical and physical assessment

Participants in the study before starting the intervention (T0) and at 5 (T5) and at 9 (T9) months after the start of the intervention program undergo to:

- *Clinical evaluation*. All subjects will undergo a clinical evaluation, with blood pressure measurement. A complete medical history is collected with particular attention to the presence of significant pathologies, the intake of drugs, and weight changes. PASE (Physical Activity Scale for the Elderly) questionnaire will be proposed to assess the degree of physical activity at T0, T5 and T9.
- *Anthropometric Evaluations*. Each patient is be subjected to measurement of body weight, and to measurement of height using a stadiometer. The body mass index (BMI) is calculated as the ratio between weight and height squared (Kg/m^2). The waist circumference is taken halfway between the superior iliac crest and the last rib. The hip circumference will also be measured. These assessments are routinely performed as part of the assessments for the clinical classification of obese patients.
- *Body composition assessment* (BIA and DXA). Body mass can be thought of in terms of a bi-compartmental model, such as fat mass (FM) and lean mass (Fat-Free Mass, FFM). Lean mass can be further divided into muscle mass (Lean Body Mass) and bone mineral content, resulting in a three-compartment model of body mass. These assessments (BIA and DXA) will be performed at the baseline (T0) and 5 and 9 months after the start of the study.

- *Performance test.* Physical performance assessment is carried out using the "Short Physical Performance Battery (SPPB)". Guralnik's SPPB scale is derived from a short battery of tests used to assess the functionality of the lower limbs. This battery consists of three tests:

  a) Balance Test. This test evaluates balance with three tests: maintaining the position with feet together for 10 seconds, then in the semi-tandem position (heel of one foot next to the big toe of the other foot) and finally tandem (heel of one foot in front of the other foot) again for 10 seconds.

  b) Gait Speed Test. This test evaluates the time used by the subject to travel 4 meters at a normal gait. The cut off used to evaluate the decrease in walking speed is independent of gender and corresponds to a speed> 0.8 m/s.

  c) Chair Stand Test (test of getting up from the chair). This test measures the time the subject takes to get up 5 times from a chair with his arms folded. The test must be performed as quickly as possible.
- *Dynamometric test.* The evaluation of the strength of the flexor muscles of the dominant hand is performed by a portable hydraulic dynamometer: Handgrip test (JAMAR, JA Preston Corp, Ontario, Canada). Three measurements are taken for each subject and the best of the three measurements is considered as the result. The cut off used to assess the decrease in strength was assigned based on gender. For men, there is a cut off <30 kg; for women, a cut off <20 kg. This test, together with the Short Physical Performance Battery (SPPB), is a strong predictor of disability and other adverse outcomes.
- *Laboratory evaluations.* All participants undergo fasting venous blood sampling comprising complete blood count, ions, creatinine, fasting blood glucose, cholesterol, LDL cholesterol, HDL cholesterol, triglycerides, insulin, hs-CRP, IL-6 and TNF-alfa.

5.5 Sub-study on the use of Diffuse Optic Spectroscopy (TD-DOS) in the evaluation of the characteristics of fat and muscular tissues in Sarco-Ob patients undergoing combined interventions of amino acidic supplementation, exercise and diet

In the context of the above described clinical trial, it opens up the opportunity to investigate the TD-DOS techniques in a subgroup of patients at time T0 and T5 of treatment (*Fig. 37*). Although the sub-study will cover only a limited group of patients, it will allow performing

an initial assessment of the possible correlation between the characterization of muscle and adipose tissue by TD-DOS with the information obtained both through procedures performed in clinical practice (anthropometric evaluations, indirect calorimetry, dynamometric and performance tests, blood chemistry analysis) and through specific study procedures (clinical evaluation, functional tests, evaluation of body composition by BIA and DXA, inflammatory cytokine, functional questionnaires).

The specific aim is an initial evaluation of the TD-DOS technique in the characterization of muscle and adipose tissue and its variations in obese sarcopenic patients subjected to combined interventions (amino acid supplementation, diet and exercise).

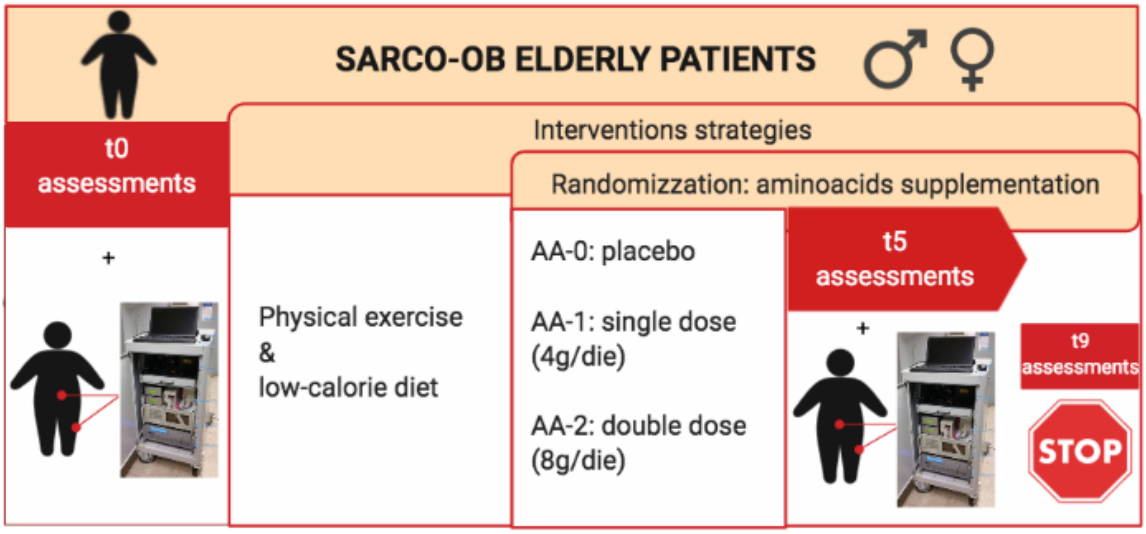

Figure 37. schematic representation of the experimental plan

5.5.1 Endpoints

1) Initial evaluation (T0) of the following parameters of abdominal muscle and adipose tissue estimated by TD-DOS.

Functional parameters:

- total volume of haemoglobin (□ M),
- tissue oxygenation level (%);

Tissue composition:

- water content (mg / cm3),
- lipid content (mg / cm3),
- collagen content (mg / cm3),

Scattering parameters related to tissue microstructure: scattering amplitude A (cm^{-1}) and power b.
2) Evaluation of the variation of the parameters estimated by TD-DOS caused by *amino acid intake* (3 levels) and *gender* (2 levels) factors after 5 months of treatment (T5).

5.5.2 Methods

TD-DOS measurements will be performed in the spectral range 600-1100 nm, by injecting the laser radiation into the tissue and collecting the scattered radiation by means of an optical fibre probe, which allows to operate with source-detector distances at 1, 2 and 3 cm to be able to probe at different depths in the tissue. The probe is placed on the skin in the area of interest.

The optical characterization of the muscle tissue will be performed with the optical probe positioned in correspondence with the right *vastus lateralis* (1/3 of the femoral length from the knee).

The abdominal region will be considered for the optical characterization of the adipose tissue. The subject will be lying in a supine position in a relaxed condition. TD-DOS measurements will be performed at least in two positions (4 cm left and right to the navel) on the abdomen.
Each measurement will be carried out at recruitment time (T0) and at T5.

5.5.3 Expected results

The clinical trials will allow getting knowledge about the effects of specific combinations of lifestyle interventions and amino acid supplementation on multidimensional frailty assessment in elderly sarcopenic or sarcopenic-obese patients. The absolute non-invasiveness and good acceptance of the optical measurements by TD-DOS instrument will allow performed measurements repeatedly over time to investigate the responsivity of sarcopenic subjects to the interventions with particular attention to gender differences.

What we expect from this sub-study is to obtain a feedback of power of this tool in investigating the structural and functional changes underlying sarcopenia and in evaluating any improvements made by intervention strategies. These skills would make this tool a potential new diagnostic technique in investigating physical frailty in the elderly.

Further, correlations analysis with parameters obtained from clinical and physical assessment currently used to classify sarcopenic subjects (such as those described in section 5.4.4) would support a possible future validation of this technology as a diagnostic tool and might lead to define a multidimensional diagnostic approach.

6 General conclusions

The study of ageing has always fascinated numerous research groups who decided to invest their activity in this field, striving to reveal the complex mechanisms underlying ageing and discover new possible therapeutic approaches to maintain and improve physical and cognitive conditions. Most of the attention should be posted on the frailty syndrome, a complex pathological age-related disease characterised by a cumulative decline in many physiological systems, with high vulnerability to poor resolution of homeostasis after a stressor event. Physical frailty is a subset of frailty, and it is substantially superimposable to sarcopenia.

Among the many unsolved aspects in the field of ageing, efforts should be addressed to the following: i) the interventions allowing the maintenance of cognitive and physical functions across the life course; ii) the sex differences in the mechanisms of ageing and cellular senescence; iii) the sex differences in the metabolic capacity of mitochondria[207]; iv) the possible differences in optimal treatment between men and women. Nowadays, these questions remain open, and obtaining complete knowledge on ageing is a stiff challenge for gerontology research[48].

In this broad field of research, my PhD work aimed to find an answer to two different open questions on physical frailty and sarcopenia: i) how to fill the lack of a reliable diagnostic method; ii) which strategy should be adopted to prevent or delay the age-related mitochondrial dysfunction affecting the skeletal muscles.

The impairment of mitochondrial bioenergetics is proved to be at the core of physical decline. Balanced formulations of essential amino acids are valuable tools to manage conditions characterised by a catabolic state, oxidative stress, or defects in energy balance[82], suggesting their potential efficacy to prevent or treat age-related physical and cognitive decline. Besides being very well-tolerated and safe, dietary supplementation with well-studied amino acid mixtures has proved to be particularly effective in promoting mitochondrial metabolism [48]. Also, muscle and fat mass structure and function changes occur during ageing, both contributing to adverse events related to physical frailty and sarcopenia. Thus, detecting structural and functional changes in these tissues could be an

efficacious strategy for an early diagnosis. In this context, diffuse optical imaging could help to overcome the lack of diagnostic tools.

In our preclinical study, the SAMP8 mouse strain has been used to investigate the pathophysiological mechanism(s) of physical decline, focusing on mitochondrial derangements in the skeletal muscles. We also explored the effectiveness of a nutraceutical approach (PD-0E7) in preventing the precocious geriatric condition. We first performed a phenotypical characterisation of the SAMP8 mice at 5, 9, 12, and 15 months of age to identify the proper timing of intervention at the early onset of motor and cognitive impairment. The study showed that early signs of inadequate general health conditions were detectable at 9 months of age, became significant at 12 months of age, and further worsened with ageing. By post-mortem examination, such events evolved parallel with a progressive impairment of the mitochondrial function in skeletal muscle.

A body of research efforts is currently devoted to boosting mitochondrial bioenergetics as novel therapeutic approaches to treat sarcopenia. We demonstrate that the dietary supplementation with the metabolic modulator PD-0E7, administered in the temporal window between 9- and 12-month of age, counteracted the age-related signs of neuromuscular decline and preserved exercise endurance in SAMP8 mice. The beneficial effect of PD-0E7 observed in the 12-month-old PD-0E7-supplemented mice might be explained by the increased mitochondrial biogenesis (as supported by increased PGC-1α and OPA-1 levels)[96]. From a translational perspective, the dietary supplementation with PD-0E7 could effectively rejuvenate mitochondria, counteracting the functional decay of skeletal muscles, potentially representing a new efficacious and safe intervention to prevent disability and physical frailty in humans[96].

In order to investigate adipose and muscle tissues and trying to overcome the lack of reliable diagnostic tool physical frailty and sarcopenia, a primary goal of my PhD research was to investigate the feasibility of using multi-distance broadband time-domain diffuse optical spectroscopy to assess the human abdomen (adipose tissue) and thigh (muscular tissue) non-invasively. Broadband absorption and reduced scattering spectra from 600 to 1100 nm were acquired at 1, 2, and 3 cm source-detector distances on healthy adult male and female volunteers and then analysed using a homogeneous model as an initial step to understanding the origin of the detected signal and how tissue should be modelled to derive quantitative information. The results exhibit an evident influence of the layered nature on the estimated optical properties. The underlying muscle makes a relevant contribution in the spectra

measured at the largest source-detector distance for thinner subjects related to blood and water absorption. More unexpectedly, also the thin superficial skin layer yields direct contamination, leading to higher water content and steeper reduced scattering spectra at the shortest distance, as also confirmed by Monte Carlo simulations. Furthermore, we found a decisive influence of gender on the estimated optical properties. This is an important issue that must be taken into account to afford future qualitative studies.

In the era of personalised and precision medicine, increasing our knowledge of adipose and muscular tissues might overcome the limitations of the traditional anthropometric indices of obesity and sarcopenia. The availability of a non-invasive technique to monitor the status of these tissues in response to nutrition, lifestyle habits, or medical treatment is fascinating for the possibilities of providing feedback and non-invasive insight. Diffuse optics is a potentially powerful option given the wealth of information it can provide – related to blood parameters, tissue composition, and microstructure. Yet, a preliminary understanding of the origin of optical measurements is a prerequisite for proposing diffuse optics in clinical studies[25].

In conclusion, an in-vivo study performed on healthy volunteers aimed to understand the potential and limitations of using broadband diffuse optical spectroscopy to non-invasively monitor subcutaneous fat layer in the abdomen skeletal muscle in the thigh. The insights obtained from this study will be used to optimise both measurement protocol and data analysis methodology for a clinical study aimed at monitoring the physical frailty in older people.

Bibliography

[1] M. Malavolta, *Biogerontologia - Dai determinanti di invecchiamento ai metodi per la determinazione dell'età biologica-*. 2018.

[2] R. Clegg, Young, Iliffe, Rikkert, "Frailty in Older People," *Lancet*, vol. 381, no. 9868, pp. 752–762, 2013, doi: 10.1016/S0140-6736(12)62167-9.

[3] W. He, D. Goodkind, and P. Kowal, "An Aging World : 2015 International Population Reports," *Aging (Albany. NY).*, no. March, p. 165, 2016.

[4] WHO, "Ageing and Life Course," 2014.

[5] A. Buch *et al.*, "Muscle function and fat content in relation to sarcopenia, obesity and frailty of old age — An overview," *Experimental Gerontology*, vol. 76. Elsevier Inc., pp. 25–32, 2016, doi: 10.1016/j.exger.2016.01.008.

[6] European Commission, "Healthy Life Years statistics," 2019, [Online]. Available: http://ec.europa.eu/health/ph_information/indicators/lifeyears_en.htm%5Cnhttp://www.tf-he.eu/index.php?option=hly_tf.

[7] L. Rodríguez-Mañas *et al.*, "Searching for an operational definition of frailty: A delphi method based consensus statement. the frailty operative definition-consensus conference project," *Journals Gerontol. - Ser. A Biol. Sci. Med. Sci.*, vol. 68, no. 1, pp. 62–67, Jan. 2013, doi: 10.1093/gerona/gls119.

[8] L. Fried *et al.*, "Frailty in older adults: evidence for a phenotype.," *J Gerontol A Biol Sci Med Sci.*, vol. 56, no. 3, pp. 146–156, 2001.

[9] A. J. Cruz-Jentoft *et al.*, "Sarcopenia: revised European consensus on definition and diagnosis," *Age Ageing*, vol. 48, pp. 16–31, 2019, doi: 10.1093/ageing/afy169.

[10] R. Calvani *et al.*, "Biomarkers for physical frailty and sarcopenia: State of the science and future developments," *Journal of Cachexia, Sarcopenia and Muscle*, vol. 6, no. 4. Wiley Online Library, pp. 278–286, 2015, doi: 10.1002/jcsm.12051.

[11] F. Landi *et al.*, "Sarcopenia as the Biological Substrate of Physical Frailty," *Clinics in Geriatric Medicine*, vol. 31, no. 3. W.B. Saunders, pp. 367–374, Aug. 01, 2015, doi: 10.1016/j.cger.2015.04.005.

[12] I. Rosenberg, "Epidemiologic and methodologic problems in determining nutritional status of older persons. (Summary comments)," *Am J Clin Nutr*, vol. 50, pp. 1231–1233, 1989.

[13] J. Morley, R. Baumgartner, R. Roubenoff, J. Mayer, and K. Nair, "Sarcopenia," *J Lab Clin Med*, vol. 137, no. 4, pp. 231–243, 2001.

[14] A. J. Cruz-Jentoft *et al.*, "Sarcopenia: European consensus on definition and diagnosis: Report of the European Working Group on Sarcopenia in Older People," *Age Ageing*, vol. 39, no. 4, pp. 412–423, Apr. 2010, doi: 10.1093/ageing/afq034.

[15] P. Francis, M. Lyons, M. Piasecki, J. Mc Phee, K. Hind, and P. Jakeman, "Measurement of muscle health in aging," *Biogerontology*, vol. 18, no. 6, pp. 901–911, 2017, doi: 10.1007/s10522-017-9697-5.

[16] T. K. Malmstrom, D. K. Miller, E. M. Simonsick, L. Ferrucci, and J. E. Morley, "SARC-F: A symptom score to predict persons with sarcopenia at risk for poor functional outcomes," *J. Cachexia. Sarcopenia Muscle*, vol. 7, no. 1, pp. 28–36, 2016, doi: 10.1002/jcsm.12048.

[17] L. Larsson *et al.*, "Sarcopenia: Aging-related loss of muscle mass and function," *Physiol. Rev.*, vol. 99, no. 1, pp. 427–511, 2019, doi: 10.1152/physrev.00061.2017.

[18] J. P. Gumucio and C. L. Mendias, "Atrogin-1, MuRF-1, and sarcopenia," *Endocrine*, vol. 43, no. 1, pp. 12–21, 2013, doi: 10.1007/s12020-012-9751-7.Atrogin-1.

[19] A. J. Cruz-Jentoft and A. A. Sayer, "Sarcopenia," *Lancet*, vol. 393, no. 10191, pp. 2636–2646, 2019, doi: 10.1016/S0140-6736(19)31138-9.

[20] D. Taaffe, T. Henwood, M. Nalls, D. Walker, T. Lang, and T. Harris, "Alterations in muscle attenuation following detraining and retraining in resistance-trained older adults," *Gerontology*, vol. 55, no. 2, pp. 217–223, 2009.

[21] M. J. Delmonico *et al.*, "Longitudinal study of muscle strength, quality, and adipose tissue infiltration," *Am. J. Clin. Nutr.*, vol. 90, no. 6, pp. 1579–1585, 2009, doi: 10.3945/ajcn.2009.28047.

[22] G. D'Antona *et al.*, "The effect of ageing and immobilization on structure and function of human skeletal muscle fibres," *J. Physiol.*, vol. 552, no. 2, pp. 499–511, 2003, doi: 10.1113/jphysiol.2003.046276.

[23] M. Finucane *et al.*, "Global Burden of Metabolic Risk Factors of Chronic Diseases Collaborating Group (Body Mass Index). National, regional, and global trends in body-mass index since 1980: systematic analysis of health examination surveys and epidemiological studies with 960 ," *Lancet*, vol. 377, no. 9765, pp. 557–567, 2011.

[24] W. Garvey and J. Mechanic, "Proposal for a Scientifically Correct and Medically Actionable Disease Classification System (ICD) for Obesity," *Obes. (Silver Spring)*, vol. 28, no. 3, pp. 484–492, 2020.

[25] P. Lanka *et al.*, "Non-invasive investigation of adipose tissue by time domain diffuse optical spectroscopy," vol. 11, no. 5, pp. 2779–2793, 2020.

[26] A. Giordano, A. Frontini, and S. Cinti, "Convertible visceral fat as a therapeutic target to curb obesity," *Nat. Rev. Drug Discov.*, vol. 15, no. 6, pp. 405–424, 2016, doi: 10.1038/nrd.2016.31.

[27] T. N. Kim *et al.*, "Impact of visceral fat on skeletal muscle mass and vice versa in a prospective cohort study: The Korean Sarcopenic Obesity Study (KSOS)," *PLoS One*, vol. 9, no. 12, pp. 1–13, 2014, doi: 10.1371/journal.pone.0115407.

[28] B. H. Goodpaster *et al.*, "The loss of skeletal muscle strength, mass, and quality in older adults: The Health, Aging and Body Composition Study," *Journals Gerontol. - Ser. A Biol. Sci. Med. Sci.*, vol. 61, no. 10, pp. 1059–1064, 2006, doi: 10.1093/gerona/61.10.1059.

[29] G. Shulman, "Ectopic fat in insulin resistance, dyslipidemia, and cardiometabolic disease," *N Engl J Med*, vol. 371, no. 12, pp. 1131–1141, 2014.

[30] L. Liu, M. Mei, S. Yang, and Q. Li, "Roles of chronic low-grade inflammation in the development of ectopic fat deposition," *Mediators Inflamm.*, 2014, doi: 10.1155/2014/418185.

[31] B. Gustafson and U. Smith, "Cytokines promote Wnt signaling and inflammation and impair the normal differentiation and lipid accumulation in 3T3-L1 preadipocytes," *J. Biol. Chem.*, vol. 281, no. 14, pp. 9507–9516, 2006, doi: 10.1074/jbc.M512077200.

[32] J. Salles *et al.*, "TNFα gene knockout differentially affects lipid deposition in liver and skeletal muscle of high-fat-diet mice," *J Nutr Biochem*, vol. 23, no. 12, pp. 1685–1693, 2012.

[33] M. J. Cartwright, T. Tchkonia, and J. L. Kirkland, "Aging in adipocytes: Potential impact of inherent, depot-specific mechanisms," *Exp. Gerontol.*, vol. 42, no. 6, pp. 463–471, 2007, doi: 10.1016/j.exger.2007.03.003.

[34] A. Valerio and E. Nisoli, "Nitric oxide, interorganelle communication, and energy flow: A novel route to slow aging," *Frontiers in Cell and Developmental Biology*, vol. 3, no. 6. 2015, doi: 10.3389/fcell.2015.00006.

[35] D. T. Villareal *et al.*, "Weight loss, exercise, or both and physical function in obese older adults," *N. Engl. J. Med.*, vol. 364, no. 13, pp. 1218–1229, 2011, doi: 10.1056/NEJMoa1008234.

[36] J. Chung, H. Kang, D. Lee, H. Lee, and Y. Lee, "Body composition and its

association with cardiometabolic risk factors in the elderly: a focus on sarcopenic obesity," *Arch Gerontol Geriatr*, vol. 56, no. 1, pp. 270–278, 2013.

[37] T. M. Manini, B. C. Clark, M. A. Nalls, B. H. Goodpaster, L. L. Ploutz-Snyder, and T. B. Harris, "Reduced physical activity increases intermuscular adipose tissue in healthy young adults," *Am. J. Clin. Nutr.*, vol. 85, no. 2, pp. 377–384, 2007, doi: 10.1093/ajcn/85.2.377.

[38] B. Goodpaster *et al.*, "Association between regional adipose tissue distribution and both type 2 diabetes and impaired glucose tolerance in elderly men and women," *Diabetes Care*, vol. 26, no. 2, pp. 372–379, 2003.

[39] A. P. Rossi *et al.*, "Predictors of ectopic fat accumulation in liver and pancreas in obese men and women," *Obesity*, vol. 19, no. 9, pp. 1747–1754, 2011, doi: 10.1038/oby.2011.114.

[40] V. Tiku, M. W. Tan, and I. Dikic, "Mitochondrial Functions in Infection and Immunity," *Trends Cell Biol.*, vol. 30, no. 4, pp. 263–275, 2020, doi: 10.1016/j.tcb.2020.01.006.

[41] H. Hoppeler and M. Fluck, "Plasticity of skeletal muscle mitochondria: structure and function," *Med Sci Sport. Exerc*, vol. 35, no. 1, pp. 95–104, 2003.

[42] Z. Arany *et al.*, "HIF-independent regulation of VEGF and angiogenesis by the transcriptional coactivator PGC-1alpha," *Nature*, vol. 451, no. 7181, pp. 1008–1012, 2008.

[43] J. Nunnari and A. Suomalainen, "Mitochondria: in sickness and in health," *Cell*, vol. 148, no. 6, pp. 1145–1159, 2012.

[44] E. Nisoli *et al.*, "Mitochondrial biogenesis in mammals: the role of endogenous nitric oxide.," *Science*, vol. 299, no. 5608, pp. 896–899, Feb. 2003, doi: 10.1126/science.1079368.

[45] E. Nisoli *et al.*, "Calorie restriction promotes mitochondrial biogenesis by inducing the expression of eNOS," *Science*, vol. 310, no. 5746, pp. 314–317, 2005.

[46] G. D'Antona *et al.*, "Branched-chain amino acid supplementation promotes survival and supports cardiac and skeletal muscle mitochondrial biogenesis in middle-aged mice," *Cell Metab.*, vol. 12, no. 4, pp. 362–372, Oct. 2010, doi: 10.1016/j.cmet.2010.08.016.

[47] A. Valerio, G. D'Antona, and E. Nisoli, "Branched-chain amino acids, mitochondrial biogenesis, and healthspan: an evolutionary perspective," *Aging (Albany. NY).*, vol. 3, no. 5, pp. 464–478, 2011, Accessed: Jun. 11, 2019. [Online].

Available: www.impactaging.com.

[48] A. Segala, E. Nisoli, and A. Valerio, "Aminoacidi essenziali, omeostasi mitocondriale e prevenzione della gfragilità nell'anziano," vol. 11, pp. 91–96, 2019.

[49] F. L. Muller, Y. Liu, and H. Van Remmen, "Complex III releases superoxide to both sides of the inner mitochondrial membrane," *J. Biol. Chem.*, vol. 279, no. 47, pp. 49064–49073, 2004, doi: 10.1074/jbc.M407715200.

[50] M. P. Murphy, "How mitochondria produce reactive oxygen species," *Biochem. J.*, vol. 417, no. 1, pp. 1–13, 2009, doi: 10.1042/BJ20081386.

[51] D. Harman, "Aging: a theory based on free radical and radiation chemistry," . *J Gerontol.*, vol. 11, no. 3, pp. 298–300, 1956.

[52] H. Frenzel and J. Feimann, "Age-dependent structural changes in the myocardium of rats. A quantitative light- and electron-microscopic study on the right and left chamber wall," *Mech Ageing Dev*, vol. 27, no. 1, pp. 29–41, 1984.

[53] G. Gouspillou *et al.*, "Mitochondrial energetics is impaired in vivo in aged skeletal muscle," *Aging Cell*, vol. 13, no. 1, pp. 39–48, 2014, doi: 10.1111/acel.12147.

[54] G. Sgarbi *et al.*, "Mitochondria hyperfusion and elevated autophagic activity are key mechanisms for cellular bioenergetic preservation in centenarians," *Aging (Albany. NY).*, vol. 6, no. 4, pp. 296–310, 2014, doi: 10.18632/aging.100654.

[55] M. Webb and D. P. Sideris, "Intimate Relations — Mitochondria and Ageing," *Int. J. Mol. Sci.*, vol. 21, no. 7580, 2020.

[56] S. Archer, "Mitochondrial dynamics--mitochondrial fission and fusion in human diseases," *N Engl J Med*, vol. 369, no. 23, pp. 2236–2251, 2013.

[57] V. Del Dotto, M. Fogazza, V. Carelli, M. Rugolo, and C. Zanna, "Eight human OPA1 isoforms, long and short: What are they for?," *Biochim. Biophys. Acta - Bioenerg.*, vol. 1859, no. 4, pp. 263–269, 2018, doi: 10.1016/j.bbabio.2018.01.005.

[58] J. M. Memme, A. T. Erlich, G. Phukan, and D. A. Hood, "Exercise and mitochondrial health," *J. Physiol.*, vol. 599, no. 3, pp. 803–817, 2021, doi: 10.1113/JP278853.

[59] A. Picca, R. Calvani, G. Sirago, H. Coelho-Junior, and E. Marzetti, "Molecular routes to sarcopenia and biomarker development: per aspera ad astra," *Curr Opin Pharmacol*, vol. 57, pp. 140–147, 2021.

[60] F. Landi *et al.*, "Sarcopenia as the Biological Substrate of Physical Frailty," *Clin. Geriatr. Med.*, vol. 31, no. 3, pp. 367–374, 2015, doi: 10.1016/j.cger.2015.04.005.

[61] K. Rockwood *et al.*, "A global clinical measure of fitness and frailty in elderly

people," *CMAJ*, vol. 173, no. 5, pp. 489–495, 2005, doi: 10.1503/cmaj.050051.

[62] X. Song, A. Mitnitski, and K. Rockwood, "Prevalence and 10-year outcomes of frailty in older adults in relation to deficit accumulation.," *J Am Geriatr Soc.*, vol. 58, no. 4, pp. 681–687, 2010.

[63] F. 3rd Gloth, J. Walston, J. Meyer, and J. Pearson, "Reliability and validity of the Frail Elderly Functional Assessment questionnaire.," *Am J Phys Med Rehabil.*, vol. 74, no. 1, pp. 45–53, 1995.

[64] H. Schuurmans, N. Steverink, S. Lindenberg, N. Frieswijk, and J. P. J. Slaets, "Old or frail: What tells us more?," *Journals Gerontol. - Ser. A Biol. Sci. Med. Sci.*, vol. 59, no. 9, pp. 962–965, 2004, doi: 10.1093/gerona/59.9.m962.

[65] R. J. J. Gobbens, M. A. L. M. Van Assen, K. G. Luijkx, and J. M. G. A. Schols, "The predictive validity of the tilburg frailty indicator: Disability, health care utilization, and quality of life in a population at risk," *Gerontologist*, vol. 52, no. 5, pp. 619–631, 2012, doi: 10.1093/geront/gnr135.

[66] S. Metzelthin *et al.*, "The Psychometric Properties of Three Self-Report Screening Instruments for Identifying Community-Dwelling Frail Elderly," *Gerontologist*, vol. 52, pp. 280–281, 2012.

[67] C. Ismail *et al.*, "Diagnostic ultrasound estimates of muscle mass and muscle quality discriminate between women with and without sarcopenia," *Front. Physiol.*, vol. 6, no. 302, pp. 1–10, 2015, doi: 10.3389/fphys.2015.00302.

[68] C. Beaudart *et al.*, "Validation of the SarQoL®, a specific health-related quality of life questionnaire for Sarcopenia," *J. Cachexia. Sarcopenia Muscle*, vol. 8, no. 2, pp. 238–244, 2017, doi: 10.1002/jcsm.12149.

[69] S. R. P. Kumar Lanka, "Advances in Broadband Time-Resolved Spectroscopy of Diffusive Media - From Physics to Clinics," Politecnico di Milano, 2019.

[70] P. Taroni, A. Pifferi, A. Torricelli, D. Comelli, and R. Cubeddu, "In vivo absorption and scattering spectroscopy of biological tissues," *Photochem Photobiol Sci.*, vol. 2, no. 2, pp. 124–9, 2003.

[71] G. Strangman, D. Boas, and J. Sutton, "Non-invasive neuroimaging using near-infrared light," *Biol Psychiatry*, vol. 52, no. 7, pp. 679–693, 2002.

[72] A. Cerussi, N. Shah, D. Hsiang, A. Durkin, J. Butler, and B. J. Tromberg, "In vivo absorption, scattering, and physiologic properties of 58 malignant breast tumors determined by broadband diffuse optical spectroscopy," *J. Biomed. Opt.*, vol. 11, no. 4, p. 044005/16, 2006, doi: 10.1117/1.2337546.

[73] P. Taroni *et al.*, "Is Collagen an Independent Risk Factor for Breast Cancer?," *Biomed. Opt. OSA Tech. Dig. (Optical Soc. Am. 2016)*, 2016.

[74] A. Pifferi *et al.*, "Spectroscopic time-resolved diffuse reflectance and transmittance measurements of the female breast at different interfiber distances," *J. Biomed. Opt.*, vol. 9, no. 6, p. 1143, 2004, doi: 10.1117/1.1802171.

[75] S. Konugolu Venkata Sekar *et al.*, "Broadband (550-1350 nm) diffuse optical characterization of thyroid chromophores," *Sci. Rep.*, vol. 8, no. 1, pp. 1–8, 2018, doi: 10.1038/s41598-018-27684-8.

[76] J. R. Mourant, T. Fuselier, J. Boyer, T. M. Johnson, and I. J. Bigio, "Predictions and measurements of scattering and absorption over broad wavelength ranges in tissue phantoms," *Appl. Opt.*, vol. 36, no. 4, p. 949, 1997, doi: 10.1364/ao.36.000949.

[77] M. Patterson, B. Chance, and B. Wilson, "Time resolved reflectance and transmittance for the non-invasive measurement of tissue optical properties," *Appl Opt*, vol. 28, no. 12, pp. 2331–2336, 1989.

[78] A. E. Civitarese *et al.*, "Calorie restriction increases muscle mitochondrial biogenesis in healthy humans," *PLoS Med.*, vol. 4, no. 3, pp. 485–494, 2007, doi: 10.1371/journal.pmed.0040076.

[79] M. Ristow *et al.*, "Antioxidants prevent health-promoting effects of physical exercise in humans," *Proc. Natl. Acad. Sci. U. S. A.*, vol. 106, no. 21, pp. 8665–8670, 2009, doi: 10.1073/pnas.0903485106.

[80] C. Farah, L. Michel, and J. Balligand, "Nitric oxide signalling in cardiovascular health and disease," *Nat Rev Cardiol*, vol. 15, no. 5, pp. 292–316, 2018.

[81] R. Vettor *et al.*, "Exercise training boosts eNOS-dependent mitochondrial biogenesis in mouse heart: role in adaptation of glucose metabolism," *Am. J. Physiol. Metab.*, vol. 306, pp. E519–E528, 2014, doi: 10.1152/ajpendo.00617.2013.

[82] C. Ruocco, A. Segala, A. Valerio, and E. Nisoli, "Essential amino acid formulations to prevent mitochondrial dysfunction and oxidative stress," *Curr. Opin. Clin. Nutr. Metab. Care*, vol. 24, no. 1, pp. 88–95, 2021, doi: 10.1097/MCO.0000000000000704.

[83] A. del Campo *et al.*, "Muscle function decline and mitochondria changes in middle age precede sarcopenia in mice," *Aging (Albany. NY).*, vol. 10, no. 1, pp. 34–55, 2018, doi: 10.18632/aging.101358.

[84] G. Distefano *et al.*, "Physical activity unveils the relationship between mitochondrial energetics, muscle quality, and physical function in older adults," *J. Cachexia. Sarcopenia Muscle*, vol. 9, no. 2, pp. 279–294, 2018, doi: 10.1002/jcsm.12272.

[85] J. Holloszy, "Regulation by exercise of skeletal muscle content of mitochondria and GLUT4," *J Physiol Pharmacol*, vol. 59, no. 7, pp. 5–18, 2008.

[86] J. E. Morley *et al.*, "Frailty consensus: A call to action," *J. Am. Med. Dir. Assoc.*, vol. 14, no. 6, pp. 392–397, 2013, doi: 10.1016/j.jamda.2013.03.022.

[87] W. P. Vermeij *et al.*, "Diet restriction delays accelerated aging and genomic stress in DNA repair deficient mice," *Nature*, vol. 537, no. 7620, pp. 427–431, 2016, doi: 10.1038/nature19329.Diet.

[88] M. P. Mattson, V. D. Longo, and M. Harvie, "Impact of intermittent fasting on health and disease processes," *Ageing Research Reviews*, vol. 39. Elsevier Ireland Ltd, pp. 46–58, 2017, doi: 10.1016/j.arr.2016.10.005.

[89] Z. M. Wang *et al.*, "Relationship of physical function to single muscle fiber contractility in older adults: Effects of resistance training with and without caloric restriction," *Journals Gerontol. - Ser. A Biol. Sci. Med. Sci.*, vol. 74, no. 3, pp. 412–419, 2019, doi: 10.1093/gerona/gly047.

[90] S. Dato, E. Hoxha, P. Crocco, F. Iannone, G. Passarino, and G. Rose, "Amino acids and amino acid sensing: implication for aging and diseases," *Biogerontology*, vol. 20, no. 1, pp. 17–31, 2019, doi: 10.1007/s10522-018-9770-8.

[91] C. H. Ko *et al.*, "Effects of enriched branched-chain amino acid supplementation on sarcopenia," *Aging (Albany. NY).*, vol. 12, no. 14, pp. 15091–15103, 2020, doi: 10.18632/aging.103576.

[92] I. Buondonno *et al.*, "From mitochondria to healthy aging: The role of branched-chain amino acids treatment: MATeR a randomized study," *Clin. Nutr.*, vol. 39, no. 7, pp. 2080–2091, 2020, doi: 10.1016/j.clnu.2019.10.013.

[93] S. Banfi *et al.*, "Supplementation with a selective amino acid formula ameliorates muscular dystrophy in mdx mice," *Sci. Rep.*, vol. 8, no. 1, pp. 1–17, 2018, doi: 10.1038/s41598-018-32613-w.

[94] F. Bifari *et al.*, "Complete neural stem cell (NSC) neuronal differentiation requires a branched chain amino acids-induced persistent metabolic shift towards energy metabolism," *Pharmacol Res*, vol. 158, no. 104863, 2020.

[95] L. Tedesco *et al.*, "A special amino-acid formula tailored to boosting cell respiration prevents mitochondrial dysfunction and oxidative stress caused by doxorubicin in mouse cardiomyocytes," *Nutrients*, vol. 12, no. 2, pp. 1–20, 2020, doi: 10.3390/nu12020282.

[96] D. Brunetti *et al.*, "Targeting multiple mitochondrial processes by a metabolic

modulator prevents sarcopenia and cognitive decline in SAMP8 mice," *Front. Pharmacol.*, 2020.

[97] A. Tchernof and J. P. Després, "Pathophysiology of human visceral obesity: An update," *Physiol. Rev.*, vol. 93, no. 1, pp. 359–404, 2013, doi: 10.1152/physrev.00033.2011.

[98] O. Addison, R. L. Marcus, P. C. Lastayo, and A. S. Ryan, "Intermuscular fat: A review of the consequences and causes," *Int. J. Endocrinol.*, 2014, doi: 10.1155/2014/309570.

[99] E. Nisoli and A. Valerio, "Healthspan and Longevity in Mammals: A Family Game for Cellular Organelles?," *Curr. Pharm. Des.*, vol. 20, no. 35, pp. 5663–5670, Sep. 2014, doi: 10.2174/1381612820666140306093651.

[100] M. Horak, J. Novak, and J. Bienertova-Vasku, "Muscle-specific microRNAs in skeletal muscle development," *Dev. Biol.*, vol. 410, no. 1, pp. 1–13, 2016, doi: 10.1016/j.ydbio.2015.12.013.

[101] D. Brown and K. Goljanek-Whysall, "microRNAs: Modulators of the underlying pathophysiology of sarcopenia?," *Ageing Res Rev*, vol. 24, no. Pt B, pp. 263–273, 2015.

[102] M. Latronico and G. Condorelli, "The might of microRNA in mitochondria," *Circ Res*, vol. 110, no. 12, pp. 1540–1542, 2012.

[103] H. Wakabayashi and K. Sakuma, "Rehabilitation nutrition for sarcopenia with disability: a combination of both rehabilitation and nutrition care management," *Journal of Cachexia Sarcopenia Muscle*, vol. 5. pp. 269–277, 2014, doi: 10.1007/s13539-014-0162-x.

[104] D. T. Villareal *et al.*, "Aerobic or resistance exercise, or both, in dieting obese older adults," *N. Engl. J. Med.*, vol. 376, no. 20, pp. 1943–1955, May 2017, doi: 10.1056/NEJMoa1616338.

[105] M. Pallas, A. Camins, M. A. Smith, G. Perry, H. G. Lee, and G. Casadesus, "From aging to Alzheimer's disease: Unveiling 'The switch' with the senescence-accelerated mouse model (SAMP8)," *Journal of Alzheimer's Disease*, vol. 15, no. 4. pp. 615–624, 2008, doi: 10.3233/JAD-2008-15408.

[106] P. Taroni *et al.*, "Breast tissue composition and its dependence on demographic risk factors for breast cancer: Non-invasive assessment by Time Domain diffuse optical spectroscopy," *PLoS One*, vol. 10, no. 6, Jun. 2015, doi: 10.1371/journal.pone.0128941.

[107] S. Konugolu Venkata Sekar *et al.*, "Broadband (600-1350 nm) Time-Resolved Diffuse Optical Spectrometer for Clinical Use," *IEEE J. Sel. Top. Quantum Electron.*, vol. 22, no. 3, 2016, doi: 10.1109/JSTQE.2015.2506613.

[108] M. E. Gómez-Gómez and S. C. Zapico, "Frailty, cognitive decline, neurodegenerative diseases and nutrition interventions," *Int. J. Mol. Sci.*, vol. 20, no. 11, 2019, doi: 10.3390/ijms20112842.

[109] T. Takeda, "Senescence-accelerated mouse (SAM): a biogerontological resource in aging research," *Neurobiol Aging*, vol. 20, no. 2, pp. 105–110, 1999.

[110] T. Takeda, M. Hosokawa, and K. Higuchi, "Senescence-accelerated mouse (SAM): a novel murine model of senescence," *Exp Gerontol*, vol. 32, no. 1–2, pp. 105–109, 1997.

[111] W. Derave, B. Eijnde, M. Ramaekers, and P. Hespel, "Soleus muscles of SAMP8 mice provide an accelerated model of skeletal muscle senescence," *Exp Gerontol*, vol. 40, no. 7, pp. 562–572, 2005.

[112] Y. Chiba *et al.*, "The senescence-accelerated mouse (SAM): a higher oxidative stress and age-dependent degenerative diseases model," *Neurochem Res*, vol. 34, no. 4, pp. 679–687, 2009.

[113] F. Derbré, A. Gratas-Delamarche, M. Gómez-Cabrera, and J. Viña, "Inactivity-induced oxidative stress: a central role in age-related sarcopenia?," *Eur J Sport Sci*, vol. 14, no. suppl 1, pp. S98-108, 2014.

[114] C. Moorwood, M. Liu, Z. Tian, and E. R. Barton, "Isometric and eccentric force generation assessment of skeletal muscles isolated from murine models of muscular dystrophies," *J. Vis. Exp.*, no. 71, pp. 1–6, 2013, doi: 10.3791/50036.

[115] M. Romanick, L. Thompson, and H. Brown-Borg, "Murine models of atrophy, cachexia, and sarcopenia in skeletal muscle," *Biochim Biophys Acta*, vol. 1832, no. 9, pp. 1410–1420, 2013.

[116] A. Y. Guo *et al.*, "Muscle mass, structural and functional investigations of senescence-accelerated mouse P8 (SAMP8)," *Exp. Anim.*, vol. 64, no. 4, pp. 425–433, 2015, doi: 10.1538/expanim.15-0025.

[117] L. Tedesco *et al.*, "Experimental evidence on the efficacy of two new metabolic modulators on mitochondrial biogenesis and function in mouse cardiomyocytes," *J. Popul. Ther. Clin. Pharmacol.*, vol. 27, no. special issue 2, pp. e12–e21, 2020.

[118] L. Tedesco *et al.*, "A specific amino acid formula prevents alcoholic liver disease in rodents," *Am. J. Physiol. - Gastrointest. Liver Physiol.*, vol. 314, no. 5, pp. G566–G582,

2018, doi: 10.1152/ajpgi.00231.2017.

[119] M. H. Ullman-Culleré and C. J. Foltz, "Body condition scoring: a rapid and accurate method for assessing health status in mice," *Lab Anim Sci*, vol. 49, no. 3, pp. 319–323, 1999, [Online]. Available: https://www.ncbi.nlm.nih.gov/pubmed/?term=Body+Condition+Scoring%3A+A+Rapid+and+Accurate+Method+for+Assessing+Health+Status+in+Mice.

[120] L. Harkema, S. Youssef, and A. de Bruin, "Pathology of Mouse Models of Accelerated Aging," *Vet Pathol*, vol. 53, no. 2, pp. 366–389, 2016.

[121] R. Lalonde and C. Strazielle, "Brain regions and genes affecting limb-clasping responses," *Brain Res Rev*, vol. 67, no. 1–2, pp. 252–259, 2011.

[122] C. Viscomi *et al.*, "In vivo correction of COX deficiency by activation of the AMPK/PGC-1α axis," *Cell Metab*, vol. 14, no. 1, pp. 80–90, 2011.

[123] K. A. Rygiel, M. Picard, and D. M. Turnbull, "The ageing neuromuscular system and sarcopenia: a mitochondrial perspective," *J. Physiol.*, vol. 594, no. 16, pp. 4499–4512, 2016, doi: 10.1113/JP271212.

[124] R. H. Houtkooper *et al.*, "The metabolic footprint of aging in mice," *Sci. Rep.*, vol. 1, 2011, doi: 10.1038/srep00134.

[125] X. Ma and J. Blenis, "Molecular mechanisms of mTOR-mediated translational control," *Nat Rev Mol Cell Biol*, vol. 10, no. 5, pp. 307–318, 2009.

[126] R. Amat, A. Planavila, S. L. Chen, R. Iglesias, M. Giralt, and F. Villarroya, "SIRT1 controls the transcription of the peroxisome proliferator-activated receptor-γ co-activator-1α(PGC-1α) gene in skeletal muscle through the PGC-1α autoregulatory loop and interaction with MyoD," *J. Biol. Chem.*, vol. 284, no. 33, pp. 21872–21880, 2009, doi: 10.1074/jbc.M109.022749.

[127] A. P. Gureev, E. A. Shaforostova, and V. N. Popov, "Regulation of Mitochondrial Biogenesis as a Way for Active Longevity: Interaction Between the Nrf2 and PGC-1α Signaling Pathways," *Front. Genet.*, vol. 10, no. 435, 2019, doi: 10.3389/fgene.2019.00435.

[128] P. Sousa-Victor *et al.*, "Geriatric muscle stem cells switch reversible quiescence into senescence," *Nature*, vol. 506, no. 7488, pp. 316–321, 2014, doi: 10.1038/nature13013.

[129] C. Griñán-Ferré, R. Corpas, D. Puigoriol-Illamola, V. Palomera-Ávalos, C. Sanfeliu, and M. Pallàs, "Understanding Epigenetics in the Neurodegeneration of Alzheimer's Disease: SAMP8 Mouse Model," *J. Alzheimer's Dis.*, vol. 62, no. 3, pp. 943–963,

2018, doi: 10.3233/JAD-170664.

[130] C. Ibebunjo *et al.*, "Genomic and Proteomic Profiling Reveals Reduced Mitochondrial Function and Disruption of the Neuromuscular Junction Driving Rat Sarcopenia," *Mol. Cell. Biol.*, vol. 33, no. 2, pp. 194–212, 2013, doi: 10.1128/mcb.01036-12.

[131] A. M. Joseph *et al.*, "The impact of aging on mitochondrial function and biogenesis pathways in skeletal muscle of sedentary high- and low-functioning elderly individuals," *Aging Cell*, vol. 11, no. 5, pp. 801–809, 2012, doi: 10.1111/j.1474-9726.2012.00844.x.

[132] C. Tezze *et al.*, "Age-Associated Loss of OPA1 in Muscle Impacts Muscle Mass, Metabolic Homeostasis, Systemic Inflammation, and Epithelial Senescence," *Cell Metab*, vol. 25, no. 6, pp. 1374–1389, 2017.

[133] T. B. Waltz *et al.*, "Sarcopenia, aging and prospective interventional strategies," *Curr Med Chem*, vol. 25, no. 40, pp. 5588–5596, 2018.

[134] G. D'Antona *et al.*, "A Peculiar Formula of Essential Amino Acids Prevents Rosuvastatin Myopathy in Mice," *Antioxidants Redox Signal.*, vol. 25, no. 11, pp. 595–608, 2016, doi: 10.1089/ars.2015.6582.

[135] K. Watson and K. Baar, "mTOR and the health benefits of exercise," *Semin Cell Dev Biol*, vol. 36, pp. 130–139, 2014.

[136] C. Goodman, "The role of mTORC1 in regulating protein synthesis and skeletal muscle mass in response to various mechanical stimuli," *Rev Physiol Biochem Pharmacol*, vol. 166, pp. 43–95, 2014.

[137] C. A. Goodman, "Role of mTORC1 in mechanically induced increases in translation and skeletal muscle mass," *J. Appl. Physiol.*, vol. 127, no. 2, pp. 581–590, 2019, doi: 10.1152/japplphysiol.01011.2018.

[138] C. S. Fry *et al.*, "Aging impairs contraction-induced human skeletal muscle mTORC1 signaling and protein synthesis," *Skelet. Muscle*, vol. 1, no. 1, p. 11, 2011, doi: 10.1186/2044-5040-1-11.

[139] J. F. Gill, G. Santos, S. Schnyder, and C. Handschin, "PGC-1α affects aging-related changes in muscle and motor function by modulating specific exercise-mediated changes in old mice," *Aging Cell*, vol. 17, no. 1, pp. 1–13, 2018, doi: 10.1111/acel.12697.

[140] J. Cunningham, J. Rodgers, D. Arlow, F. Vazquez, V. Mootha, and P. Puigserver, "mTOR controls mitochondrial oxidative function through a YY1-PGC-1alpha

transcriptional complex," *Nature*, vol. 450, no. 7170, pp. 736–740, 2007.

[141] S. M. Schieke *et al.*, "The mammalian target of rapamycin (mTOR) pathway regulates mitochondrial oxygen consumption and oxidative capacity," *J. Biol. Chem.*, vol. 281, no. 37, pp. 27643–27652, 2006, doi: 10.1074/jbc.M603536200.

[142] J. J. Dominy, Y. Lee, Z. Gerhart-Hines, and P. Puigserver, "Nutrient-dependent regulation of PGC-1alpha's acetylation state and metabolic function through the enzymatic activities of Sirt1/GCN5," *Biochim Biophys Acta*, vol. 1804, no. 8, pp. 1676–83, 2010.

[143] Q. Ma, "Role of Nrf2 in oxidative stress and toxicity," *Annu. Rev. Pharmacol. Toxicol.*, vol. 53, no. 1, pp. 401–426, 2013, doi: 10.1146/annurev-pharmtox-011112-140320.

[144] M. Ristow and K. Schmeisser, "Mitohormesis: Promoting health and lifespan by increased levels of reactive oxygen species (ROS)," *Dose-Response*, vol. 12, no. 2, pp. 288–341, 2014, doi: 10.2203/dose-response.13-035.Ristow.

[145] I. Ryoo and M. Kwak, "Regulatory crosstalk between the oxidative stress-related transcription factor Nfe2l2/Nrf2 and mitochondria," *Toxicol Appl Pharmacol*, vol. 359, pp. 24–33, 2018.

[146] T. Varanita *et al.*, "The OPA1-dependent mitochondrial cristae remodeling pathway controls atrophic, apoptotic, and ischemic tissue damage," *Cell Metab*, vol. 21, no. 6, pp. 834–44, 2015.

[147] S. Cogliati *et al.*, "Mitochondrial cristae shape determines respiratory chain supercomplexes assembly and respiratory efficiency," *Cell*, vol. 155, no. 1, pp. 160–171, 2013.

[148] R. Acin-Perez and J. A. Enriquez, "The function of the respiratory supercomplexes: The plasticity model," *Biochim. Biophys. Acta - Bioenerg.*, vol. 1837, no. 4, pp. 444–450, 2014, doi: 10.1016/j.bbabio.2013.12.009.

[149] J. A. Enriquez and G. Lenaz, "Coenzyme Q and the respiratory Chain: Coenzyme Q pool and mitochondrial supercomplexes," *Mol. Syndromol.*, vol. 5, no. 3–4, pp. 119–140, 2014, doi: 10.1159/000363364.

[150] R. Acín-Pérez *et al.*, "Respiratory complex III is required to maintain complex I in mammalian mitochondria," *Mol Cell*, vol. 13, no. 6, pp. 805–815, 2004.

[151] G. Civiletto *et al.*, "Opa1 overexpression ameliorates the phenotype of two mitochondrial disease mouse models," *Cell Metab*, vol. 21, no. 6, pp. 845–854, 2015.

[152] C. Greggio *et al.*, "Enhanced Respiratory Chain Supercomplex Formation in Response to Exercise in Human Skeletal Muscle," *Cell Metab.*, vol. 25, no. 2, pp.

301–311, 2017, doi: 10.1016/j.cmet.2016.11.004.

[153] G. E. Walker, P. Marzullo, R. Ricotti, G. Bona, and F. Prodam, "The pathophysiology of abdominal adipose tissue depots in health and disease," *Horm. Mol. Biol. Clin. Investig.*, vol. 19, no. 1, pp. 57–74, Jan. 2014, doi: 10.1515/hmbci-2014-0023.

[154] S. Cinti, "Adipose Organ Development and Remodeling," in *Comprehensive Physiology*, vol. 8, 2018, pp. 1357–1431.

[155] K. Sun, C. M. Kusminski, and P. E. Scherer, "Adipose tissue remodeling and obesity.," *J. Clin. Invest.*, vol. 121, no. 6, pp. 2094–2101, 2011, doi: 10.1172/JCI45887.

[156] G. Marcelin, A. L. M. Silveira, L. B. Martins, A. V. M. Ferreira, and K. Clément, "Deciphering the cellular interplays underlying obesityinduced adipose tissue fibrosis," *J. Clin. Invest.*, vol. 129, no. 10, pp. 4032–4040, 2019, doi: 10.1172/JCI129192.

[157] Gijs H. Goossens, "The Metabolic Phenotype in Obesity: Fat Mass, Body Fat Distribution, and Adipose Tissue Function," *Obes Facts*, vol. 10, pp. 207–215, 2017, Accessed: Sep. 11, 2019. [Online]. Available: https://www.ncbi.nlm.nih.gov/pmc/articles/PMC5644968/pdf/ofa-0010-0207.pdf.

[158] M. Longo *et al.*, "Adipose Tissue Dysfunction as Determinant of Obesity-Associated Metabolic Complications," *Int. J. Mol. Sci.*, vol. 20, no. 2358, 2019, Accessed: Sep. 10, 2019. [Online]. Available: https://www.ncbi.nlm.nih.gov/pmc/articles/PMC6539070/pdf/ijms-20-02358.pdf.

[159] L. Tankó, Y. Bagger, P. Alexandersen, P. Larsen, and C. Christiansen, "Central and peripheral fat mass have contrasting effect on the progression of aortic calcification in postmenopausal women," *Eur Hear. J*, vol. 24, no. 16, pp. 1531–1537, 2003.

[160] R. E. Van Pelt, E. M. Evans, K. B. Schechtman, A. A. Ehsani, and W. M. Kohrt, "Contributions of total and regional fat mass to risk for cardiovascular disease in older women," *Am. J. Physiol. - Endocrinol. Metab.*, vol. 282, no. 5 45-5, pp. 1023–1028, 2002, doi: 10.1152/ajpendo.00467.2001.

[161] B. F. Palmer, "The sexual dimorphism of obesity," *Mol. Cell. Endocrinol.*, vol. 31, no. 3, pp. 477–479, 2013, doi: 10.1016/j.mce.2014.11.029.The.

[162] M. Williams, G. Hunter, T. Kekes-Szabo, S. Snyder, and M. Treuth, "Regional fat distribution in women and risk of cardiovascular disease," *Am J Clin Nutr*, vol. 65,

no. 3, pp. 855–860, 1997.

[163] R. E. Van Pelt, C. M. Jankowski, W. S. Gozansky, R. S. Schwartz, and W. M. Kohrt, "Lower-body adiposity and metabolic protection in postmenopausal women," *J. Clin. Endocrinol. Metab.*, vol. 90, no. 8, pp. 4573–4578, 2005, doi: 10.1210/jc.2004-1764.

[164] G. Bos *et al.*, "Opposite contributions of trunk and leg fat mass with plasma lipase activities: The hoorn study," *Obes. Res.*, vol. 13, no. 10, pp. 1817–1823, 2005, doi: 10.1038/oby.2005.221.

[165] A. Krauze *et al.*, "Sex and body mass index implications on gluteofemoral subcutaneous tissue morphology visualized by ultrasonography – preliminary study," *J. Ultrason.*, vol. 19, no. 77, pp. 105–112, 2019, doi: 10.15557/JoU.2019.0015.

[166] G. Conti *et al.*, "Proteomic and ultrastructural analysis of cellulite— new findings on an old topic," *Int. J. Mol. Sci.*, vol. 21, no. 6, 2020, doi: 10.3390/ijms21062077.

[167] G. Ganesan *et al.*, "Diffuse optical spectroscopic imaging of subcutaneous adipose tissue metabolic changes during weight loss," *Int. J. Obes.*, vol. 40, no. 8, pp. 1292–1300, 2016, doi: 10.1038/ijo.2016.43.

[168] V. A. Hughes, W. R. Frontera, R. Roubenoff, W. J. Evans, and M. A. Fiatarone Singh, "Longitudinal changes in body composition in older men and women: Role of body weight change and physical activity," *Am. J. Clin. Nutr.*, vol. 76, no. 2, pp. 473–481, 2002, doi: 10.1093/ajcn/76.2.473.

[169] G. B. Forbes, "Longitudinal changes in adult fat-free mass: Influence of body weight," *Am. J. Clin. Nutr.*, vol. 70, no. 6, pp. 1025–1031, 1999, doi: 10.1093/ajcn/70.6.1025.

[170] D. L. Waters, R. N. Baumgartner, P. J. Garry, and B. Vellas, "Advantages of dietary, exercise-related, and therapeutic interventions to prevent and treat sarcopenia in adult patients: an update.," *Clin. Interv. Aging*, vol. 5, pp. 259–270, 2010, doi: 10.2147/cia.s6920.

[171] L. Józsa, M. Järvinen, M. Kvist, M. Lehto, and A. Mikola, "Capillary density of tenotomized skeletal muscles. I. Experimental study in the rat.," *Eur J Appl Physiol Occup Physiol*, vol. 44, no. 2, pp. 175–181, 1980.

[172] Y. Kano, S. Shimegi, H. Takahashi, K. Masuda, and S. Katsuta, "Changes in capillary luminal diameter in rat soleus muscle after hind-limb suspension," *Acta Physiol Scand*, vol. 169, no. 4, pp. 271–276, 2000.

[173] K. Tyml and O. Mathieu-Costello, "Structural and functional changes in the

microvasculature of disused skeletal muscle," *Front Biosci*, vol. 6, pp. D45-52, 2001.

[174] L. Gliemann *et al.*, "Resveratrol modulates the angiogenic response to exercise training in skeletal muscles of aged men," *Am. J. Physiol. - Hear. Circ. Physiol.*, vol. 307, no. 8, pp. H1111–H1119, 2014, doi: 10.1152/ajpheart.00168.2014.

[175] R. T. Hepple, S. L. M. Mackinnon, J. M. Goodman, S. G. Thomas, and M. J. Plyley, "Resistance and aerobic training in older men: Effects on VO(2peak) and the capillary supply to skeletal muscle," *J. Appl. Physiol.*, vol. 82, no. 4, pp. 1305–1310, 1997, doi: 10.1152/jappl.1997.82.4.1305.

[176] L. B. Verdijk, T. Snijders, T. M. Holloway, J. Van Kraenburg, and L. J. C. Van Loon, "Resistance Training Increases Skeletal Muscle Capillarization in Healthy Older Men," *Med. Sci. Sport. Exerc.*, vol. 48, no. 11, pp. 2157–2164, 2016.

[177] T. Snijders *et al.*, "Muscle fibre capillarization is a critical factor in muscle fibre hypertrophy during resistance exercise training in older men," *J. Cachexia. Sarcopenia Muscle*, vol. 8, no. 2, pp. 267–276, 2017, doi: 10.1002/jcsm.12137.

[178] K. Deruisseau, A. Kavazis, and S. Powers, "Selective downregulation of ubiquitin conjugation cascade mRNA occurs in the senescent rat soleus muscle," *Exp Gerontol*, vol. 40, no. 6, pp. 526–531, 2005.

[179] R. Whipple, L. Wolfson, and P. Amerman, "The relationship of knee and ankle weakness to falls in nursing home residents: an isokinetic study," *J Am Geriatr Soc*, vol. 35, no. 1, pp. 13–20, 1987.

[180] L. Larsson and T. Ansved, "Effects of ageing on the motor unit," *Prog Neurobiol*, vol. 45, no. 5, pp. 397–458, 1995.

[181] A. D. Mora *et al.*, "Towards next-generation time-domain diffuse optics for extreme depth penetration and sensitivity," *Biomed. Opt. Express*, vol. 6, no. 5, p. 1749, 2015, doi: 10.1364/BOE.6.001749.

[182] A. Pifferi *et al.*, "Performance assessment of photon migration instruments: the MEDPHOT protocol," *Appl. Opt.*, vol. 44, no. 11, p. 2104, 2005, doi: 10.1364/AO.44.002104.

[183] H. Wabnitz *et al.*, "Performance assessment of time-domain optical brain imagers, part 1: basic instrumental performance protocol," *J. Biomed. Opt.*, vol. 19, no. 8, p. 086010, 2014, doi: 10.1117/1.JBO.19.8.086010.

[184] A. Pifferi, P. Taroni, G. Valentini, and S. Andersson-Engels, "Real-time method for fitting time-resolved reflectance and transmittance measurements with a Monte Carlo model," *Appl. Opt.*, vol. 37, no. 13, p. 2774, 1998, doi: 10.1364/ao.37.002774.

[185] E. Alerstam, T. Svensson, and S. Andersson-Engels, "Parallel computing with graphics processing units for high-speed Monte Carlo simulation of photon migration," *J. Biomed. Opt.*, vol. 13, no. 6, p. 060504, 2008, doi: 10.1117/1.3041496.

[186] R. Cubeddu, A. Pifferi, P. Taroni, A. Torricelli, and G. Valentini, "Experimental test of theoretical models for time-resolved reflectance," *Med. Phys*, vol. 23, no. 9, pp. 1625–1633, 1996.

[187] P. Taroni, A. Bassi, D. Comelli, A. Farina, R. Cubeddu, and A. Pifferi, "Diffuse optical spectroscopy of breast tissue extended to 1100 nm," *J. Biomed. Opt.*, vol. 14, no. 5, p. 054030, 2009, doi: 10.1117/1.3251051.

[188] S. K. V. Sekar *et al.*, "Diffuse optical characterization of collagen absorption from 500 to 1700 nm," *J. Biomed. Opt.*, vol. 22, no. 1, p. 015006, 2017, doi: 10.1117/1.jbo.22.1.015006.

[189] S. Prahl, "Assorted Spectra." .

[190] C. D'Andrea *et al.*, "Time-resolved spectrally constrained method for the quantification of chromophore concentrations and scattering parameters in diffusing media.," *Opt. Express*, vol. 14, no. 5, pp. 1888–1898, 2006, doi: 10.1364/OE.14.001888.

[191] H. Ding, J. Q. Lu, W. A. Wooden, P. J. Kragel, and X. H. Hu, "Refractive indices of human skin tissues at eight wavelengths and estimated dispersion relations between 300 and 1600 nm," *Phys. Med. Biol.*, vol. 51, no. 6, pp. 1479–1489, 2006, doi: 10.1088/0031-9155/51/6/008.

[192] A. N. Bashkatov, E. A. Genina, V. I. Kochubey, and V. V Tuchin, "Optical properties of human skin, subcutaneous and mucous tissues in the wavelength range from 400 to 2000 nm," *J. Phys. D. Appl. Phys.*, vol. 38, no. 15, pp. 2543–2555, Aug. 2005, doi: 10.1088/0022-3727/38/15/004.

[193] C. R. Simpson, M. Kohl, M. Essenpreis, and M. Cope, "Near-infrared optical properties of ex vivo human skin and subcutaneous tissues measured using the Monte Carlo inversion technique," *Phys. Med. Biol.*, vol. 43, no. 9, pp. 2465–2478, 1998, doi: 10.1088/0031-9155/43/9/003.

[194] M. Cesari *et al.*, "Hemoglobin Levels and Skeletal Muscle: Results From the InCHIANTI Study," *Journals Gerontol. Ser. A Biol. Sci. Med. Sci.*, vol. 59, no. 3, pp. M249–M254, 2004, doi: 10.1093/gerona/59.3.M249.

[195] S. B. Heymsfield, V. Stevens, R. Noel, C. McManus, J. Smith, and D. Nixon, "Biochemical composition of muscle in normal and semistarved human subjects:

Relevance to anthropometric measurements," *Am. J. Clin. Nutr.*, vol. 36, no. 1, pp. 131–142, 1982, doi: 10.1093/ajcn/36.1.131.

[196] T. Cortázar, M. Guzmán-Alonso, H. Novoa, and M. Riaño, "Water content at different skin depths and the influence of moisturizing formulations," *Ski. Res Technol*, vol. 21, no. 3, pp. 35–40, 2016.

[197] S. L. Jacques and S. A. Prah, "Mie scattering from collagen fibers," 1998. .

[198] E. Dransfield, "Intramuscular composition and texture of beef muscles," *J. Sci. Food Agric.*, vol. 28, no. 9, pp. 833–842, 1977.

[199] L. S. L. Arakaki, W. A. Ciesielski, B. D. Thackray, E. O. Feigl, and K. A. Schenkman, "Simultaneous Optical Spectroscopic Measurement of Hemoglobin and Myoglobin Saturations and Cytochrome aa3 Oxidation In Vivo," *Appl Spectrosc*, vol. 64, no. 9, pp. 973–979, 2010.

[200] A. Van Dorn, "COVID-19 and readjusting clinical trials," *Lancet*, vol. 396, no. 10250, pp. 523–524, 2020.

[201] Collaborative Geriatric Medicine Research, "Age and frailty are independently associated with increased COVID-19 mortality and increased care needs in survivors: results of an international multi-centre study," *Age Ageing*, 2021.

[202] X. Zhang, A. Lewis, J. Moley, and J. Brestoff, "A systematic review and meta-analysis of obesity and COVID-19 outcomes," *Sci Rep*, vol. 11, no. 1, p. 7193, 2021.

[203] L. Kompaniyets *et al.*, "Body Mass Index and Risk for COVID-19-Related Hospitalization, Intensive Care Unit Admission, Invasive Mechanical Ventilation, and Death - United States, March-December 2020," *MMWR Morb Mortal Wkly Rep*, vol. 70, no. 10, pp. 355–361, 2021.

[204] R. Aquilani *et al.*, "Effects of oral amino acid supplementation on long-term-care-acquired infections in elderly patients," *Arch Gerontol Geriatr*, vol. 52, no. 3, pp. 123–128, 2011.

[205] C.-D. Liao *et al.*, "Effects of elastic resistance exercise on body composition and physical capacity in older women with sarcopenic obesity: A CONSORT-compliant prospective randomized controlled trial," *Medicine (Baltimore).*, vol. 96, no. 23, p. e7115, 2017, doi: 10.1097/MD.0000000000007115.

[206] S. W. Huang, J. W. Ku, L. F. Lin, C. De Liao, L. C. Chou, and T. H. Liou, "Body composition influenced by progressive elastic band resistance exercise of sarcopenic obesity elderly women: A pilot randomized controlled trial," *Eur. J. Phys. Rehabil. Med.*, vol. 53, no. 4, pp. 556–563, 2017, doi: 10.23736/S1973-9087.17.04443-4.

[207] R. Ventura-Clapier *et al.*, "Mitochondria: a central target for sex differences in pathologies.," *Clin. Sci.*, vol. 131, no. 9, pp. 803–822, May 2017, doi: 10.1042/CS20160485.

Appendix A: Supplementary Information for Section 4.3

Absorption and reduced scattering spectra measured on the abdominal region. Spectra for the five positions at ρ=2 for all the 10 subjects.

Subject #1

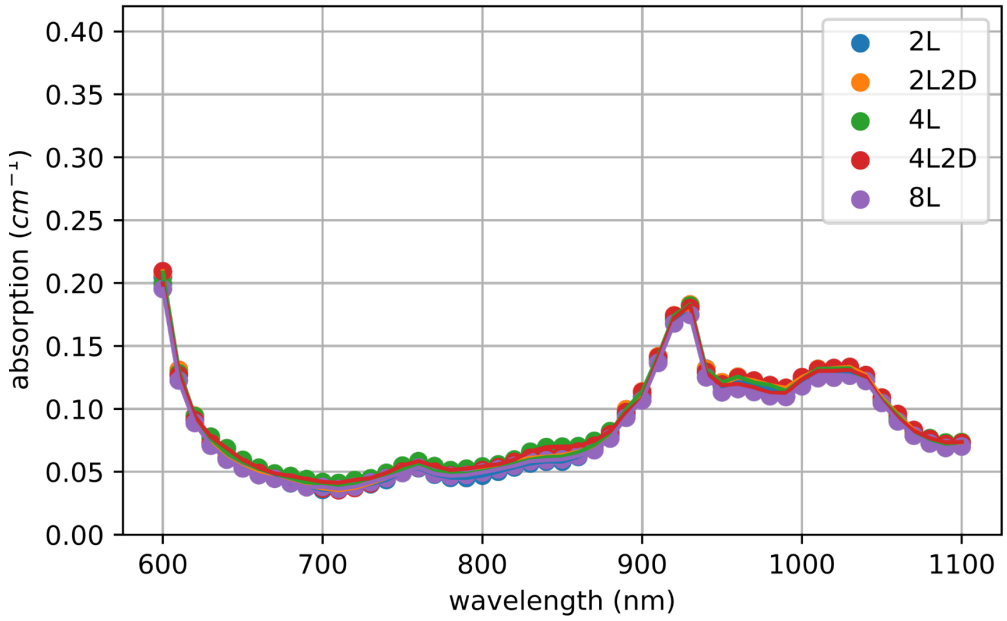

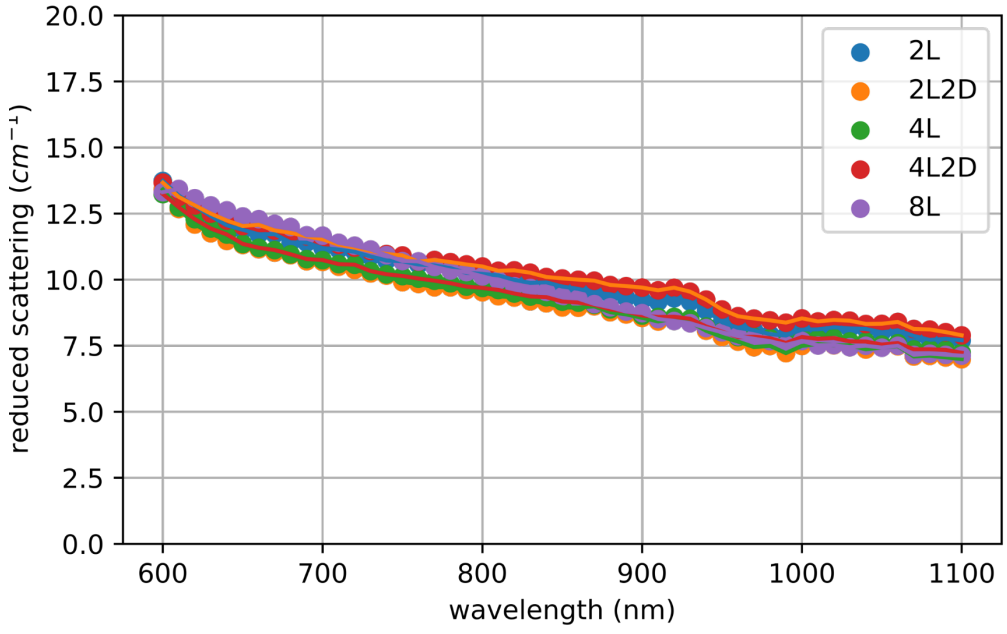

Subject #2

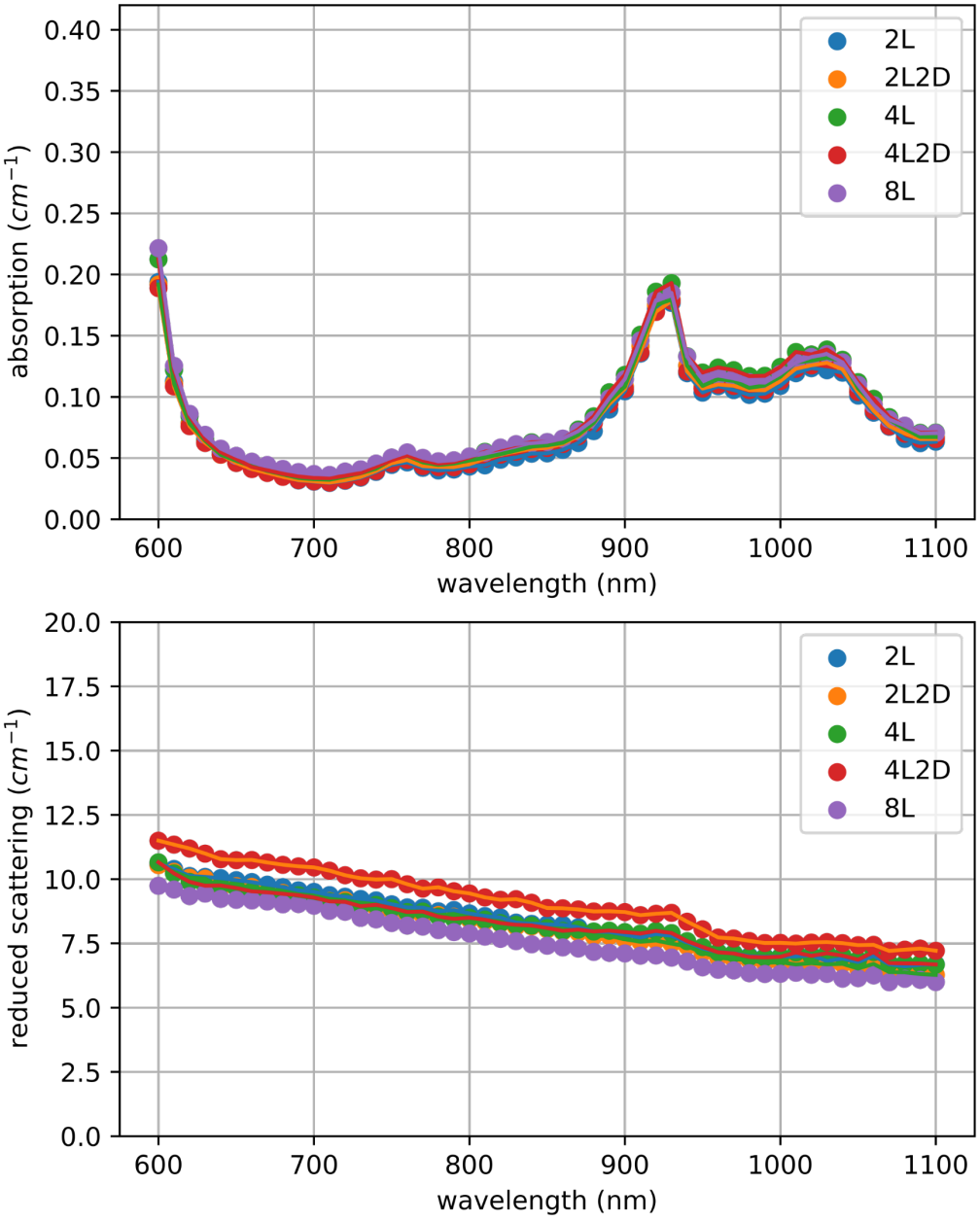
absorption (cm^{-1})
0.40
0.35
0.30
0.25
0.20
0.15
0.10
0.05
0.00
600
700
800
900
1000
1100
wavelength (nm)
2L
2L2D
4L
4L2D
8L
reduced scattering (cm^{-1})
20.0
17.5
15.0
12.5
10.0
7.5
5.0
2.5
0.0
600
700
800
900
1000
1100
wavelength (nm)
2L
2L2D
4L
4L2D
8L

Subject #3

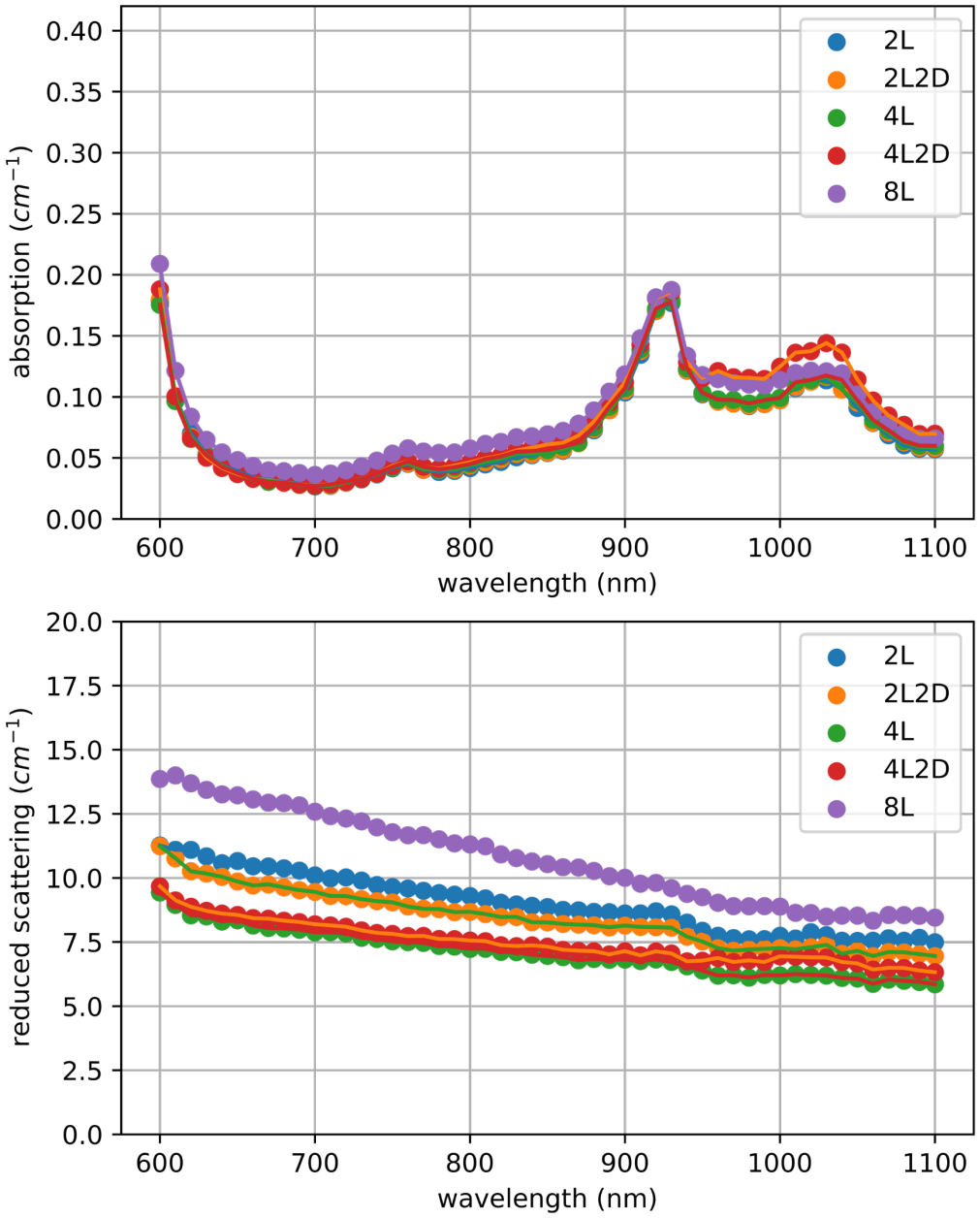
absorption (cm^{-1})
0.40
0.35
0.30
0.25
0.20
0.15
0.10
0.05
0.00
600
700
800
900
1000
1100
wavelength (nm)
2L
2L2D
4L
4L2D
8L
reduced scattering (cm^{-1})
20.0
17.5
15.0
12.5
10.0
7.5
5.0
2.5
0.0
600
700
800
900
1000
1100
wavelength (nm)
2L
2L2D
4L
4L2D
8L

Subject #4

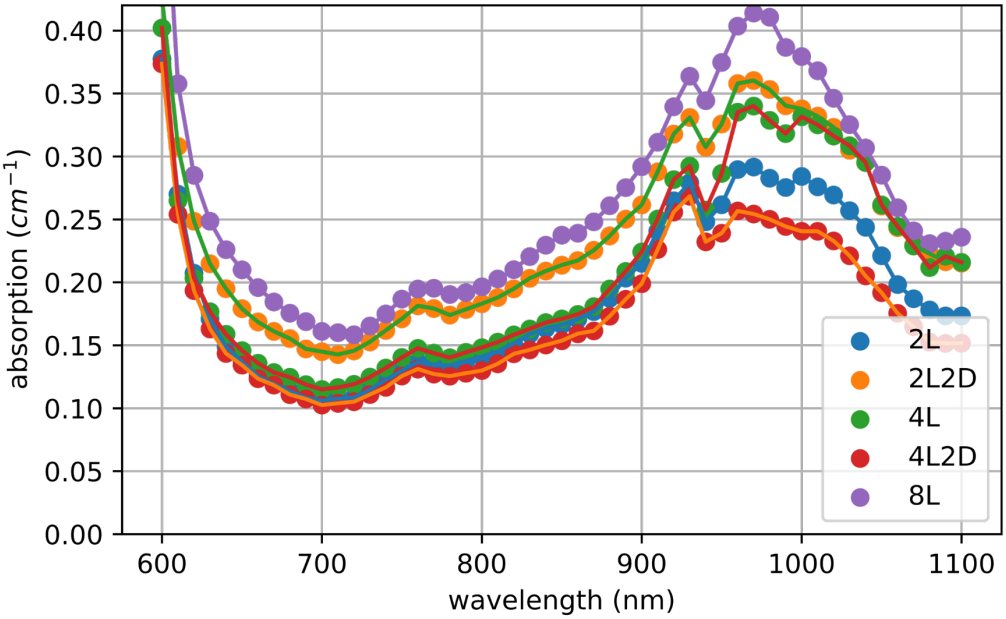
absorption (cm^{-1})
0.40
0.35
0.30
0.25
0.20
0.15
0.10
0.05
0.00
600
700
800
900
1000
1100
wavelength (nm)
2L
2L2D
4L
4L2D
8L

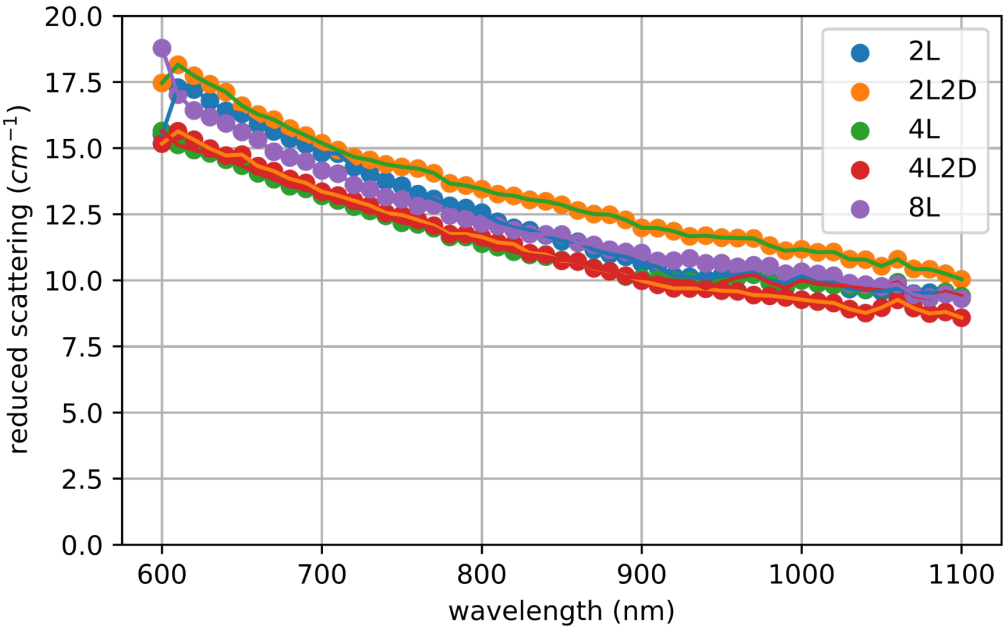
reduced scattering (cm^{-1})
20.0
17.5
15.0
12.5
10.0
7.5
5.0
2.5
0.0
600
700
800
900
1000
1100
wavelength (nm)
2L
2L2D
4L
4L2D
8L

Subject #5

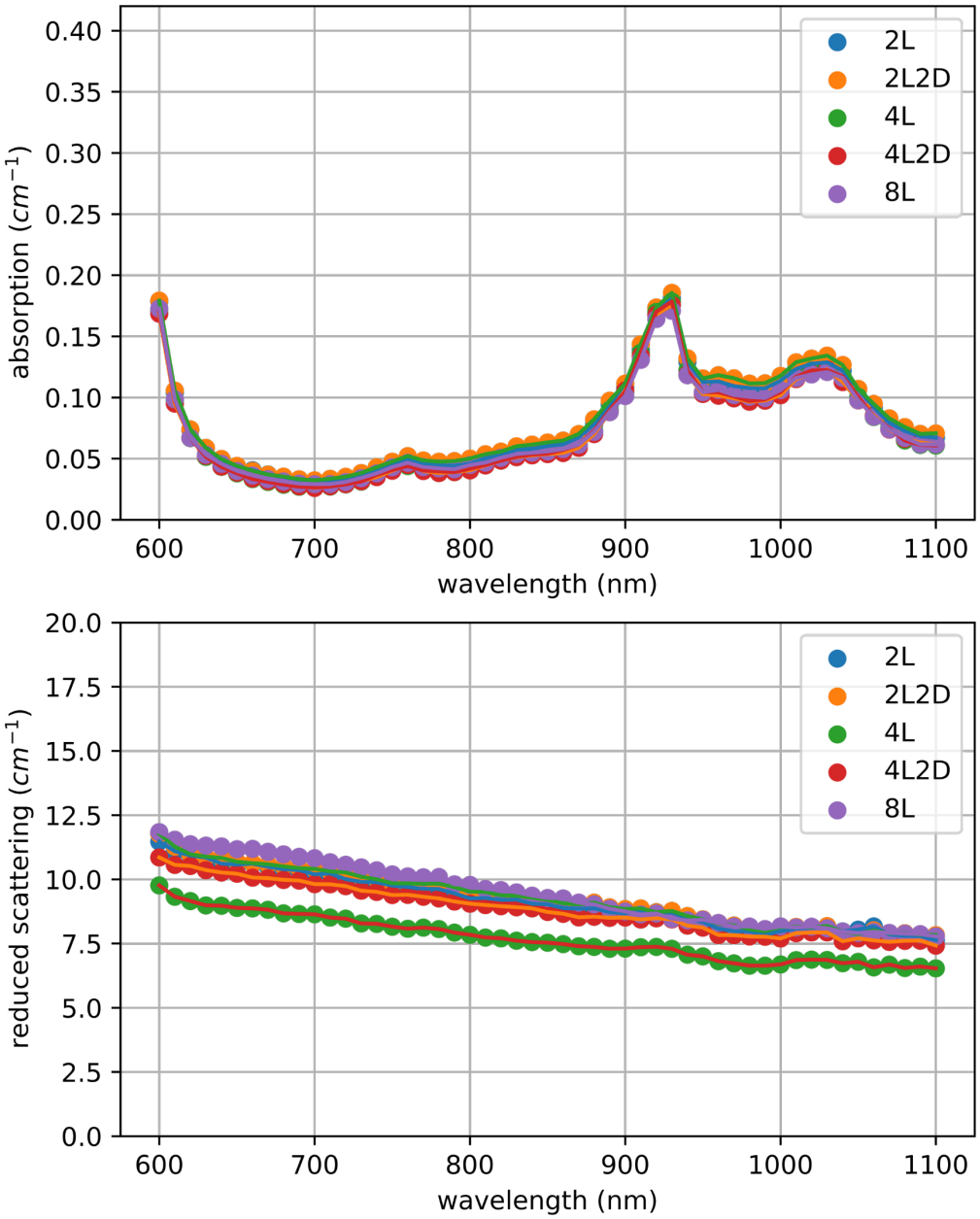
absorption (cm^{-1})
0.40
0.35
0.30
0.25
0.20
0.15
0.10
0.05
0.00
600
700
800
900
1000
1100
wavelength (nm)
2L
2L2D
4L
4L2D
8L
reduced scattering (cm^{-1})
20.0
17.5
15.0
12.5
10.0
7.5
5.0
2.5
0.0
600
700
800
900
1000
1100
wavelength (nm)
2L
2L2D
4L
4L2D
8L

Suject #6

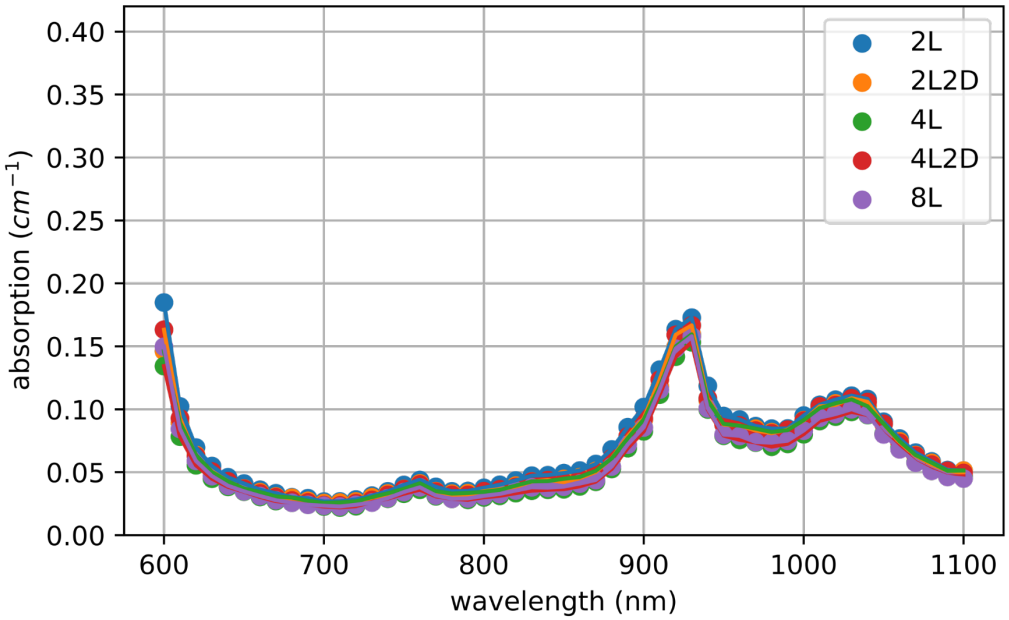
absorption (cm^{-1})
0.40
0.35
0.30
0.25
0.20
0.15
0.10
0.05
0.00
600
700
800
900
1000
1100
wavelength (nm)
2L
2L2D
4L
4L2D
8L

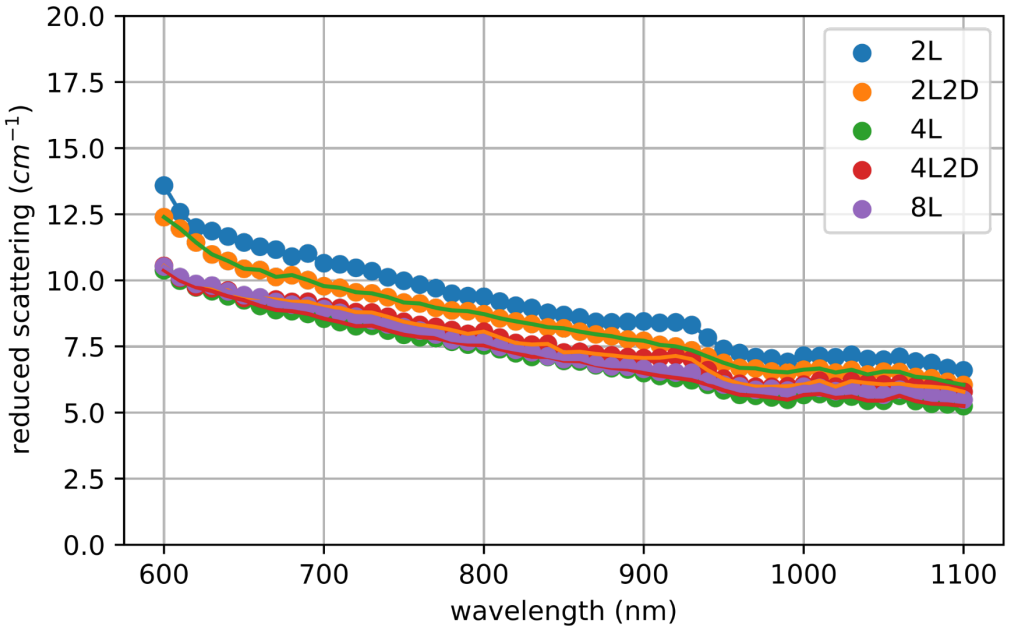
reduced scattering (cm^{-1})
20.0
17.5
15.0
12.5
10.0
7.5
5.0
2.5
0.0
600
700
800
900
1000
1100
wavelength (nm)
2L
2L2D
4L
4L2D
8L

Subject #7

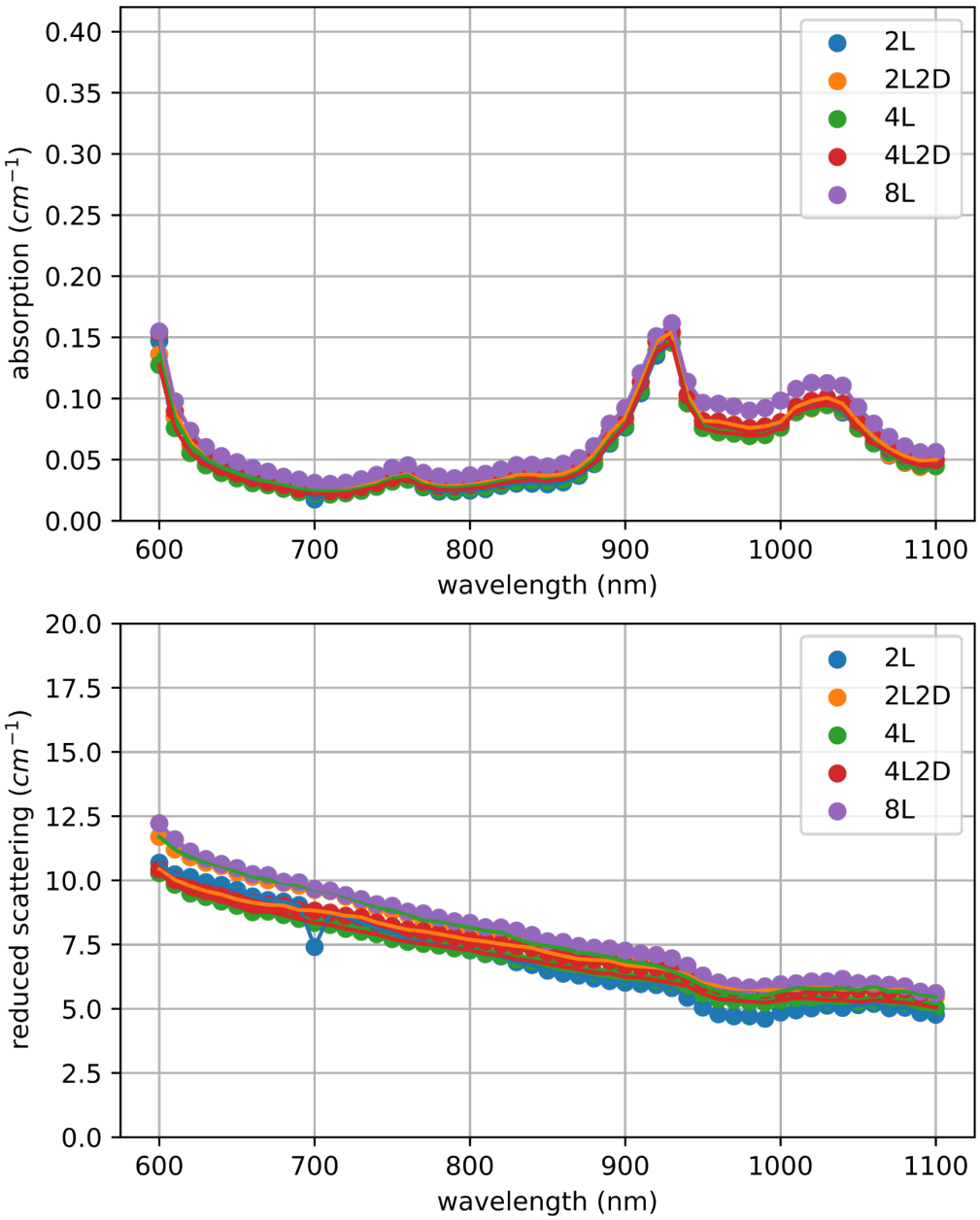
absorption (cm^{-1})
0.40
0.35
0.30
0.25
0.20
0.15
0.10
0.05
0.00
600
700
800
900
1000
1100
wavelength (nm)
2L
2L2D
4L
4L2D
8L
reduced scattering (cm^{-1})
20.0
17.5
15.0
12.5
10.0
7.5
5.0
2.5
0.0
600
700
800
900
1000
1100
wavelength (nm)
2L
2L2D
4L
4L2D
8L

Subject #8

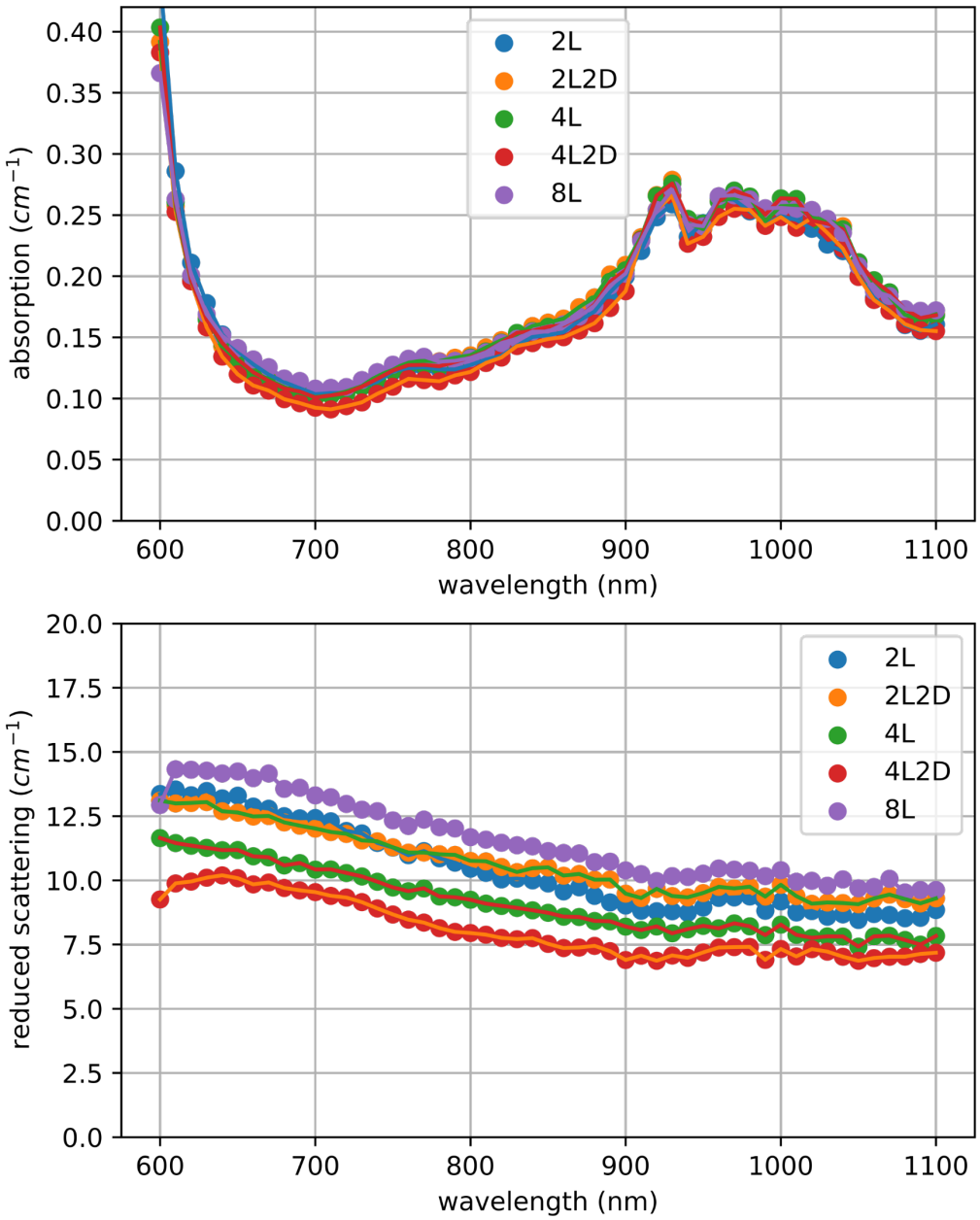
2L
2L2D
4L
4L2D
8L
absorption (cm^{-1})
0.40
0.35
0.30
0.25
0.20
0.15
0.10
0.05
0.00
600
700
800
900
1000
1100
wavelength (nm)
reduced scattering (cm^{-1})
20.0
17.5
15.0
12.5
10.0
7.5
5.0
2.5
0.0
600
700
800
900
1000
1100
wavelength (nm)

Subject #9

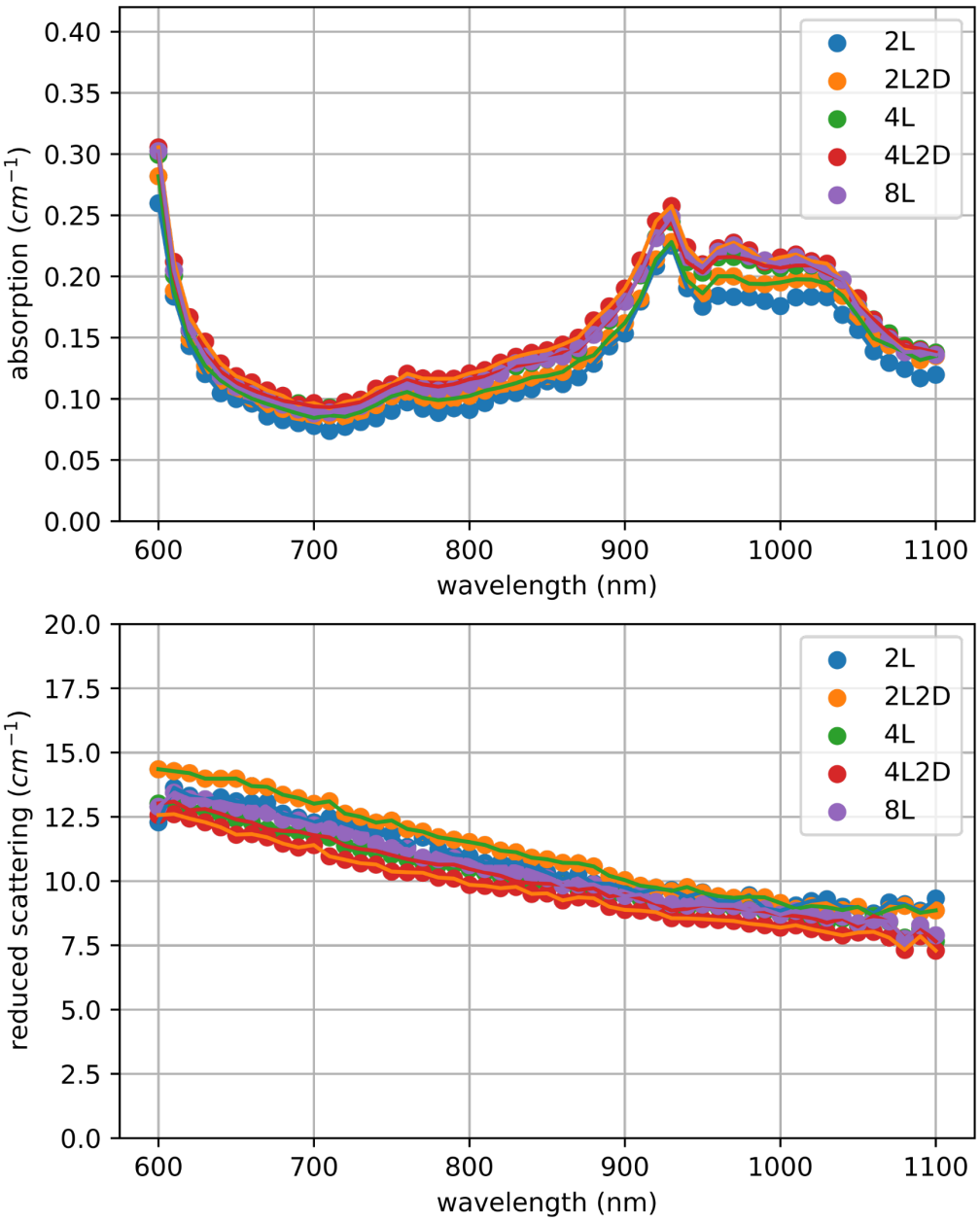
absorption (cm^{-1})
0.40
0.35
0.30
0.25
0.20
0.15
0.10
0.05
0.00
600
700
800
900
1000
1100
wavelength (nm)
2L
2L2D
4L
4L2D
8L
reduced scattering (cm^{-1})
20.0
17.5
15.0
12.5
10.0
7.5
5.0
2.5
0.0
600
700
800
900
1000
1100
wavelength (nm)
2L
2L2D
4L
4L2D
8L

Subject #10

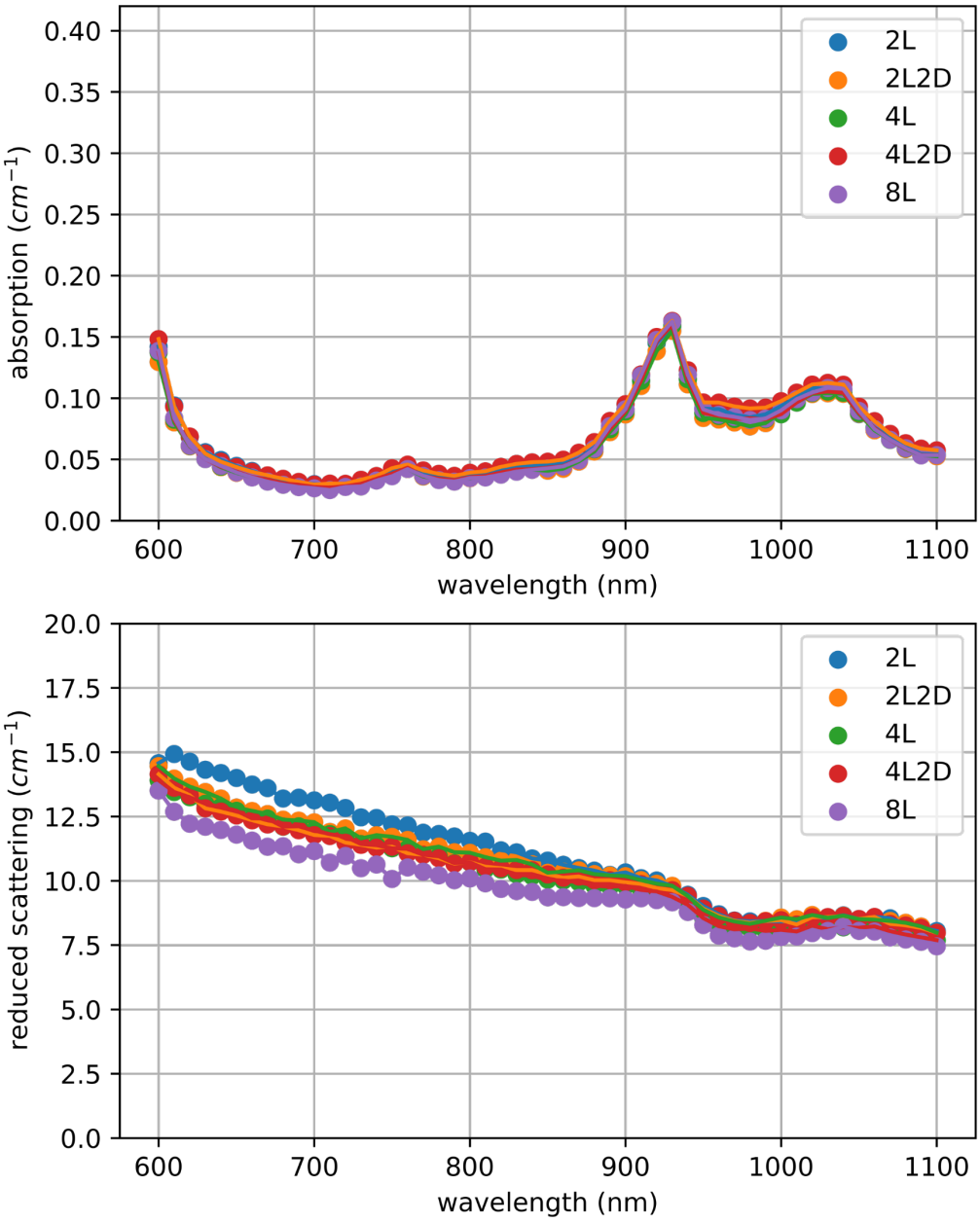
absorption (cm^{-1})
0.40
0.35
0.30
0.25
0.20
0.15
0.10
0.05
0.00
600
700
800
900
1000
1100
wavelength (nm)
2L
2L2D
4L
4L2D
8L
reduced scattering (cm^{-1})
20.0
17.5
15.0
12.5
10.0
7.5
5.0
2.5
0.0
600
700
800
900
1000
1100
wavelength (nm)
2L
2L2D
4L
4L2D
8L

Absorption spectra for the five positions (2L= 2 cm left to the navel, 4L= 4 cm left to the navel, 4L2D= 4 cm left 2cm down to the navel, 2L2D= 2 cm left 2cm down to the navel, 8L= 8 cm left to the navel) measured on the abdominal region. Spectra with mean values from all the subjects at the three interfibre distances.

Rho1

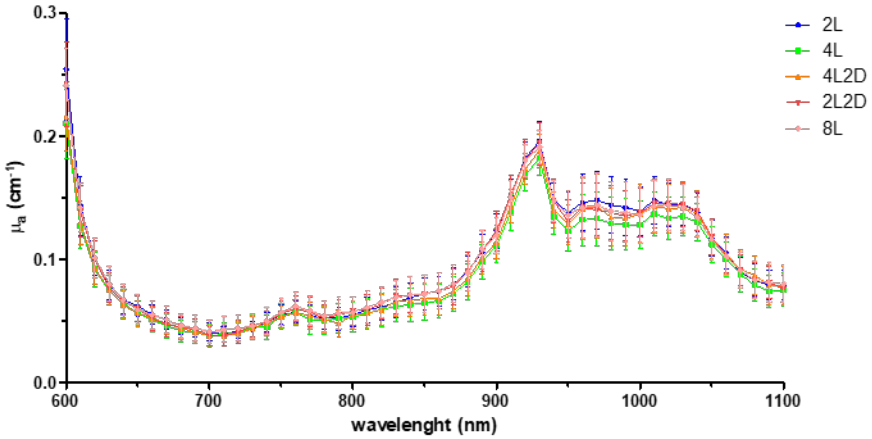

Rho2

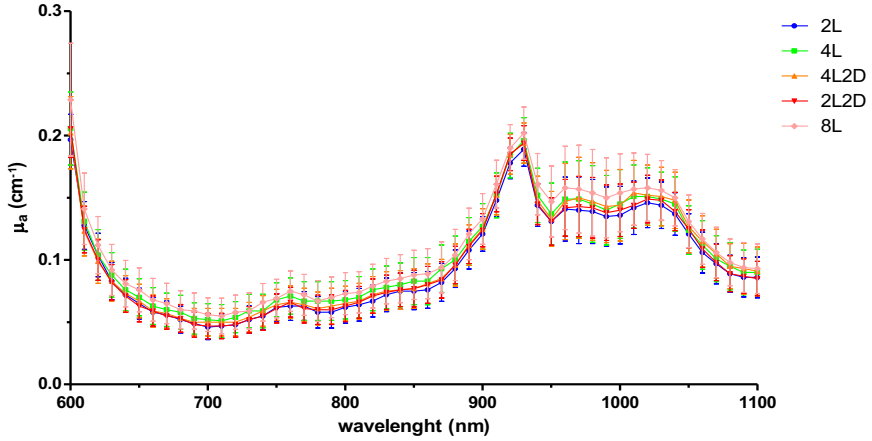

Rho3

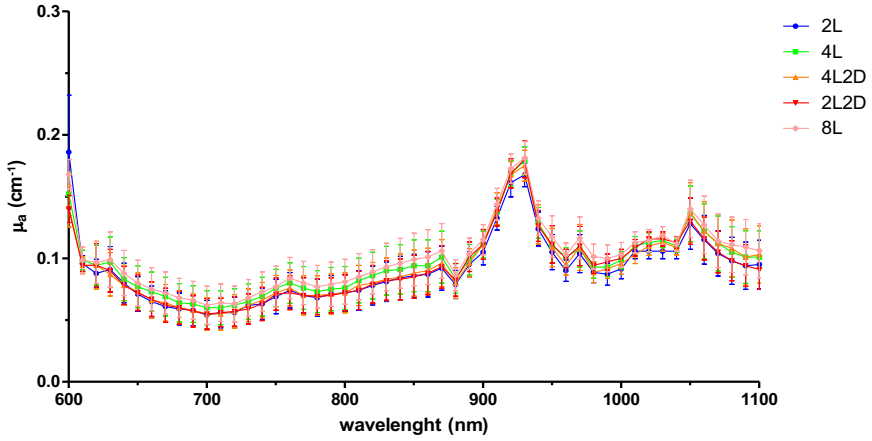

Comparison of the absorption coefficients in the range of wavelengths 600-1100nm at the different tested positions.

Rho1

wavelenght (nm)	2L vs 4L	2L vs 4L2D	2L vs 2L2D	2L vs 8L	4L vs 4L2D	4L vs 2L2D	4L vs 8L	4L2D vs 2L2D	4L2D vs 8L	2L2D vs 8L
600	***	***	ns	ns	ns	***	***	**	*	ns
610	ns	ns	ns	ns	ns	ns	ns	ns	ns	ns
620	ns	ns	ns	ns	ns	ns	ns	ns	ns	ns
630	ns	ns	ns	ns	ns	ns	ns	ns	ns	ns
640	ns	ns	ns	ns	ns	ns	ns	ns	ns	ns
650	ns	ns	ns	ns	ns	ns	ns	ns	ns	ns
660	ns	ns	ns	ns	ns	ns	ns	ns	ns	ns
670	ns	ns	ns	ns	ns	ns	ns	ns	ns	ns
680	ns	ns	ns	ns	ns	ns	ns	ns	ns	ns
690	ns	ns	ns	ns	ns	ns	ns	ns	ns	ns
700	ns	ns	ns	ns	ns	ns	ns	ns	ns	ns
710	ns	ns	ns	ns	ns	ns	ns	ns	ns	ns
720	ns	ns	ns	ns	ns	ns	ns	ns	ns	ns
730	ns	ns	ns	ns	ns	ns	ns	ns	ns	ns
740	ns	ns	ns	ns	ns	ns	ns	ns	ns	ns
750	ns	ns	ns	ns	ns	ns	ns	ns	ns	ns
760	ns	ns	ns	ns	ns	ns	ns	ns	ns	ns
770	ns	ns	ns	ns	ns	ns	ns	ns	ns	ns
780	ns	ns	ns	ns	ns	ns	ns	ns	ns	ns
790	ns	ns	ns	ns	ns	ns	ns	ns	ns	ns
800	ns	ns	ns	ns	ns	ns	ns	ns	ns	ns
810	ns	ns	ns	ns	ns	ns	ns	ns	ns	ns
820	ns	ns	ns	ns	ns	ns	ns	ns	ns	ns
830	ns	ns	ns	ns	ns	ns	ns	ns	ns	ns
840	ns	ns	ns	ns	ns	ns	ns	ns	ns	ns
850	ns	ns	ns	ns	ns	ns	ns	ns	ns	ns
860	ns	ns	ns	ns	ns	ns	ns	ns	ns	ns
870	ns	ns	ns	ns	ns	ns	ns	ns	ns	ns
880	ns	ns	ns	ns	ns	ns	ns	ns	ns	ns
890	ns	ns	ns	ns	ns	ns	ns	ns	ns	ns
900	ns	ns	ns	ns	ns	ns	ns	ns	ns	ns
910	ns	ns	ns	ns	ns	ns	ns	ns	ns	ns
920	ns	ns	ns	ns	ns	ns	ns	ns	ns	ns
930	ns	ns	ns	ns	ns	ns	ns	ns	ns	ns
940	ns	ns	ns	ns	ns	ns	ns	ns	ns	ns
950	ns	ns	ns	ns	ns	ns	ns	ns	ns	ns
960	ns	ns	ns	ns	ns	ns	ns	ns	ns	ns
970	ns	ns	ns	ns	ns	ns	ns	ns	ns	ns
980	ns	ns	ns	ns	ns	ns	ns	ns	ns	ns
990	ns	ns	ns	ns	ns	ns	ns	ns	ns	ns
1000	ns	ns	ns	ns	ns	ns	ns	ns	ns	ns
1010	ns	ns	ns	ns	ns	ns	ns	ns	ns	ns
1020	ns	ns	ns	ns	ns	ns	ns	ns	ns	ns
1030	ns	ns	ns	ns	ns	ns	ns	ns	ns	ns
1040	ns	ns	ns	ns	ns	ns	ns	ns	ns	ns
1050	ns	ns	ns	ns	ns	ns	ns	ns	ns	ns
1060	ns	ns	ns	ns	ns	ns	ns	ns	ns	ns
1070	ns	ns	ns	ns	ns	ns	ns	ns	ns	ns
1080	ns	ns	ns	ns	ns	ns	ns	ns	ns	ns
1090	ns	ns	ns	ns	ns	ns	ns	ns	ns	ns
1100	ns	ns	ns	ns	ns	ns	ns	ns	ns	ns

Statistical analysis was performed with two-way ANOVA and Bonferroni's multiple comparison test. Error bars represent SEM; n=10; ns=not significant, *p<0.05, **p<0.01, ***p<0.001. Outliers values are removed from the dataset.

Rho 2

wavelenght (nm)	2L vs 4L	2L vs 4L2D	2L vs 2L2D	2L vs 8L	4L vs 4L2D	4L vs 2L2D	4L vs 8L	4L2D vs 2L2D	4L2D vs 8L	2L2D vs 8L
600	ns	ns	ns	***	ns	ns	*	ns	**	*
610	ns	ns	ns	ns	ns	ns	ns	ns	ns	ns
620	ns	ns	ns	ns	ns	ns	ns	ns	ns	ns
630	ns	ns	ns	ns	ns	ns	ns	ns	ns	ns
640	ns	ns	ns	ns	ns	ns	ns	ns	ns	ns
650	ns	ns	ns	ns	ns	ns	ns	ns	ns	ns
660	ns	ns	ns	ns	ns	ns	ns	ns	ns	ns
670	ns	ns	ns	ns	ns	ns	ns	ns	ns	ns
680	ns	ns	ns	ns	ns	ns	ns	ns	ns	ns
690	ns	ns	ns	ns	ns	ns	ns	ns	ns	ns
700	ns	ns	ns	ns	ns	ns	ns	ns	ns	ns
710	ns	ns	ns	ns	ns	ns	ns	ns	ns	ns
720	ns	ns	ns	ns	ns	ns	ns	ns	ns	ns
730	ns	ns	ns	ns	ns	ns	ns	ns	ns	ns
740	ns	ns	ns	ns	ns	ns	ns	ns	ns	ns
750	ns	ns	ns	ns	ns	ns	ns	ns	ns	ns
760	ns	ns	ns	ns	ns	ns	ns	ns	ns	ns
770	ns	ns	ns	ns	ns	ns	ns	ns	ns	ns
780	ns	ns	ns	ns	ns	ns	ns	ns	ns	ns
790	ns	ns	ns	ns	ns	ns	ns	ns	ns	ns
800	ns	ns	ns	ns	ns	ns	ns	ns	ns	ns
810	ns	ns	ns	ns	ns	ns	ns	ns	ns	ns
820	ns	ns	ns	ns	ns	ns	ns	ns	ns	ns
830	ns	ns	ns	ns	ns	ns	ns	ns	ns	ns
840	ns	ns	ns	ns	ns	ns	ns	ns	ns	ns
850	ns	ns	ns	ns	ns	ns	ns	ns	ns	ns
860	ns	ns	ns	ns	ns	ns	ns	ns	ns	ns
870	ns	ns	ns	ns	ns	ns	ns	ns	ns	ns
880	ns	ns	ns	ns	ns	ns	ns	ns	ns	ns
890	ns	ns	ns	ns	ns	ns	ns	ns	ns	ns
900	ns	ns	ns	ns	ns	ns	ns	ns	ns	ns
910	ns	ns	ns	ns	ns	ns	ns	ns	ns	ns
920	ns	ns	ns	ns	ns	ns	ns	ns	ns	ns
930	ns	ns	ns	ns	ns	ns	ns	ns	ns	ns
940	ns	ns	ns	ns	ns	ns	ns	ns	ns	ns
950	ns	ns	ns	ns	ns	ns	ns	ns	ns	ns
960	ns	ns	ns	ns	ns	ns	ns	ns	ns	ns
970	ns	ns	ns	ns	ns	ns	ns	ns	ns	ns
980	ns	ns	ns	ns	ns	ns	ns	ns	ns	ns
990	ns	ns	ns	ns	ns	ns	ns	ns	ns	ns
1000	ns	ns	ns	ns	ns	ns	ns	ns	ns	ns
1010	ns	ns	ns	ns	ns	ns	ns	ns	ns	ns
1020	ns	ns	ns	ns	ns	ns	ns	ns	ns	ns
1030	ns	ns	ns	ns	ns	ns	ns	ns	ns	ns
1040	ns	ns	ns	ns	ns	ns	ns	ns	ns	ns
1050	ns	ns	ns	ns	ns	ns	ns	ns	ns	ns
1060	ns	ns	ns	ns	ns	ns	ns	ns	ns	ns
1070	ns	ns	ns	ns	ns	ns	ns	ns	ns	ns
1080	ns	ns	ns	ns	ns	ns	ns	ns	ns	ns
1090	ns	ns	ns	ns	ns	ns	ns	ns	ns	ns
1100	ns	ns	ns	ns	ns	ns	ns	ns	ns	ns

Statistical analysis was performed with two-way ANOVA and Bonferroni's multiple comparison test. Error bars represent SEM; n=10; ns=not significant, *p<0.05, **p<0.01, ***p<0.001. Outliers values are removed from the dataset.

Rho 3

wavelenght (nm)	2L vs 4L	2L vs 4L2D	2L vs 2L2D	2L vs 8L	4L vs 4L2D	4L vs 2L2D	4L vs 8L	4L2D vs 2L2D	4L2D vs 8L	2L2D vs 8L
600	***	***	***	ns	ns	ns	ns	ns	**	***
610	ns	ns	ns	ns	ns	ns	ns	ns	ns	ns
620	ns	ns	ns	ns	ns	ns	ns	ns	ns	ns
630	ns	ns	ns	ns	ns	ns	ns	ns	ns	ns
640	ns	ns	ns	ns	ns	ns	ns	ns	ns	ns
650	ns	ns	ns	ns	ns	ns	ns	ns	ns	ns
660	ns	ns	ns	ns	ns	ns	ns	ns	ns	ns
670	ns	ns	ns	ns	ns	ns	ns	ns	ns	ns
680	ns	ns	ns	ns	ns	ns	ns	ns	ns	ns
690	ns	ns	ns	ns	ns	ns	ns	ns	ns	ns
700	ns	ns	ns	ns	ns	ns	ns	ns	ns	ns
710	ns	ns	ns	ns	ns	ns	ns	ns	ns	ns
720	ns	ns	ns	ns	ns	ns	ns	ns	ns	ns
730	ns	ns	ns	ns	ns	ns	ns	ns	ns	ns
740	ns	ns	ns	ns	ns	ns	ns	ns	ns	ns
750	ns	ns	ns	ns	ns	ns	ns	ns	ns	ns
760	ns	ns	ns	ns	ns	ns	ns	ns	ns	ns
770	ns	ns	ns	ns	ns	ns	ns	ns	ns	ns
780	ns	ns	ns	ns	ns	ns	ns	ns	ns	ns
790	ns	ns	ns	ns	ns	ns	ns	ns	ns	ns
800	ns	ns	ns	ns	ns	ns	ns	ns	ns	ns
810	ns	ns	ns	ns	ns	ns	ns	ns	ns	ns
820	ns	ns	ns	ns	ns	ns	ns	ns	ns	ns
830	ns	ns	ns	ns	ns	ns	ns	ns	ns	ns
840	ns	ns	ns	ns	ns	ns	ns	ns	ns	ns
850	ns	ns	ns	ns	ns	ns	ns	ns	ns	ns
860	ns	ns	ns	ns	ns	ns	ns	ns	ns	ns
870	ns	ns	ns	ns	ns	ns	ns	ns	ns	ns
880	ns	ns	ns	ns	ns	ns	ns	ns	ns	ns
890	ns	ns	ns	ns	ns	ns	ns	ns	ns	ns
900	ns	ns	ns	ns	ns	ns	ns	ns	ns	ns
910	ns	ns	ns	ns	ns	ns	ns	ns	ns	ns
920	ns	ns	ns	ns	ns	ns	ns	ns	ns	ns
930	ns	ns	ns	ns	ns	ns	ns	ns	ns	ns
940	ns	ns	ns	ns	ns	ns	ns	ns	ns	ns
950	ns	ns	ns	ns	ns	ns	ns	ns	ns	ns
960	ns	ns	ns	ns	ns	ns	ns	ns	ns	ns
970	ns	ns	ns	ns	ns	ns	ns	ns	ns	ns
980	ns	ns	ns	ns	ns	ns	ns	ns	ns	ns
990	ns	ns	ns	ns	ns	ns	ns	ns	ns	ns
1000	ns	ns	ns	ns	ns	ns	ns	ns	ns	ns
1010	ns	ns	ns	ns	ns	ns	ns	ns	ns	ns
1020	ns	ns	ns	ns	ns	ns	ns	ns	ns	ns
1030	ns	ns	ns	ns	ns	ns	ns	ns	ns	ns
1040	ns	ns	ns	ns	ns	ns	ns	ns	ns	ns
1050	ns	ns	ns	ns	ns	ns	ns	ns	ns	ns
1060	ns	ns	ns	ns	ns	ns	ns	ns	ns	ns
1070	ns	ns	ns	ns	ns	ns	ns	ns	ns	ns
1080	ns	ns	ns	ns	ns	ns	ns	ns	ns	ns
1090	ns	ns	ns	ns	ns	ns	ns	ns	ns	ns
1100	ns	ns	ns	ns	ns	ns	ns	ns	ns	ns

Statistical analysis was performed with two-way ANOVA and Bonferroni's multiple comparison test. Error bars represent SEM; n=10; ns=not significant, **p<0.01, ***p<0.001. Outliers values are removed from the dataset.

Reduced scattering spectra for the five positions (2L= 2 cm left to the navel, 4L= 4 cm left to the navel, 4L2D= 4 cm left 2cm down to the navel, 2L2D= 2 cm left 2cm down to the navel, 8L= 8 cm left to the navel) measured on the abdominal region. Spectra with mean values from all the subjects at the three interfibre distances.

Rho1

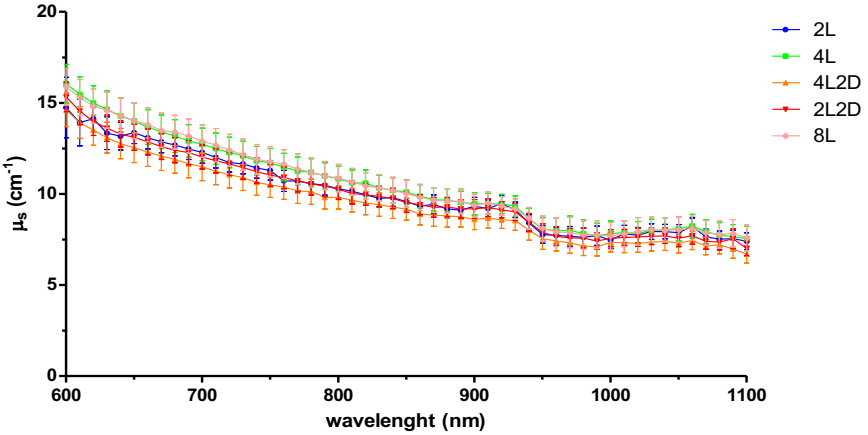

Rho2

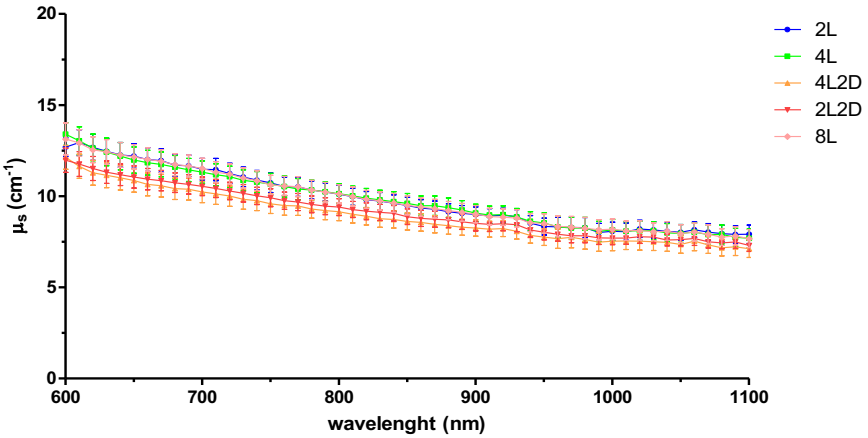

Rho3

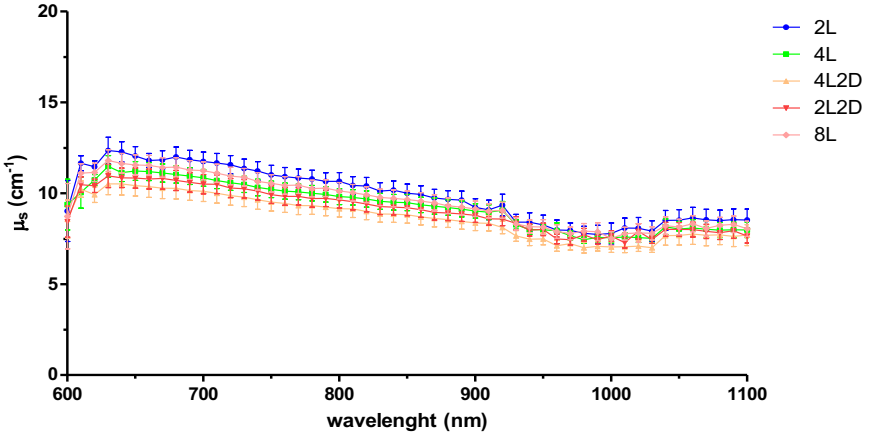

Comparison of the reduced scattering coefficients in the range of wavelengths 600-1100nm at the different tested positions.

Rho1

wavelenght (nm)	2L vs 4L	2L vs 4L2D	2L vs 2L2D	2L vs 8L	4L vs 4L2D	4L vs 2L2D	4L vs 8L	4L2D vs 2L2D	4L2D vs 8L	2L2D vs 8L
600	ns	ns	ns	ns	ns	ns	ns	ns	ns	ns
610	ns	ns	ns	ns	ns	ns	ns	ns	ns	ns
620	ns	ns	ns	ns	ns	ns	ns	ns	ns	ns
630	ns	ns	ns	ns	ns	ns	ns	ns	ns	ns
640	ns	ns	ns	ns	ns	ns	ns	ns	ns	ns
650	ns	ns	ns	ns	ns	ns	ns	ns	ns	ns
660	ns	ns	ns	ns	ns	ns	ns	ns	ns	ns
670	ns	ns	ns	ns	ns	ns	ns	ns	ns	ns
680	ns	ns	ns	ns	ns	ns	ns	ns	ns	ns
690	ns	ns	ns	ns	ns	ns	ns	ns	ns	ns
700	ns	ns	ns	ns	ns	ns	ns	ns	ns	ns
710	ns	ns	ns	ns	ns	ns	ns	ns	ns	ns
720	ns	ns	ns	ns	ns	ns	ns	ns	ns	ns
730	ns	ns	ns	ns	ns	ns	ns	ns	ns	ns
740	ns	ns	ns	ns	ns	ns	ns	ns	ns	ns
750	ns	ns	ns	ns	ns	ns	ns	ns	ns	ns
760	ns	ns	ns	ns	ns	ns	ns	ns	ns	ns
770	ns	ns	ns	ns	ns	ns	ns	ns	ns	ns
780	ns	ns	ns	ns	ns	ns	ns	ns	ns	ns
790	ns	ns	ns	ns	ns	ns	ns	ns	ns	ns
800	ns	ns	ns	ns	ns	ns	ns	ns	ns	ns
810	ns	ns	ns	ns	ns	ns	ns	ns	ns	ns
820	ns	ns	ns	ns	ns	ns	ns	ns	ns	ns
830	ns	ns	ns	ns	ns	ns	ns	ns	ns	ns
840	ns	ns	ns	ns	ns	ns	ns	ns	ns	ns
850	ns	ns	ns	ns	ns	ns	ns	ns	ns	ns
860	ns	ns	ns	ns	ns	ns	ns	ns	ns	ns
870	ns	ns	ns	ns	ns	ns	ns	ns	ns	ns
880	ns	ns	ns	ns	ns	ns	ns	ns	ns	ns
890	ns	ns	ns	ns	ns	ns	ns	ns	ns	ns
900	ns	ns	ns	ns	ns	ns	ns	ns	ns	ns
910	ns	ns	ns	ns	ns	ns	ns	ns	ns	ns
920	ns	ns	ns	ns	ns	ns	ns	ns	ns	ns
930	ns	ns	ns	ns	ns	ns	ns	ns	ns	ns
940	ns	ns	ns	ns	ns	ns	ns	ns	ns	ns
950	ns	ns	ns	ns	ns	ns	ns	ns	ns	ns
960	ns	ns	ns	ns	ns	ns	ns	ns	ns	ns
970	ns	ns	ns	ns	ns	ns	ns	ns	ns	ns
980	ns	ns	ns	ns	ns	ns	ns	ns	ns	ns
990	ns	ns	ns	ns	ns	ns	ns	ns	ns	ns
1000	ns	ns	ns	ns	ns	ns	ns	ns	ns	ns
1010	ns	ns	ns	ns	ns	ns	ns	ns	ns	ns
1020	ns	ns	ns	ns	ns	ns	ns	ns	ns	ns
1030	ns	ns	ns	ns	ns	ns	ns	ns	ns	ns
1040	ns	ns	ns	ns	ns	ns	ns	ns	ns	ns
1050	ns	ns	ns	ns	ns	ns	ns	ns	ns	ns
1060	ns	ns	ns	ns	ns	ns	ns	ns	ns	ns
1070	ns	ns	ns	ns	ns	ns	ns	ns	ns	ns
1080	ns	ns	ns	ns	ns	ns	ns	ns	ns	ns
1090	ns	ns	ns	ns	ns	ns	ns	ns	ns	ns
1100	ns	ns	ns	ns	ns	ns	ns	ns	ns	ns

Statistical analysis was performed with two-way ANOVA and Bonferroni's multiple comparison test. Error bars represent SEM; n=10; ns=not significant. Outliers values are removed from the dataset.

Rho2

wavelenght (nm)	2L vs 4L	2L vs 4L2D	2L vs 2L2D	2L vs 8L	4L vs 4L2D	4L vs 2L2D	4L vs 8L	4L2D vs 2L2D	4L2D vs 8L	2L2D vs 8L
600	ns	ns	ns	ns	*	**	ns	ns	ns	*
610	ns	**	*	ns	**	*	ns	ns	*	*
620	ns	**	*	ns	**	ns	ns	ns	*	ns
630	ns	**	*	ns	*	ns	ns	ns	*	ns
640	ns	*	ns	ns	*	ns	ns	ns	*	ns
650	ns	**	*	ns	ns	ns	ns	ns	**	ns
660	ns	**	ns	ns	*	ns	ns	ns	**	ns
670	ns	**	ns	ns	*	ns	ns	ns	**	ns
680	ns	**	ns	ns	*	ns	ns	ns	**	ns
690	ns	**	ns	ns	ns	ns	ns	ns	**	ns
700	ns	*	ns	ns	ns	ns	ns	ns	**	ns
710	ns	**	ns	ns	ns	ns	ns	ns	*	ns
720	ns	*	ns	ns	ns	ns	ns	ns	*	ns
730	ns	*	ns	ns	ns	ns	ns	ns	*	ns
740	ns	ns	ns	ns	ns	ns	ns	ns	ns	ns
750	ns	*	ns	ns	ns	ns	ns	ns	ns	ns
760	ns	ns	ns	ns	ns	ns	ns	ns	ns	ns
770	ns	ns	ns	ns	ns	ns	ns	ns	ns	ns
780	ns	ns	ns	ns	ns	ns	ns	ns	ns	ns
790	ns	ns	ns	ns	ns	ns	ns	ns	ns	ns
800	ns	ns	ns	ns	ns	ns	ns	ns	ns	ns
810	ns	ns	ns	ns	ns	ns	ns	ns	ns	ns
820	ns	ns	ns	ns	ns	ns	ns	ns	ns	ns
830	ns	ns	ns	ns	ns	ns	ns	ns	ns	ns
840	ns	ns	ns	ns	ns	ns	ns	ns	ns	ns
850	ns	ns	ns	ns	ns	ns	ns	ns	ns	ns
860	ns	ns	ns	ns	ns	ns	ns	ns	ns	ns
870	ns	ns	ns	ns	ns	ns	ns	ns	ns	ns
880	ns	ns	ns	ns	ns	ns	ns	ns	ns	ns
890	ns	ns	ns	ns	ns	ns	ns	ns	ns	ns
900	ns	ns	ns	ns	ns	ns	ns	ns	ns	ns
910	ns	ns	ns	ns	ns	ns	ns	ns	ns	ns
920	ns	ns	ns	ns	ns	ns	ns	ns	ns	ns
930	ns	ns	ns	ns	ns	ns	ns	ns	ns	ns
940	ns	ns	ns	ns	ns	ns	ns	ns	ns	ns
950	ns	ns	ns	ns	ns	ns	ns	ns	ns	ns
960	ns	ns	ns	ns	ns	ns	ns	ns	ns	ns
970	ns	ns	ns	ns	ns	ns	ns	ns	ns	ns
980	ns	ns	ns	ns	ns	ns	ns	ns	ns	ns
990	ns	ns	ns	ns	ns	ns	ns	ns	ns	ns
1000	ns	ns	ns	ns	ns	ns	ns	ns	ns	ns
1010	ns	ns	ns	ns	ns	ns	ns	ns	ns	ns
1020	ns	ns	ns	ns	ns	ns	ns	ns	ns	ns
1030	ns	ns	ns	ns	ns	ns	ns	ns	ns	ns
1040	ns	ns	ns	ns	ns	ns	ns	ns	ns	ns
1050	ns	ns	ns	ns	ns	ns	ns	ns	ns	ns
1060	ns	ns	ns	ns	ns	ns	ns	ns	ns	ns
1070	ns	ns	ns	ns	ns	ns	ns	ns	ns	ns
1080	ns	ns	ns	ns	ns	ns	ns	ns	ns	ns
1090	ns	ns	ns	ns	ns	ns	ns	ns	ns	ns
1100	ns	ns	ns	ns	ns	ns	ns	ns	ns	ns

Statistical analysis was performed with two-way ANOVA and Bonferroni's multiple comparison test. Error bars represent SEM; n=10; ns=not significant, *p<0.05, **p<0.01. Outliers values are removed from the dataset.

Rho3

wavelenght (nm)	2L vs 4L	2L vs 4L2D	2L vs 2L2D	2L vs 8L	4L vs 4L2D	4L vs 2L2D	4L vs 8L	4L2D vs 2L2D	4L2D vs 8L	2L2D vs 8L
600	ns	ns	ns	ns	ns	ns	ns	ns	ns	ns
610	**	*	ns	ns	ns	ns	ns	ns	ns	ns
620	ns	*	ns	ns	ns	ns	ns	ns	ns	ns
630	ns	***	**	ns	ns	ns	ns	ns	*	ns
640	ns	***	**	ns	ns	ns	ns	ns	ns	ns
650	ns	***	ns	ns	ns	ns	ns	ns	ns	ns
660	ns	**	ns	ns	ns	ns	ns	ns	ns	ns
670	ns	**	ns	ns	ns	ns	ns	ns	ns	ns
680	ns	***	*	ns	ns	ns	ns	ns	ns	ns
690	ns	***	*	ns	ns	ns	ns	ns	ns	ns
700	ns	***	*	ns	ns	ns	ns	ns	ns	ns
710	ns	***	ns	ns	ns	ns	ns	ns	ns	ns
720	ns	***	*	ns	ns	ns	ns	ns	ns	ns
730	ns	**	ns	ns	ns	ns	ns	ns	ns	ns
740	ns	**	ns	ns	ns	ns	ns	ns	ns	ns
750	ns	**	ns	ns	ns	ns	ns	ns	ns	ns
760	ns	**	ns	ns	ns	ns	ns	ns	ns	ns
770	ns	**	ns	ns	ns	ns	ns	ns	ns	ns
780	ns	**	ns	ns	ns	ns	ns	ns	ns	ns
790	ns	**	ns	ns	ns	ns	ns	ns	ns	ns
800	ns	**	ns	ns	ns	ns	ns	ns	ns	ns
810	ns	*	ns	ns	ns	ns	ns	ns	ns	ns
820	ns	**	ns	ns	ns	ns	ns	ns	ns	ns
830	ns	*	ns	ns	ns	ns	ns	ns	ns	ns
840	ns	*	ns	ns	ns	ns	ns	ns	ns	ns
850	ns	ns	ns	ns	ns	ns	ns	ns	ns	ns
860	ns	*	ns	ns	ns	ns	ns	ns	ns	ns
870	ns	ns	ns	ns	ns	ns	ns	ns	ns	ns
880	ns	ns	ns	ns	ns	ns	ns	ns	ns	ns
890	ns	ns	ns	ns	ns	ns	ns	ns	ns	ns
900	ns	ns	ns	ns	ns	ns	ns	ns	ns	ns
910	ns	ns	ns	ns	ns	ns	ns	ns	ns	ns
920	ns	*	ns	ns	ns	ns	ns	ns	ns	ns
930	ns	ns	ns	ns	ns	ns	ns	ns	ns	ns
940	ns	ns	ns	ns	ns	ns	ns	ns	ns	ns
950	ns	ns	ns	ns	ns	ns	ns	ns	ns	ns
960	ns	ns	ns	ns	ns	ns	ns	ns	ns	ns
970	ns	ns	ns	ns	ns	ns	ns	ns	ns	ns
980	ns	ns	ns	ns	ns	ns	ns	ns	ns	ns
990	ns	ns	ns	ns	ns	ns	ns	ns	ns	ns
1000	ns	ns	ns	ns	ns	ns	ns	ns	ns	ns
1010	ns	ns	ns	ns	ns	ns	ns	ns	ns	ns
1020	ns	ns	ns	ns	ns	ns	ns	ns	ns	ns
1030	ns	ns	ns	ns	ns	ns	ns	ns	ns	ns
1040	ns	ns	ns	ns	ns	ns	ns	ns	ns	ns
1050	ns	ns	ns	ns	ns	ns	ns	ns	ns	ns
1060	ns	ns	ns	ns	ns	ns	ns	ns	ns	ns
1070	ns	ns	ns	ns	ns	ns	ns	ns	ns	ns
1080	ns	ns	ns	ns	ns	ns	ns	ns	ns	ns
1090	ns	ns	ns	ns	ns	ns	ns	ns	ns	ns
1100	ns	ns	ns	ns	ns	ns	ns	ns	ns	ns

Statistical analysis was performed with two-way ANOVA and Bonferroni's multiple comparison test. Error bars represent SEM; n=10; ns=not significant, *p<0.05, **p<0.01, ***p<0.001. Outliers values are removed from the dataset.

Appendix B: Supplementary Information for Section 4.4

Tissue composition, blood oxygenation, and scatter parameters for all the subjects at the three source detector separations for location at 4 cm to the left of the navel

Subject #	ρ	Hb μM	HbO_2 μM	THb μM	StO_2 %	lipid g/cm³	water g/cm³	collagen g/cm³	bkg cm^{-1}	A cm^{-1}	b
0	1	2.74	6.67	9.41	71%	0.521	0.284	0.383	0.001	14.29	1.62
	2	1.07	13.70	14.76	93%	0.662	0.141	0.469	0.004	11.88	1.06
	3	1.50	14.31	15.81	91%	0.718	0.139	0.309	0.007	10.45	0.85
1	1	3.95	24.29	28.24	86%	0.318	0.124	0.412	0.028	13.82	2.09
	2	7.13	28.20	35.34	80%	0.375	0.091	0.086	0.049	13.80	2.10
	3	6.29	26.07	32.35	81%	0.374	0.124	0.016	0.062	12.66	1.69
2	1	3.07	7.23	10.30	70%	0.675	0.199	0.000	0.005	13.92	1.57
	2	4.67	14.74	19.40	76%	0.520	0.121	0.087	0.029	15.60	1.97
	3	5.55	13.14	18.69	70%	0.347	0.076	0.033	0.032	12.67	2.40
3	1	3.77	24.53	28.30	87%	0.605	0.255	0.242	0.056	22.76	1.21
	2	4.53	29.80	34.33	87%	0.554	0.308	0.197	0.084	19.95	0.96
	3	5.33	38.33	43.66	88%	0.339	0.564	0.268	0.068	17.14	0.62
4	1	2.50	6.75	9.25	73%	0.799	0.185	0.001	0.007	12.51	0.97
	2	2.65	10.11	12.77	79%	0.847	0.131	0.000	0.009	11.56	0.98
	3	1.92	13.82	15.74	88%	0.837	0.072	0.017	0.011	10.96	0.98
5	1	2.35	19.93	22.27	89%	0.567	0.179	0.398	0.017	15.75	1.49
	2	3.01	22.74	25.75	88%	0.694	0.178	0.271	0.032	13.95	1.18
	3	3.44	23.00	26.44	87%	0.649	0.243	0.330	0.046	14.26	0.99
6	1	1.99	27.63	29.62	93%	0.684	0.195	0.347	0.051	16.80	1.41
	2	2.90	30.38	33.28	91%	0.750	0.218	0.256	0.045	13.57	1.09
	3	3.43	30.22	33.65	90%	0.614	0.334	0.377	0.050	14.49	0.98
7	1	2.27	4.26	6.53	65%	0.676	0.198	0.000	0.006	13.65	0.68
	2	1.36	17.00	18.36	93%	0.777	0.118	0.174	0.006	13.97	0.84
	3	1.96	16.06	18.02	89%	0.803	0.124	0.073	0.008	12.68	0.79
8	1	2.77	25.38	28.15	90%	0.646	0.189	0.343	0.006	16.41	1.34
	2	3.13	25.57	28.69	89%	0.781	0.163	0.141	0.017	14.05	1.00
	3	3.19	25.47	28.67	89%	0.754	0.237	0.147	0.026	14.47	0.79
9	1	1.46	16.99	18.45	92%	0.573	0.158	0.450	0.006	16.77	1.56
	2	1.59	18.22	19.80	92%	0.718	0.144	0.221	0.013	13.54	0.98
	3	2.04	16.96	19.01	89%	0.798	0.133	0.110	0.022	13.64	0.88
10	1	2.12	8.75	10.87	80%	0.689	0.135	0.274	0.000	12.65	1.33
	2	1.66	12.89	14.55	89%	0.765	0.109	0.249	0.005	11.01	0.87
	3	2.20	13.48	15.68	86%	0.820	0.106	0.138	0.013	10.69	0.73
11	1	1.96	15.63	17.59	89%	0.762	0.128	0.267	0.014	14.18	1.00
	2	1.97	15.83	17.79	89%	0.807	0.117	0.241	0.017	11.16	0.78
	3	2.51	15.49	18.00	86%	0.836	0.125	0.118	0.031	11.78	0.68
12	1	2.18	6.25	8.43	74%	0.778	0.173	0.000	0.008	13.46	0.74
	2	1.33	13.48	14.81	91%	0.788	0.077	0.080	0.007	11.71	0.82
	3	1.34	10.36	11.70	89%	0.788	0.126	0.000	0.011	10.26	0.48
13	1	2.89	7.11	10.00	71%	0.779	0.135	0.111	0.000	14.57	1.11
	2	2.02	8.42	10.44	81%	0.823	0.097	0.145	0.009	10.95	0.79
	3	2.41	9.03	11.44	79%	0.843	0.095	0.085	0.020	10.65	0.69

14	1	2.13	10.17	12.30	83%	0.644	0.157	0.252	0.000	14.94	1.51
	2	1.67	12.78	14.45	88%	0.761	0.125	0.221	0.007	11.96	1.08
	3	1.64	11.60	13.24	88%	0.810	0.109	0.119	0.008	10.23	0.83
15	1	1.56	17.74	19.30	92%	0.707	0.116	0.288	0.014	12.91	1.37
	2	1.66	19.89	21.54	92%	0.680	0.153	0.278	0.026	10.40	1.06
	3	2.54	21.06	23.60	89%	0.835	0.164	0.103	0.032	11.95	0.83
16	1	2.45	11.71	14.16	83%	0.663	0.136	0.301	0.014	13.38	1.35
	2	2.40	14.58	16.98	86%	0.781	0.132	0.287	0.029	11.95	0.86
	3	2.80	14.47	17.27	84%	0.739	0.172	0.297	0.042	12.30	0.76
17	1	3.03	22.13	25.16	88%	0.567	0.219	0.661	0.021	14.35	1.20
	2	2.95	23.06	26.01	89%	0.731	0.187	0.363	0.044	12.01	0.82
	3	4.19	20.67	24.86	83%	0.664	0.229	0.343	0.057	12.05	0.74
18	1	2.71	18.63	21.35	87%	0.579	0.224	0.422	0.002	16.67	1.47
	2	2.54	17.84	20.38	88%	0.712	0.184	0.328	0.032	15.22	1.06
	3	3.27	16.89	20.16	84%	0.698	0.281	0.165	0.046	14.53	0.84
19	1	2.47	16.14	18.60	87%	0.753	0.144	0.112	0.003	10.60	1.32
	2	2.93	16.49	19.43	85%	0.863	0.143	0.002	0.022	9.93	0.93
	3	2.37	17.12	19.49	88%	0.791	0.159	0.133	0.040	10.98	0.88
20	1	1.64	15.53	17.17	90%	0.735	0.147	0.191	0.005	14.84	1.00
	2	1.59	15.96	17.55	91%	0.850	0.118	0.074	0.009	11.02	0.69
	3	1.76	14.84	16.60	89%	0.859	0.112	0.013	0.019	11.37	0.65
21	1	4.20	24.22	28.42	85%	0.757	0.195	0.004	0.021	13.96	1.09
	2	4.80	23.75	28.54	83%	0.826	0.208	0.138	0.057	14.07	0.89
	3	4.44	26.81	31.25	86%	0.683	0.292	0.255	0.079	14.07	0.68
22	1	3.25	17.78	21.03	85%	0.851	0.175	0.003	0.013	13.02	0.88
	2	3.08	23.22	26.29	88%	0.865	0.162	0.010	0.041	13.79	0.80
	3	3.30	25.09	28.40	88%	0.737	0.238	0.106	0.053	14.28	0.71
23	1	3.91	22.44	26.34	85%	0.589	0.216	0.323	0.013	16.12	1.47
	2	4.24	23.47	27.71	85%	0.729	0.205	0.215	0.036	14.58	1.09
	3	4.21	26.06	30.27	86%	0.619	0.299	0.311	0.053	15.36	0.84
24	1	3.58	18.10	21.68	83%	0.716	0.200	0.351	0.047	15.24	1.21
	2	3.46	21.97	25.43	86%	0.765	0.247	0.368	0.070	12.15	0.79
	3	4.67	23.51	28.18	83%	0.615	0.305	0.381	0.077	12.30	0.73
25	1	2.68	7.73	10.41	74%	0.822	0.192	0.000	0.007	12.77	0.93
	2	2.57	12.52	15.09	83%	0.851	0.110	0.000	0.011	11.77	0.92
	3	1.77	15.36	17.13	90%	0.864	0.094	0.044	0.011	11.14	0.65

THb = total hemoglobin content | StO_2 = oxygen saturation | bkg = wavelength independent value added as a fitting parameter to account for possible tissue absorbers not included in the fitting procedures and for limitations of the theoretical model.

Tissue composition, blood oxygenation, and scatter parameters for all the subjects at the three source detector separations for location at 4 cm to the right of the navel

Subject #	ρ	Hb µM	HbO_2 µM	THb µM	StO_2 %	lipid g/cm³	water g/cm³	collagen g/cm³	bkg cm^{-1}	A cm^{-1}	b
0	1	3.69	5.11	8.81	58%	0.545	0.364	0.135	0.000	14.40	1.65
	2	2.07	11.67	13.74	85%	0.721	0.139	0.238	0.000	12.60	1.19
	3	1.70	11.42	13.12	87%	0.783	0.129	0.184	0.005	12.14	0.88
1	1	5.17	16.40	21.57	76%	0.418	0.190	0.125	0.014	15.92	2.11
	2	5.96	20.40	26.36	77%	0.413	0.123	0.078	0.044	15.81	1.97
	3	5.24	21.10	26.34	80%	0.402	0.148	0.057	0.058	14.01	1.71
2	1	2.97	6.13	9.11	67%	0.625	0.170	0.000	0.004	12.52	1.89
	2	4.15	13.48	17.63	76%	0.567	0.091	0.018	0.009	13.03	2.05
	3	6.11	9.74	15.85	61%	0.329	0.028	0.048	0.014	15.02	3.23
3	1	4.10	27.87	31.98	87%	0.563	0.269	0.335	0.043	20.29	1.28
	2	5.06	29.61	34.67	85%	0.650	0.248	0.131	0.066	17.07	0.95

	3	3.74	33.98	37.71	90%	0.510	0.447	0.484	0.068	16.15	0.50
4	1	2.42	5.48	7.90	69%	0.756	0.184	0.000	0.007	12.81	0.88
	2	2.52	9.67	12.20	79%	0.843	0.115	0.000	0.010	11.91	0.91
	3	2.00	13.26	15.27	87%	0.827	0.077	0.001	0.012	11.43	0.92
5	1	2.81	14.30	17.10	84%	0.490	0.212	0.424	0.005	16.68	1.67
	2	2.90	16.23	19.12	85%	0.690	0.170	0.218	0.029	14.72	1.18
	3	2.95	17.44	20.39	86%	0.730	0.220	0.118	0.052	15.12	0.87
6	1	3.02	22.27	25.29	88%	0.671	0.189	0.336	0.037	17.81	1.46
	2	2.94	25.75	28.69	90%	0.743	0.207	0.280	0.052	14.17	1.01
	3	3.24	28.22	31.46	90%	0.616	0.324	0.371	0.053	13.95	0.92
7	1	2.38	3.11	5.50	57%	0.572	0.175	0.000	0.005	13.55	0.62
	2	2.31	8.11	10.43	78%	0.781	0.158	0.001	0.009	13.52	0.68
	3	1.51	16.18	17.69	91%	0.841	0.119	0.072	0.009	13.72	0.67
8	1	2.01	20.94	22.95	91%	0.711	0.146	0.228	0.006	18.12	1.16
	2	2.73	23.27	26.00	89%	0.808	0.136	0.105	0.014	15.05	0.93
	3	2.40	24.38	26.78	91%	0.746	0.192	0.258	0.017	15.58	0.81
9	1	2.56	11.24	13.80	81%	0.700	0.135	0.152	0.000	14.55	1.49
	2	1.66	13.59	15.25	89%	0.796	0.107	0.149	0.012	12.65	0.89
	3	1.95	14.45	16.40	88%	0.819	0.116	0.073	0.025	13.14	0.81
10	1	3.61	10.49	14.10	74%	0.605	0.169	0.438	0.000	14.60	1.48
	2	2.31	14.43	16.75	86%	0.779	0.121	0.309	0.000	10.74	0.81
	3	2.64	13.89	16.53	84%	0.865	0.119	0.131	0.013	11.31	0.68
11	1	2.05	10.09	12.14	83%	0.754	0.117	0.188	0.003	15.61	1.06
	2	1.97	12.43	14.40	86%	0.806	0.109	0.171	0.017	13.22	0.84
	3	2.38	12.45	14.84	84%	0.863	0.113	0.040	0.033	13.57	0.75
12	1	2.13	5.26	7.38	71%	0.732	0.164	0.001	0.008	13.37	0.73
	2	1.37	12.34	13.71	90%	0.786	0.071	0.090	0.006	11.52	0.84
	3	1.73	11.74	13.47	87%	0.794	0.067	0.001	0.011	10.85	0.82
13	1	2.06	7.01	9.08	77%	0.780	0.105	0.174	0.000	13.16	0.93
	2	1.98	8.28	10.26	81%	0.848	0.100	0.128	0.011	11.29	0.63
	3	2.79	9.91	12.70	78%	0.850	0.102	0.063	0.021	12.89	0.67
14	1	2.15	3.64	5.79	63%	0.686	0.211	0.000	0.006	13.22	0.79
	2	1.02	8.91	9.93	90%	0.771	0.099	0.231	0.008	14.94	1.08
	3	1.18	9.81	10.99	89%	0.780	0.089	0.162	0.013	13.49	0.83
15	1	1.59	19.10	20.69	92%	0.595	0.163	0.449	0.009	14.09	1.34
	2	1.82	20.67	22.49	92%	0.719	0.146	0.343	0.024	12.13	1.16
	3	2.54	19.14	21.68	88%	0.734	0.188	0.161	0.046	13.49	0.92
16	1	2.57	10.18	12.75	80%	0.709	0.146	0.208	0.001	13.40	1.21
	2	2.69	12.85	15.54	83%	0.788	0.122	0.161	0.018	12.44	0.88
	3	2.49	14.01	16.50	85%	0.763	0.133	0.212	0.038	13.32	0.83
17	1	3.58	16.95	20.53	83%	0.647	0.209	0.415	0.013	16.17	1.03
	2	3.42	18.97	22.38	85%	0.771	0.158	0.340	0.031	13.69	0.72
	3	4.05	18.49	22.54	82%	0.725	0.210	0.275	0.043	13.88	0.64
18	1	2.34	15.67	18.01	87%	0.597	0.186	0.298	0.001	16.51	1.56
	2	2.86	16.75	19.61	85%	0.782	0.152	0.123	0.012	13.08	1.08
	3	2.58	15.94	18.52	86%	0.748	0.173	0.144	0.026	13.90	0.95
19	1	2.31	18.17	20.48	89%	0.715	0.159	0.119	0.008	11.69	1.21
	2	1.99	19.10	21.09	91%	0.823	0.134	0.150	0.018	10.51	0.87
	3	2.47	19.41	21.89	89%	0.833	0.151	0.077	0.029	10.31	0.79
20	1	2.38	7.50	9.88	76%	0.803	0.189	0.001	0.008	13.31	0.79
	2	2.71	11.43	14.14	81%	0.833	0.130	0.000	0.010	11.87	0.87
	3	2.07	13.20	15.27	86%	0.845	0.086	0.001	0.013	11.77	0.84
21	1	3.43	17.18	20.61	83%	0.847	0.148	0.000	0.013	12.92	0.84
	2	3.45	21.60	25.05	86%	0.875	0.133	0.002	0.031	13.02	0.76
	3	3.19	23.16	26.35	88%	0.795	0.187	0.065	0.053	14.00	0.62
22	1	3.66	19.30	22.96	84%	0.866	0.189	0.001	0.013	12.84	0.89
	2	3.31	26.70	30.01	89%	0.847	0.153	0.008	0.032	13.74	0.81
	3	2.64	26.99	29.62	91%	0.705	0.225	0.221	0.040	14.69	0.68
23	1	4.13	21.30	25.44	84%	0.593	0.225	0.247	0.012	17.34	1.49

	2	3.99	23.30	27.29	85%	0.760	0.186	0.173	0.028	16.35	1.16
	3	3.65	26.42	30.07	88%	0.632	0.251	0.277	0.043	17.20	0.97
24	1	3.59	13.03	16.62	78%	0.774	0.170	0.024	0.026	15.23	1.10
	2	3.33	17.30	20.62	84%	0.771	0.175	0.286	0.056	13.56	0.83
	3	3.81	19.52	23.34	84%	0.773	0.261	0.235	0.079	13.67	0.64
25	1	2.52	6.64	9.16	73%	0.778	0.207	0.001	0.007	13.63	0.76
	2	2.87	12.44	15.30	81%	0.829	0.139	0.000	0.010	12.42	0.85
	3	2.37	14.76	17.14	86%	0.823	0.104	0.000	0.012	12.31	0.77

THb = total hemoglobin content | StO_2 = oxygen saturation | bkg = wavelength independent value added as a fitting parameter to account for possible tissue absorbers not included in the fitting procedures and for limitations of the theoretical model.

Tissue composition, blood oxygenation, and scatter parameters for all the subjects at the three source detector separations for location at 1/3 of the femoral length on the right thigh (*vastus lateralis* muscle)

Subject #	ρ	Hb µM	HbO_2 µM	THb µM	StO_2 %	lipid g/cm³	water g/cm³	collagen g/cm³	bkg cm⁻¹	A cm⁻¹	b
0	1	6.70	11.44	18.14	63%	0.001	0.857	1.367	0.055	12.03	1.74
	2	4.69	17.18	21.87	79%	0.162	0.501	1.738	0.084	10.73	1.33
	3	4.55	16.90	21.45	79%	0.258	0.556	1.268	0.113	9.73	1.02
1	1	6.25	28.88	35.13	82%	0.165	0.511	1.671	0.147	13.65	1.34
	2	8.92	43.32	52.25	83%	0.163	0.520	1.654	0.150	9.97	1.06
	3	21.85	31.76	53.61	59%	0.004	0.287	1.386	0.064	8.25	2.56
2	1	3.50	16.44	19.94	82%	0.786	0.184	0.188	0.009	10.84	1.25
	2	3.32	15.21	18.54	82%	0.799	0.166	0.158	0.048	10.57	0.87
	3	2.86	15.76	18.62	85%	0.789	0.181	0.108	0.065	9.91	0.69
3	1	5.42	19.92	25.34	79%	0.615	0.267	0.487	0.111	14.43	0.96
	2	5.69	23.49	29.19	80%	0.545	0.334	0.566	0.152	12.10	0.63
	3	7.56	26.25	33.81	78%	0.445	0.381	0.698	0.149	10.48	0.72
4	1	4.15	24.75	28.89	86%	0.607	0.279	0.645	0.068	13.05	0.96
	2	4.01	23.58	27.59	85%	0.664	0.307	0.674	0.116	11.28	0.72
	3	4.84	27.24	32.07	85%	0.512	0.381	0.647	0.121	10.32	0.74
5	1	4.45	21.25	25.69	83%	0.192	0.459	1.754	0.123	11.70	1.32
	2	3.60	24.47	28.07	87%	0.258	0.491	1.779	0.152	8.85	0.88
	3	8.20	32.39	40.59	80%	0.196	0.509	1.422	0.149	8.43	1.03
6	1	6.55	21.34	27.89	77%	0.674	0.298	0.508	0.080	16.21	1.27
	2	5.69	22.65	28.35	80%	0.658	0.339	0.530	0.123	12.28	0.89
	3	4.90	23.52	28.42	83%	0.515	0.438	0.756	0.130	10.62	0.83
7	1	2.71	10.85	13.56	80%	0.789	0.169	0.258	0.033	11.97	0.91
	2	3.28	12.44	15.72	79%	0.769	0.181	0.247	0.067	10.25	0.79
	3	2.51	13.04	15.56	84%	0.764	0.216	0.386	0.083	9.61	0.69
8	1	3.53	14.00	17.53	80%	0.863	0.127	0.061	0.018	12.45	0.66
	2	3.29	14.76	18.06	82%	0.862	0.129	0.128	0.044	10.62	0.58
	3	2.75	14.60	17.35	84%	0.793	0.151	0.231	0.057	10.01	0.57
9	1	3.75	14.58	18.34	80%	0.651	0.267	0.576	0.079	16.64	1.19
	2	2.00	17.66	19.66	90%	0.578	0.283	0.796	0.110	12.86	0.81
	3	2.37	18.47	20.84	89%	0.543	0.325	0.682	0.124	10.36	0.73
10	1	8.19	20.09	28.28	71%	0.342	0.506	1.431	0.102	14.73	1.14
	2	8.12	20.31	28.43	71%	0.293	0.479	1.415	0.129	11.39	0.92
	3	13.63	22.54	36.16	62%	0.489	0.574	0.593	0.143	10.27	0.86
11	1	3.05	12.06	15.11	80%	0.813	0.145	0.223	0.024	10.90	0.64
	2	3.59	11.57	15.16	76%	0.809	0.148	0.180	0.053	9.96	0.59
	3	3.35	12.48	15.84	79%	0.792	0.138	0.211	0.066	9.80	0.56
12	1	2.60	10.04	12.63	79%	0.649	0.222	0.437	0.072	15.48	0.90
	2	2.64	10.88	13.51	80%	0.733	0.252	0.433	0.105	10.90	0.55
	3	3.17	13.75	16.92	81%	0.691	0.261	0.331	0.124	9.35	0.50

13	1	2.76	12.83	15.59	82%	0.750	0.196	0.484	0.044	12.42	0.94
	2	2.86	12.19	15.05	81%	0.717	0.197	0.488	0.088	10.90	0.78
	3	3.11	13.79	16.90	82%	0.722	0.216	0.357	0.104	9.91	0.65
14	1	5.30	11.20	16.50	68%	0.507	0.291	0.750	0.086	15.99	1.28
	2	5.34	15.18	20.52	74%	0.584	0.330	0.827	0.107	12.27	0.71
	3	8.78	16.75	25.53	66%	0.587	0.351	0.311	0.111	10.55	0.67
15	1	1.95	15.66	17.61	89%	0.639	0.245	0.577	0.054	13.12	0.93
	2	1.92	16.18	18.10	89%	0.713	0.233	0.541	0.095	11.29	0.68
	3	1.97	18.90	20.87	91%	0.663	0.243	0.402	0.098	10.01	0.68
16	1	2.04	13.74	15.78	87%	0.790	0.133	0.125	0.008	11.13	0.80
	2	2.54	12.93	15.47	84%	0.852	0.121	0.080	0.030	10.32	0.70
	3	2.19	11.85	14.04	84%	0.817	0.132	0.129	0.044	9.88	0.61
17	1	3.81	19.83	23.63	84%	0.209	0.543	1.499	0.131	13.70	1.00
	2	2.99	22.32	25.31	88%	0.342	0.457	1.607	0.155	10.26	0.74
	3	5.09	24.81	29.90	83%	0.322	0.493	1.427	0.153	8.88	0.83
18	1	3.88	12.14	16.02	76%	0.664	0.175	0.278	0.002	13.73	1.16
	2	3.41	13.41	16.82	80%	0.782	0.143	0.178	0.028	11.48	0.78
	3	3.02	13.36	16.38	82%	0.800	0.145	0.231	0.045	11.34	0.72
19	1	3.23	15.12	18.35	82%	0.644	0.283	0.463	0.056	10.13	0.93
	2	3.54	16.93	20.48	83%	0.680	0.250	0.534	0.087	8.98	0.74
	3	3.21	18.70	21.91	85%	0.676	0.252	0.517	0.095	8.51	0.67
21	1	4.18	9.52	13.71	69%	0.830	0.107	0.000	0.008	10.12	0.74
	2	3.99	10.38	14.37	72%	0.909	0.118	0.001	0.032	9.71	0.46
	3	3.55	9.86	13.41	74%	0.868	0.121	0.069	0.047	9.59	0.42
22	1	3.67	16.95	20.62	82%	0.829	0.157	0.004	0.032	10.20	0.69
	2	4.03	18.54	22.57	82%	0.863	0.176	0.024	0.073	9.62	0.56
	3	3.26	19.55	22.80	86%	0.815	0.176	0.168	0.089	9.23	0.48
23	1	3.14	18.94	22.08	86%	0.784	0.180	0.233	0.062	12.05	0.97
	2	3.36	23.20	26.55	87%	0.762	0.229	0.532	0.089	10.03	0.70
	3	4.59	22.26	26.86	83%	0.733	0.267	0.361	0.113	9.54	0.61
24	1	2.36	12.28	14.64	84%	0.746	0.183	0.281	0.059	11.03	0.89
	2	2.89	12.64	15.52	81%	0.798	0.216	0.289	0.094	9.83	0.65
	3	2.14	15.16	17.31	88%	0.747	0.210	0.407	0.104	9.43	0.57
25	1	3.01	10.32	13.33	77%	0.851	0.149	0.001	0.026	8.75	0.76
	2	3.21	13.23	16.43	80%	0.877	0.157	0.115	0.058	8.22	0.59
	3	2.90	14.74	17.64	84%	0.830	0.151	0.178	0.071	8.17	0.57

THb = total hemoglobin content | StO_2 = oxygen saturation | bkg = wavelength independent value added as a fitting parameter to account for possible tissue absorbers not included in the fitting procedures and for limitations of the theoretical model.

Absorption and reduced scattering spectra at the three source detector separations measured on the abdominal region (4 cm left to the navel and 4 cm right to the navel respectively on the left and on the right) for all the subjects

Subject #0

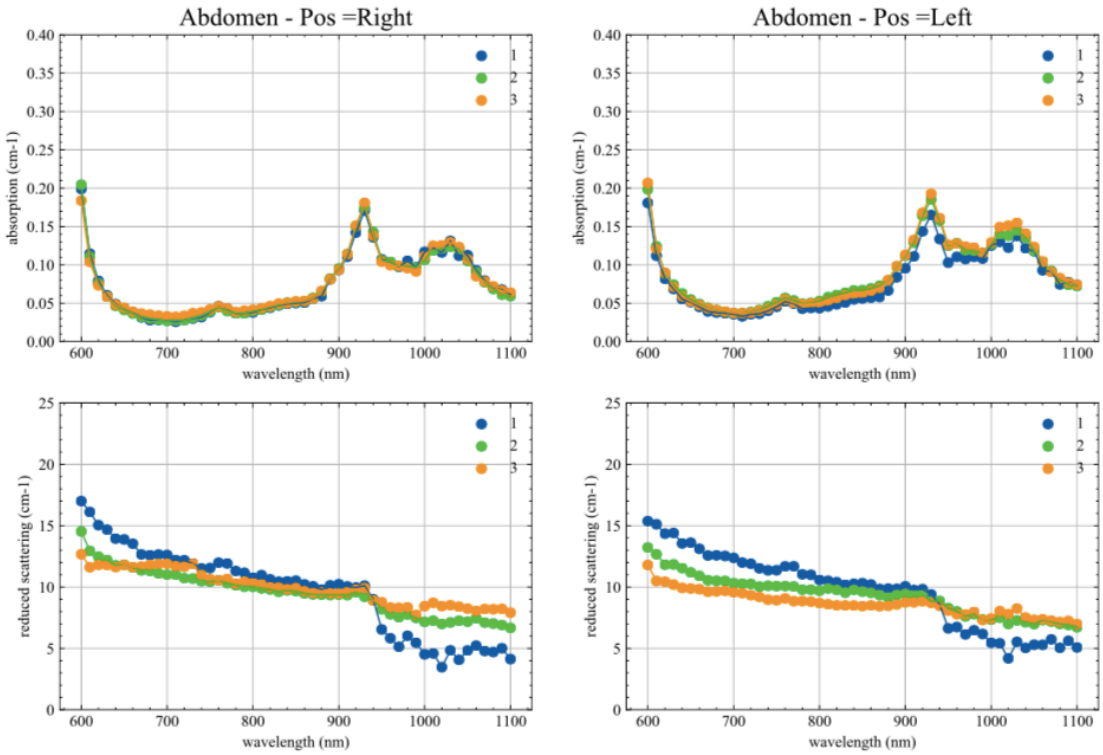

Subject #1

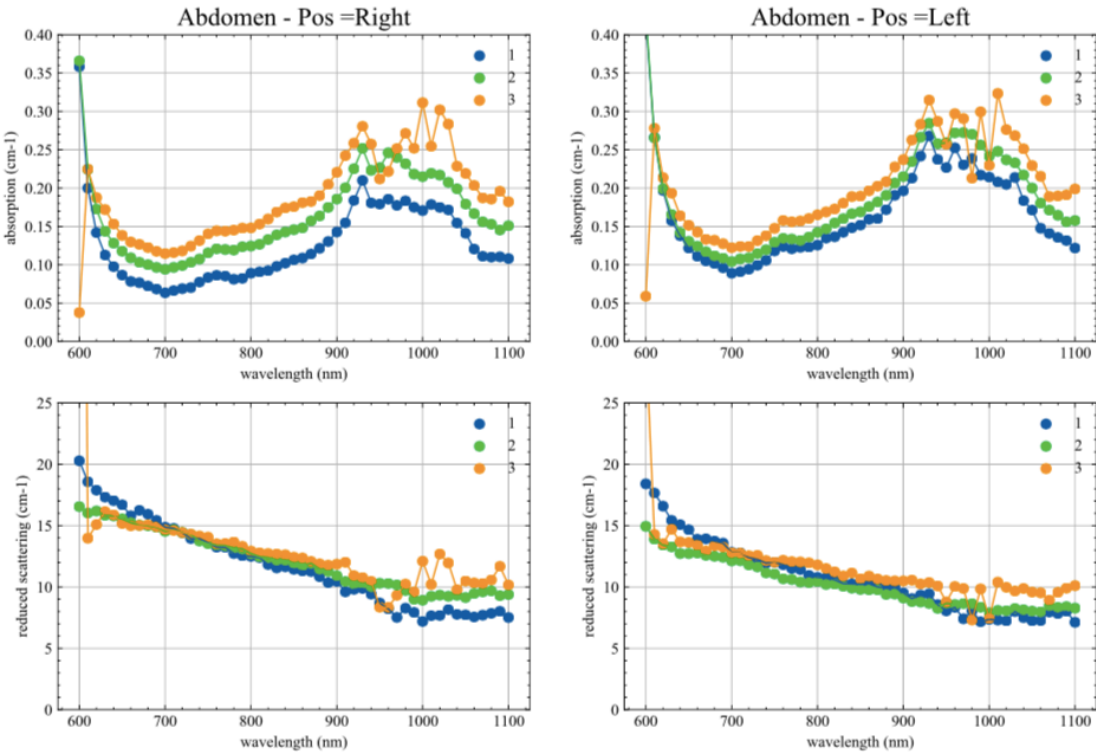

Subject #2

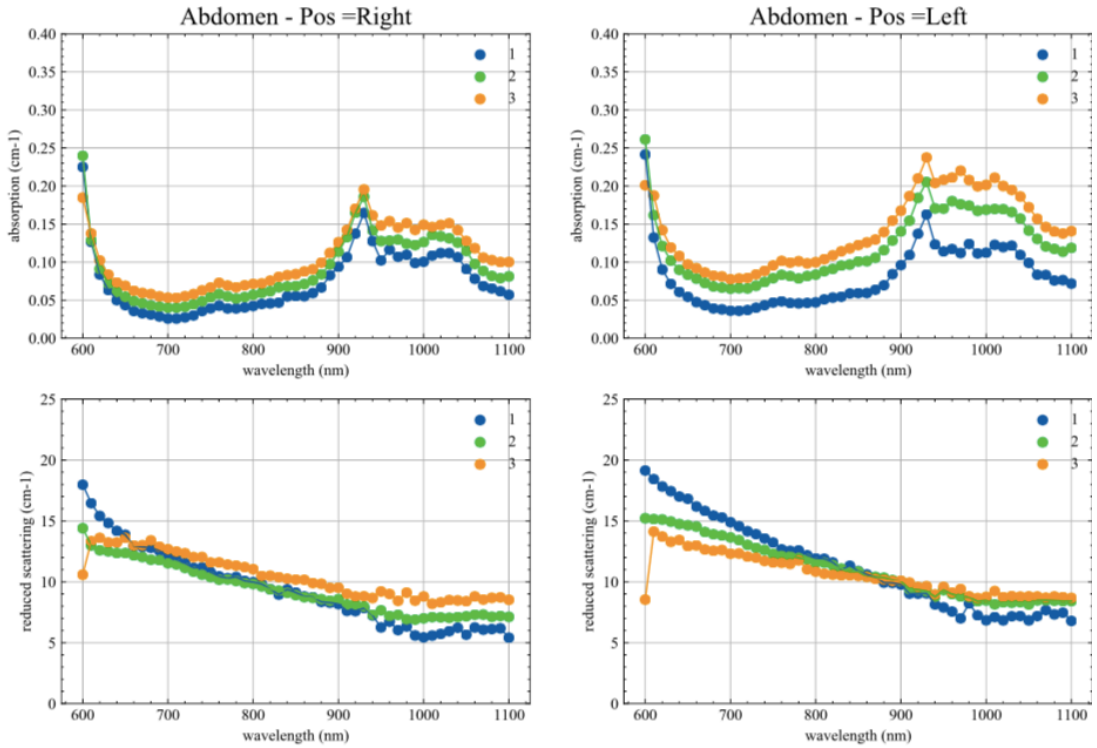

Subject #3

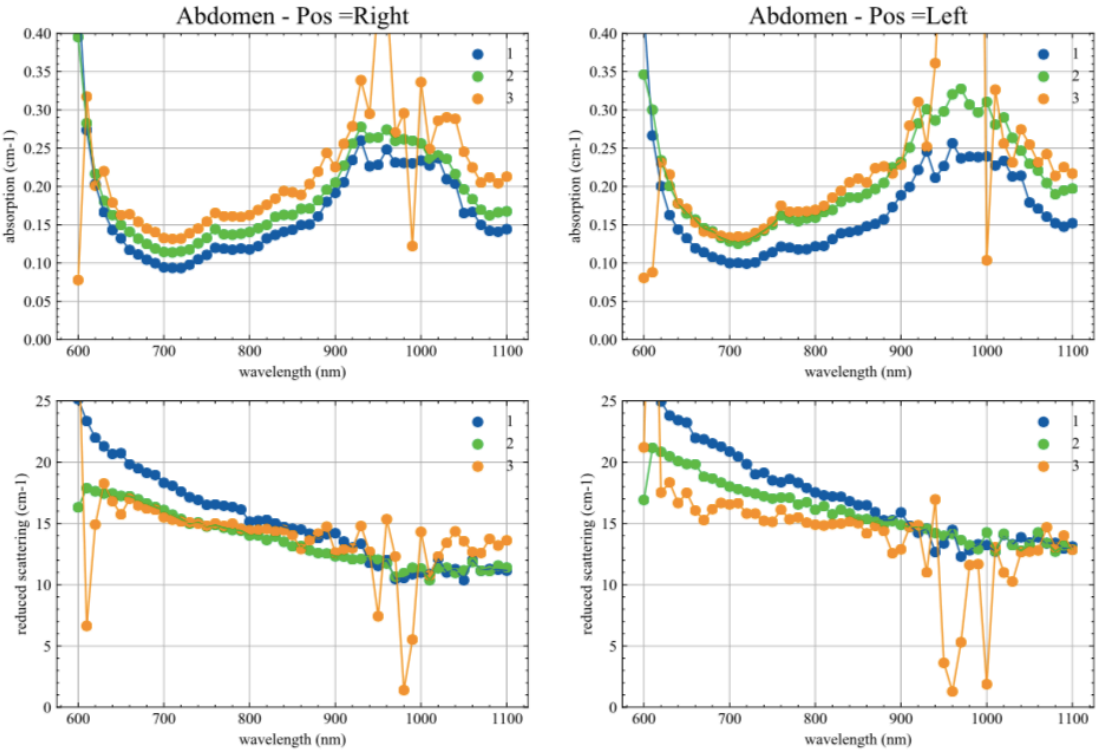

Subject #4

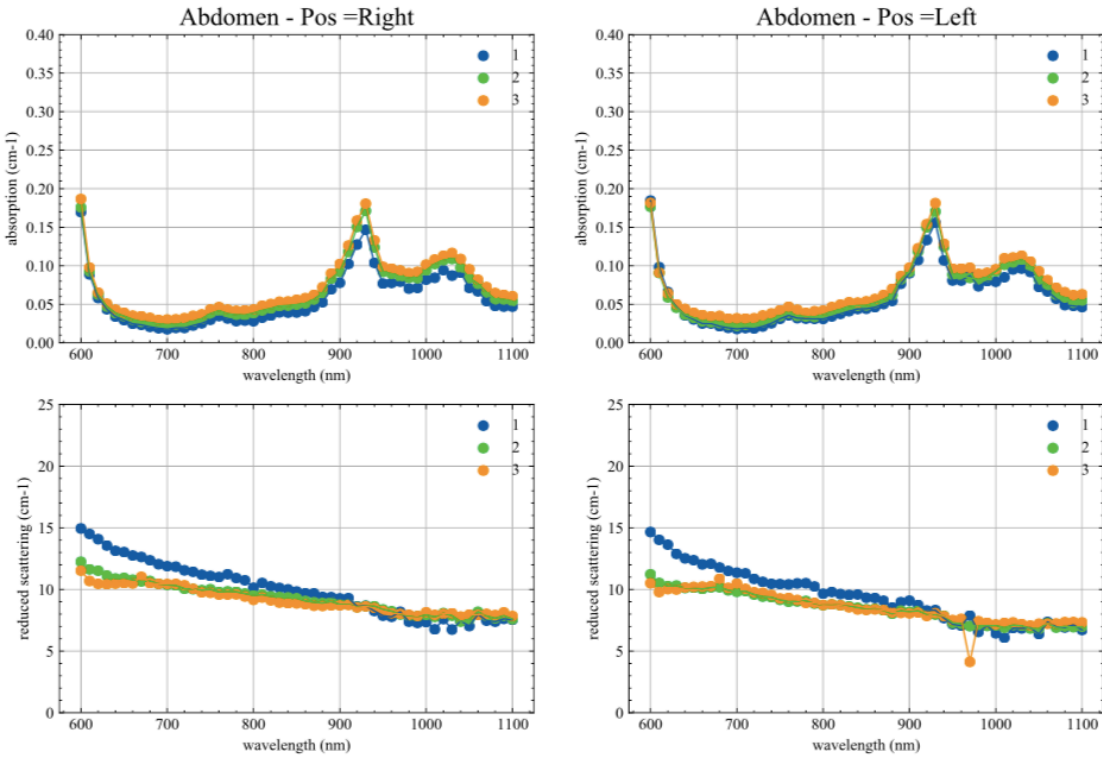

Subject #5

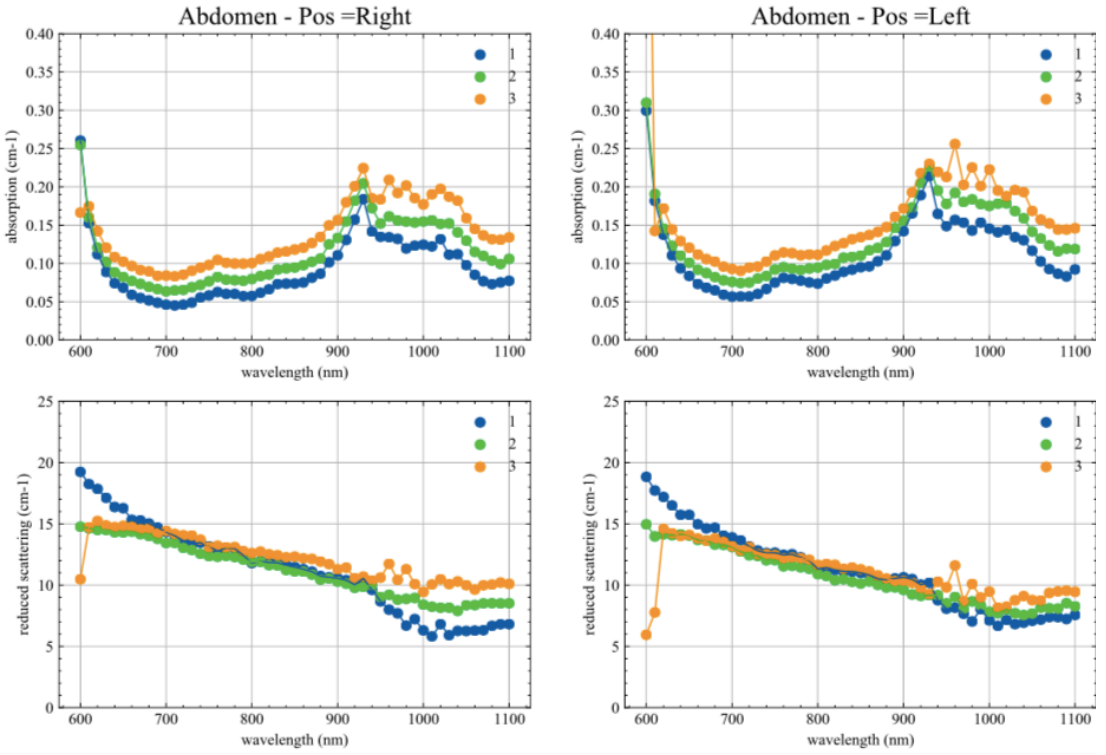

Subject #6

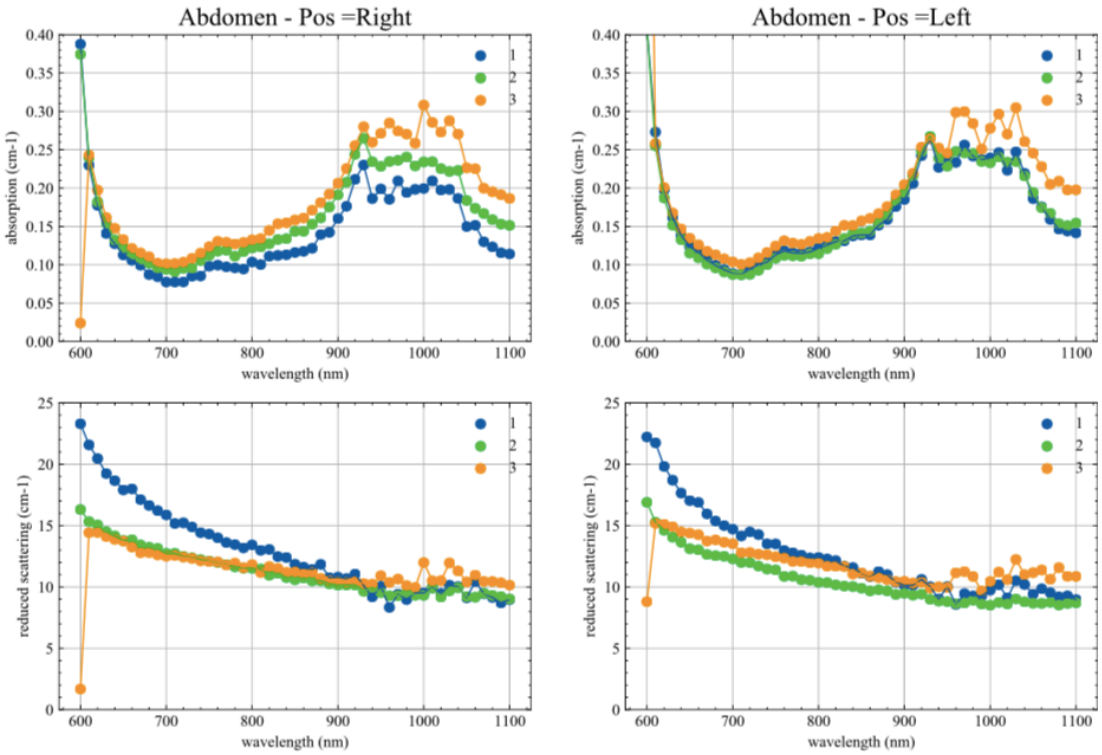

Subject #7

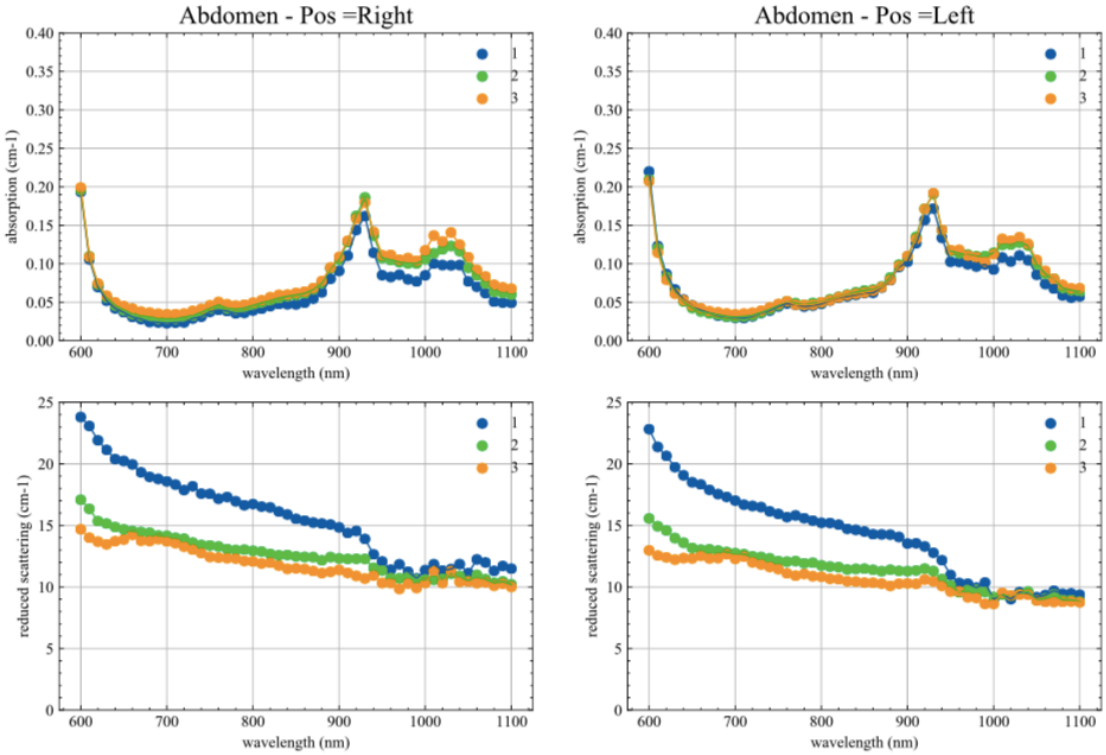

Subject #8

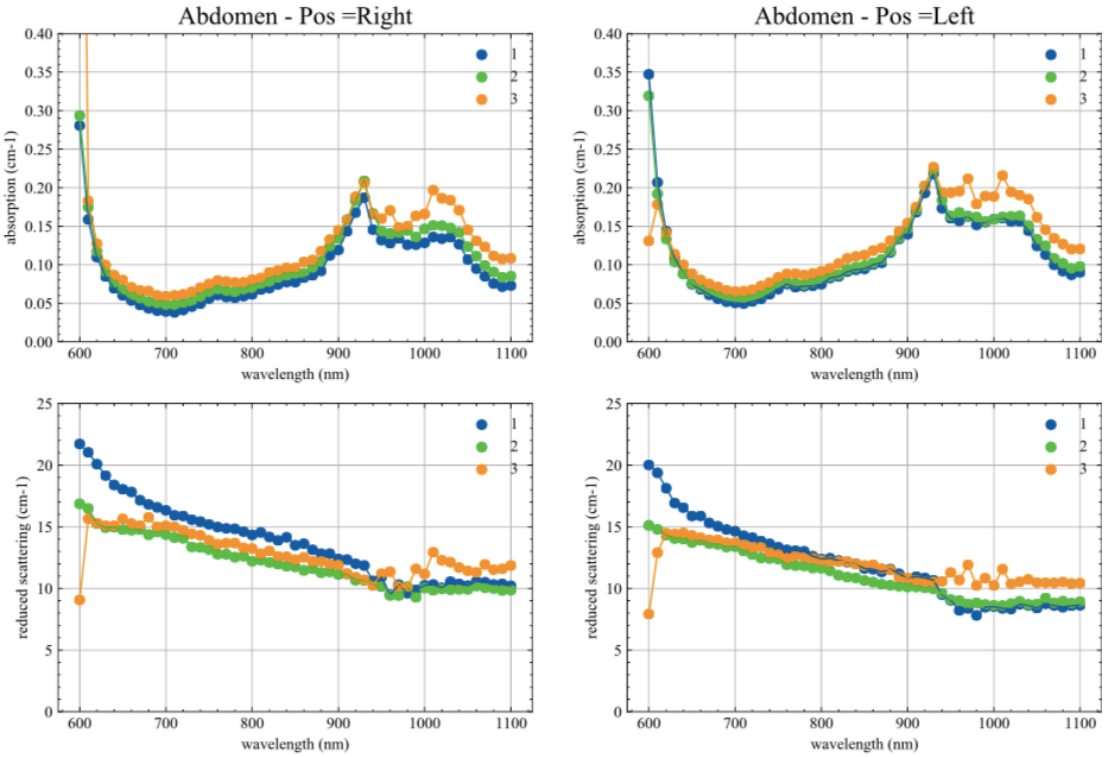

Subject #9

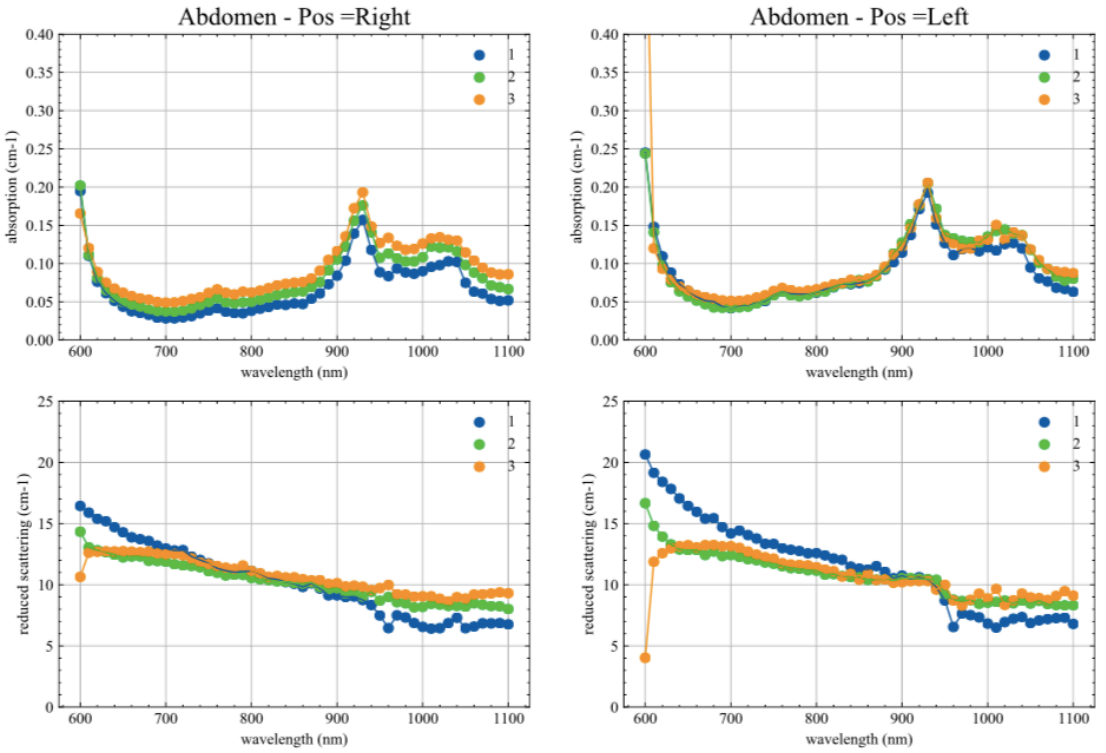

Subject #10

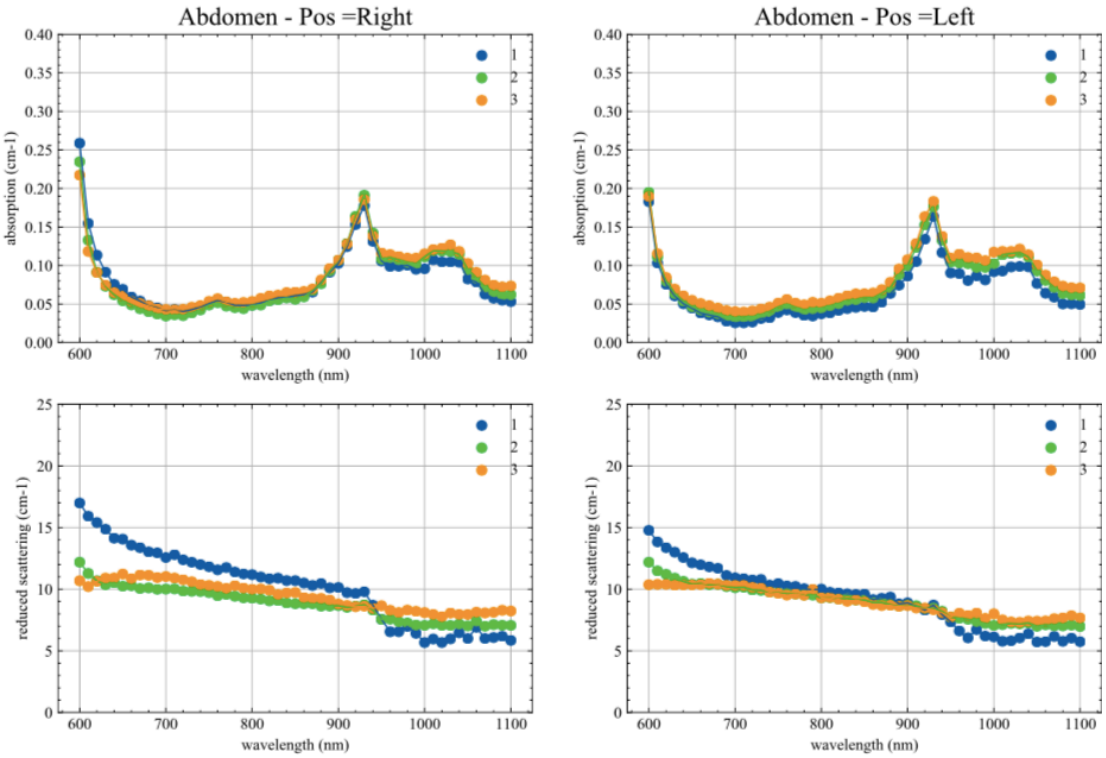

Subject #11

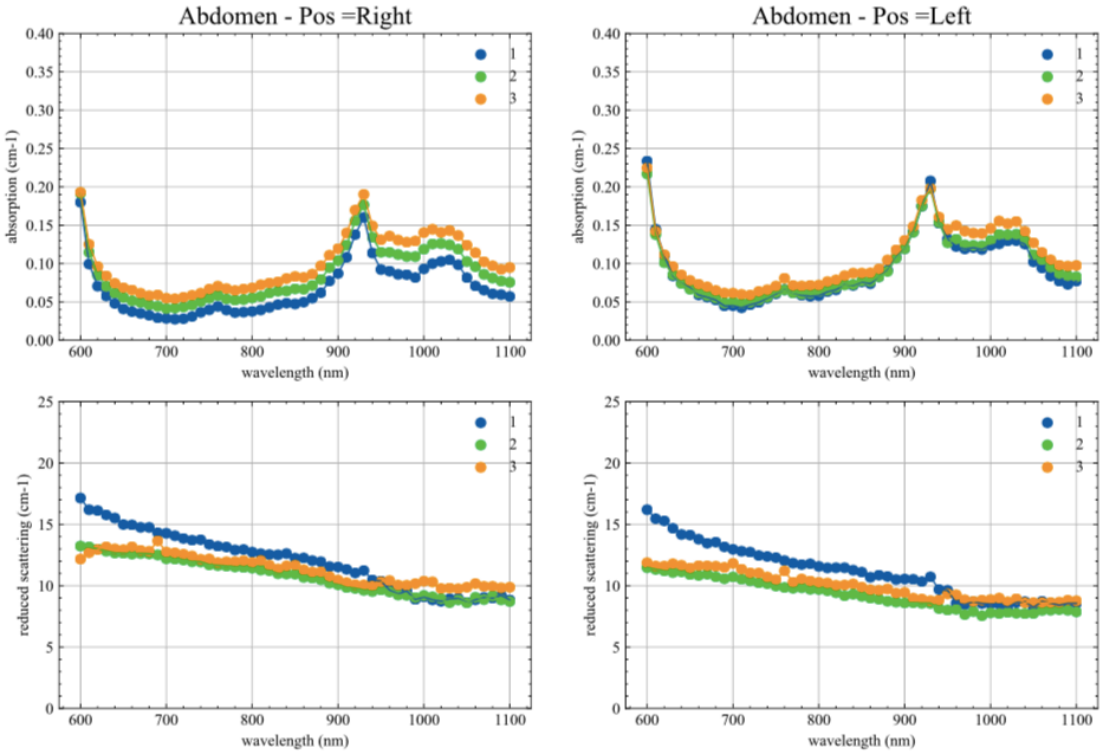

Subject #12

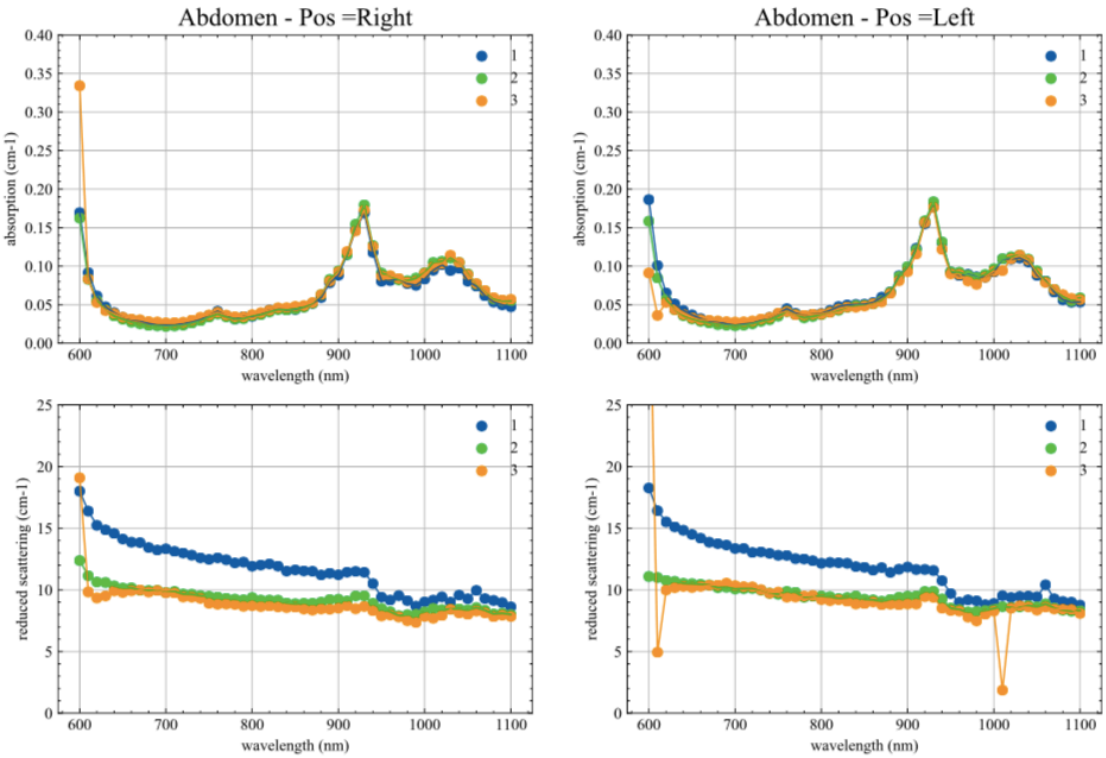

Subject #13

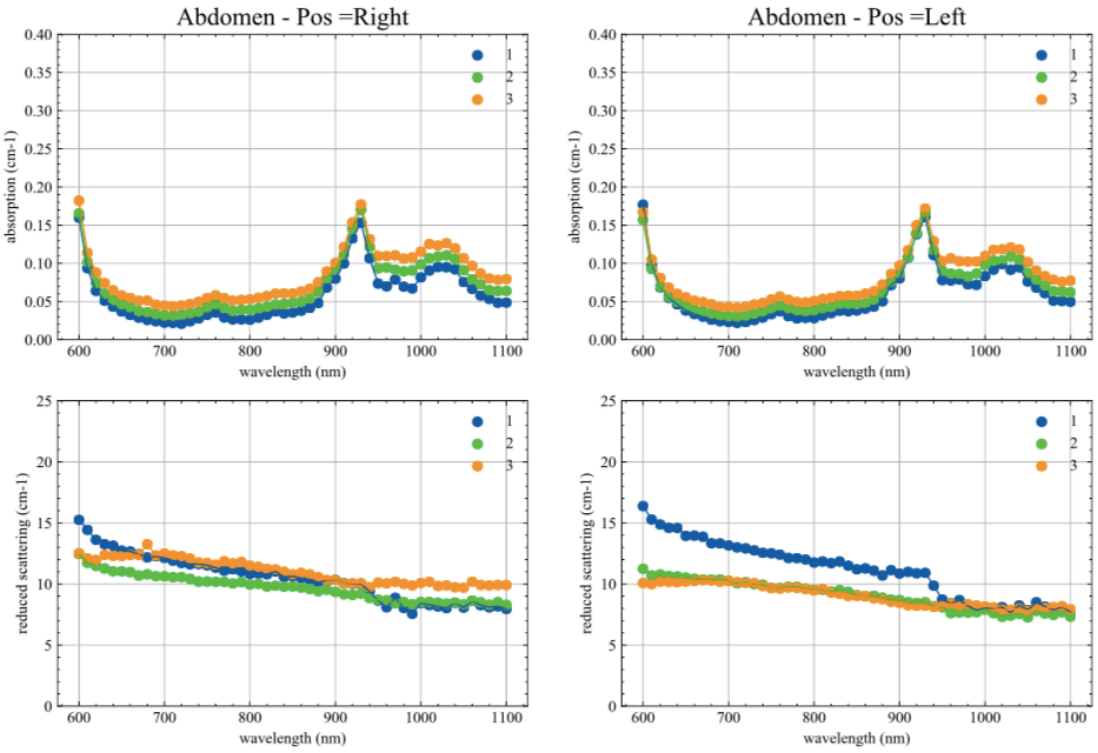

Subject #14

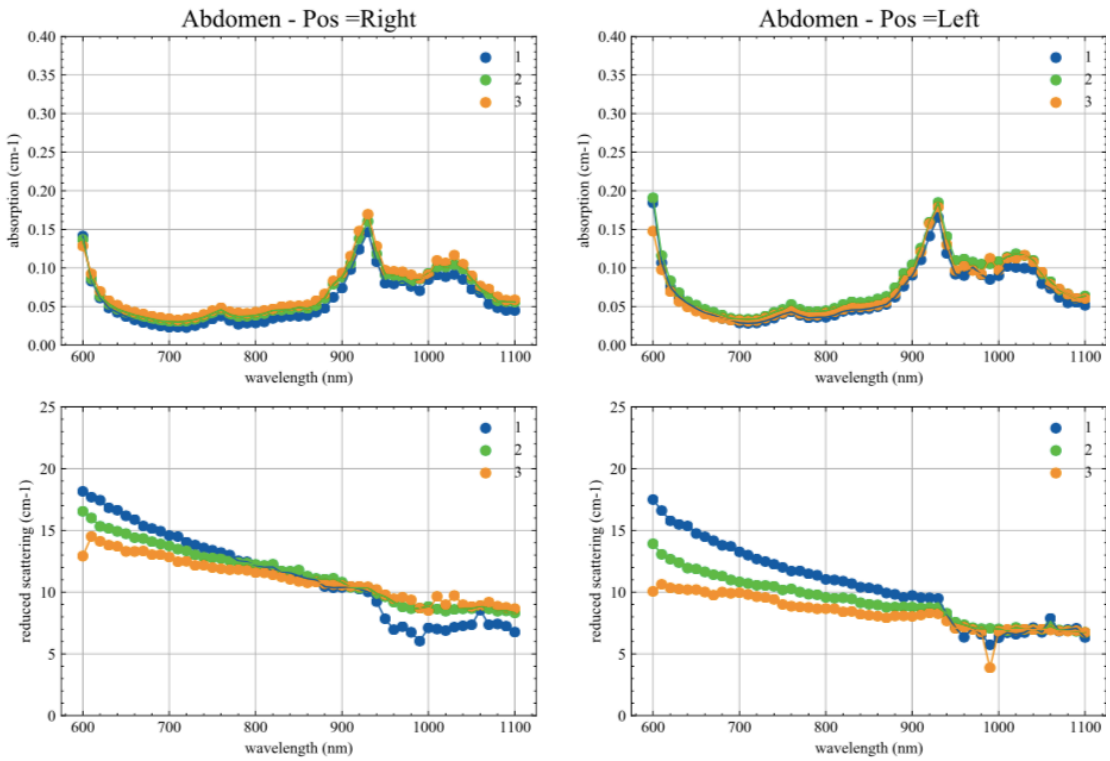

Subject #15

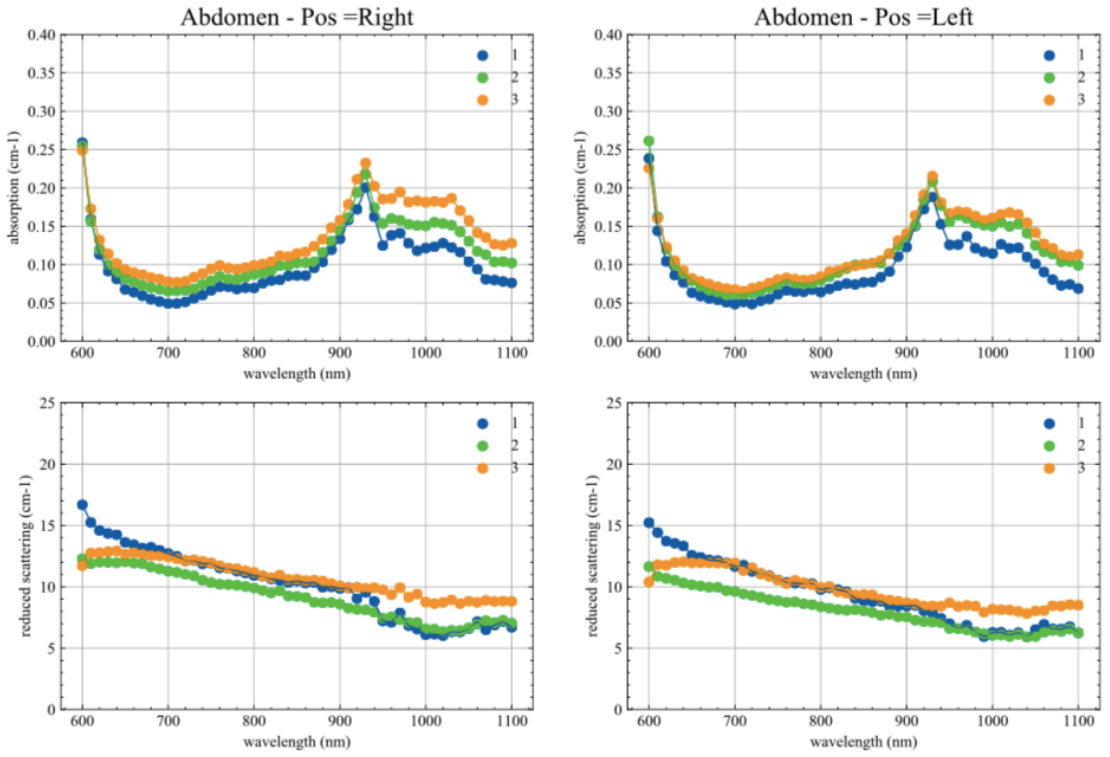

Subject #16

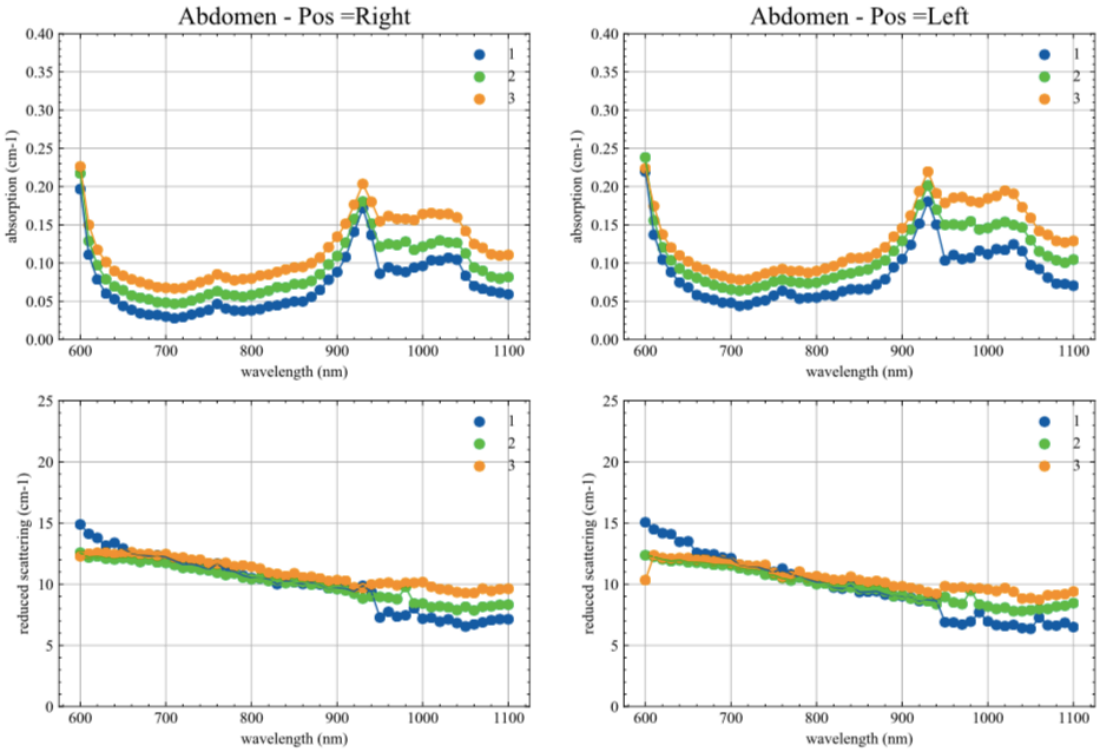

Subject #17

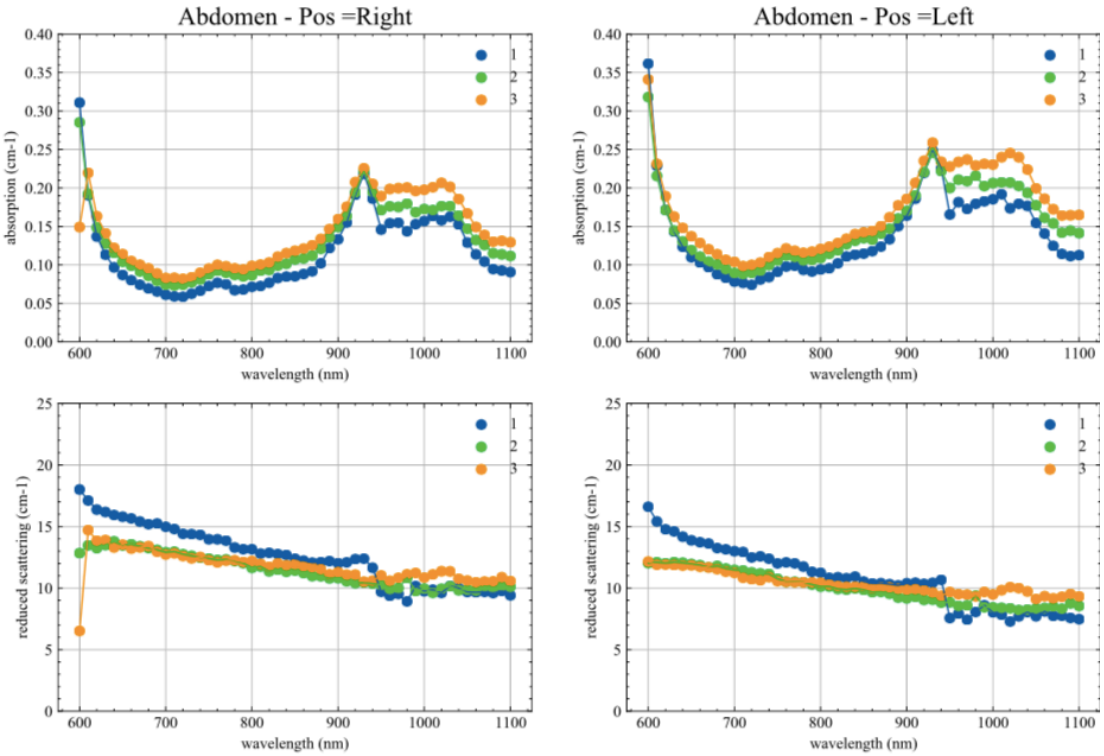

Subject #18

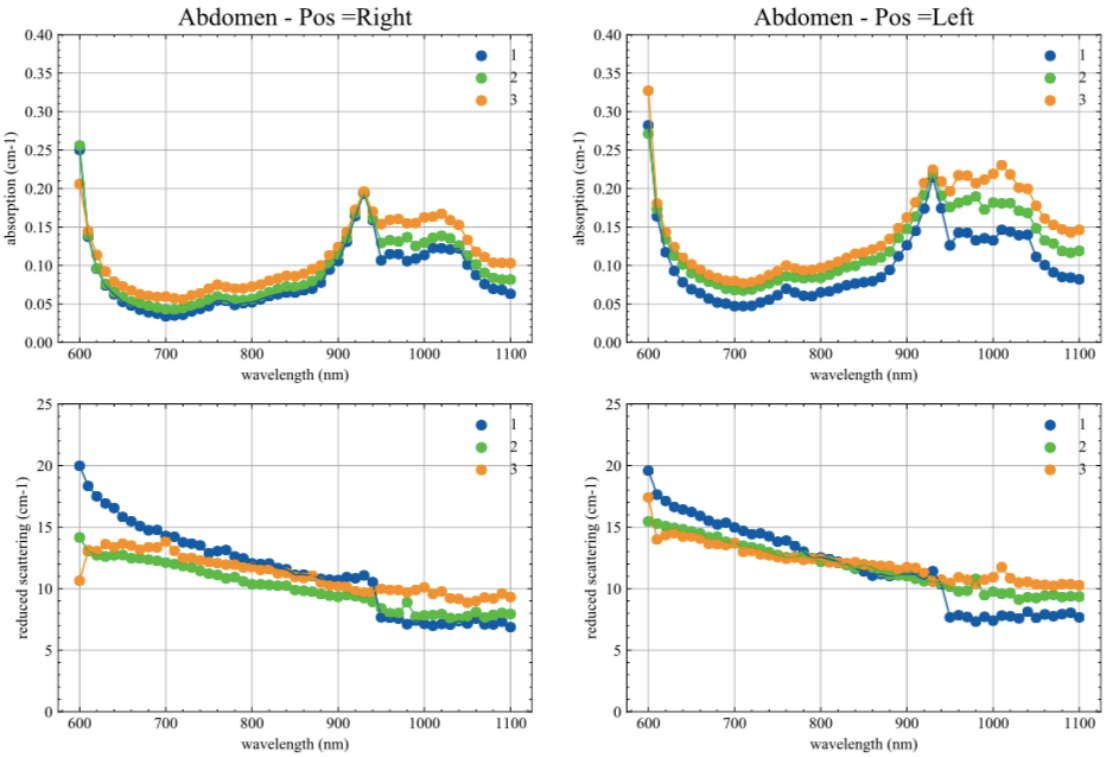

Subject #19

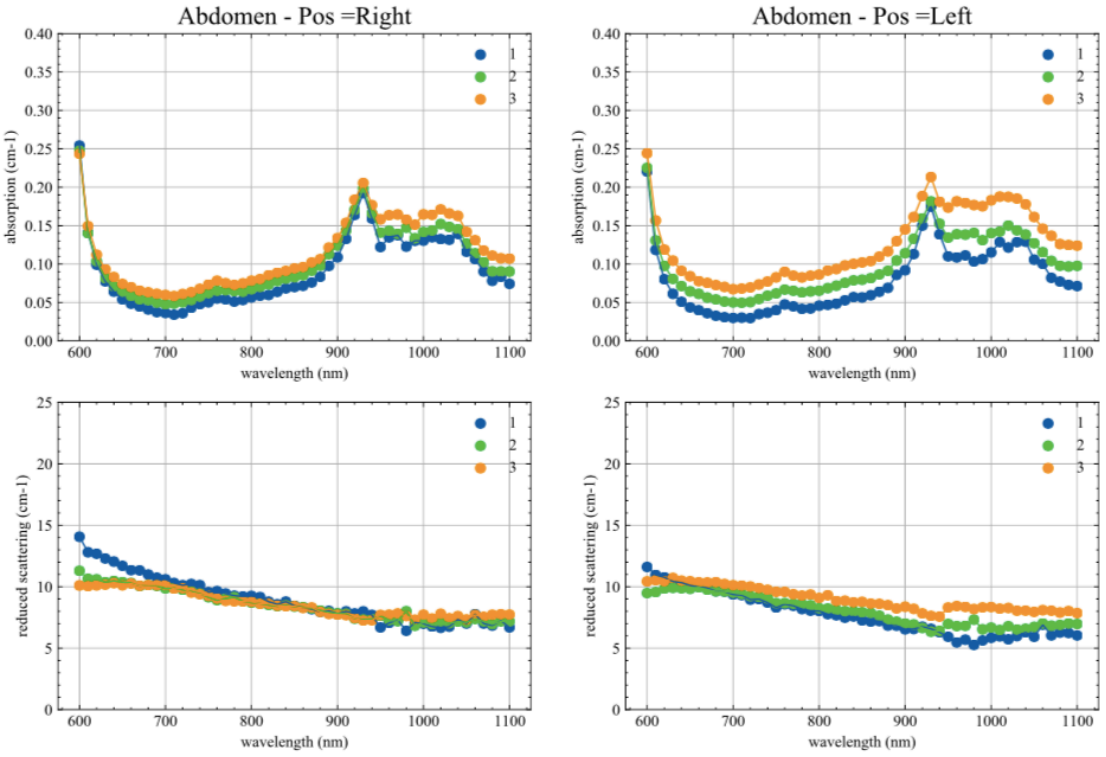

Subject #20

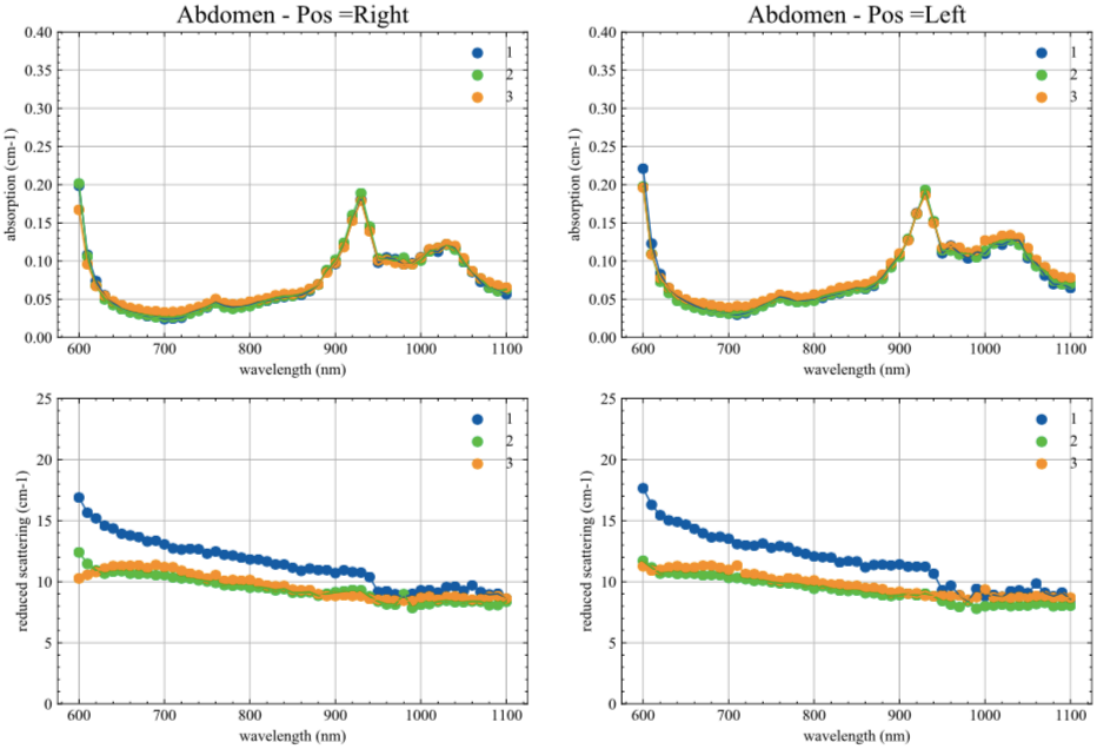

Subject #21

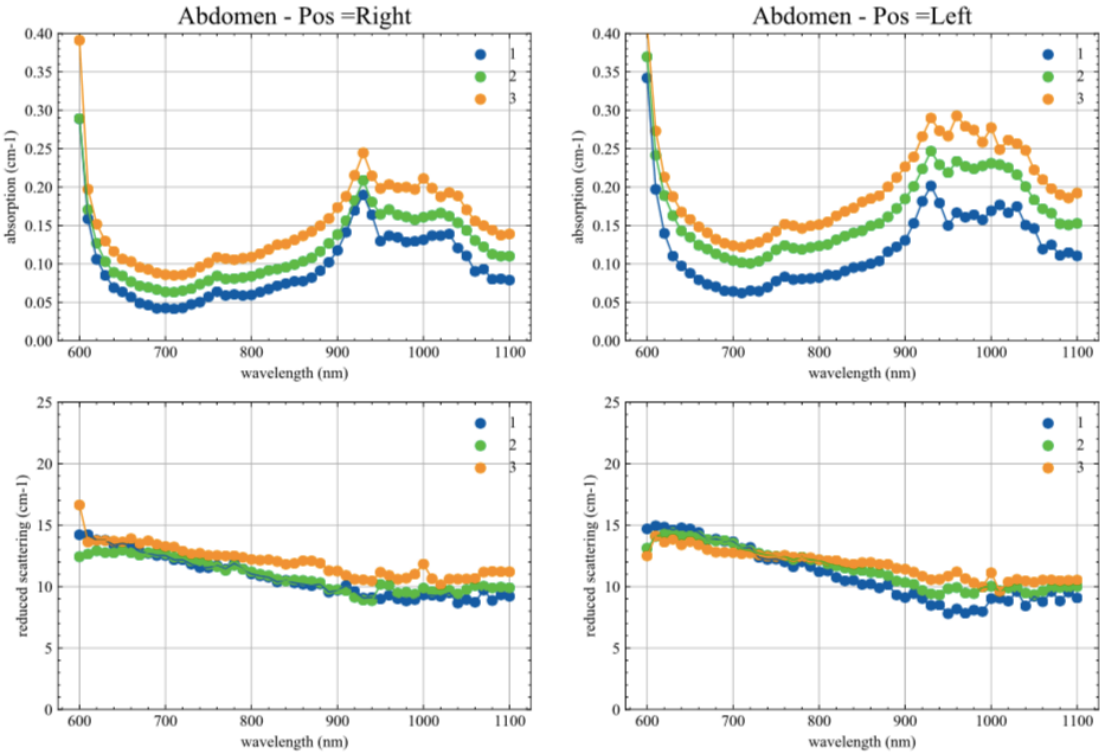

Subject #22

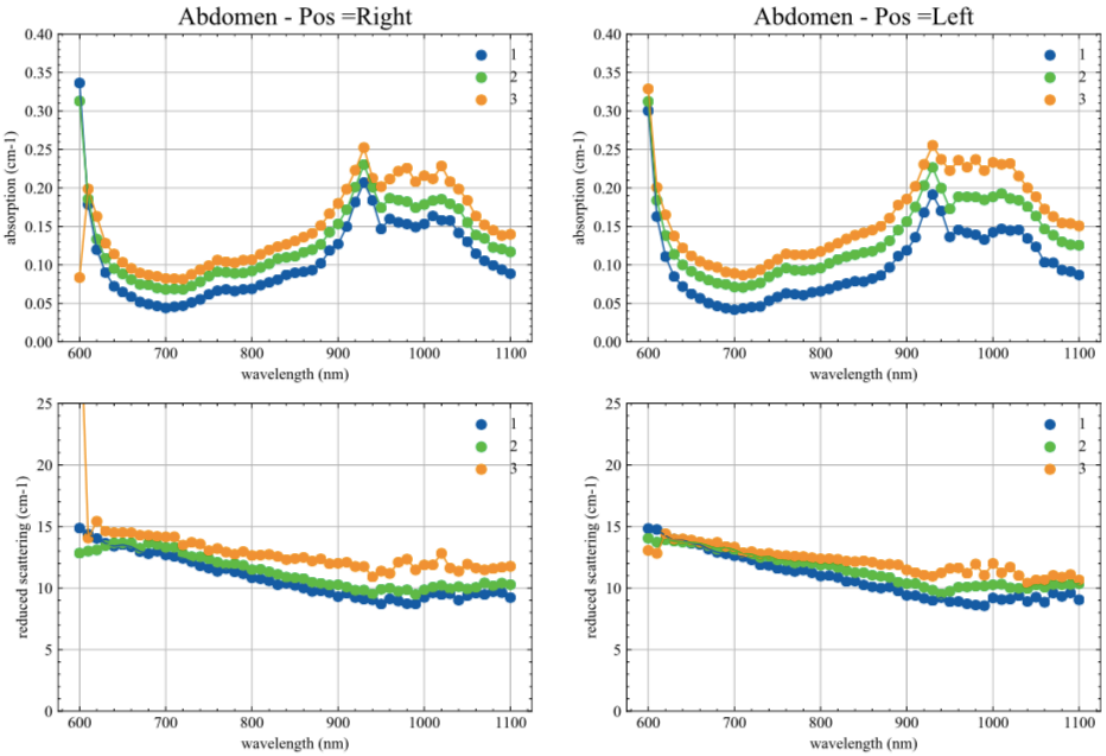

Subject #23

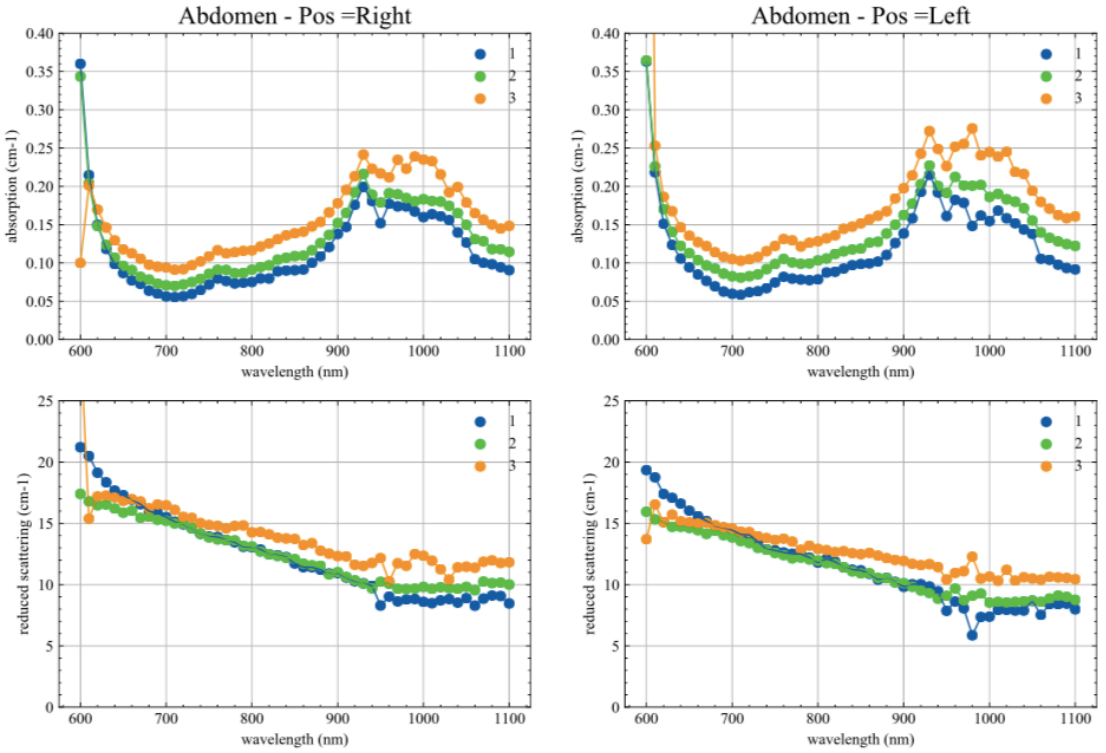

Subject #24

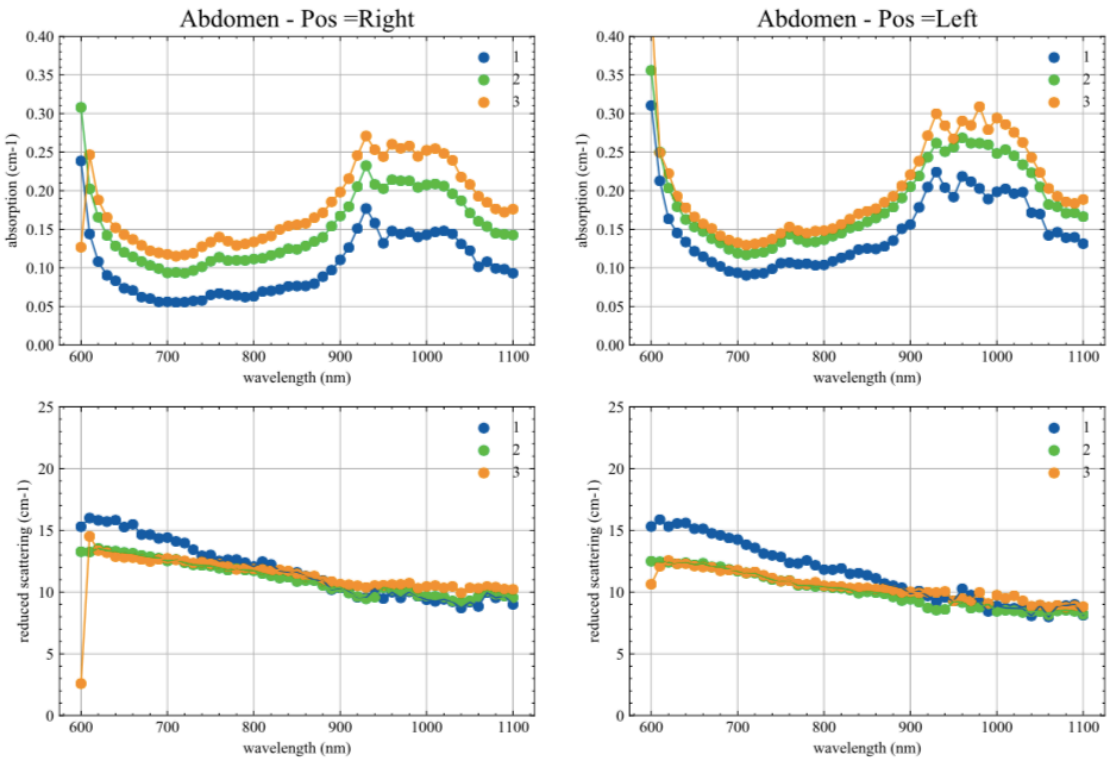

Subject #25

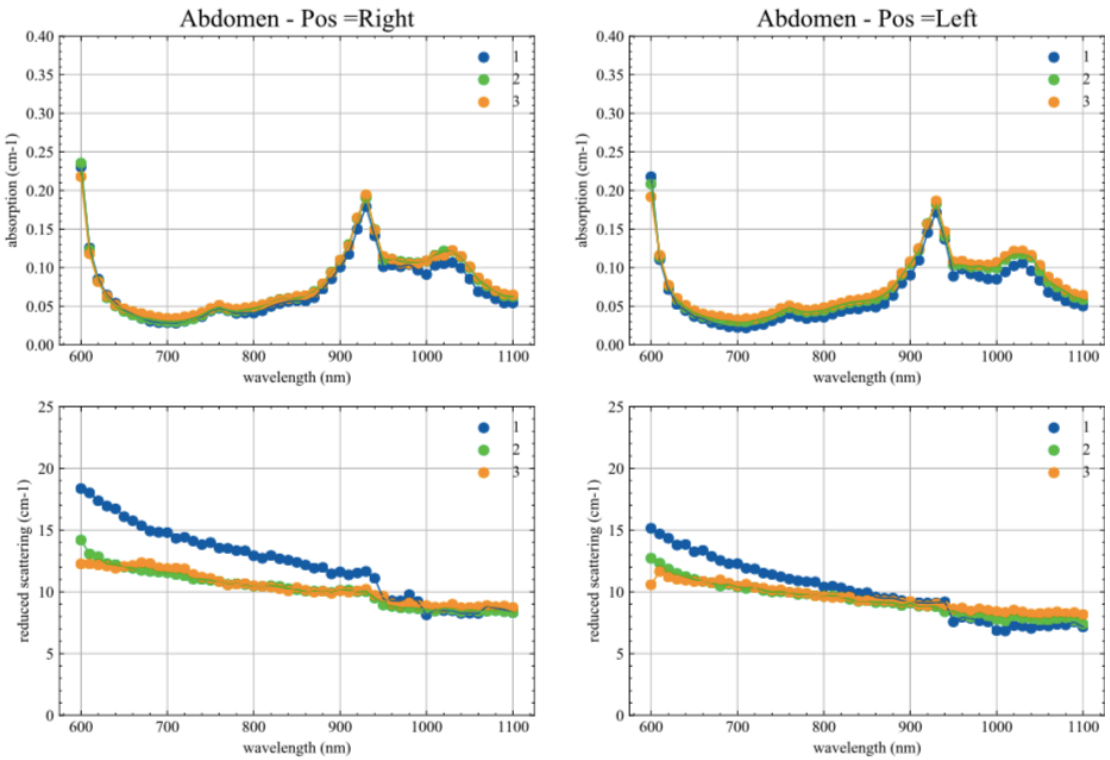

Absorption and reduced scattering spectra at the three source detector separations measured at 1/3 of the femoral length on the right thigh (*vastus lateralis* muscle). Spectra for the 3

Subject #0

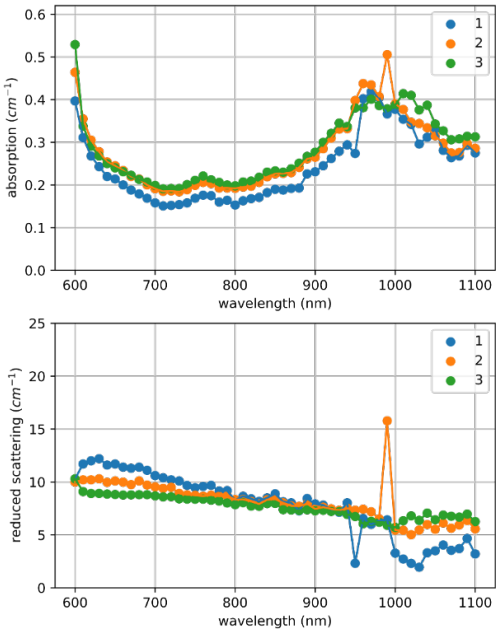

Subject #1

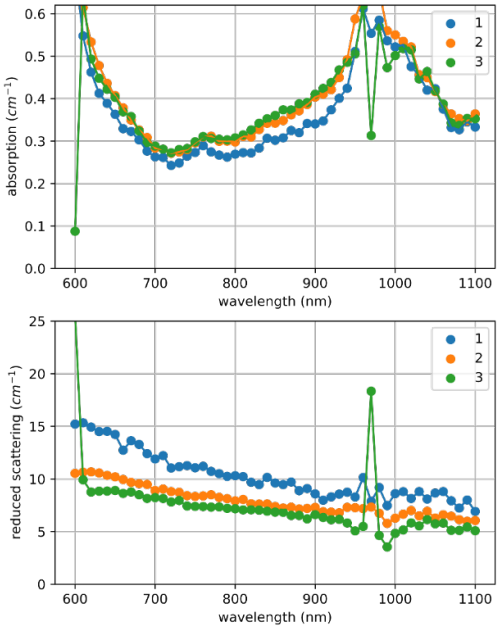

Subject #2

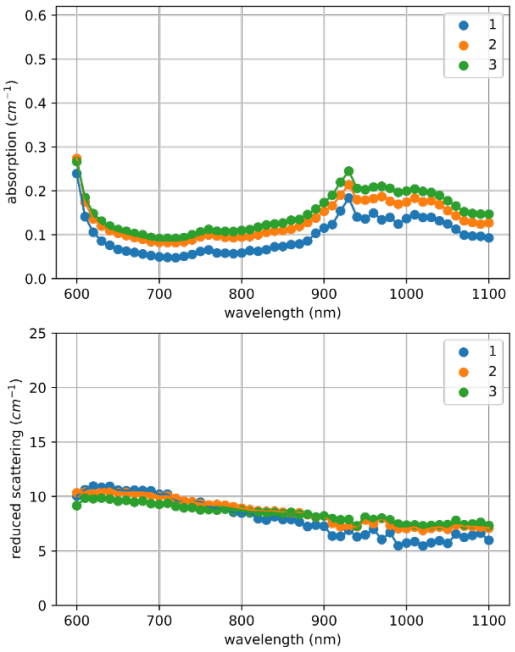

Subject #3

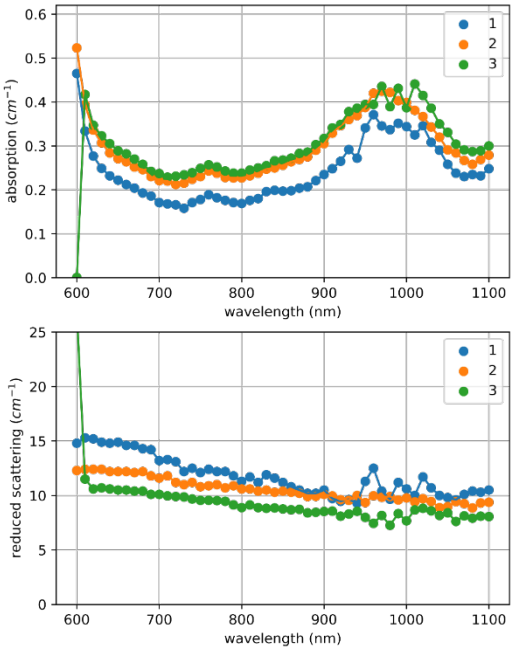

Appendix B: Supplementary Information for Section 4.4

Subject #4

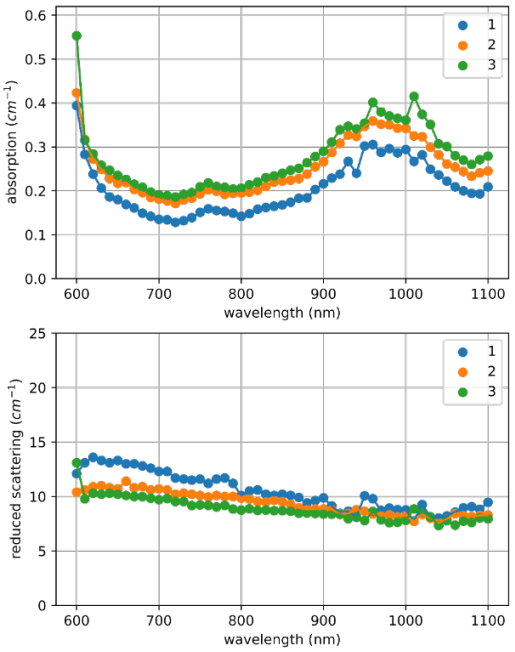

Subject #5

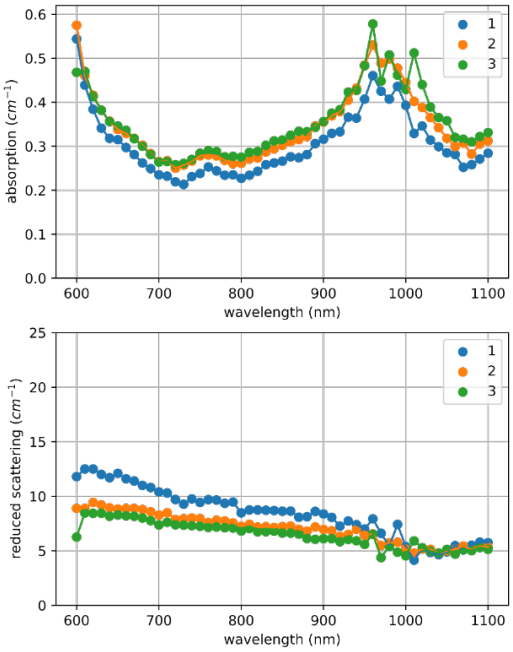

Subject #6

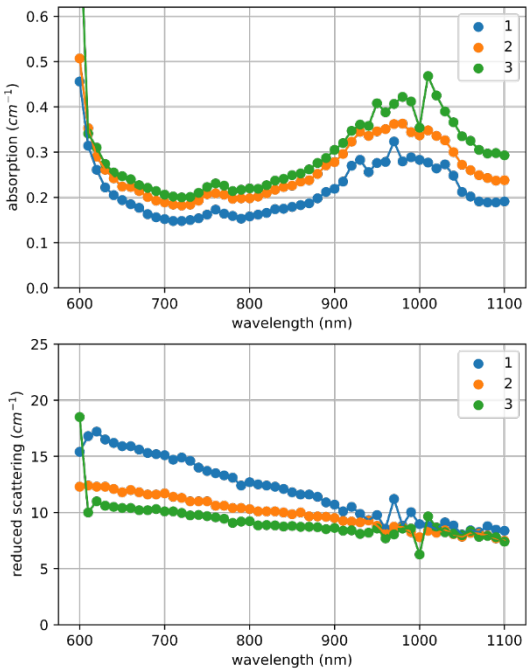

Subject #7

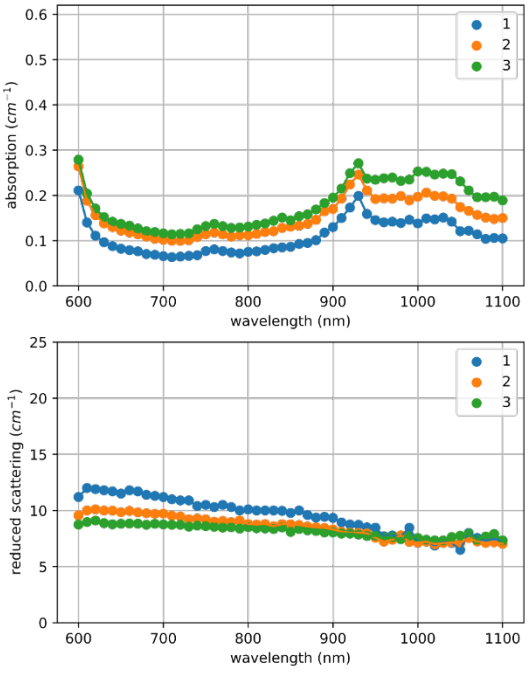

Appendix B: Supplementary Information for Section 4.4

Subject #8

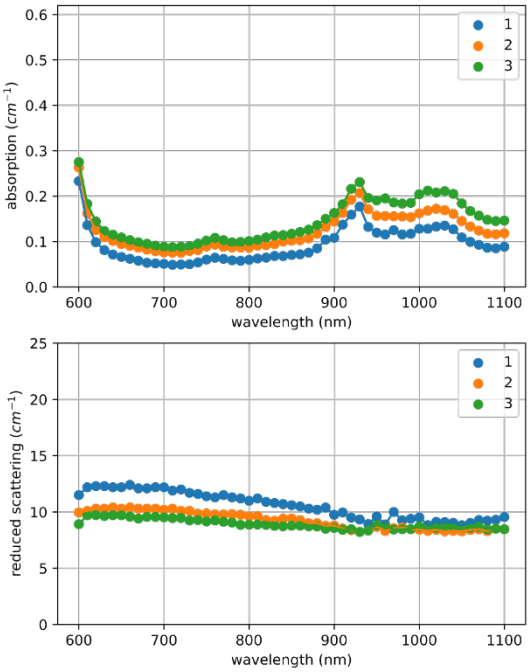

Subject #9

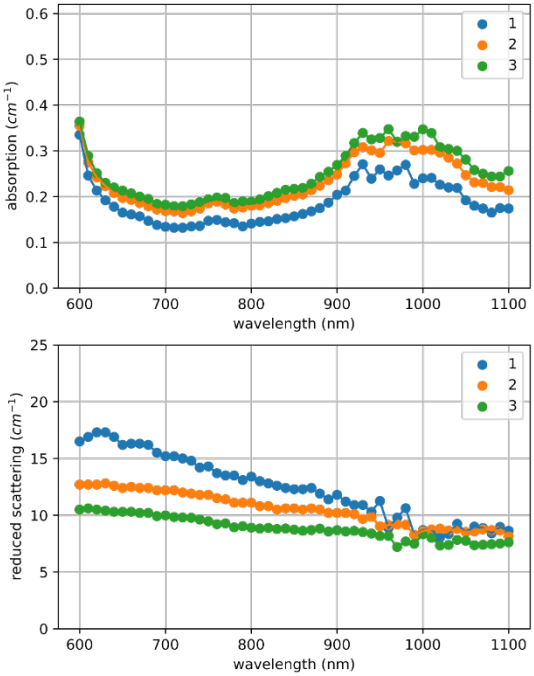

Subject #10

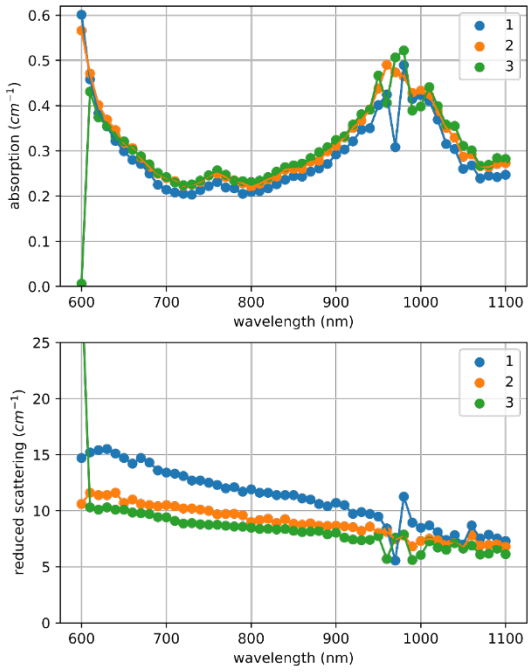

Subject #11

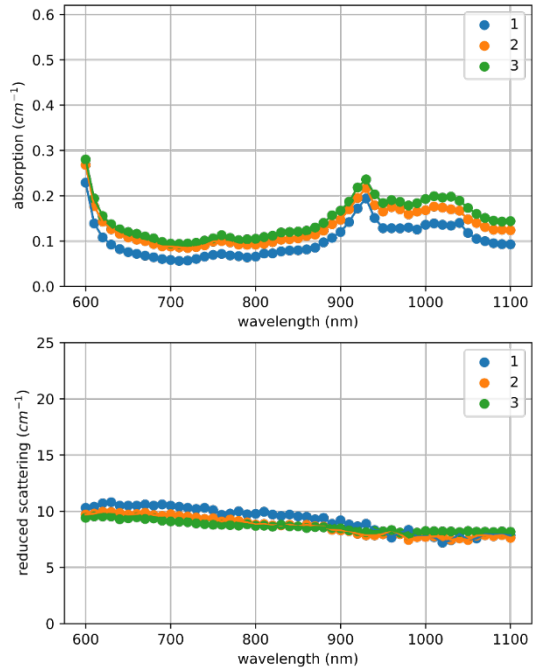

Subject #12

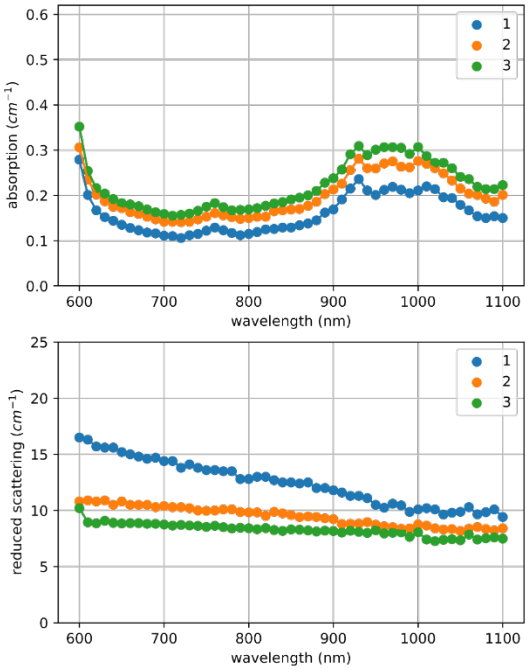

Subject #13

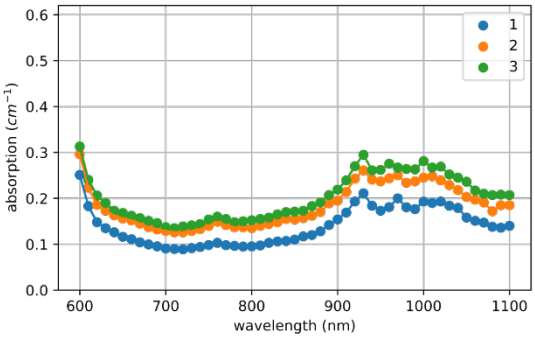

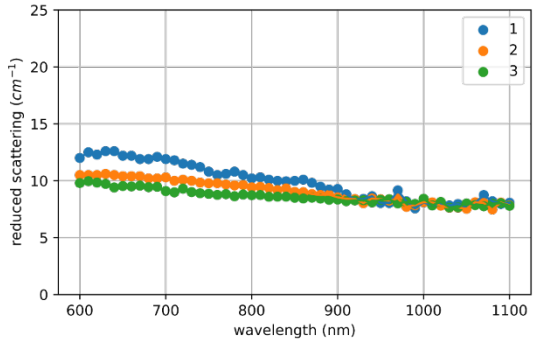

Subject #14

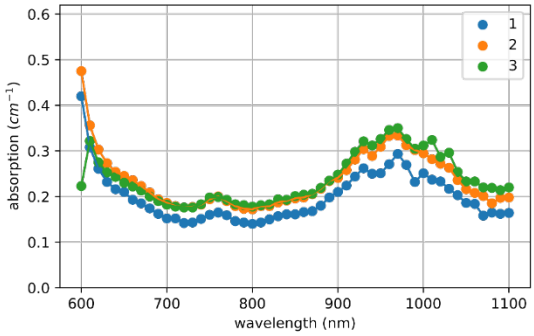

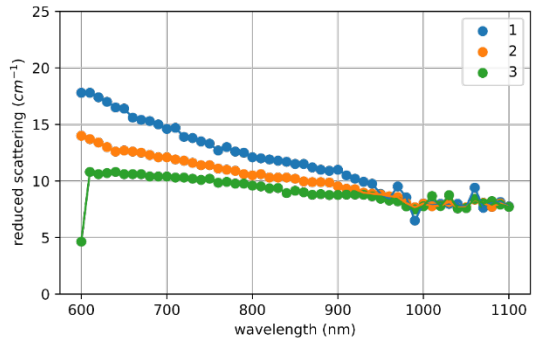

Subject #15

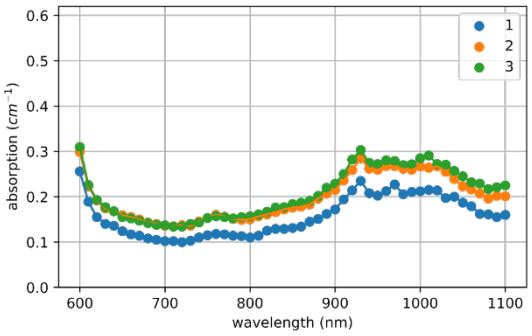

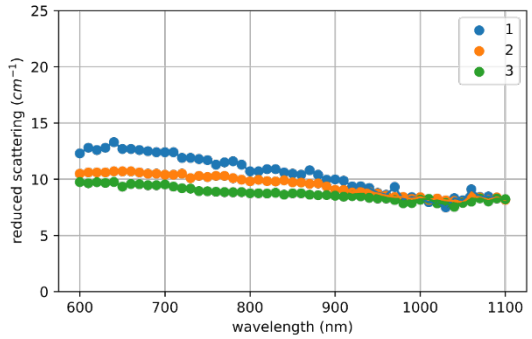

Appendix B: Supplementary Information for Section 4.4

Subject #16

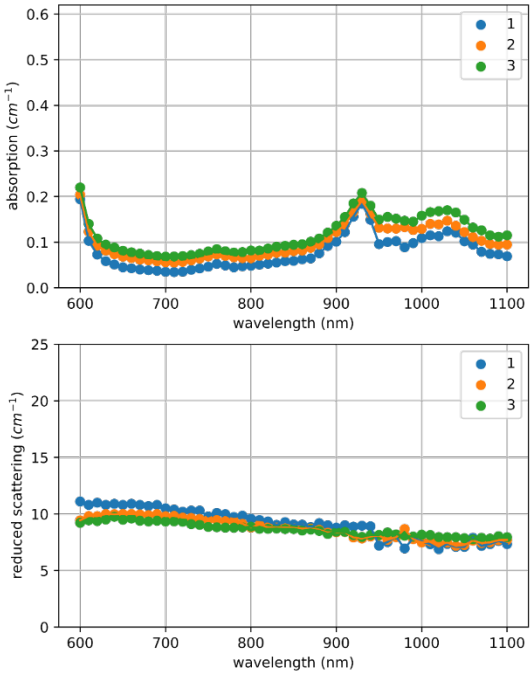

Subject #17

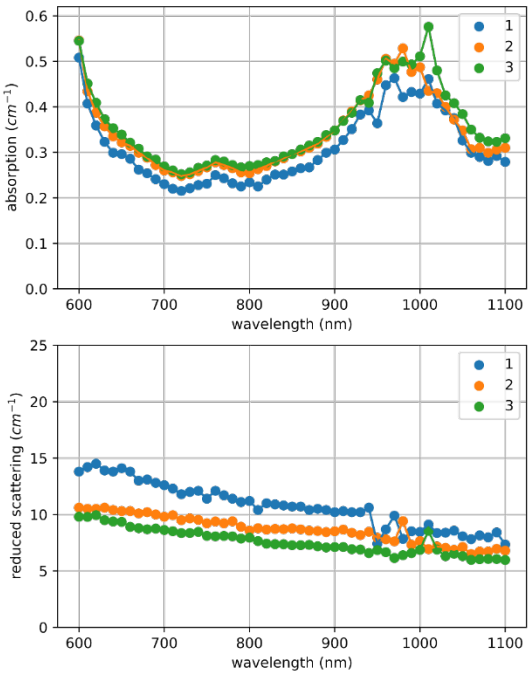

Subject #18

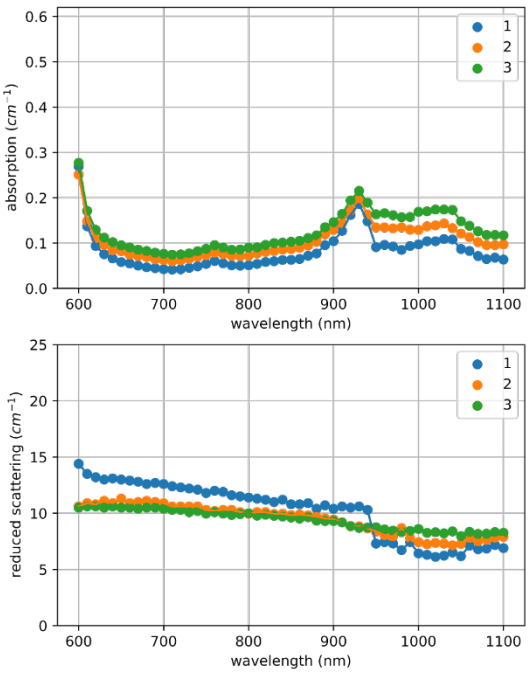

Subject #19

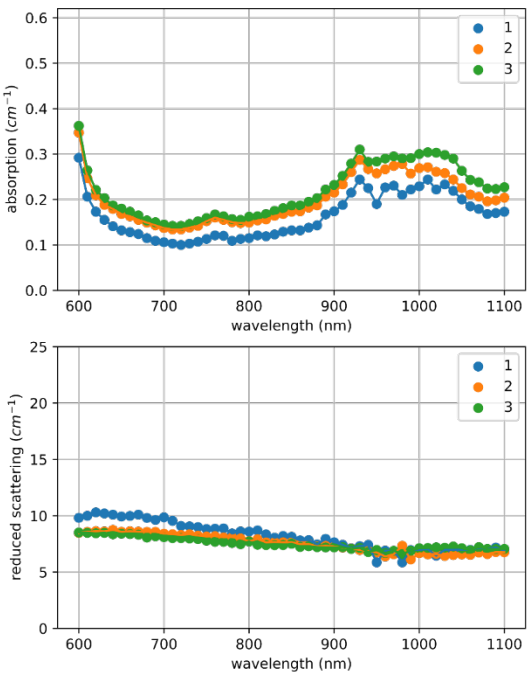

Subject #21

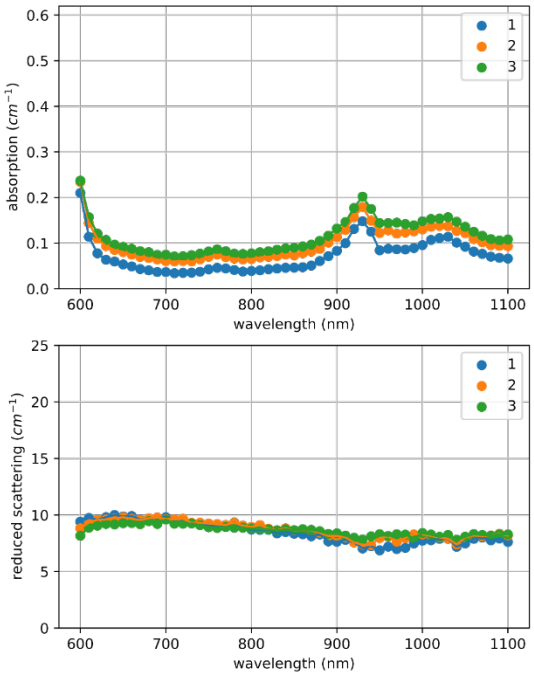

Subject #22

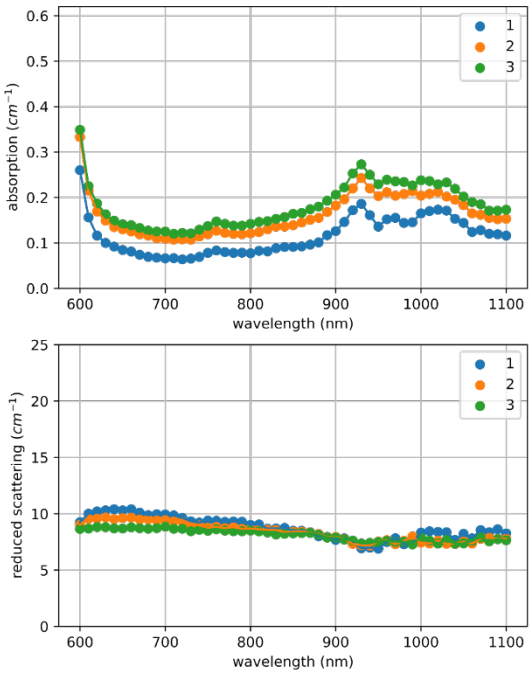

Subject #23

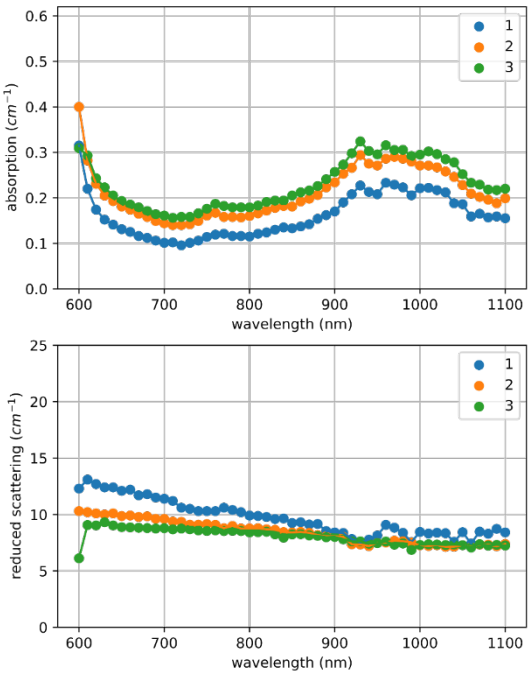

Subject #24

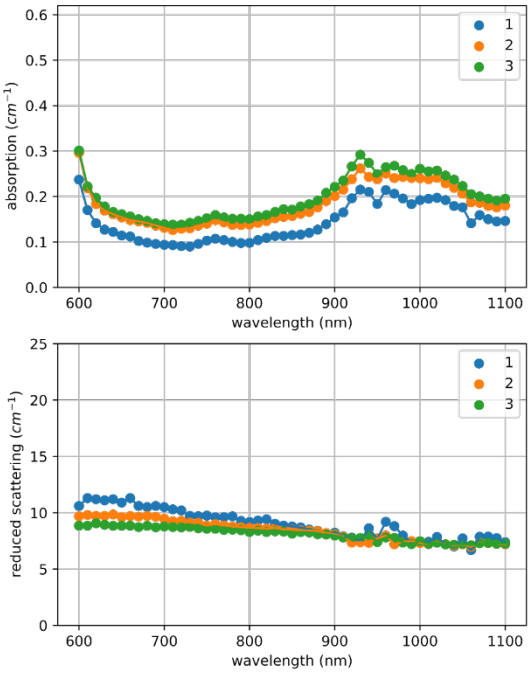

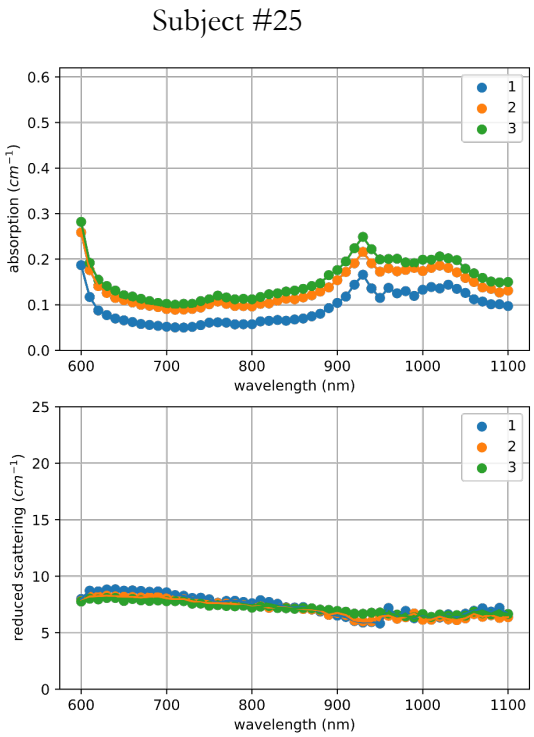
Subject #25
absorption (cm^{-1})
wavelength (nm)
reduced scattering (cm^{-1})
wavelength (nm)
1
2
3

Absorption spectra for the three positions (Left= 4cm left to navel, Right= 4cm right to navel, 1/3 of the femoral length on the right thigh) tested. Spectra with mean values from all the subjects at the three interfibre distances.

Rho1

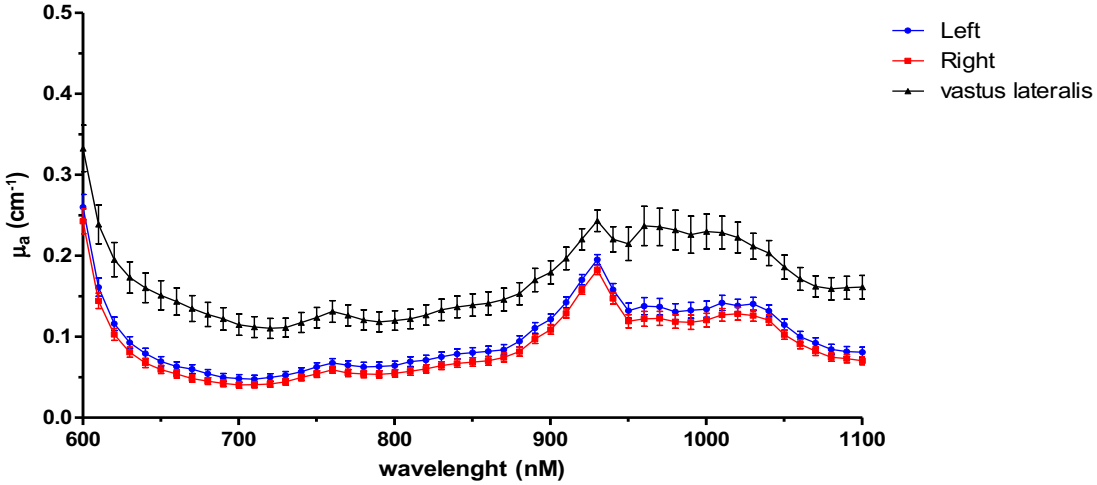

Rho2

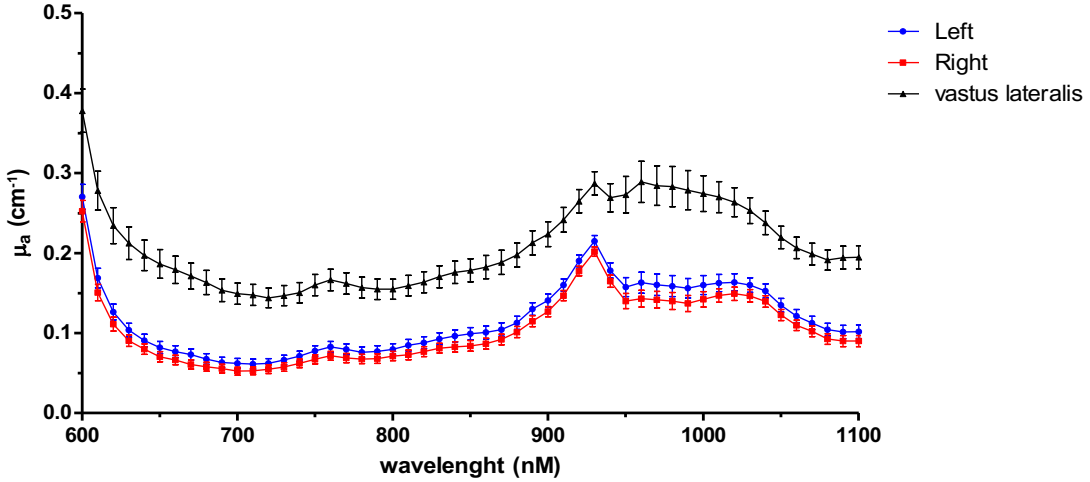

Rho3

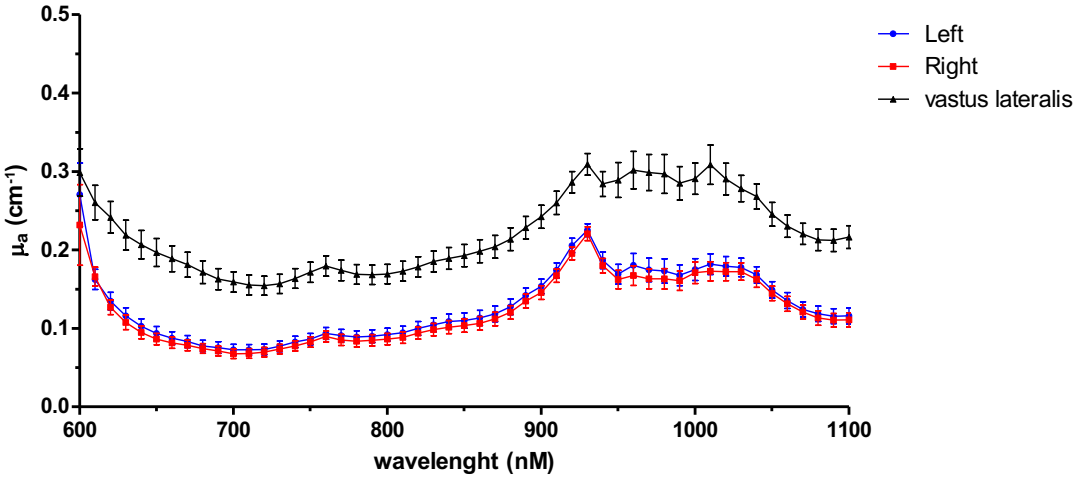

Comparison of the absorption coefficients in the range of wavelengths 600-1100nm at the different tested positions.

	rho1			rho2			rho3		
wavelenght (nm)	Left vs Right	Left vs vastus lateralis	Right vs vastus lateralis	Left vs Right	Left vs vastus lateralis	Right vs vastus lateralis	Left vs Right	Left vs vastus lateralis	Right vs vastus lateralis
600	ns	***	***	ns	***	***	ns	ns	**
610	ns	***	***	ns	***	***	ns	***	***
620	ns	***	***	ns	***	***	ns	***	***
630	ns	***	***	ns	***	***	ns	***	***
640	ns	***	***	ns	***	***	ns	***	***
650	ns	***	***	ns	***	***	ns	***	***
660	ns	***	***	ns	***	***	ns	***	***
670	ns	***	***	ns	***	***	ns	***	***
680	ns	***	***	ns	***	***	ns	***	***
690	ns	***	***	ns	***	***	ns	***	***
700	ns	***	***	ns	***	***	ns	***	***
710	ns	***	***	ns	***	***	ns	***	***
720	ns	***	***	ns	***	***	ns	***	***
730	ns	***	***	ns	***	***	ns	***	***
740	ns	***	***	ns	***	***	ns	***	***
750	ns	***	***	ns	***	***	ns	***	***
760	ns	***	***	ns	***	***	ns	***	***
770	ns	***	***	ns	***	***	ns	***	***
780	ns	***	***	ns	***	***	ns	***	***
790	ns	***	***	ns	***	***	ns	***	***
800	ns	***	***	ns	***	***	ns	***	***
810	ns	**	***	ns	***	***	ns	***	***
820	ns	***	***	ns	***	***	ns	***	***
830	ns	***	***	ns	***	***	ns	***	***
840	ns	***	***	ns	***	***	ns	***	***
850	ns	***	***	ns	***	***	ns	***	***
860	ns	***	***	ns	***	***	ns	***	***
870	ns	***	***	ns	***	***	ns	***	***
880	ns	***	***	ns	***	***	ns	***	***
890	ns	***	***	ns	***	***	ns	***	***
900	ns	***	***	ns	***	***	ns	***	***
910	ns	**	***	ns	***	***	ns	***	***
920	ns	**	***	ns	***	***	ns	***	***
930	ns	**	***	ns	***	***	ns	***	***
940	ns	***	***	ns	***	***	ns	***	***
950	ns	***	***	ns	***	***	ns	***	***
960	ns	***	***	ns	***	***	ns	***	***
970	ns	***	***	ns	***	***	ns	***	***
980	ns	***	***	ns	***	***	ns	***	***
990	ns	***	***	ns	***	***	ns	***	***
1000	ns	***	***	ns	***	***	ns	***	***
1010	ns	***	***	ns	***	***	ns	***	***
1020	ns	***	***	ns	***	***	ns	***	***
1030	ns	***	***	ns	***	***	ns	***	***
1040	ns	***	***	ns	***	***	ns	***	***
1050	ns	***	***	ns	***	***	ns	***	***
1060	ns	***	***	ns	***	***	ns	***	***
1070	ns	***	***	ns	***	***	ns	***	***
1080	ns	***	***	ns	***	***	ns	***	***
1090	ns	***	***	ns	***	***	ns	***	***
1100	ns	***	***	ns	***	***	ns	***	***

Appendix B: Supplementary Information for Section 4.4

Statistical analysis was performed with two-way ANOVA and Bonferroni's multiple comparison test. Error bars represent SEM; n=25; ns=not significant, **p<0.01, ***p<0.001. Outliers values are removed from the dataset.

Reduced scattering spectra for the three positions (Left= 4cm left to navel, Right= 4cm right to navel, 1/3 of the femoral length on the right thigh) tested. Spectra with mean values from all the subjects at the three interfibre distances.

Rho1

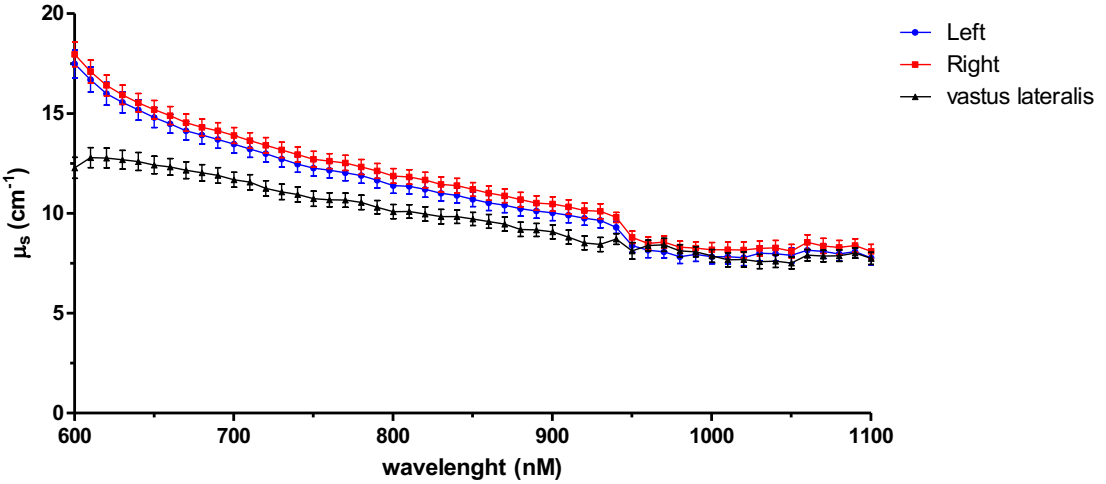

Rho2

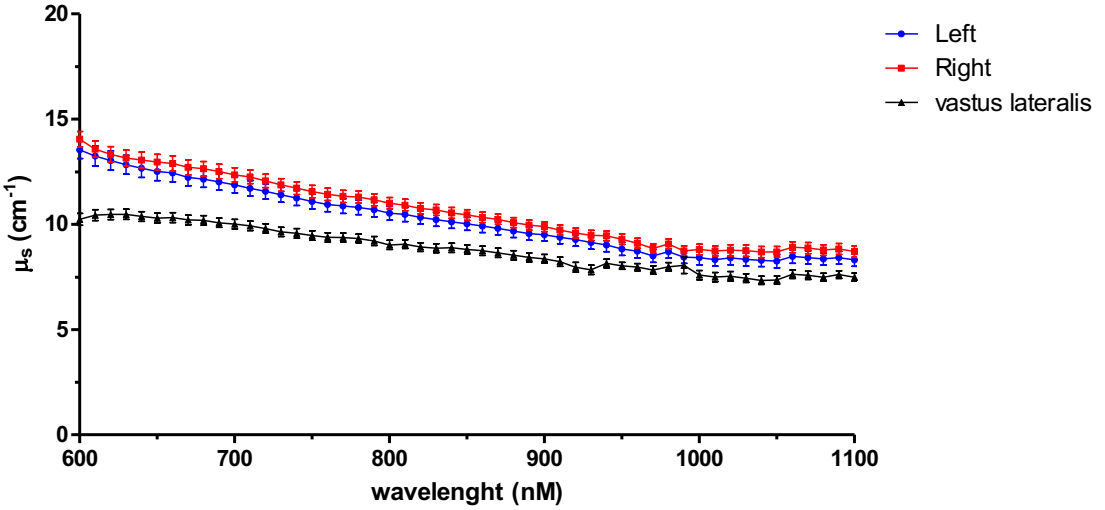

Rho3

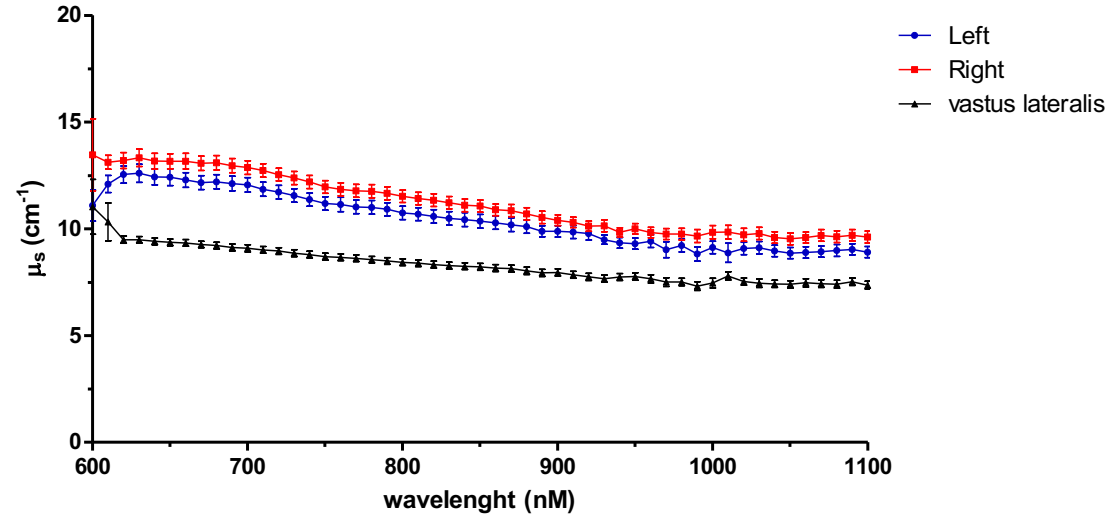

Comparison of the reduced scattering coefficients in the range of wavelengths 600-1100nm at the different tested positions.

	rho1			rho2			rho3		
wavelenght (nm)	Left vs Right	Left vs vastus lateralis	Right vs vastus lateralis	Left vs Right	Left vs vastus lateralis	Right vs vastus lateralis	Left vs Right	Left vs vastus lateralis	Right vs vastus lateralis
600	ns	***	***	ns	***	***	***	ns	***
610	ns	***	***	ns	***	***	ns	***	***
620	ns	***	***	ns	***	***	ns	***	***
630	ns	***	***	ns	***	***	ns	***	***
640	ns	***	***	ns	***	***	ns	***	***
650	ns	***	***	ns	***	***	ns	***	***
660	ns	***	***	ns	***	***	ns	***	***
670	ns	***	***	ns	***	***	ns	***	***
680	ns	***	***	ns	***	***	ns	***	***
690	ns	***	***	ns	***	***	ns	***	***
700	ns	***	***	ns	***	***	ns	***	***
710	ns	***	***	ns	***	***	ns	***	***
720	ns	***	***	ns	***	***	ns	***	***
730	ns	***	***	ns	***	***	ns	***	***
740	ns	**	***	ns	***	***	ns	***	***
750	ns	**	***	ns	***	***	ns	***	***
760	ns	**	***	ns	***	***	ns	***	***
770	ns	**	***	ns	***	***	ns	***	***
780	ns	*	***	ns	***	***	ns	***	***
790	ns	**	***	ns	***	***	ns	***	***
800	ns	*	***	ns	***	***	ns	***	***
810	ns	*	***	ns	***	***	ns	***	***
820	ns	*	***	ns	***	***	ns	***	***
830	ns	ns	***	ns	***	***	ns	***	***
840	ns	ns	***	ns	**	***	ns	***	***
850	ns	ns	**	ns	**	***	ns	***	***
860	ns	ns	**	ns	**	***	ns	***	***
870	ns	ns	**	ns	**	***	ns	***	***
880	ns	ns	**	ns	**	***	ns	***	***
890	ns	ns	*	ns	*	***	ns	***	***
900	ns	ns	**	ns	**	***	ns	***	***
910	ns	ns	**	ns	**	***	ns	***	***
920	ns	*	***	ns	***	***	ns	***	***
930	ns	*	***	ns	**	***	ns	***	***
940	ns	ns	ns	ns	ns	**	ns	**	***
950	ns	ns	ns	ns	ns	**	ns	**	***
960	ns	ns	ns	ns	ns	*	ns	***	***
970	ns	ns	ns	ns	ns	ns	ns	**	***
980	ns	ns	ns	ns	ns	*	ns	***	***
990	ns	ns	ns	ns	ns	ns	ns	**	***
1000	ns	ns	ns	ns	ns	**	ns	**	***
1010	ns	ns	ns	ns	ns	**	ns	ns	***
1020	ns	ns	ns	ns	ns	**	ns	**	***
1030	ns	ns	ns	ns	ns	**	ns	**	***
1040	ns	ns	ns	ns	ns	**	ns	**	***
1050	ns	ns	ns	ns	ns	**	ns	*	***
1060	ns	ns	ns	ns	ns	**	ns	*	***
1070	ns	ns	ns	ns	ns	**	ns	**	***
1080	ns	ns	ns	ns	ns	**	ns	**	***
1090	ns	ns	ns	ns	ns	**	ns	**	***
1100	ns	ns		ns	ns	**	ns	**	***

Appendix B: Supplementary Information for Section 4.4

Statistical analysis was performed with two-way ANOVA and Bonferroni's multiple comparison test. Error bars represent SEM; n=25; ns=not significant, *p<0.05, **p<0.01, ***p<0.001. Outliers values are removed from the dataset.

Absorption spectra with mean values from all the subjects at the three interfibre distances for the three tested positions.

Abdomen 4 cm left to the navel (4L)

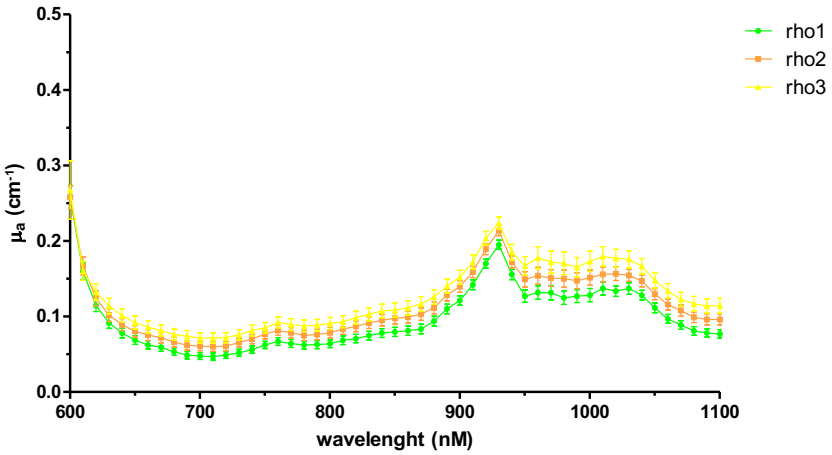

Abdomen 4 cm right to the navel (4R)

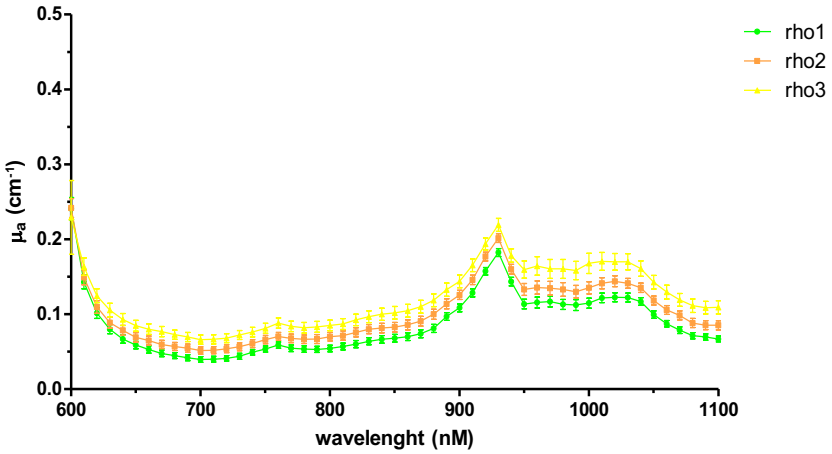

***Vastus lateralis* (VL)**

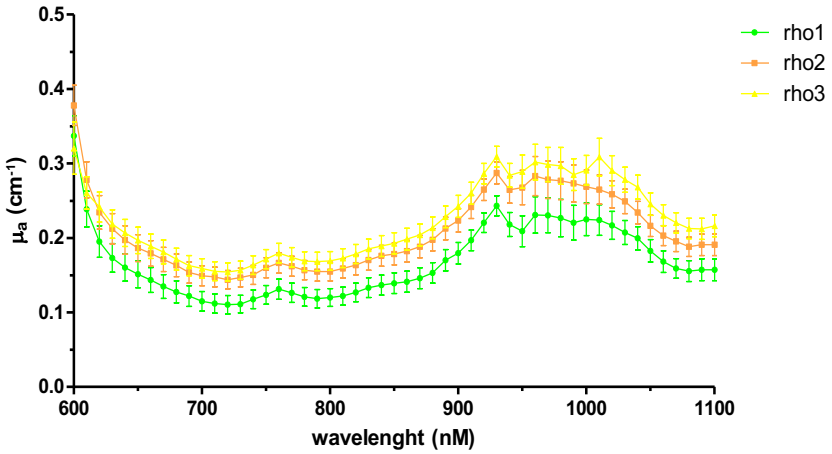

Comparison of the absorption coefficients in the range of wavelengths 600-1100nm at the three interfibre distances.

	4L			4R			VL		
wavelenght (nm)	rho1 vs rho2	rho1 vs rho3	rho2 vs rho3	rho1 vs rho2	rho1 vs rho3	rho2 vs rho3	rho1 vs rho2	rho1 vs rho3	rho2 vs rho3
600	ns	ns	ns	ns	ns	ns	***	ns	***
610	ns	ns	ns	ns	ns	ns	***	ns	ns
620	ns	ns	ns	ns	ns	ns	***	***	ns
630	ns	**	ns	ns	*	ns	***	***	ns
640	ns	**	ns	ns	*	ns	***	***	ns
650	ns	**	ns	ns	*	ns	***	***	ns
660	ns	**	ns	ns	**	ns	***	***	ns
670	ns	**	ns	ns	**	ns	***	***	ns
680	ns	**	ns	ns	**	ns	***	***	ns
690	ns	***	ns	ns	**	ns	***	***	ns
700	ns	**	ns	ns	**	ns	***	***	ns
710	ns	***	ns	ns	**	ns	***	***	ns
720	ns	**	ns	ns	**	ns	***	***	ns
730	ns	**	ns	ns	**	ns	***	***	ns
740	ns	***	ns	ns	**	ns	***	***	ns
750	ns	**	ns	ns	**	ns	***	***	ns
760	ns	***	ns	ns	**	ns	***	***	ns
770	ns	***	ns	ns	**	ns	***	***	ns
780	ns	***	ns	ns	**	ns	***	***	ns
790	ns	***	ns	ns	**	ns	***	***	ns
800	ns	***	ns	ns	***	ns	***	***	ns
810	ns	***	ns	ns	**	ns	***	***	ns
820	ns	***	ns	ns	***	ns	***	***	ns
830	ns	***	ns	ns	***	ns	***	***	ns
840	ns	***	ns	ns	***	ns	***	***	ns
850	ns	***	ns	ns	***	ns	***	***	ns
860	ns	***	ns	ns	***	ns	***	***	ns
870	*	***	ns	ns	***	ns	***	***	ns
880	ns	***	ns	ns	***	ns	***	***	ns
890	ns	***	ns	ns	***	ns	***	***	ns
900	ns	***	ns	ns	***	ns	***	***	ns
910	ns	***	ns	ns	***	ns	***	***	ns
920	*	***	ns	ns	***	ns	***	***	ns
930	*	***	ns	ns	***	ns	***	***	*
940	ns	***	ns	ns	***	ns	***	***	ns
950	*	***	ns	ns	***	*	***	***	ns
960	*	***	**	ns	***	**	***	***	ns
970	ns	***	*	ns	***	*	***	***	ns
980	**	***	*	ns	***	*	***	***	ns
990	*	***	ns	ns	***	**	***	***	ns
1000	**	***	*	ns	***	***	***	***	ns
1010	ns	***	**	ns	***	**	***	***	***
1020	**	***	*	ns	***	*	***	***	***
1030	ns	***	*	ns	***	**	***	***	**
1040	ns	***	ns	ns	***	*	***	***	***
1050	ns	***	ns	ns	***	ns	***	***	**
1060	ns	***	ns	ns	***	ns	***	***	**
1070	ns	***	ns	ns	***	ns	***	***	*
1080	ns	***	ns	ns	***	ns	***	***	*
1090	ns	***	ns	ns	***	ns	***	***	ns
1100	ns	***	ns	ns	***	ns	***	***	*

Statistical analysis was performed with two-way ANOVA and Bonferroni's multiple comparison test. Error bars represent SEM; n=26 for abdomen positions, n=25 for *vastus lateralis* position; ns=not significant, *p<0.05, **p<0.01, ***p<0.001. Outliers values are removed from the dataset.

Reduced scattering spectra with mean values from all the subjects at the three interfibre distances for the three tested positions.

Abdomen 4 cm left to the navel (4L)

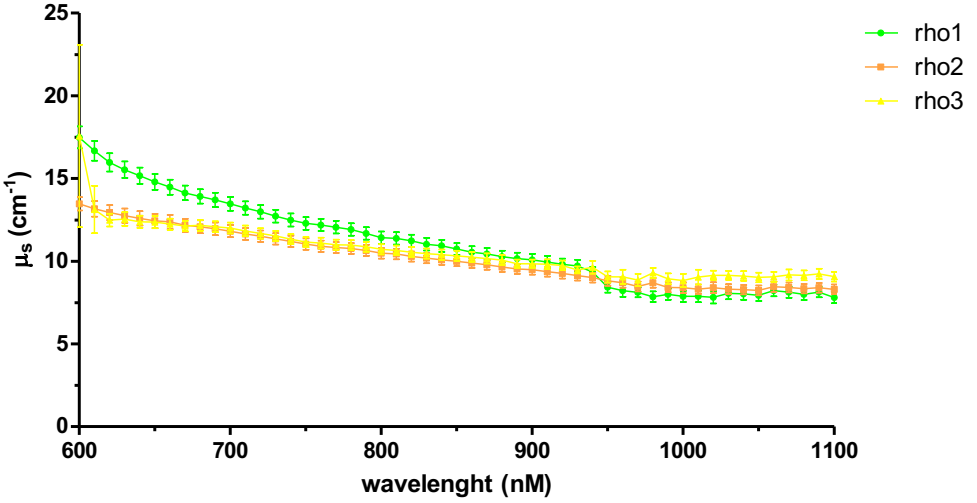

Abdomen 4 cm right to the navel (4R)

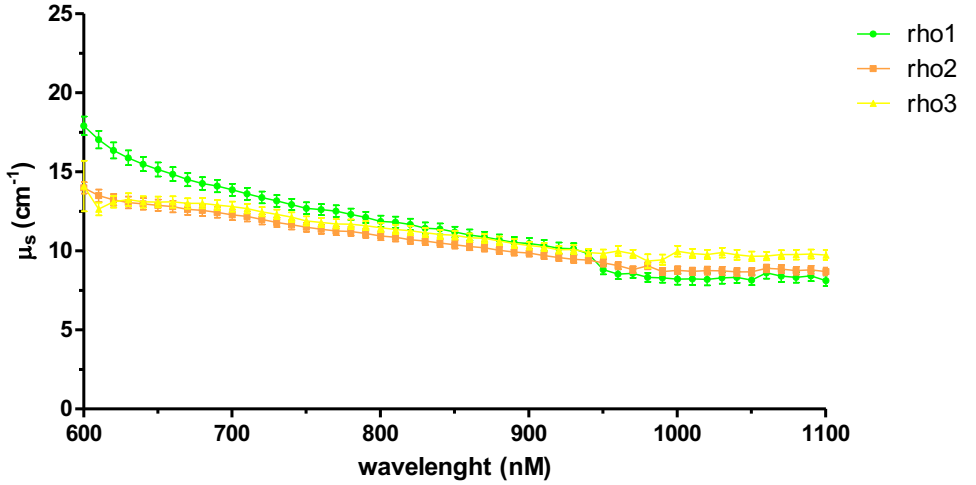

Vastus lateralis (VL)

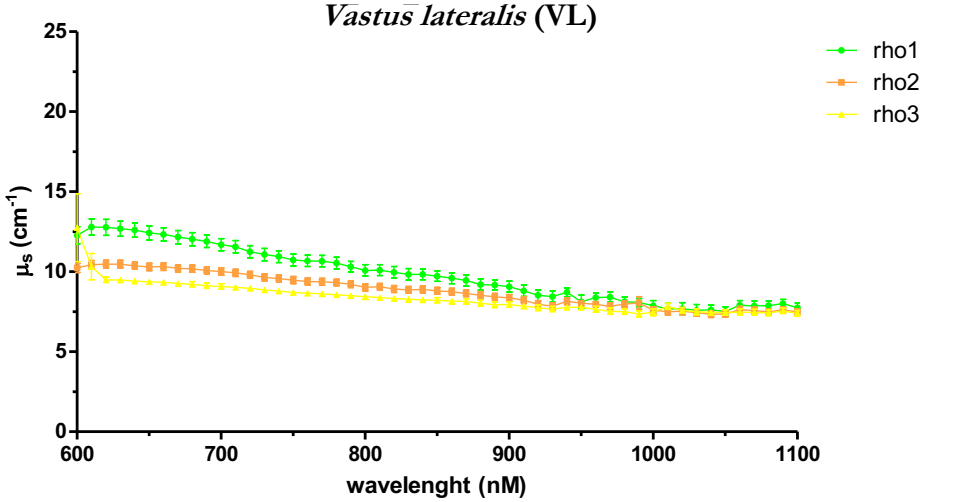

Comparison of the reduced scattering coefficients in the range of wavelengths 600-1100nm at the three interfibre distances.

	4L			4R			VL		
wavelenght (nm)	rho1 vs rho2	rho1 vs rho3	rho2 vs rho3	rho1 vs rho2	rho1 vs rho3	rho2 vs rho3	rho1 vs rho2	rho1 vs rho3	rho2 vs rho3
600	***	ns	***	***	***	ns	***	ns	***
610	***	***	ns	***	***	ns	***	***	ns
620	***	***	ns	***	***	ns	***	***	ns
630	**	**	ns	***	***	ns	***	***	ns
640	*	**	ns	***	***	ns	***	***	ns
650	*	*	ns	***	***	ns	***	***	ns
660	ns	ns	ns	***	***	ns	***	***	ns
670	ns	ns	ns	***	***	ns	***	***	ns
680	ns	ns	ns	***	**	ns	***	***	ns
690	ns	ns	ns	***	**	ns	***	***	ns
700	ns	ns	ns	***	*	ns	***	***	ns
710	ns	ns	ns	***	ns	ns	***	***	ns
720	ns	ns	ns	***	ns	ns	**	***	ns
730	ns	ns	ns	***	ns	ns	**	***	ns
740	ns	ns	ns	**	ns	ns	**	***	ns
750	ns	ns	ns	**	ns	ns	*	***	ns
760	ns	ns	ns	**	ns	ns	**	***	ns
770	ns	ns	ns	**	ns	ns	**	***	ns
780	ns	ns	ns	*	ns	ns	*	***	ns
790	ns	ns	ns	ns	ns	ns	ns	***	ns
800	ns	ns	ns	ns	ns	ns	ns	***	ns
810	ns	ns	ns	ns	ns	ns	ns	***	ns
820	ns	ns	ns	ns	ns	ns	ns	***	ns
830	ns	ns	ns	ns	ns	ns	ns	***	ns
840	ns	ns	ns	ns	ns	ns	ns	***	ns
850	ns	ns	ns	ns	ns	ns	ns	***	ns
860	ns	ns	ns	ns	ns	ns	ns	**	ns
870	ns	ns	ns	ns	ns	ns	ns	**	ns
880	ns	ns	ns	ns	ns	ns	ns	*	ns
890	ns	ns	ns	ns	ns	ns	ns	*	ns
900	ns	ns	ns	ns	ns	ns	ns	ns	ns
910	ns	ns	ns	ns	ns	ns	ns	ns	ns
920	ns	ns	ns	ns	ns	ns	ns	ns	ns
930	ns	ns	ns	ns	ns	ns	ns	ns	ns
940	ns	ns	ns	ns	ns	ns	ns	ns	ns
950	ns	ns	ns	ns	ns	ns	ns	ns	ns
960	ns	ns	ns	ns	***	ns	ns	ns	ns
970	ns	ns	ns	ns	**	ns	ns	ns	ns
980	ns	ns	ns	ns	ns	ns	ns	ns	ns
990	ns	ns	ns	ns	*	ns	ns	ns	ns
1000	ns	ns	ns	ns	***	**	ns	ns	ns
1010	ns	ns	ns	ns	***	*	ns	ns	ns
1020	ns	ns	ns	ns	***	ns	ns	ns	ns
1030	ns	ns	ns	ns	***	*	ns	ns	ns
1040	ns	ns	ns	ns	***	*	ns	ns	ns
1050	ns	ns	ns	ns	***	ns	ns	ns	ns
1060	ns	ns	ns	ns	*	ns	ns	ns	ns
1070	ns	ns	ns	ns	**	ns	ns	ns	ns
1080	ns	ns	ns	ns	***	ns	ns	ns	ns
1090	ns	ns	ns	ns	***	ns	ns	ns	ns
1100	ns	ns	ns	ns	***	ns	ns	ns	ns

Statistical analysis was performed with two-way ANOVA and Bonferroni's multiple comparison test. Error bars represent SEM; n=26 for abdomen positions, n=25 for *vastus lateralis* position; ns=not significant, *p<0.05, **p<0.01, ***p<0.001. Outliers values are removed from the dataset.